Alternative protective coatings for hot stamped automotive body parts

Damien Close

UNIVERSITÉ DE LORRAINE

École doctorale SESAMES

THÈSE

Pour l'obtention du titre de :

DOCTEUR DE L'UNIVERSITÉ DE LORRAINE

CHIMIE

Spécialité : Chimie, Electrochimie et Science des Matériaux

Présentée par :

DAMIEN CLOSE

Alternative protective coatings for hot stamped automotive body parts

---

Soutenance publique le 22 Mars 2018 à Metz devant le jury composé de :

Juan CREUS	Professeur LaSIE, Université de La Rochelle - La Rochelle, France	Rapporteur
Marjorie OLIVIER	Professeur Faculté Polytechnique de Mons - Mons, Belgique	Rapporteur
Muriel VERON	Professeur Grenoble INP, SIMAP - Grenoble, France	Examinatrice
Albert TIDU	Professeur LEM3, Université de Lorraine - Metz, France	Examinateur
Nathalie ALLAIN	Professeur LEM3, Université de Lorraine - Metz, France	Examinatrice
Nicolas STEIN	Maître de Conférences HDR IJL, Université de Lorraine - Metz, France	Directeur de thèse
Clotilde BOULANGER	Professeur IJL, Université de Lorraine - Metz, France	Invitée
Régis LALLEMENT	Dr. -Ing Daimler AG - Sindelfingen, Allemagne	Invité

Institut Jean Lamour – Equipe 208 – 1 Boulevard Arago 57078 Metz CEDEX

Université de Lorraine – Pôle M4 : matière, matériaux, métallurgie, mécanique

Conformément aux exigences de l'École Doctorale SESAMES, la thèse étant rédigée en anglais, l'introduction, les objectifs, les résumés des chapitres 4, 5 et 6 ainsi que la conclusion sont également rédigés en français.

This work has been carried out at the *Institut Jean Lamour (IJL)* and at the *laboratory of study of microstructures, mechanics and material sciences (LEM3)* of the Université de Lorraine (UL) in the framework of an industrial project in cooperation with the Daimler AG.

First of all, I would like to express my sincere gratitude to Dr. Nicolas Stein, Prof. Nathalie Allain and Prof. Albert Tidu for their continuous support and input throughout the entire thesis. Their help in regard to the various scientific and technical challenges I encountered as well as the insightful comments on the manuscript helped me to improve my work. I enjoyed the endless brain storming sessions in which we were trying to understand the Zn-Mn alloys. My sincere thanks go to my advisor Nicolas for his outstanding supervision, his personal support in the rough phases as well as for sharing his immense knowledge with me. I am deeply grateful for everything I learned from you.

All this would not have been possible without the support of Dr. Régis Lallement, who originally had the idea about this interesting topic and initiated the project. He has taught me a lot about academic and industrial environments, which was an important requirement to conduct this thesis. Beyond, I would like to express my gratitude to Dr. Peter Feuser for his great expertise in the domain of hot forming, his valuable supervision and his numerous comments which improved the quality of this thesis. I am also thankful to Mr. Raschke, Prof. Paul Dick and Mr. Bachmann for the opportunity of conducting this research and for initiating the financial support. I am also appreciative to Prof. Merklein who provided me the opportunity to carry out hot stamping experiments as well as to Dr. Sven Hildering for his support with the research facilities.

I would like to thank Prof. Marjorie Olivier, Prof. Muriel Veron, Prof. Juan Creus, and Prof. Clotilde Boulanger for being part of my thesis committee and for their helpful comments on the manuscript and the presentation. I am also thankful to Prof. Albert Tidu who made me the honor of being the president of the committee.

Furthermore, I would like to take the opportunity to thank Florian Claudel for his support in the last months of my PhD thesis. I am also thankful to my colleagues from the IJL and LEM3 laboratories for their contribution in conducting the experiments, in particular Dr. Julien Guyon for his FIB-SEM and EBSD analyses, Dr. Sebastien Diliberto and Laetitia Garoux for the XRD analyses, Dr. Marie Georgel for the Raman measurements as well as Dr. Abdel Danine and Prof. Jaafar Ghanbaja for the TEM analyses. Thanks to Estelle, Nicolas, Jamal, Thu Hang, Victor, Romain, Daniela, Alexander and Florian for their support in the experiments as well as to José Lopez for the construction of the electroplating cell. I also would like to thank the staff of the RD/KSO, TF/VFT and RD/KRU departments, in particular Dr. Michael Bayer and Carmen Schmidt for their help in the characterisation studies. I also have a thought for Bernard for his contribution in the start of the project.

Lastly, I would like to express my gratitude to my family and friends for their support during the last years as well as to my partner, Anna, who has encouraged me during the entire process. I am thankful for your understanding, your patience, your love and your humour, which have brightened up the sometimes dark days of thesis writing.

SUMMARY

Alternative protective coating systems for hot stamped automotive body parts

Various coatings are currently available for press-hardened steels used for the automotive construction, mainly with the aim of providing good anticorrosive properties to the body components. In order to improve performance of the coated products in terms of hot formability, corrosion protection and suitability for subsequent manufacturing processes, steelmakers and car manufacturers investigated various alternative coating materials. Only a few solutions resulted in a serial production. The aim of this study is to proceed to a screening of the performance of current coating variants, to identify new concepts for alternative coating materials and assess their suitability for the hot stamping application.

The present work is focused on the study of Zn-Mn alloy coatings. Various electroplating baths and electric parameters were studied in order to determine optimal deposition conditions for obtaining Zn-Mn alloys with high Mn contents. The deposits obtained on large-scale steel plates were characterized with regards to their crystallographic, microstructural and anticorrosive properties. The behavior of the coating materials during austenitizing treatment was studied after heat treatment to different temperatures and heating durations. A particular attention was given to the evolution of the composition, the interdiffusion phases formed as well as to the presence of oxidation and evaporation mechanisms at high temperature. At last, the forming properties of the alternative coating materials and their susceptibility for liquid metal embrittlement were assessed on the basis of direct hot stamping experiments.

KEY WORDS

Coatings

Electrodeposition

Microstructural Characterization

Corrosion Protection

Hot Stamping

Surface Engineering

RÉSUMÉ

Revêtements alternatifs pour pièces automobiles embouties à chaud

De nombreux revêtements sont actuellement disponibles pour les aciers emboutis à chaud et trempés pour le domaine de la construction automobile. Afin d'augmenter les performances des produits actuels en termes d'aptitude à la mise en forme à chaud, de résistance contre la corrosion et de compatibilité avec les procédés de fabrication ultérieurs, les constructeurs automobiles et les sidérurgistes ont développé de nombreux types de matériaux alternatifs. Peu de produits ont trouvé une place importante dans l'utilisation industrielle. L'objectif de ce travail est de procéder à une vue d'ensemble des performances des produits actuels, d'identifier de nouveaux concepts de revêtements et d'étudier leur compatibilité pour l'application de la mise en forme à chaud.

Cette étude porte sur les revêtements d'alliages de Zn-Mn. De nombreux bains électrolytiques et paramètres électriques ont été étudiés afin de déterminer des conditions de déposition optimales pour obtenir des alliages Zn-Mn avec une forte teneur en Mn. Les propriétés cristallographiques, microstructurales et anticorrosives de couches obtenues sur des plaques d'acier de grandes dimensions ont été caractérisées avec de nombreuses techniques. La compatibilité des couches protectrices pour le traitement d'austénitisation a été évaluée après des traitements thermiques à différentes températures et durées de chauffe. Une attention particulière a été portée sur l'évolution de la composition et des phases d'interdiffusion formées, ainsi que sur l'apparition de mécanismes d'oxydation et d'évaporation à haute température. Enfin, l'aptitude à la mise en forme à chaud et notamment la susceptibilité à la fissuration par métaux liquides de ces nouveaux revêtements ont été évaluées par des essais d'emboutissage.

MOTS CLÉS

Revêtements

Électrodéposition

Caractérisation microstructurale

Protection contre la corrosion

Emboutissage à chaud

Traitement de surface

Table of contents

List of abbreviations

AAS	Atomic Absorption Spectroscopy
Ac_3	Austenite formation finish temperature
BIW	Body-In-White
BSE	Back Scattered Electrons
CV	Cyclic Voltammetry
DP	Dual-Phase steel
e	Coating thickness
E	Potential
EBSD	Electron Backscatter Diffraction
E_{corr}	Corrosion potential
EDS	Energy Dispersive X-ray Spectroscopy
EQCM	Electrochemical Quartz Crystal Microbalance
F	Faraday's constant
f	Resonance frequency
FEG	Field Emission Gun
FIB	Focused Ion Beam
GA	Galvannealed
GDOES	Glow-Discharge Optical Electron Spectroscopy
GI	Galvanized
HTC	Heat Transfer Coefficient
i	Current density
i_{corr}	Corrosion current density
JCPDS	Joint Committee on Powder Diffraction Standards
K	Constant of Sauerbrey
LME	Liquid Metal Embrittlement
M	Molar Mass
M_f	Martensite finish temperature
M_s	Martensite start temperature
η	Current efficiency
OCP	Open Circuit Potential
OEM	Original Equipment Manufacturer
P_c	Contact pressure
PEG	Polyethylene Glycol
PHS	Press-Hardened Steel
Q	Electric charge
R_p	Polarization resistance
S_a	Surface roughness
SCE	Standard Calomel Electrode
SE	Secondary Electrons
SEM	Scanning Electron Microscopy

SHE	Standard Hydrogen Electrode
STEM	Scanning Transmission Electron Microscope
T	Temperature
t	Time
t_0	Initial blank thickness
T_{max}	Maximal blank temperature
t_{aust}	Austenitizing time
TEM	Transmission Electron Microscope
TRIP	Transformation-Induced Plasticity steel
T_f	Furnace temperature
UHSS	Ultra-High-Strength Steel
VDA	Verband der Automobilindustrie e.V.
WDS	Wavelength Dispersive Spectroscopy
XRD	X-ray Diffraction
z	Number of electrons
λ	Wavelength of the incident X-radiation
ρ	Volumic mass

Introduction [EN]

With the aim of decreasing the emissions related to the consumption of vehicles, in particular for the emission of carbon dioxide, car manufacturers count on the lightening of the bodies, which is mainly achieved by the use of low-density materials such as aluminum, magnesium, composites and by the insertion of cold formed steel components with high strength [1, 2]. In addition, in order to ensure the best behavior of the car bodies in the event of a crash and fulfill the constantly evolving car safety regulations like NHTSA and NCAP standards, car manufacturers have developed many active protection measures such as sensors, driver assistance systems or airbags. In addition, passive safety is ensured by the design of bodies with various materials with tailored properties. While soft materials such as multiple phase steels are required in the crumple zones of the cars in order to absorb the energy in the event of a crash, the passenger compartment must remain rigid to protect the occupants and generally consist of steels with a high yield strength [1]. For these structures, press-hardened components with an ultra-high-strength of up to 1500 MPa and a relatively low total elongation at rupture of about 6 % and consisting of manganese-boron steel such as the 22MnB5 steel grade are commonly used [1, 3]. These materials were first implemented in 1984 in car bodies and their use has progressively increased until reaching an estimated number of 600 million parts in 2015 [4]. Such parts are manufactured by the hot stamping process during which steel blanks are austenitized to a temperature range of 900-950 °C for several minutes, transferred to press tools for forming or for calibration of the final geometries [3]. By carrying out a rapid cooling of the heated blanks with cooled tools, a martensitic structure is formed, which permits to achieve a significant increase of the mechanical strength of the final components. In order to avoid oxidation and decarburization of steel during heat treatment and avoid the issues implied by the use of bare steel in terms of corrosion, various coating systems have been developed and investigated by the automotive industry [3]. Nowadays, two metallic coating products are established in the serial production, namely galvanized and aluminized coatings. Their use mainly depends on the geometries of the components and on the required performance of the parts, in particular in terms of corrosion protection. A particular interest was found for Zn-based coatings, mainly with the aim of providing sacrificial protection to steel.

Several key development tracks have been found in hot stamping applications, such as the development of new design concepts with the use of tailored-rolled blanks or tailored-tempered parts to achieve the desired component strength and ductility [2]. Moreover, new heating technologies such as conduction and induction heating are currently under development in order to optimize the manufacturing processes [5]. Another promising approach is the development of innovative materials concepts for coating materials for the hot stamping application. The range of functionalities required for the coating materials comprises good thermal stability during austenitizing treatment, good hot formability, adequate suitability for subsequent processes such as painting and joining as well as high anticorrosive performance.

However, challenges are encountered by steelmakers and car manufacturers in the optimization of the manufacturing process and the corresponding costs and the achievement of good performance with current coating systems. In fact, austenitizing treatment induces changes in the composition of the initial coatings and influences performance of the products, in particular in terms of corrosion protection. In the case of aluminized steels, no sacrificial corrosion protection is provided after hot stamping, contrary to galvanized steel. However, galvanized coatings have a low hot formability due to the formation of cracks in substrate steel related to liquid metal embrittlement and require a more complex manufacturing process than aluminized parts. The present work is dedicated to the electrodeposition and the study of the properties of alternative Zn-Mn alloy coatings prior to and post to high temperature processes and hot stamping, with the aim of finding a compromise between the advantages of current aluminized and galvanized products, namely good formability at high temperature and the achievement of sacrificial protection for steel.

Introduction [FR]

Dans l'objectif de réduire les émissions liées à la consommation des véhicules, et en particulier des émissions de dioxyde de carbone, l'industrie automobile mise sur la réduction du poids des véhicules, qui peut principalement être obtenue en utilisant des matériaux à faible densité comme l'aluminium, le magnésium, les composites ou en utilisant des aciers formés à froid à très haute résistance mécanique [1, 2].

En outre, et afin d'assurer une protection maximale dans le cas d'un crash et de répondre aux exigences de plus en plus strictes des standards mondiaux tels que NHTSA ou NCAP en matière de sécurité routière, de nombreuses méthodes et technologies de protection actives telles que des capteurs, des outils d'assistance ou des airbags ont été développées par les constructeurs automobiles. De plus, la sécurité passive des passagers est assurée par la conception de carrosseries avec de nombreux types de matériaux possédant des propriétés sur mesure. D'une part, des matériaux relativement ductiles tels que les aciers multiphasés sont souhaités dans certaines zones des carrosseries telles que l'avant ou l'arrière du véhicule afin d'absorber l'énergie lors d'un accident. D'autre part, l'habitacle de véhicules doit rester le plus intact possible afin de protéger les passagers et sont, de ce fait, généralement faits d'aciers avec un faible taux de déformation [1].

Une grande partie de ces pièces de structures est constituée d'aciers présentant une ultra-haute résistance mécanique de 1500 MPa et une faible élongation à la rupture d'environ 6 % [1, 3]. Ces aciers de type Manganese-Bore tels que le 22MnB5 ont fait leur première apparition en 1984 dans le domaine automobile et leur production a subi une très forte hausse au point d'atteindre un nombre estimé de pièces de 600 millions en 2015 [4]. Ces pièces sont fabriquées par le procédé d'emboutissage à chaud, c'est à dire après austénitisation de tôles à une température de 900-950 °C pendant plusieurs minutes suivie d'une mise en forme à chaud et d'une trempe thermique dans les outils de presse [3]. Le refroidissement rapide des tôles permet d'activer la transformation d'une phase austénitique en phase martensitique, ce qui conduit à une augmentation considérable des propriétés mécaniques des pièces. Dans le but d'éviter l'oxydation et la décarburation de l'acier lors du traitement thermique d'austénitisation et de réduire l'exposition des pièces aux environnement corrosifs lors de l'utilisation d'aciers nus dans la carrosserie automobile, de nombreux types de revêtements ont été développés par l'industrie automobile et les sidérurgistes [3].

Actuellement, deux revêtements métalliques, à savoir les produits aluminiés et galvanisés, ont pris une place importante dans la production en série de pièces automobiles. Leur utilisation dépend des géométries des pièces et des propriétés souhaitées, notamment en termes de protection contre la corrosion. Un intérêt particulier a été trouvé pour les aciers revêtus de couches basées sur des alliages de zinc qui permettent d'obtenir une protection cathodique du substrat.

Ces dernières années, le domaine de l'emboutissage à chaud de pièces de carrosserie automobiles a fait l'objet de plusieurs axes d'étude et de recherche, tel que le développement de nouveaux concepts comme l'utilisation de flans soudés, laminés ou tempérés sur mesure pour réduire le poids des pièces et obtenir le comportement mécanique désiré pour la structure [2]. De plus, de nouvelles méthodes de chauffage par conduction ou induction font actuellement l'objet de recherches avec pour objectif d'optimiser le procédés de fabrication [5]. Un autre axe d'étude concerne le développement et l'élaboration de nouveaux types de revêtements protecteurs pour l'emboutissage à chaud qui doivent répondre à un large panel d'exigences, notamment une bonne stabilité thermique pendant le traitement d'austénitisation, une bonne compatibilité avec les procédés de traitement ultérieux tels que la peinture et l'assemblage, ainsi que de hautes performances anticorrosives et une bonne aptitude à la mise en forme à chaud.

Cependant, de nombreux défis sont rencontrés par les constructeurs automobiles et les sidérurgistes dans l'optimisation des procédés de fabrication et de leurs coûts ainsi que dans l'obtention de performances optimales avec les produits commerciaux actuels. En effet, le traitement d'austénitisation des plaques revêtues modifie considérablement la composition et la microstructure des revêtements initiaux, et par conséquent les performances des produits finaux, notamment en termes de protection contre la corrosion. Dans le cas d'aciers aluminiés, aucune protection cathodique active n'est obtenue après emboutissage à chaud, contrairement aux aciers galvanisés pour lesquels la présence de zinc permet de protéger l'acier de la corrosion. Cependant, ces derniers possèdent une faible aptitude à la mise en forme à chaud dû au phénomène de fissuration par métaux liquides, ce qui implique l'utilisation d'un procédé de fabrication plus complexe et plus coûteux que pour des aciers aluminiés.

Cette étude est dédiée à la sélection de matériaux prometteurs sur la base de recherches bibliographiques et des exigences vis-à-vis de l'application de mise en forme à chaud. Les alliages de Zn-Mn sélectionnés seront élaborés par électrodéposition après une étude exhaustive des conditions électrolytiques et seront caractérisés avant et après traitements thermiques et essais d'emboutissages avec pour objectifs de déterminer les propriétés des nouveaux types de revêtements pour cette application et évaluer leurs performances par rapport aux produits standards.

1. State of the art about coating systems for press-hardened parts

1.1 Hot stamping in the automotive industry

1.1.1 Automotive bodies

Nowadays, various steel grades are combined in passenger vehicles to reduce fuel consumption by manufacturing lightweight body parts and to achieve good performance in crash safety. This particularity is a response to increasingly stringent international regulations for vehicle emissions such as the long-term goal of 95 g of carbon dioxide emissions per kilometre and the constantly evolving rules for passengers safety requirements such as EuroNCAP or NHTSA [6-8].

Two categories of steel body parts can be distinguished, namely cold and hot formed components. On the one hand, cold formed standard steels with strengths of about 500 MPa and a high ductility with total elongations of up to 60 % can be implemented in the vehicle body in order to absorb energy during a crash by undergoing severe plastic deformation [1]. However, steel grades with high ductility and standard strength are responsible for the intrusion of external structures into the passenger compartment or the failure of the structures in presence of high stresses. Advanced High-Strength Steels (AHSS) such as Dual-Phase (DP) and Transformation-Induced Plasticity (TRIP) steels were developed for the cold forming application to increase mechanical strength of the components [9]. According to Naganathan and Penter, manufacturing of AHSS parts involves challenges such as low formability at room temperature and considerable springback [10].

On the other hand, hot formed components provide good formability and reduced springback, along with outstanding mechanical properties after quenching in the press tools, namely after the press-hardening process. Their use has increased drastically in the last years for safety-related anti-intrusion parts and structural reinforcements in order to prevent intrusion into the passenger compartment and to improve the structure stability against buckling and roll-over [6, 11]. The current work is dedicated to the study of protective coatings for the latter hot formed body parts.

1.1.2 Hot stamped body parts

The hot stamping process was originally developed and patented by the “Norrbottens Järnverk AB” in 1977, after a first announcement for a European patent on hot stamping in Sweden in 1973 [12, 13]. Blanks of hardenable steel are heated to austenitic state and formed to the desired final shape and simultaneously cooled down for obtaining a martensitic structure. The original application of the hot stamping method was the manufacturing of saw blades and lawn mower blades with ultra-high strength [14]. The first hot formed steel components were used in 1984 in the automotive application for door

intrusion beams in the SAAB 9000 passenger cars [3]. The original body part was made of a 22MnB5 steel and provided an ultimate tensile strength of 1200 MPa [15].

The first serial production of hot formed automotive components started in 1986 by Plannja AB [13]. Further supply contracts were then signed with many car manufacturers in the early 1990s, generalizing the use of hot stamped parts in the car bodies. In fact, the number of manufactured components increased from 3 million parts per year in 1987 to approximately 107 million parts per year in 2007 [10]. A further increase has been observed in the last years, with a global demand of 300 million parts in 2011 and an estimated number of 600 million parts in 2015 along with the diversification of the structure components in the car bodies [4]. More than 130 hot stamping production lines have been built by 2011 to respond to the growing demand from car manufacturers [8]. A particular growth was found to take place in the Asian/Pacific region [4].

According to Jesner and Gelder, the number of press-hardened steel parts in automotive Body-In-White (BIW) increased up to 50 parts per vehicle in the recent years [16]. Hot stamped steels are currently implemented in various locations in the body. The typical components are A and B-pillar reinforcements, side impact protection, bumpers, door pillar reinforcement, rear and front end cross members or roof frames [14]. About 12 % of the car body weight of the current S-Class is made of hot formed steel components, as presented in Figure 1 [17].

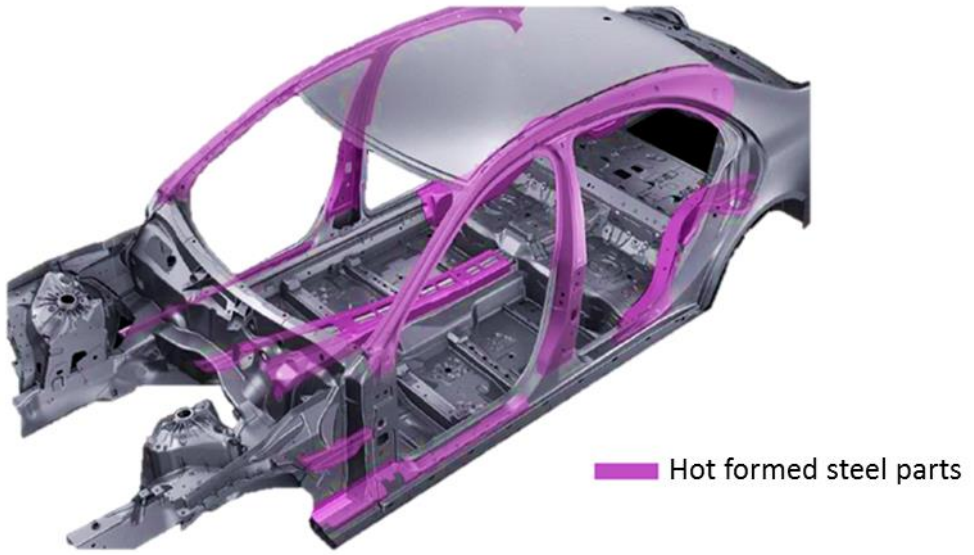

Figure 1: Distribution of hot formed steels in the car body of the current Mercedes-Benz S-Class (2013) [17].

The application of new generation steel components coupled with advanced manufacturing processes and tailored mechanical properties will help the automotive industry to meet the demand for lighter vehicles without the added expense of alternative lightweight materials such as Aluminum or Magnesium, which imply a CO_2 footprint five to ten times higher than that of AHSS [18]. The use of AHSS has shown considerable advantages in terms of lightweight conception with a reduction of 25 % of the BIW mass and a reduction of fuel consumption of more than 5 % compared to conventional steel automotive bodies, along

with little or no increase of BIW manufacturing costs [8, 18]. In fact, the drastic increase of the mechanical strength of hot formed components permits to reduce the thickness required for the parts to ensure good crash performance, thus reducing the weight of the vehicle BIW. A particular interest was found by car manufacturers for partial press-hardening of body parts with heated tools with the aim of manufacturing body components with tailored ductility and strength [2].

1.2 Press-hardening process

Boron alloys such as 22MnB5, 27MnCrB5 and 37MnB4 steels were reported to produce a fully martensitic microstructure, which is responsible for the considerable increase of strength after press-hardening [14]. The current study will be dedicated to the study of hot stamping of 22MnB5 steel, which is the most established base material for hot stamped automotive components.

The main commercial products are supplied by ArcelorMittal S.A., ThyssenKrupp Steel Europe AG or Voestalpine GmbH for the european automotive market and are available with different manufacturing processes, surface treatments and protective coatings.

The chemical composition of 22MnB5 steels is listed in Table 1.

Table 1: Chemical composition of 22MnB5 steel in wt.% [19, 20].

Elements	**C**	**Mn**	**Si**	**P**	**S**	**Al**	**Ti**	**Cr**	**B**
Composition (wt.%)	0.19-0.25	1.10-1.40	0.00-0.40	0.000-0.025	0.000-0.015	0.020-0.060	0.02-0.05	0.15-0.35	0.0008-0.0050

In order to achieve advanced mechanical properties, small fractions of Boron, Carbon, Manganese or Chromium are added to steel. The adjustement of the Carbon content permits to stabilize austenite and control the strength after quenching [3, 14]. Boron is added in order to increase hardenability of steel by retarding the heterogeneous nucleation of ferrite at austenite grain boundaries [3]. It results in a lower critical cooling rate and an extension of the process window for hot forming [10, 13]. Chrome and Manganese were stated to slightly increase the tensile strength of the quenched steel and improve hardenability by retarding austenite decomposition and bainite transformation [10, 14, 21].

The structure of the as-delivered 22MnB5 steel consists of a mixture of about 75 % ferrite and 25 % pearlite and has a moderate strength of 600 MPa and a high ductility of about 25 % [3, 13, 14, 20]. During forming of full austenitic steel at high temperature, the strength of approximately 200 MPa and the ductility of about 40 % make large plastic deformation possible [3]. After press-hardening of the blanks in the press tools, steel parts have an ultra-high strength of approximately 1500 MPa and a relatively low elongation at fracture of about 6 %, characteristic of a fully martensitic microstructure [11]. A good dimensional accuracy of the body parts is obtained, as springback is effectively suppressed due to the phase transformation from austenite to martensite during simultaneous forming and quenching of

the parts within the dies [2, 9]. The main mechanical properties of the 22MnB5 steel prior to and post to hot stamping are summarized in Table 2.

Table 2: Mechanical properties of as-delivered and hot stamped 22MnB5 steel [2, 20, 22].

	22MnB5 As-delivered	**22MnB5 Hot stamped**
Tensile strength UTS (MPa)	500-700	1300-1600
Yield strength YS (MPa)	300-550	950-1250
Total elongation A_{80}	≥ 10	> 6

As presented in Figure 2, press-hardening of 22MnB5 components leads to a significant increase of the flow stress. During quenching, austenite (fcc) transforms into martensite (bct) (Figure 2 b)) [14].

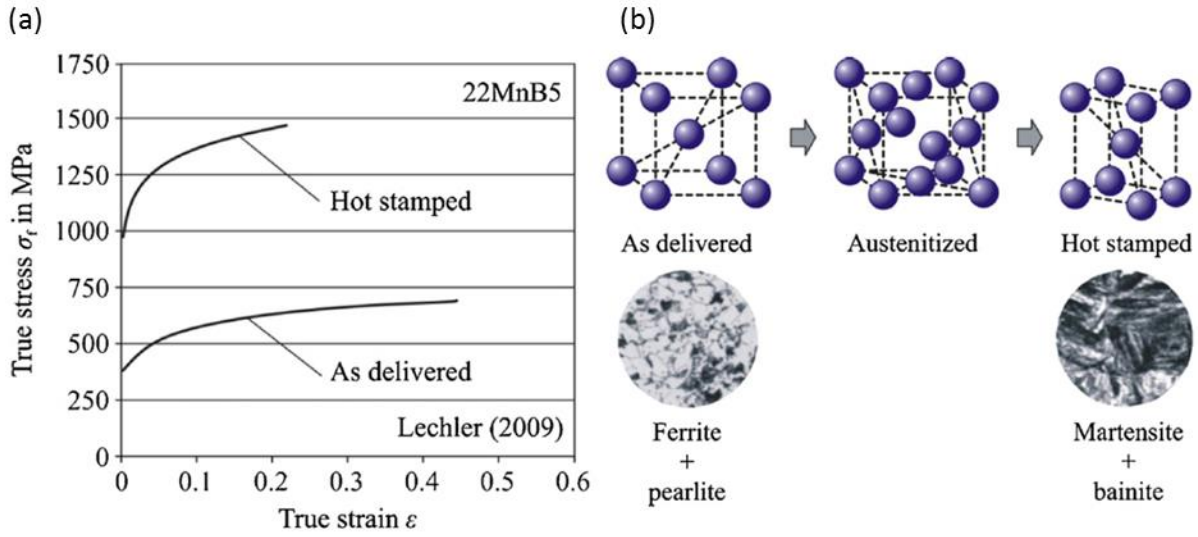

Figure 2: Flow curves of 22MnB5 steel prior to and post to hot stamping (a) and microstructure of 22MnB5 steel during hot stamping (b); from [14].

Austenite starts to decompose into martensite at a temperature of 410 °C corresponding to the martensite start temperature (M_s) and stops forming at 230 °C, temperature corresponding to the martensite finish temperature (M_f) for 22MnB5 steel [10, 23]. These values were found to vary in the literature [11, 21, 24-26], as the composition of steel and in particular carbon influences the martensitic formation temperature domain. Besides, the use of longer austenitization times during heat treatment [23] and the presence of plastic deformation during quenching lead to a reduction of the martensite start (M_s) temperature [13, 25].

In order to achieve the target mechanical properties of the final press-hardened components, it is important to take into account the cooling rate of the austenitized components. Fan et al. reported that ferrite and pearlite form when very low cooling rates of 2-5 °C/s are used [21]. At cooling rates of 10-16 °C/s, a mixed microstructure of ferrite and bainite forms, while at cooling rates of 20-25 °C/s, a fully bainitic microstructure is obtained

[13, 21]. Merklein and Lechler [27] reported that a critical cooling rate of 27 °C/s is required to complete a fully martensitic transformation in the press dies. As very high cooling rates up to 100 K/s are generally used during industrial hot forming, the bainite formation cannot take place, irrespective of the strain rate [28].

The Heat Transfer Coefficient (HTC) between press tool and workpiece was reported by Merklein et al. [29] to increase as a function of contact pressure, due to the increase in the effective contact surface area, as confirmed by Brosius et al. [30]. A low temperature of the press tools was stated to increase the cooling rate due to a higher temperature difference between tools and workpiece [31]. Quenching of the parts is mainly conducted by the use of cooling ducts in the forming tools with fluid coolant such as water. Moreover, the coating system was found to have a significant influence on the heat exchange during quenching and on the tribological properties in the frictional relevant areas. A decreasing friction coefficient was observed with increasing sheet temperature [29, 32].

1.3 Direct and indirect hot stamping processes

Two methods are established in the manufacturing of hot formed components for the automotive application, namely the direct and the indirect processes. Both methods are presented in Figure 3.

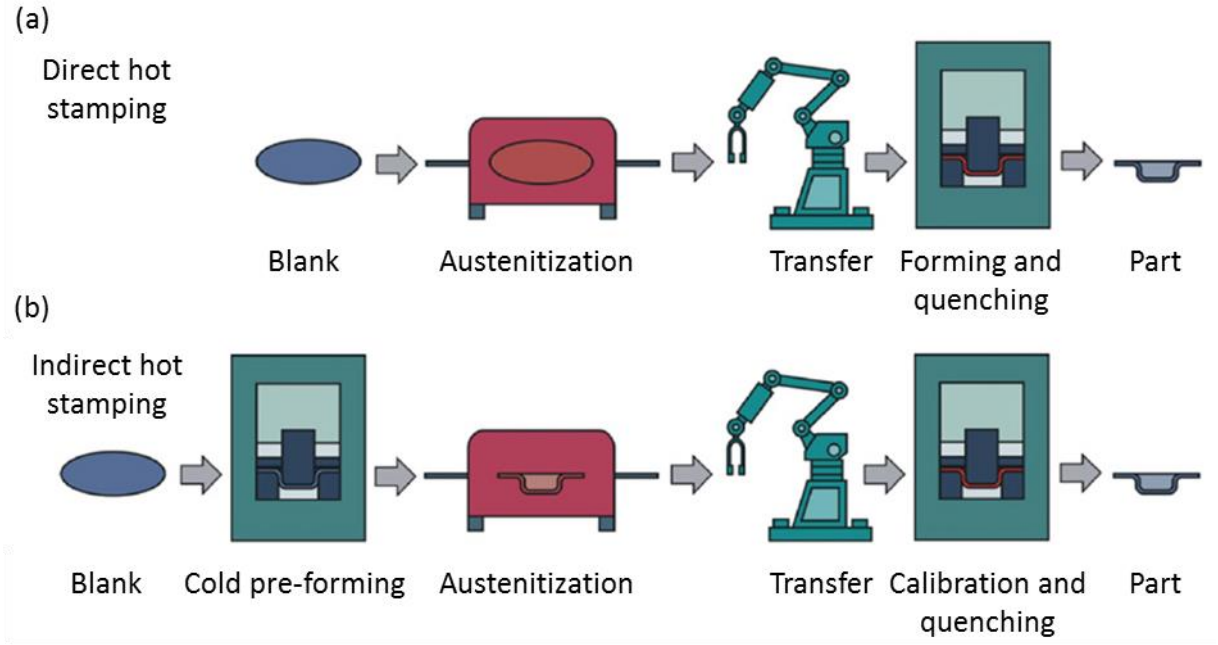

Figure 3: Schematic of direct (a) and indirect (b) hot stamping processes; from [14].

In direct hot stamping, coiled 22MnB5 material is cut out into blanks and inserted into a furnace at 900 to 950 °C to austenitize the steel substrate [3]. After a certain heating duration, blanks are transferred to press tools, hot formed and quenched in a single stroke in press tools with internally water-cooled dies in order to increase heat transfer and accelerate quenching. This means that only one press unit is required to manufacture UHSS parts by direct hot stamping.

Indirect hot stamping process involves an additional forming step at room temperature with conventionnal cold drawing press tools [10, 11]. The pre-formed blanks are then heated for austenitization in a continuous feed-furnace and finally transferred to the second press unit. This last step permits to form a martensitic structure by quenching of the austenitized parts and to calibrate the final shape of the components.

A schematic of the process stages and relevant parameters during press-hardening is presented in Figure 4.

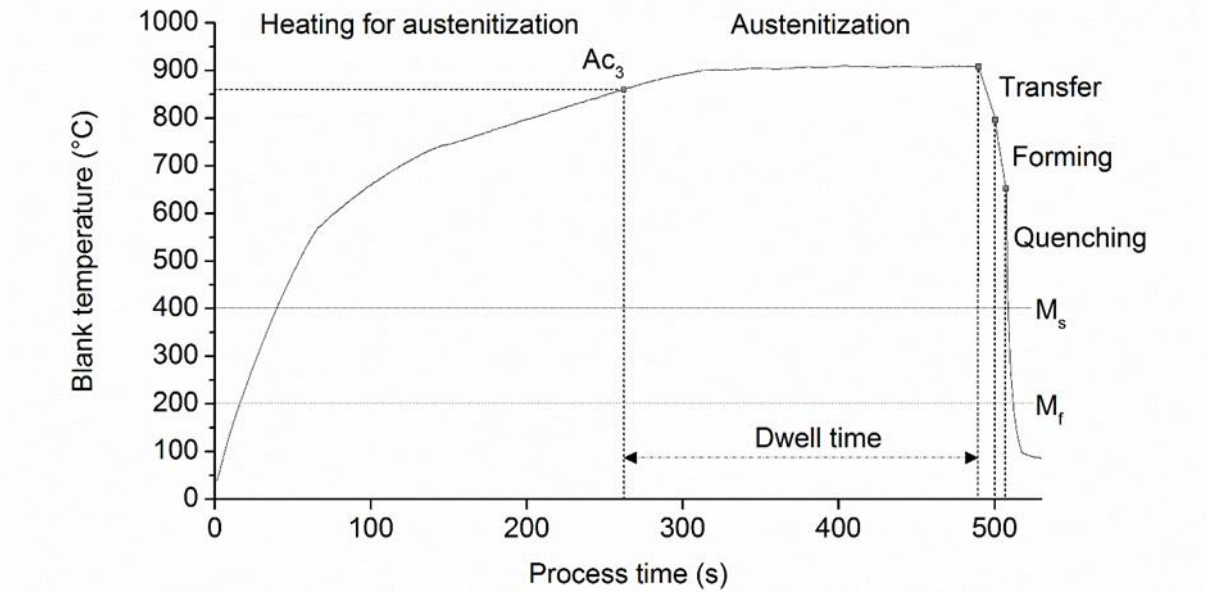

Figure 4: Schematic of the press-hardening process of hot formed body components with relevant parameters.

Hot stamped components are generally heated by radiation and convective flow of heat in continuous furnaces [10]. The heating procedure has a great influence on the properties of the parts and the process efficiency. The achievement of homogeneous blank temperatures, along with short heating times to reduce processing time for hot stamping is of high interest in the manufacturing process of automotive parts. The use of alternative heating technologies with shorter cycle times such as induction or conduction heating was reported in several works [5, 14, 33, 34]. The energy efficiency of induction heating was found to be up to two times higher than conventional heating process.

A temperature of at least 850 °C was stated to be required to form a full austenite structure in 22MnB5 steel, which corresponds to the Ac_3 temperature [29, 32]. Kuepferle et al. reported a temperature range of 830-890 °C [26], while a value of 825 °C was reported by Karbasian et al. [35]. The blanks are then kept at a temperature above the austenitizing temperature for a duration called dwell time, comprised between 3 and 10 minutes [3]. This annealing time is defined with regard to the material gauge, the coating used, the hot stamping line and the process window required [35]. Transfer of heated blanks to press tools generally takes 3-8 s [13, 36, 37] and should be kept as low as possible in order to carry out forming at temperatures higher than the martensite start temperature (Figure 4) [14]. As a consequence, the forming process generally occurs in the temperature range 650-850 °C [2].

Cooling should proceed with closed dies until the temperature of the parts drops below 200 °C [8, 35]. Hardening of the parts in the tools requires approximately 10 s [13]. The completion of the transfer, stamping and the cooling steps during the direct hot stamping is evaluated between 15 to 25 seconds [10].

As forming and quenching take place in separate press tools during indirect hot stamping, several consecutive cold forming operations can be carried out in order to achieve very complex shapes, contrarily to direct hot stamping which involves a unique forming step at high temperature [10]. Moreover, an important extent of the cutting of the parts, in particular for holes and edges, can be carried out on non-hardened materials prior to press-hardening. This characteristic permits to reduce the use of costly trimming techniques such as lasers or coated mechanical tools and to optimize maintenance costs [38]. However, indirect hot stamping involves higher costs due to the use of an additionnal forming unit for room temperature deformation compared to direct hot stamping [8].

Bare 22MnB5 press-hardened steels were initially used for UHSS components in the automotive bodies. However, the use of bare components induces challenges in terms of manufacturability due to the formation of an oxide scale on the surface of the parts and a decarburization of steel during austenitizing treatment prior to hot stamping [3, 39, 40]. Higher temperatures and heating times lead to an increase in the friction coefficient for 22MnB5 steel due to the increase of the amount of oxides generated during heat treatment [10]. In fact, limitation of scale formation is preferable for protecting dies from scale accumulation and abrasive wear, since the hardness of the oxide layer is up to a factor of 5 higher than that of 22MnB5 steel [41]. Therefore, a removal of the oxide scale, for instance by abrasive blasting, is necessary. The main method for reducing the amount of oxides is to use a controlled furnace atmosphere [7, 39]. This method may induce higher costs due to the use of inert gas and cannot completely avoid oxidation, since transfer, forming and cooling of the sheet metal are carried out under ambient atmosphere. A further approach for avoiding or at least reducing high temperature oxidation of steel is to use oxidation preventive oil during heat treatment [42]. However, the most important issue of the use of bare steel for the hot stamping application is the absence of corrosion protection, which implies an extended use of secondary protection measures in order to ensure good performance to the final products, as discussed in Section 1.4.

In order to increase performance and processability of hot stamped components, Original Equipment Manufacturers (OEMs) have investigated and developed various protective metallic coatings. The development and the approval of alternative coating materials for this application implicate a complex profile on required functionalities, ranging from good anticorrosive performance, excellent formability to good compatibility with subsequent manufacturing processes such as painting or joining.

The use of either the indirect or the direct hot stamping processes partly depends on the complexity of the parts geometries, for which one or several forming steps are required. Besides, the behavior of coating materials during cold and hot forming plays an essential role in the selection of the manufacturing routes of hot stamped components.

Two coating products are mainly used in the automotive industry for press-hardened components, namely the galvanized and aluminized coatings. Direct hot stamping is currently used for manufacturing aluminized components, since the aluminized layer provides good formability at high temperature and prevents the base material from oxidizing during heat treatment. The parts can then be directly painted without surface treatment. Indirect hot stamping is used for manufaturing galvanized parts, since the Zn coating is not suitable for hot forming due to cracking induced by Liquid Metal Embrittlement (LME). Scaling of the galvanized coating occurs during heat treatment, a costly surface cleaning treatment is required for ensuring good subsequent painting and joining processes [43]. More information regarding the behavior and properties of current coatings during hot stamping will be reported in Section 1.5.

In the framework of this thesis, the investigation of the forming behavior of alternative coating systems will be based on the direct hot stamping process, since this manufacturing route is the most common method compared to indirect hot stamping.

1.4 Challenges in corrosion protection of press-hardened steel parts

This part is dedicated to the corrosion mechanisms involved in automotive bodies and to the evaluation criteria of anticorrosive performance of hot formed components for a better understanding of the behavior of the various coating systems and to define the requirements of the alternative coating products studied in the present work.

1.4.1 Corrosion of car bodies

According to the work of Lefèvre, corrosion mechanisms of car bodies can be classified into five categories: generalized corrosion, galvanic corrosion, perforating corrosion, cosmetic corrosion and pitting corrosion [44].

Generalized corrosion can be observed for non-painted parts undergoing high temperature stages such as exhaust pipes or engines and is characterized by uniform corrosion mechanisms and the absence of galvanic coupling.

Galvanic corrosion occurs when metals with different electrochemical behaviors are brought into contact. The less noble metal, that is to say the one with the lowest electrochemical potential, acts as an anode and is oxidized. This mechanism is considered as an advantage if steel structures are coated with a material with a lower electrochemical potential than that of iron, such as zinc. In that case, the coating acts as a sacrificial material and protects steel from corrosion. In the literature data, this property is defined as protection by sacrificial anode or sacrificial protection. It appears that this corrosion mechanism is also called cathodic corrosion protection. In this work, both terms will be alternatively used. In the case of coatings providing no or low cathodic protection, corrosion occurs on the coating and the base substrate simultaneously.

Perforating corrosion, or crevice corrosion, is the most critical corrosion phenomenon on vehicles, as it can lead to the perforation of body parts, thereby affecting the functional properties of the vehicles. This mechanism is usually observed in cavities or in areas with stagnant solution or salted electrolytes, which creates a differential aeration cell, as presented in Figure 5. Car bodies contain a multitude of box sections and joints which can lead to crevice corrosion if an unsufficient run-off takes place [45]. Corrosion starts on an interior surface of a part, penetrates the sheet and is eventually visible at the exterior surface [46].

Due to the confinement of the electrolyte in the crevice, the input of oxygen into the crevice is blocked and a galvanic coupling between rich and poor O_2 regions takes place. The accumulation of cations is compensated by the input of chloride anions, leading to the formation of metallic chlorides according to the following reaction:

$$M^{n+} + Cl^- + n\ H_2O \longrightarrow MOH_n + Cl^- + n\ H^+$$

The local decrease in pH causes an acceleration of the metal dissolution and the reaction is autocatalytic [8].

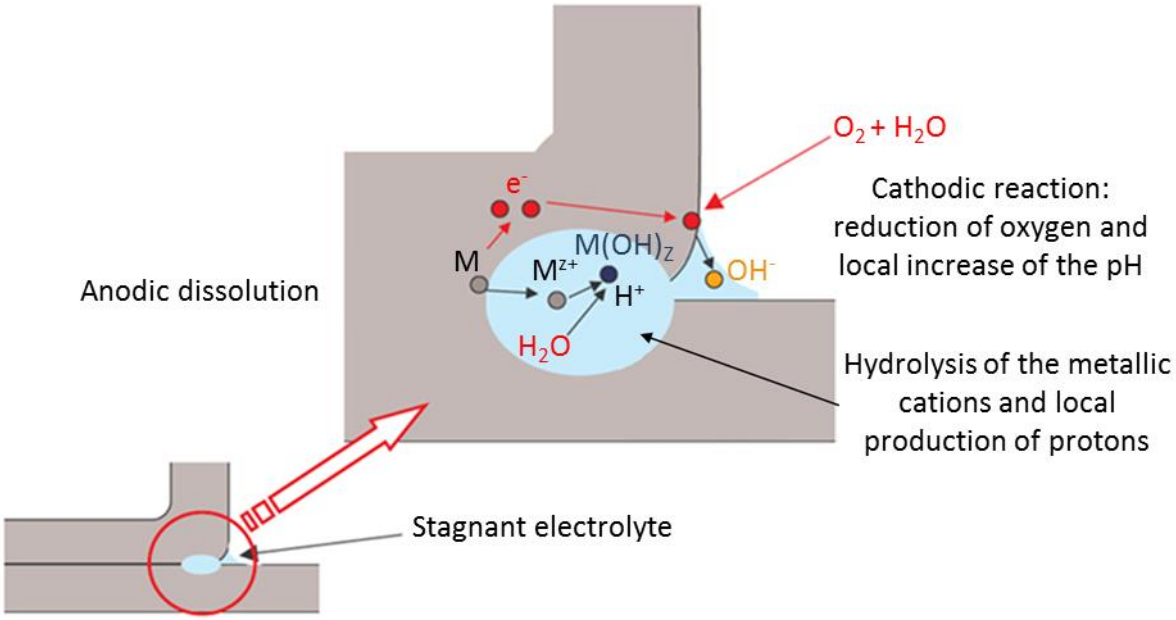

Figure 5: Schematic of the corrosion mechanisms occurring in the event of crevice corrosion; from [44].

Pitting corrosion is a localized attack, usually caused by the presence of chlorides and can be considered similar to perforating corrosion. This corrosion type is a self-initiating form of crevice corrosion in which corrosion generates a pit or a crevice and propagates until eventually perforating the metal. This phenomenon takes place on heterogeneous areas of metals, breaks in protective films, defects or imperfections [45].

Cosmetic corrosion depicts a corrosive attack on exterior surfaces where the paint film is damaged [46] and is generally induced by insufficient thickness of the coating systems, or by the local damage of the protective layers, such as stone chipping or cracks [43]. The behavior

of steel parts coated with a zinc or zinc-alloy layer and painted in the event of cosmetic corrosion is shown in Figure 6.

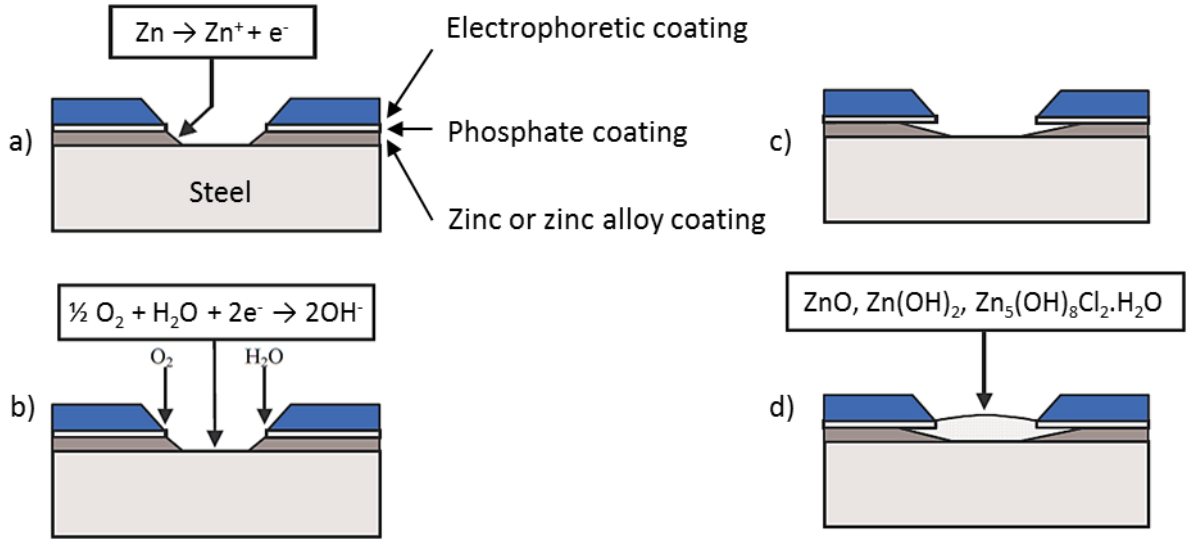

Figure 6: Schematic of corrosion mechanisms of Zn-coated and painted steel in the event of cosmetic corrosion: dissolution of Zn (a), formation of hydroxide anions (b), cathodic delamination of paints (c) and precipitation of corrosion products (d); from [44].

Due to the direct contact of steel with the corrosive environment on a damaged area, a corrosion current is induced on the surface of the coated product. The first corrosion mechanism is the preferential dissolution of the zinc coating (Figure 6 a)), while electrons are heading towards cathodic sites, namely the steel substrate. Due to the cathodic reaction of oxygen occurring on the base material, hydroxide anions are formed (Figure 6 b)). In the case of very humid media, such as those used in cyclic corrosion tests, a cathodic delamination of the paints can appear and cause the enlargement of the scribe, as shown in Figure 6 c). Zinc corrosion products, which composition depends on the corrosive environment, form and precipitate in the damaged area. Red rust eventually appears when a sufficient amount of Zn corroded, as the scribe width and thereby the bare surface increase [44]. In the case of a bare steel part or steel coated with a layer providing no cathodic protection, the anodic area is located on the surface of both substrate and coating materials, while the cathodic area is located on the phosphate conversion layer. This implies that the oxidation reaction at the steel substrate is not hindered and can lead to perforation of the base material [8].

The protective effect of coating systems is generally refered to a passive corrosion protection for which corrosion mechanisms are prevented by the passivation of the materials or by the use of secondary measures, or to an active corrosion protection when a sacrifical effect is provided by the less noble metal such as a Zn-containing layer [8].

The above-mentioned corrosion mechanisms do not fully depict the behavior of coated Press-Hardened Steel (PHS) parts, as they present different layers and compositions due to heat treatment prior to press-hardening. More information about the performance of the current coated products is presented in the following part.

1.4.2 Corrosion protection of hot formed components

Corrosion protection of hot formed steel parts involves more challenges than cold formed parts, due to the austenitizing treatment required for increasing mechanical properties of the components. In fact, chemical diffusion takes place at high temperature and leads to a modification of the composition of the coating, in particular to a diffusion of iron into the protective layer. The relatively high amounts of iron in the coating surface result in a decrease of anticorrosion performance of the products and in the formation of red rust in the event of corrosion. Therefore, a strong dependency of the heating parameters such as temperature, dwell time and heating rate during manufacturing process of the components was observed on the anticorrosive performance, in particular for Zn-based coatings [37]. In the case of hot formed components, the appearance of red rust in corrosive media does not reveal any degradation of the functions of the base material, but only indicates the presence of iron in the outer surface of the product [47-49]. However, the formation of red rust depreciates the visual quality of the product and should be avoided [43].

Several secondary protection measures are used in the automotive industry in order to ensure high anticorrosive performance of hot formed components. Electrophoretic Coating (E-Coat) is the most widespread solution to protect vehicles from corrosion [43]. Various E-Coat thicknesses are required for automotive BIW, depending on the location of the components and their exposure to aggressive media. A standard thickness of 18-29 µm was stated to be required for PHS parts at Daimler AG and varies due to the complex geometries of the bodies. Moreover, seam sealing process is used on parts or assemblies in the BIW in order to increase corrosion resistance. Body parts located in the floor area, such as side or rear rails, are generally protected from stone chipping with covers, under-floor protections or PVC seams. Finally, the injection of wax in cavities in critical assembly areas permits to avoid stagnancy of corrosive media and to reduce risks of crevice corrosion. It should be noted that hot formed components are generally protected by only one paint layer, namely the E-Coat, since they are not implemented in visible areas of the vehicles [43].

1.4.3 Assessment criteria and anticorrosion performance of current coatings for hot formed components

Cyclic corrosion tests

With the aim of simulating the behavior of materials over the lifespan of the vehicles, various accelerated corrosion tests were developed and reported in the literature, such as salt spray tests and cyclic corrosion tests. LeBozec et al. [50] studied various accelerated corrosion tests in the automotive industry in order to define the particularity of each test and the performance of steel and zinc-coated materials. The authors stated that continuous neutral salt spray tests with 5 wt.% NaCl like the DIN EN ISO 9227 test should not be used for the prediction of durability of steel-based materials. In fact, tests carried out under continual wetness provide results different than those experienced on field vehicles, for which

intervals of dryness are present [45]. As laboratory tests do not depict the same conditions as the real-world conditions, they should be used only for fundamental understanding [51].

Cyclic corrosion tests such as the VDA 621-415 proposed by the German association Verband Der Automobilindustrie (VDA) were developed to define a standard assessment method for german OEMs with a greater similarity to the behavior observed on automotive components. The test conditions of the latter were redefined in 2013 with the development of the new VDA 233-102 [43]. In addition to standard tests, car manufacturers developed their internal competences and facilities to establish internal rules for qualifying new construction features, materials or assembly concepts [43]. Moreover, field surveys or monitor car tests permit to estimate the lifespan of the vehicles and gather knowledge about the worldwide aggressive environments [52].

Corrosion testing

Cosmetic corrosion is generally investigated by applying a scribe down to the base material after electrophoretic deposition. After appropriate exposure to a corrosive medium such as a cyclic corrosion test in horizontal or vertical position, blisters and red rust form on each side of the scribe [43]. The scribes are generally 1 mm wide and 100 mm long and are applied by carbide cutters or by a laser technique. In the case of mechanical scribing, the operation is carried out several times in order to reach the base material. The scribe creepback, that is to say the delamination of the protective coating on each side of the scribe, can be measured by an optical method or by visual inspection. The mean and the maximum scribe creepback are generally measured.

Perforating corrosion is generally investigated by carrying out corrosion tests on non-painted panels. During the corrosion test, the surface of the samples is observed regularly to spot the apparition of red rust. Corrosion products are then removed from the surface by chemical dissolution. Surface cartography of the corrosion attack can be performed to determine the attack depth [43]. A further possibility for evaluating the perforating corrosion is to measure the scribe depth by cross section or by laser triangulation, as reported in the work of Dosdat et al. [37].

Investigation of the behavior of coating products on cut-edges is generally carried out on painted panels with a cyclic corrosion test. The size and distribution of the blisters formed on edges are assessed by visual tests, cross-sections or linear measurements.

Sacrificial corrosion protection of Zn-coated steel parts is generally investigated by means of galvanostatic dissolution [47, 53-55]. The difference in the electrochemical potentials between coating and substrate materials can be ascertained with this method. Moreover, significant information regarding the distribution of the Zn-Fe interdiffusion layers formed during heat treatment and their relative proportion in the coating can be evaluated. More information about this method will be reported in the next part.

Anticorrosive performance of commercial coating products

In this part, the anticorrosive properties of both main coating products, namely galvanized and aluminized coatings are reviewed according to the above-mentioned assessment criteria. More information regarding the properties of the latter coatings is presented in Section 1.5.

Dosdat et al. [37] reported that GI coatings are significantly more resistant to cosmetic corrosion than aluminized samples and therefore present a lower scribe delamination, as confirmed by Allély et al. [48]. Both coatings present equivalent mass losses and attack depths on non-painted panels [37]. A similar behavior in perforating corrosion in scribe lines was reported for aluminized and galvanized products [37, 48]. The protection of GI coatings against cut-edge creepback was reported by Dosdat et al. [37] to be much higher than for aluminized parts. This result can be explained by the sacrificial effect of the zinc-based layer.

Cathodic corrosion protection of aluminized parts was reported by Allély et al. [56] to be very low due to the difference of less than 50 mV between the potentials of the aluminized coating and steel after hot stamping. The Al-Si layer can therefore not be considered as a sacrificial coating [53]. The electrochemical potentials of the diffusion layers formed during hot stamping (Section) were stated to differ, mostly due to the variation of the Al content in the layers, but remain at a potential similar than that of steel [48, 57, 58]. However, the latter can be considered as an active coating due to the formation of corrosion products with a low dissolution rate. As stated in the works of Allély et al. [48, 56], in the case of damages of the protective layers such as scribes or cracks during a VDA 233-102 cyclic corrosion test, Al-Si and exposed steel corrode simultaneously, forming Al, Si and Fe corrosion products which precipitate in the form of hydroxides and aluminosilicates. These corrosion products fill the cavities and cause a barrier effect on the diffusion of oxygen toward steel surface and reduce corrosion mechanisms.

As mentioned previously, galvanized coatings provide sacrificial protection to steel. Figure 7 presents the influence of the hot stamping process on the electrochemical potential of galvanized steel, and thus the sacrificial effect of the Zn layer for steel.

As shown in Figure 7 and reported in the works of Luckeneder et al. [54] and Autengruber et al. [47], the duration for anodic coating dissolution post to press-hardening is two times higher than for the as-deposited coating, mainly because of the increased coating thickness [59]. Moreover, several potential stages appear during anodic dissolution and can be related to the presence of phase with different compositions, namely a zinc-rich and an iron-rich intermetallic phases. These phases will be discussed in detail later.

The first stage is the dissolution of the zinc-rich Γ_1-phase with a potential of approximately -0.55 V vs. SHE. After a certain time depending on the composition of the coating, a second dissolution stage with a potential about 200 mV lower than that of steel occurs and corresponds to the α-Fe(Zn) phase. The overshooting potential between both phases is not explained [59].

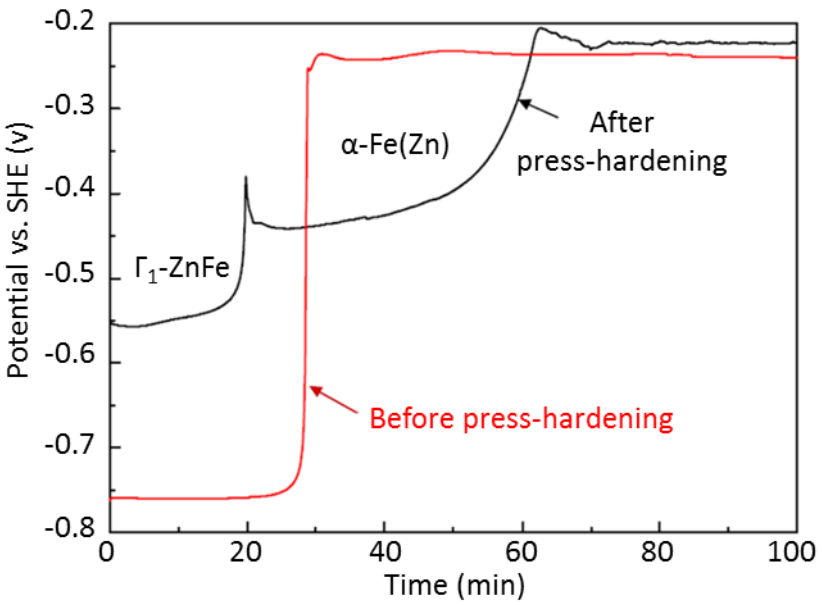

Figure 7: Evolution of the electrochemical potential of a galvanized coating prior to (red line) and post to hot forming (black line) by means of galvanostatic dissolution; Electrolyte: 100 g l^{-1} $ZnSO_4 \cdot 7H_2O$ + 200 g l^{-1} NaCl; T = 35 °C; aerated; i = 11.76 mA cm^{-2}; Potential vs. SHE; from [54].

As observed in Figure 7, both Γ_1- and α-phases provide cathodic protection to steel substrate, with a more pronounced effect for the Γ_1-phase due to its lower electrochemical potential [59]. Fleischanderl et al. [60] reported that the Zn content in the galvanized coating should be high enough to provide adequate cathodic protection of the base material. Indeed, the α-Fe(Zn) layer should have a Zn content in the range of 17-44 wt.% to obtain a sufficient sacrificial effect. The zinc-rich intermetallic layer should contain 70-95 wt.% Zn. After dissolution of both Zn-Fe phases, the potential reaches that of steel. It should be noted that presented potential values and dissolution times can differ in the case of different heat treatment conditions and coating thicknesses. In fact, as reported earlier, the Γ_1-phase can disappear during heat treatment and thereby reduce cathodic protection of steel substrate. In order to ensure sufficient cathodic corrosion protection of steel parts, stable manufacturing processes are required for the deposition of layers with reproducible composition, thickness and properties, as well as for the hot stamping of parts with identical heat treatment conditions such as heating rate, heating temperature and time or transfer duration.

Recent discussions between car manufacturers and steelmakers have revealed challenges in achieving acceptable process windows for manufacturing GI parts with regard to the dwell time along with sufficient sacrificial protection. A larger process window for hot stamping and better corrosion protection are obtained when thicker coatings are used [43].

To sum up, it appears that aluminized coatings provide comparable performance with regard to GI coatings in terms of perforation corrosion due to the formation of stable corrosion products. However, galvanized coatings provide lower scribe creepback and a higher protective effect on cut-edges. Moreover, a higher cosmetic corrosion protection is achieved

in the case of galvanized components compared to the Al-Si-coated product. The higher anticorrosive performance of the galvanized coating can be related to the Zn-containing layer, providing sacrificial corrosion protection to steel, contrary to the aluminized product. Therefore, the present work is based on the study of Zn-alloy coating with an anticorrosive behavior similar to that of the galvanized coating.

1.5 Current coating products for hot stamped body parts

The main challenge encountered by steelmakers in the development of coatings for hot stamping is, contrary to cold formed components, the high temperature treatment prior to forming. Due to chemical diffusion between substrate and coating materials, performance of the initial coating can be strongly affected.

Several target properties should be taken into account in the development of protective coatings for hot stamped parts. The coating materials should have a good behavior during heat treatment for press-hardening with a low exposure to oxidation and evaporation and limited diffusion of iron into the coating. Moreover, they should provide good suitability for forming processes, in particular for the cost-effective direct hot stamping method, with for instance a good adhesion to steel, limited oxide scale formation along with no adhesion with press tools, as well as no LME cracking. Moreover, high anticorrosive properties and good compatibility with subsequent painting and joining processes are required.

In the last decade, european car manufacturers have shown a high interest in two coated materials, namely aluminized and galvanized products, resulting in a wide use of both systems for BIW components. Besides these both coating systems, many further materials were investigated for this application. A summary of the state of the art about the performance of commercial and development coating systems is presented in the following part. A particular attention will be given to the galvanized coating, as the present work is dedicated to the study of alternative Zn-based coatings.

1.5.1 Galvanized coatings

Introduction and initial properties

Galvanized (GI) coatings are widely used on cold rolled sheet steel products due to their effective cathodic corrosion protection and adequate formability [3]. The first use of this coating system for the hot stamping application was reported by Fleischanderl et al. [53]. This 15-µm coating generally contains 0.2 wt.% Al and is deposited by continuous hot-dip galvanizing with a bath temperature comprised between 400 °C and 495 °C [53]. The addition of Al was reported to form a thin $Fe_2Al_{5-x}Zn_x$ phase at the interface between liquid zinc and steel during hot-dipping, inhibiting the formation of brittle Fe-Zn intermetallic phases and thereby improving the coating formability during deformation at room temperature. Moreover, the use of Al permits to form a superficial protective layer mainly consisting of Al_2O_3 during heat treatment, protecting the underlying zinc-containing coating from oxidation and evaporation at high temperature [3, 61].

Figure 8 shows cross-sectional micrographs of an as-deposited hot-dip galvanized coating. The coating consists of two Zn-Fe alloys, namely the ζ-phase with a Fe content of about 5 wt.%, the η-phase with a Fe content of at most 0.03 wt.%, as well as the above-mentioned $Fe_2Al_{5-x}Zn_x$ inhibition layer [3, 62].

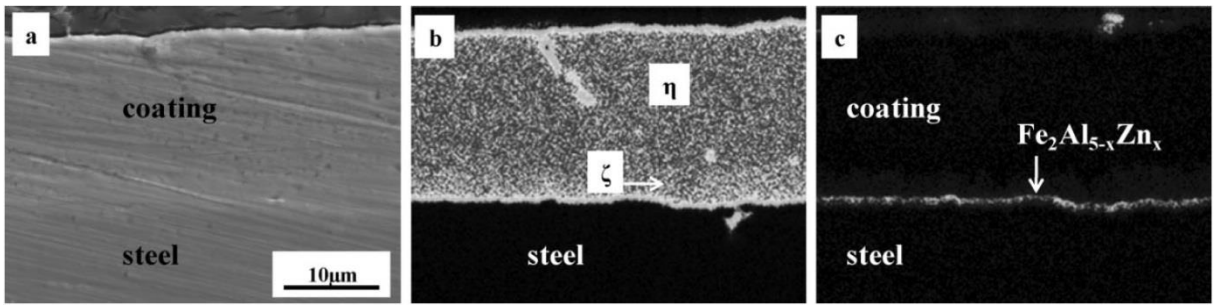

Figure 8: Cross-sectional SEM micrographs of an as-produced GI coating: microstructure (a), Zn distribution with the ζ- and η-phases (b) and Al distribution with the $Fe_2Al_{5-x}Zn_x$ inhibition layer (c) obtained by Wavelength Dispersive Spectroscopy (WDS) [3].

High temperature evolution

The thickness of the coating was stated by Faderl et al. [38] to increase from 15 µm to 20-35 µm after hot stamping. Diffusion of Fe into the Zn coating takes place, in particular for high temperatures and heating times and induces a change of the initial coating composition by forming interdiffusion and oxide layers. The amount of Zn decreases gradually towards the coating/steel interface [3].

The cross-sectional micrographs of a galvanized steel sheet after heat treatment at 900 °C in air for 4 min is presented in Figure 9.

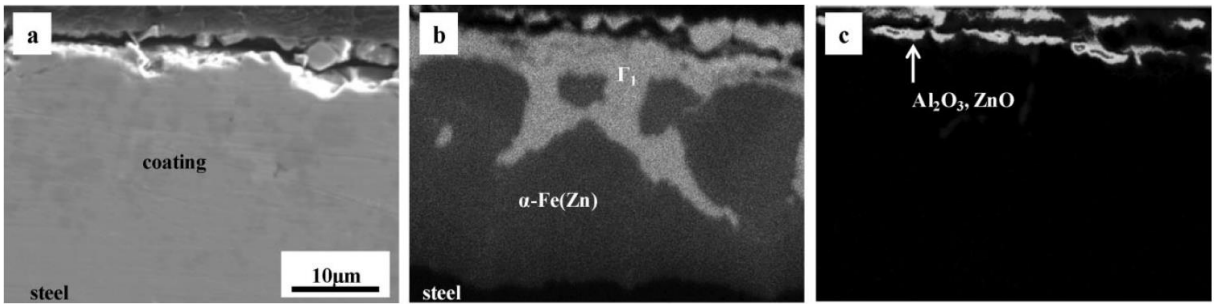

Figure 9: Cross-sectional SEM micrographs of a GI coating after heating at 900 °C in air for 4 min: microstructure (a), Zn distribution (b) and Al distribution (c) obtained by WDS [3].

Fan et al. reported that the heat treated coating consists of an oxide layer, a zinc-rich Fe-Zn intermetallic layer, and a layer of α-Fe with Zn in solid solution. Autengruber et al. [59] stated that the oxide layer is mainly composed of an upper layer of ZnO and a lower layer of Al_2O_3. Further oxides from the steel alloying elements, such as B, Cr and Mn were also observed [59, 63]. Zn oxides are increasingly added to the 200-nm-thick Al oxide layer for temperatures above 700 °C, in particular for high temperatures and heating times [51, 64, 65].

The lower part of the coating consists of the α-Fe phase with at most 35 wt.% Zn in solid solution. The Fe-Zn intermetallic layer located below the oxide scale was identified as the zinc-rich Γ_1-phase containing about 26 wt.% Fe and formed with the peritectic reaction at 782 °C from liquid Zn and solid α-Fe phase (Figure 10) [62]. Due to the progressive diffusion of iron from the substrate steel to the coating during heat treatment, this phase was found to be gradually consumed by the underlying α-Fe phase [3].

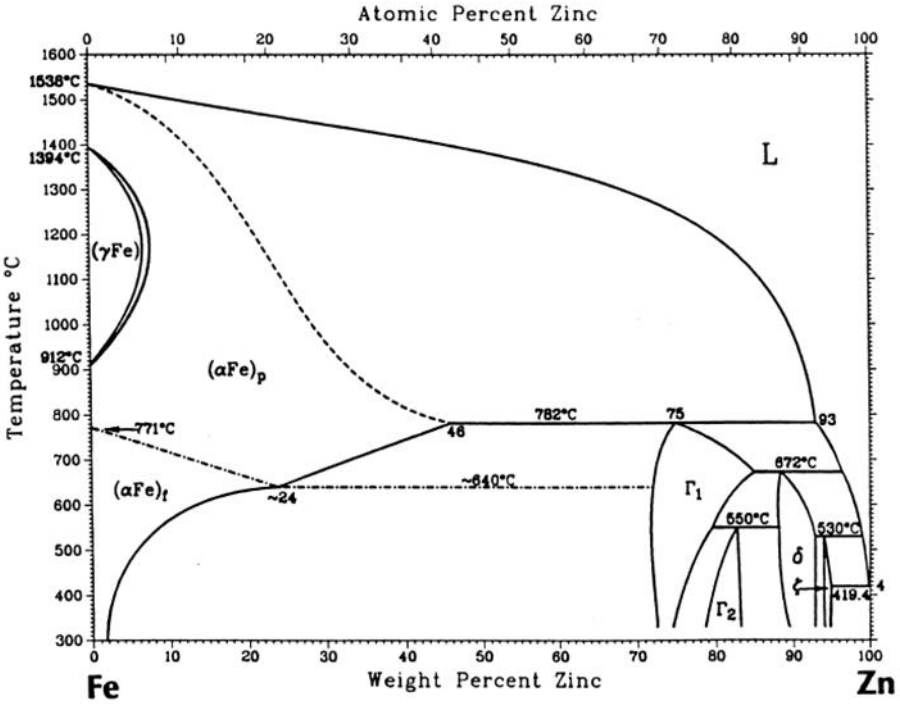

Figure 10: Fe-Zn binary phase diagram [62].

Further intermetallic phases may form, depending on the Fe content in the top of the coating. The Γ_2, δ and ζ phases form when the layer contains a low amount of Fe. The iron content in the coating after hot stamping mainly depends on the initial coating thickness, the initial Fe, Al and Zn contents as well as on the heating conditions [3].

Many researchers highlighted a significant dependency of the coating composition on the corrosion resistance of the hot stamped GI steels. Particularly, the Fe content of the layers induces changes in the electrochemical potential of the heat treated coating, and affects sacrificial corrosion protection, as discussed in Section 1.4.3.

Autengruber et al. [59] investigated the formation of intermetallic phases at various temperatures during the austenitization process of GI steels. Fe diffusion started at 500 °C and formed an interdiffusion layer containing 10 wt.% Fe at the interface steel/coating. A temperature of 550 °C led to the formation of a single δ-Zn-Fe phase in the coating with 11 wt.% Fe. A continuous conversion from δ-Zn-Fe to Γ_1-Zn-Fe phase takes place between 600 °C and 700 °C. At 750 °C, a Zn-saturated α-Fe with 72 wt.% Fe forms at the steel/coating interface. Further heating of the specimens resulted in more conversion of α-Fe with Zn in solution [59]. At temperatures above 782 °C, a solid-liquid reaction with the growth of the α-Fe solid solution at the expense of liquid Zn occurs. During cooling below 782 °C, the liquid

Zn and a part of the α-Fe phase transform to the Γ_1-phase, while the α-Fe is stabilized to room temperature. Although the α-Fe phase has a low solubility for Zn at lower temperatures, a single layer of α-Fe with a high Zn content is observed at room temperature. This can be explained by the fast cooling carried out during press-hardening, preventing the decomposition of the α-Fe with a high Zn content [3].

Zn has a low boiling point of 908 °C in standard atmosphere [66]. In an inert Ar atmosphere, Zn was found to evaporate at temperatures above 600 °C, leading to a coating mostly composed of a α-Fe solid solution [3]. In addition, the rate of evaporation of Zn in Argon at 1 atm pressure was reported to increase slowly at lower temperatures and rapidly at higher temperatures of up to 850 °C [67]. Moreover, the ZnO layer formed on the top surface of the coating due to the residual O_2 content in the heating furnace at 600 °C was found to sublimate at higher temperatures, forming gaseous Zn metal vapor and oxygen. The loss of Zn during heating in a protective atmosphere can therefore be explained by the combination of Zn evaporation and ZnO sublimation [3]. It is therefore necessary to carry out heat treatment in an oxidizing atmosphere, as reported by Fleischanderl et al. [53]. Further surface defects such as zinc blisters or burn-offs were reported by Singh et al. to be caused by the manual handling of the blanks, the presence of contaminants on the blanks and on the furnace rollers, or by too high temperatures and heating times in the furnace equipments in presence of a protective atmosphere [51].

Liquid Metal Embrittlement (LME) of Zn-based coatings

The terms macrocracks and microcracks are used in the literature and describe respectively the appearance of LME mechanisms and the formation of cracks due to mechanical issues such as friction between steel and die [66, 68, 69]. Genderen et al. reported that the tribological aspects have to be taken into consideration while studying LME mechanisms, since the most sensitive areas for microcrack formation were those with the most intense tool contact, indicating that Zn embrittlement is not the only cause of crack formation [70]. Hensen et al. [71] reported a significant decrease in microcrack depth by the use of lubrication during direct hot stamping due to the reduction of the shear stresses on the surface materials, as confirmed by Drillet et al. [68]. Janik et al. [69] proposed that cracks formed across the α-Fe(Zn)/austenite interface of parts during hot forming can also be induced by microstructural defects such as oxides, inclusions or pre-existing cracks in α-Fe(Zn). Drillet et al. [68] reported that microcracks initiate in the coating and propagate inside steel in a very thin ferrite (and/or bainite) layer located below the coating. The authors proposed that this interface layer forms due to a too low cooling speed along with a high level of deformation, or due to decarburization prior to hot-dip coating.

Mechanisms of LME

Since most Fe-Zn intermetallic phases, exempt from the α-Fe phase with Zn in solid solution, have a melting point much below the furnace temperatures used during heat treatment for hot stamping, some liquid phases may be present in the coating during forming. The critical temperature-composition range for the formation of LME is presented in Figure 11 a). In this

case, liquid Zn penetrates the austenite grain boundaries during high temperature deformation and causes a weakening and a decohesion of those grain boundaries [71]. This results in the formation of cracks in the coating and in the base material. This phenomenon is commonly called Liquid Metal Embrittlement (LME). The presence of cracks in the steel substrate may lead to challenges in functional properties of the final products, in particular in corrosion protection, crash safety and structural durability.

Fan et al. [3] stated that LME is generally observed between two metals with a low mutual solubility which do not form intermetallic compounds during heat treatment. As shown in Figure 10, the solubility of Zn is very low in γ-Fe while the α–phase provides a high solubility of Zn. However, both phases were reported to be sensitive to Zn embrittlement. The grain boundaries in α-Fe(Zn) appear to be already wetted by liquid Zn before the application of tensile loading stresses [9]. The cracks were stated to initiate at the solid α-Fe(Zn)/liquid zinc interface of the coating and to propagate along the austenite grain boundaries under the action of surface tensile stresses [72].

Besides, the LME mechanisms are presumably caused by the adsorption-induced weakening of interatomic bonds at the tip of cracks, facilitating decohesion of the grain boundaries [3]. Hensen et al. [71] reported that cracks form when a concentration of stress exceeds the maximum strain capacity of the material. No valid explanation could be made for a possible increase of stresses in the case of the GI product compared to other materials free from cracks. However, the presence of zinc in the fractured surface of a hot formed GI part was found to be responsible for the lowering of the strain capacity of the Zn-coated steel and for the appearance of cracks.

Figure 11 b) shows the SEM-EDS micrograph of a cross section of a GI steel part after direct hot stamping, with the identification of the corresponding phases.

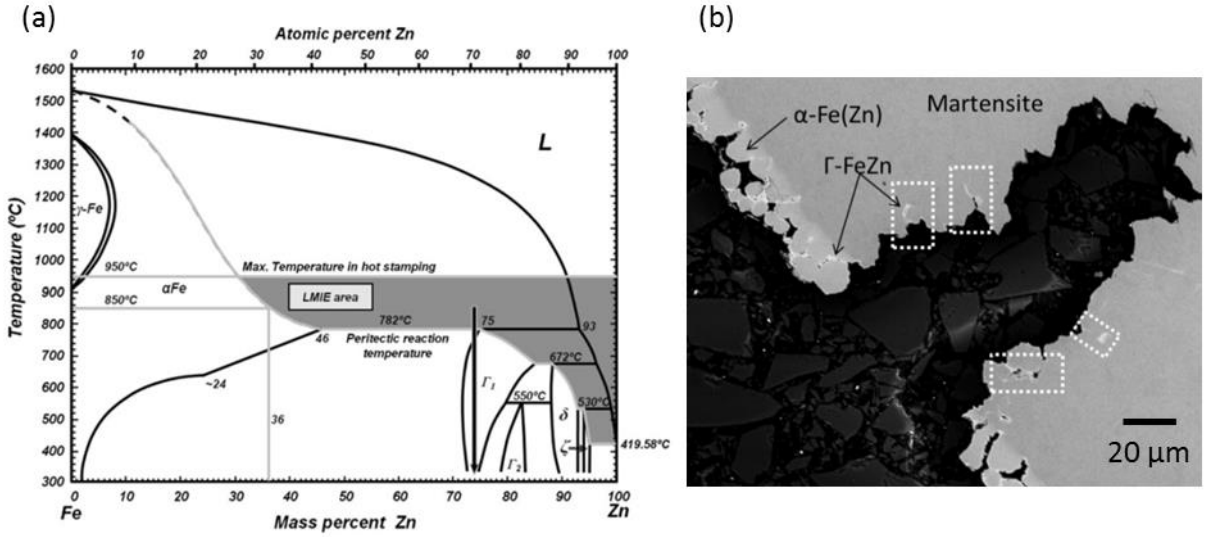

Figure 11: Binary Fe-Zn phase diagram with the temperature-composition range (in gray) in which LME is likely to occur during direct hot forming (a) [9] and back-scattered (BSE) cross-sectional SEM-micrograph of a crack formed during direct hot stamping of galvanized steel (b) [43].

The diffusion of the zinc-rich Γ-phase into the steel substrate can be observed in the brighter areas in the coating as well as along the crack formed in the base material, which is a typical mechanism of LME.

From the literature data, it can be considered that cracks with a depth of at most 10 µm in the base material are acceptable and do presumably not influence the functional properties of the body components [71]. However, the amount and the depth of cracks can be barely predicted, since many factors such as initial coating characteristics, heating parameters, process stability or parts geometries may influence LME formation.

Prevention of LME

The LME mechanisms were reported by Genderen et al. [70] to depend on three factors, namely the stress level, the mechanical susceptibility of the sustrate material and the presence of liquid phases during hot forming. All three factors must be present to cause LME. The removal of at least one factor was stated by the same authors to prevent the appearance of LME during direct hot stamping. Moreover, cracks caused by LME can be prevented by a suitable choice of coating composition, coating thickness and process parameters [71].

Several approaches were proposed in the literature to avoid or at least to reduce LME during direct hot stamping of GI steels [3]. The main approach is the use of the indirect hot stamping for manufacturing GI components. This method permits to avoid simultaneous presence of mechanical stresses and liquid metal in the coating by carrying out forming and heat treatment processes separately. Since most of the deformation is completed before heating, no LME takes place during hot press forming [9].

A second possibility for avoiding LME is to carry out an additional heat treatment on GI coatings in order to activate chemical diffusion between coating and substrate materials. An iron content of at least 70 wt.% pemits to avoid LME during hot press forming [73]. The formation of α-Fe(Zn) is thereby more readily achieved compared to conventional GI coatings, along with the reduced amount of liquid phases [9]. This approach resulted in the development of the so-called galvannealed (GA) coating, which will be discussed in Appendix 1.

Furthermore, extended dwell times during heat treatment of GI coatings could reduce the amount of liquid Zn during forming. A reduction in the depth of microcracks by the use of extended dwell times was reported in the literature [9, 71]. However, a reduction of productivity can be expected due to the extended heating time.

In a similar way, the use of thinner Zn layers was reported to cause a reduction of the micro- and macrocrack depth on hot formed parts [71] since the time for converting the Zn coating to a full α-Fe(Zn) layer during heat treatment can be significantly reduced [3]. However, a narrower process window during heat treatment prior to hot stamping can be expected for ensuring sufficient corrosion protection.

An alternative manufacturing route consists in reducing the forming temperature below the peritectic transformation temperature of 782 °C by increasing transfer time in order to reduce or avoid the presence of liquid phases during forming step, since liquid Zn transforms to solid Γ_1-phase below this temperature [3]. Li et al. reported the formation of cracks with depths of more than 100 µm for a forming temperature range of 830-778 °C [72]. At a forming temperature of 700-732 °C, the cracks could not be completely avoided but their depth was significantly reduced. According to Lee et al. [9], this approach may cause a considerable reduction of the strength of the hot formed components, since a transformation of the austenite to ferrite and bainite could take place. Moreover, a rupture of the brittle Γ_1-phase was reported by Fan et al. to occur [3].

A further approach consists in avoiding the presence of liquid phases during high temperature forming by increasing melting temperature of the coating, in particular by alloying Zn with adequate elements. This approach was used by several researchers for the development of alternative coating systems and will be the central point of the current work, as Zn-Mn alloy coatings will be deposited and characterized for the direct hot stamping application.

Processability of galvanized steel and parts

Galvanized parts are industrially manufactured with the indirect hot stamping process, which allows manufacturing components with complex geometries, since several consecutive forming steps at low temperature can be carried out in order to obtain the target geometries. However, an increase of the manufacturing costs of GI coated parts is induced by the additional press tools required for the cold pre-forming steps prior to press-hardening stage of the process as well as by the appropriate heating and transfer equipments for processing individual pre-formed parts [8]. In addition, the presence of liquid phases during hot stamping was reported to cause the adhesion of Zn to press dies, which can increase the maintenance costs of the production lines [3].

As stated in the previous section, GI steel parts are hot stamped in an oxidizing atmosphere, inducing the formation of a poorly adhering oxide scale on top of the coating [64]. This particularity was found to positively reduce Zn loss during heating. However, an increase of the electrical contact resistance for Resistance Spot Welding (RSW) was reported to occur in presence of oxides, affecting manufacturability of the hot stamped components [3, 51]. In addition, a zinc oxide layer with a thickness higher than 2 µm was stated to have a negative effect on the E-coat adherence and thereby on the corrosion resistance of the painted products [74]. Therefore, a surface treatment should be carried out after hot stamping by abrasive blasting with steel or glass granulate, corundum or dry ice, in order to remove the oxide scale [75]. The Fe-Zn coating was found to be not affected by this cleaning method [64], although a possible loss of zinc-rich phases could occur. It is important to note that surface post-treatment increases manufacturing costs, notably due to the cleaning equipment and the individual handling of formed parts.

Despite the higher production costs of GI coated parts compared to aluminized parts [68], the presence of cathodic protection provided by the zinc-containing layer increases performance of body components in corrosive environments. A particular attention should be given to the control of the process parameters during heat treatment, since anticorrosive properties are sensitive to process parameters [43].

Galvanized manganese-boron steels were first used in 2008 for hot stamped vehicle components [8] and are commercially available under the trade names PHS-Ultraform (Voestalpine GmbH) or USIBOR GI (ArcelorMittal S.A.).

1.5.2 Aluminized coatings

Introduction and initial properties

The aluminizing process is generally carried out by hot-dipping 22MnB5 steel into a molten Al alloy bath with a near-eutectic composition containing 88 wt.% Al, 9 wt.% Si and 3 wt.% Fe at a temperature of about 670 °C [3]. The purpose of the use of Si in the molten bath is to form a Fe_2SiAl_7 inhibition layer at the coating/substrate interface, which permits to prevent the rapid formation of a hard and brittle intermetallic Fe_2Al_5 phase onto the steel substrate during hot dipping and to obtain a flat coating/steel interface along with a multilayered microstructure [3, 76]. As shown in Figure 12 a), the coating consists of an Al-Si eutectic matrix separated by a 5-µm-thick Fe_2SiAl_7 inhibition layer. A thin layer of Fe_2Al_5 and $FeAl_3$ was also observed at the interface between the Fe_2SiAl_7 and steel [3].

High temperature evolution

The coating was reported to melt at approximately 580 °C [33, 39, 77]. An increase of the coating thickness from 25-30 µm to 35-45 µm occurs after heat treatment due to an enrichment of the layer with Fe by chemical diffusion, in particular at high temperatures and long dwell times [3, 37]. During heat treatment in air, a compact thin oxide layer consisting of Al_2O_3 forms on the surface of the coating [3]. The phase evolution of the Al-Si coating during heat treatment was found to vary in the literature, most probably due to the influence of the heating rate, heating time, temperature and initial coating thickness on the high temperature behavior of the coating. As illustrated in the cross-sectional Scanning Electron Microscopy (SEM) micrograph of the aluminized coating post to hot stamping presented in Figure 12 b), five layers are generally reported in the literature data [3, 48, 78].

According to Fan et al., the first layer located on the coating surface consists of the $FeAl_2$ phase, while several works identified it as the Fe_2Al_5 phase [3]. This difference may result from the gradual increase of Fe content in the coating during heat treatment. The second layer was identified as the τ_1-Fe_2SiAl_2 phase. The third layer consists of the same phases as those formed in the first layer, namely $FeAl_2$ or Fe_2Al_5, depending on the literature data. The fourth layer was reported to be similar to the second layer. Finally, the fifth layer located at the interface coating/substrate was found to have a gradually increasing Fe content toward the steel substrate and to consist of the Fe_3Al phase. A transition from layered to island-type

morphology of the diffusion layers formed during heat treatment was reported to occur, in particular in the case of high heating rates [3]. More comprehensive investigations of the phase formation of aluminized steels during heat treatment are reported in the works of Windmann et al. [76, 79].

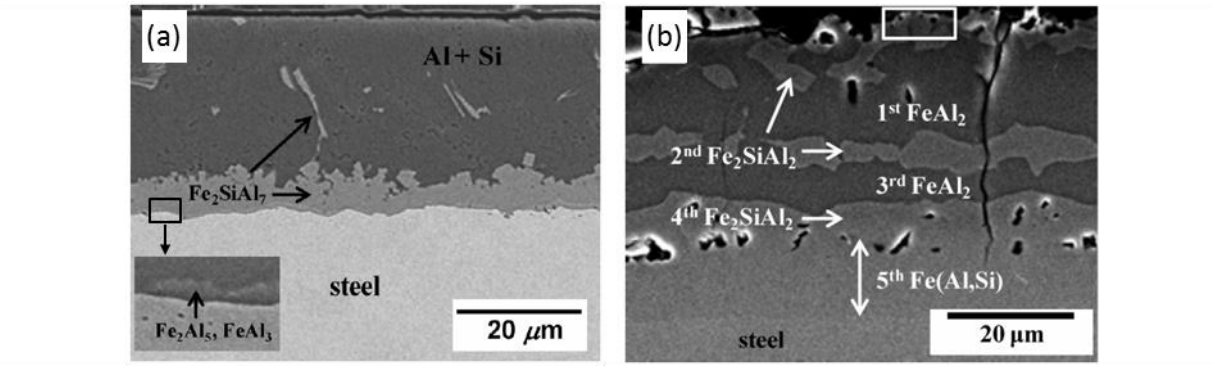

Figure 12: Cross-sectional SEM micrographs of an aluminized steel prior to (a) and post to heat treatment (b) at 930 °C for 5 min in air with a heating rate of 10 °C.s^{-1} in air; from [3].

As shown in Figure 12 b, voids can appear in the aluminized coating after hot stamping, namely below the oxide layer and in the interdiffusion layer. Their formation was found to be promoted as the heating time increases. Fan et al. [3] proposed that the voids formed below the oxide layer are formed due to atomic diffusion of Al atoms outwardly to form the surface oxide or inwardly to form the Fe-Al intermetallic phases, which could create vacancies in the coating. A further possible explanation is that Al atoms of the Fe-Al intermetallic phases can react with moisture and form H_2 gas and thereby induce the formation of voids [77]. Voids formed in the coating are most likely associated with a difference in the diffusivity of Fe or Al in the Fe_2SiAl_2 diffusion layers, which is commonly known as the Kirkendall effect [3, 58].

During heat treatment of aluminized steels, cracks are likely to form in the coating, even if no deformation occurs. The origin of these cracks was reported by Fan et al. to result from the thermal expansion coefficient of the brittle intermetallic phases and the steel substrate [3]. Moreover, the coating can break into segments during plastic deformation and a higher density of finer cracks is observed at higher strain rates [80, 81]. It is important to note that the cracks do not propagate beyond the diffusion layer [48, 56, 80]. In fact, the thermal expansion coefficient of the diffusion zone was found to be close to that of the substrate steel [77]. Moreover, this layer has a much lower hardness than the rest of the coating and the martensite steel substrate, which could explain why microcracks do not propagate [3]. The study of Zhong-Xiang et al. [81] stated that microcracks formed in the Al-Si coating may induce interfacial debonding of the coating in presence of stress concentration, as confirmed by Fan et al. [21]. It should be noted that the exposed bare steel areas within the cracks and defects can induce issues in terms of corrosion protection as steel corrodes [48, 79].

Processability of aluminized steel and parts

Aluminized steel parts are manufactured by direct hot stamping. Indirect hot stamping is problematic due to the lower forming limits of the Al-Si layer during cold deformation compared to the 22MnB5 base material [29]. A total coating thickness of 40 µm should not be exceeded to ensure a sufficient weldability of the components [14].

In order to improve paintability of body components and to increase electrophoretic coating adhesion, a chemical pre-treatment is generally carried out prior to painting by dipping the BIW into a zinc phosphate solution to form a phosphate conversion film on the surface [82]. A hydrogen bond is then created between the phosphate coating and the electrophoretic coating [57]. The phosphate coating does not form on the surface of hot formed aluminized steel because the oxide film inhibits the etching reaction by the phosphating solution [57, 83]. However, a good paint adhesion can be achieved by a sufficient roughness of the coating after hot forming. It should be mentioned that roughness and friction coefficient of the heat treated aluminized coating were found to increase as heating time and heating temperature increase [77, 78, 84]. It should be noted that liquid Al was reported by Fan et al. to adhere to the furnace rollers during hot stamping, which increases maintenance costs of the equipments [3].

The use of the aluminized coating for press-hardened body components was first patented in 2000 by ArcelorMittal [85]. The product is commercially available under the trade name of Usibor® 1500P (ArcelorMittal) or MBW 1500 (ThyssenKrupp) and will be further named Al-Si in the present work.

1.5.3 Further protective coating systems

In this part, the properties and performance of other protective coating systems based on Zn alloys are reviewed. Further products, such as multilayered and Al-based coatings are reported in Appendix 1. It should be noted that some of these products remained as development investigation tracks, or may be in use in the serial production of vehicles, but in a limited extend compared to galvanized and aluminized coatings.

Zn-Fe coatings

In order to improve suitability of the GI coating for direct hot forming, an additional heat treatment in the range of 480-520 °C, called galvannealing, can be carried out on the non-hardened galvanized product to pre-activate α-Fe(Zn) formation betweeen the steel substrate and the coating and to thereby reduce the amount of liquid phases in the coating [3]. Moreover, galvannealing permits to break down the Fe_2Al_5 inhibition layer and to form the aforementioned Al_2O_3 oxide scale prior to carrying out heat treatment for hot stamping. This results in a reduced heating time to eliminate liquid Zn by the growth of the α-Fe(Zn) phase [9]. The resulting Zn-Fe coated product is then processed with the conventional direct hot stamping method. These coatings are commonly known as galvannealed (GA) products and are commercially available under the names Usibor GA (ArcelorMittal) or PHS-Ultraform GA (Voestalpine) for direct and indirect hot stamping [68]. An additional galvannealed

product was recently commercialized for direct hot stamping of press-hardened parts with a 20MnB5 steel grade with an optimized manufacturing route to avoid the formation of micro- and macro-cracks [86]. Compared to the GI coating, a lower Al content of 0.13-0.14 wt.% is added to the molten Zn bath for deposition in order to facilitate the formation of Fe-Zn intermetallic phases during galvannealing and heat treatment prior to hot forming [3].

The oxide layer formed on GA components during heat treatment mainly consists of ZnO enriched by Cr and Mn [69]. However, contrary to GI hot stamped parts, no surface cleaning treatment was stated to be required for the GA coating, since a homogeneous phosphating and good paint adhesion can be achieved [40, 48, 68]. The spot weldability of GA steel parts was found to depend on the amount of oxides formed on the coating surface during heat treatment, inducing increased contact resistance, risks of splashing and electrode degradation. As a result, low temperature and dwell times improve weldability [70].

Cracking of galvannealed parts during direct hot stamping was reported by Schwinghammer et al. to depend on the heating time, the forming temperature and the initial coating thickness [55]. A strong reduction of the crack depth was observed for longer dwell times and for reduced coating thicknesses, caused by the reduction of the amount of liquid Zn during forming [55, 73].

Similarly to the GI coating, the process parameters used during galvannealing and heat treatment prior to hot forming have a significant influence on the corrosion protection behavior, as confirmed by Genderen et al. [70]. Dosdat et al. [37] reported a similar behavior for GI and GA coatings and better behavior than aluminized parts in terms of perforating, cosmetic and cut-edge corrosion. Allély et al. [48] stated that perforation corrosion protection of GA parts decreases with the severity of the austenitizing heat treatment. Schwinghammer et al. reported higher protective behavior in terms of flange corrosion, cosmetic corrosion and cathodic protection for increased initial thickness of the GA coating and lower dwell times.

Zn-Ni coatings

The aim of the alloying of Zinc with Nickel is to increase the melting temperature of the layer and thereby reduce or suppress the probability of the presence of liquid phases which may diffuse into steel grain boundaries and generate LME. The electrodeposited 10.6-µm-thick Zn-Ni coating contains 11 wt.% Ni and 0.6 wt.% Fe and is composed of a uniform intermetallic γ-Ni_5Zn_{21} phase. It should be noted that this alloy is metastable since the γ-phase was reported to form for Ni contents of at most 14 wt.% in equilibrium state [3]. A melting point of 881 °C was reported by Köyer et al. for the corresponding alloy [87]. The thickness of the coating increases to 20-25 µm after hot stamping [8]. The phase evolution and the microstructure of electrodeposited Zn-Ni coatings during heat treatment were reported in the work of Kondratiuk et al. [88]. After heat treatment, an α-ferrite with Zn and Ni in solid solution forms at the interface substrate/coating, while a Ni-rich γ-$Zn_xNi_yFe_z$ forms on the upper part of the coating. The amount of the latter phase was found to decrease in favor of α-Fe with Zn and Ni in solid solution when extended heating times were used [89].

An oxide layer containing zinc oxide as well as manganese oxide diffusing from the steel substrate formed on the surface of the heat treated coating [88, 90]. No nickel oxides were observed. A thicker oxide layer was formed compared to galvanized coatings, reportedly due to the absence of an initial alumina layer preventing oxidation kinetics [88]. A removal of the oxide scale was stated by Köyer et al. to be facultative, although an improvement in the subsequent processes can be achieved [87]. A good compatibility of the layers with painting, adhesive bonding and welding processes was achieved after hot forming. The hot forming behavior of Zn-Ni was investigated by Kondratiuk et al. and showed a lower friction coefficient than Al-Si-coated blanks [91]. Zn-Ni-coated products were reported to be suitable for both direct and indirect hot stamping, partly due to the high melting point of the alloy. Moreover, a potential difference of 300 mV between the coating and steel substrate was obtained after heat treatment at 880 °C for 5 min. A higher corrosion resistance for Zn-Ni coatings than GI and GA coatings was reported by Fan et al. [3] during cyclic corrosion tests. Moreover, the heating time was stated to have no significant effect on corrosion resistance [3, 49]. Direct hot formed GA and Zn-Ni coated components were reported by Reini et al. to be used in the GM group in passenger vehicles for the first time [92]. The Zn-Ni-coated product was available under the trade name GammaProtect® (ThyssenKrupp Steel Europe) for hot stamped body parts and its production was stopped for patent-related reasons and due to work safety issues related to the use of carcinogenic Ni [93, 94].

1.5.4 Performance of commercial coatings for the hot stamping application

According to the information from the literature data regarding the properties of current coating products for the hot stamping application presented in the last sections, it appears that limits are encountered by all coating materials in terms of hot formability, corrosion protection or subsequent processing, thereby implying a compromise in the performance during the selection of the most appropriate materials for the manufacturing of components. The characteristic challenges and advantages of the main current coatings are summarized in Table 3.

It is clear that the main motivations in the development of optimal coating products are the achievement of good anticorrosive performance, in particular of sacrifical protection, and of good hot formability with the suppression of the susceptibility of the coating materials to LME. As stated earlier, only two commercial products, namely aluminized and galvanized steels have found the interest of OEMs for a wide-scale manufacturing of hot formed components. Both products will be considered as state-of-the-art coatings in the framework of the definition of alternative promising materials and of the study of the performance of new Zn-Mn coating materials compared to commercial products.

Table 3: Advantages and challenges implied by current coating products for hot forming of automotive steel parts; from [3].

	Advantages	Challenges
Aluminized coating	- Good barrier corrosion resistance - No need for phosphating - No surface treatment required	- Coating brittleness - Liquid Al adhesion - No cathodic corrosion protection
Galvanized coating	- Cathodic corrosion resistance	- LME - Oxides removal - Brittleness of coating
Galvannealed coating	- Reduction / avoidance of LME - Cathodic corrosion resistance	- Brittleness of coating - High Fe content
Zn-Ni alloy coating	- No LME - Cathodic corrosion resistance	- Higher costs - Health concerns
Aluminide coating	- Good formability - Good barrier corrosion resistance	- Liquid Al adhesion - No cathodic corrosion protection
Hybrid coating	- Cathodic corrosion resistance	- Formation of brittle Fe-Al intermetallics - Higher costs

The next section will be dedicated to the definition of potential promising alternative coating materials and to the review of their properties with regard to the requirements for the hot forming application.

1.6 Alternative coating systems for press-hardened parts

This part is focused on the definition of alternative coating systems for hot stamping applications with a potential increase of the performance of current products in terms of anticorrosive and hot forming properties. On the basis of the comprehensive literature research reported in the last section, several single and multi layer coating systems were considered to provide interesting properties and are presented in Section 1.6.1. Zn-Mn alloy coatings were selected as the most promising investigation track, due to higher anticorrosive properties and higher melting point compared to pure Zn layers. The target properties and performance of the corresponding deposits are reported in Section 1.6.2. Finally, Section 1.6.3 concerns the deposition of Zn-Mn alloys, in particular by electroplating.

1.6.1 Identification of promising alternative coatings

Two main concepts have been identified in the literature for protective coating for automotive press-hardened parts, in accordance with the coating systems reported in Section 1.5. The first system involves the use of single layer coatings, mostly based on organic or zinc alloy coatings. The second concept involves the use of multilayer coatings in order to combine functional properties of different materials, in particular by using additional protective layers onto current coated products to improve their performance. On the basis of both concepts, various alternative coating systems with promising properties

have been proposed in the framework of this study and resulted in patent applications. The various systems are summarized in Table 4.

Coating systems presented in Table 4 a) are based on the use of various Zn alloy layers with presumed advanced properties compared to standard galvanized products. On the basis of high-temperature phase diagrams found in the literature data, the use of Zn alloys such as Zn-Mn and Zn-Co is likely to increase the melting temperature of the coating and thereby to reduce or avoid the susceptibility to LME during direct hot stamping, as reported in Section 1.5.1. In fact, melting temperatures of 567 °C and 740 °C can be obtained with the use of 1 wt.% Co and 23 wt.% Mn respectively, compared to a melting temperature of about 420 °C for pure Zn. In addition, higher anticorrosive properties may be achieved by the use of Zn alloys compared to pure Zn layers, depending on the alloying element [95, 96]. In the case of Zn-Co alloy coatings, more stable corrosion products were found to form compared to pure Zn coatings, which permits to increase anticorrosive performance [97, 98]. However, metallic Co has an electrochemical potential (-0.28 V/SHE) higher than that of both Fe and Zn metals (-0.44 V/SHE and -0.76 V/SHE, respectively), which means that the cathodic corrosion protection of steel is likely to decrease by the use of Co as alloying element for Zn compared to pure Zn coatings. On the other hand, higher anticorrosive properties were reported in the case of Zn-Mn alloy coatings due to the combination of stable corrosion products and to the increase of sacrifical protection of steel due to the lower electrochemical potential of Mn (-1.18 V/SHE) compared to that of Zn and Fe. On the basis of these results, it appears that Zn-Mn coatings show the most promising anticorrosive properties compared to Zn-Co alloys, along with the possibility to increase the melting temperature of the coating compared to pure Zn deposits. Therefore, the present work will be dedicated to the study of single-layer Zn-Mn alloy coatings. The properties of this coating system will be reported in detail in the following part (Section 1.6.2).

The use of an intermediate Zn alloy layer such as Zn-Mn, Zn-Co or Zn-Mn-Co between a pure Zn layer and steel may permit to reduce or avoid the formation of cracks due to LME during direct hot stamping due to the increased melting temperature of the Zn alloy layer compared to pure Zn. The presence of Zn-based coatings most probably provides good anticorrosive protection to steel, in particular cathodic protection. It can be assumed that the use of an additional protective layer above the Zn-based layers and consisting for instance of oxides possibly permits to reduce or avoid evaporation and oxidation mechanisms of the underlying materials, in particular of Zn. The reduction of these effects may be beneficial for ensuring sufficient sacrificial corrosion protection and good compatibility with subsequent processes such as joining and painting [99].

Multilayer coatings presented in Table 4 b) consist of metallic Mn or Zn alloy layers such as Zn-Mn or Zn-Co alloys separated from the base material with an intermediary layer. The use of the latter materials is expected to provide cathodic corrosion protection to steel. The intermediary layer can consist of an aluminized coating or a ceramic material and is likely to hamper interdiffusion processes between the Zn-based layers and steel, which would result

in the increase of the amount of remaining metallic Zn in the coatings after hot stamping, beneficial for sacrificial corrosion protection.

Table 4: Promising single and multi layer coating systems for hot formed automotive components identified in the framework of the present study.

(a)

Publication	DE102014004652		WO2015149918			DE102014004650		
Reference	[95]		[96]			[99]		
Third layer	-		-			Protective surface layer against oxidation, evaporation or passivation layer (facultative)		
Second layer	-		-			Zn		
First layer	ZnCo	ZnMn	ZnMn	ZnCo	ZnMnCo	ZnCo	ZnMn	Zn alloy
Substrate	Press-hardenable or deep-drawing steel							

(b)

Publication	DE102014004656				WO2015149901			DE102014004657		DE102014004651	
Reference	[100]				[101]			[102]		[103]	
Third layer	Protective surface layer against oxidation, evaporation or passivation layer (facultative)				-			-		Protective surface layer against oxidation, evaporation or passivation layer	
Second layer	Zn	Zn alloy	ZnCo	ZnMn	ZnCo	ZnMn	Mn	ZnCo	ZnMn	ZnCo	ZnMn
First layer	Protective layer against interdiffusion and LME				AlSi			AlSi		AlSi	
Substrate	Press-hardenable or deep-drawing steel										

(c)

Publication	DE102014004649			WO2015149900				
Reference	[104]			[105]				
Third layer	Protective surface layer against oxidation, evaporation or passivation layer (facultative)			Protective surface layer against oxidation, evaporation or passivation layer (facultative)				
Second layer	ZnCo	ZnMn	Zn alloy	ZnCo	ZnMn	Co	Mn	Zn alloy
First layer	Zn			Zn				
Substrate	Press-hardenable or deep-drawing steel							

In addition, by using an intermediary layer such as an aluminized coating between steel and Zn-based layers, it can be assumed that the penetration of liquid Zn-rich phases towards the steel substrate as well as the appearance of cracks related to LME (see Section 1.5.1) can be hindered or at least reduced [100-103]. This particularity may permit to obtain good suitability for direct hot stamping of the coated products.

It can be assumed that the use of an additional protective layer located above the metallic Mn and Zn alloy layer and consisting for instance of oxides possibly permits to reduce or avoid evaporation and oxidation mechanisms of the underlying materials [100, 103].

Multilayer coating systems presented in Table 4 c) consist of a pure Zn layer coated by a layer consisting of Zn alloys such as Zn-Co or Zn-Mn or of metallic Co or Mn [104, 105]. As mentioned earlier, the use of Zn alloys may permit to achieve higher corrosion protection than a single layer Zn coating and to increase the melting temperature of the coating, thereby reducing the susceptibility of coated steel to LME. The use of metallic Co or Mn aims for the formation of a chemical diffusion gradient with the underlying Zn layer during heat treatment, which may lead to a considerable increase of the melting point of the underlying coating, thereby reducing the amount of liquid phases during hot stamping responsible for LME. In a similar way to coating systems mentioned earlier, the use of an additional superficial layer consisting for instance of oxides may permit to reduce evaporation and oxidation mechanisms of the underlying materials during heat treatment.

1.6.2 Properties of alternative Zn-Mn alloy coatings

Motivation

The investigation of alternative Zn-based coating products with good suitability for direct hot stamping has been the focus of many researchers. As stated by Steinhoff et al., the improvement of material properties of galvanized press-hardened parts providing robust and reproducible direct hot stamping manufacturing processes as well as sufficient cathodic corrosion protection constitute a priority in the coating development [6]. The reduction or suppression of the LME phenomenon for galvanized coatings during direct hot stamping plays a major role in the achievement of good formability with the possibility, depending on the geometries of the parts, of using either the indirect or the direct hot stamping method. Moreover, the use of Zn-based coatings would provide cathodic protection of steel structures, implying reduced secondary protection measures along with lower production costs. As discussed in Section 1.5.1, several methods permit to avoid or at least to reduce the formation of LME during direct hot stamping of galvanized steel parts. The present work is based on the study of alternative Zn alloy coatings with advanced forming and anticorrosive properties than the current galvanized products. In the framework of the literature review about potential alternative Zn-based materials, Zinc-Manganese (Zn-Mn) alloys turned to provide a good compromise in terms of high temperature stability and corrosion protection.

High temperature properties

The alloying of Zn with Mn permits to obtain a significant increase of the melting temperature of the coating, as presented in the Zn-Mn equilibrium phase diagram in Figure 13. The susceptibility to LME during direct hot forming can thereby be reduced compared to a galvanized part since less or no liquid phases are present at high temperature during forming. Moreover, a reduction of chemical diffusion during heat treatment could be achieved due to the presence of a solid coating for a longer time until reaching the melting temperature of the alloy. This characteristic could reduce the formation of interdiffusion alloys with substrate steel and preserve anticorrosion properties of the coating.

As reported in the work of Okamoto et al. [106], 18 crystallographic phases were identified for Zn-Mn alloys. Many parts of the assessed diagram should be considered tentative or qualitative, in particular for the ε phase domain, due to disagreement in the literature data. No attempts were made to calculate the phase diagram thermodynamically [106]. As hot forming generally takes place at temperatures in the range 600-800 °C, liquid phases can be avoided during forming if the Mn content in the Zn-Mn coating is high enough. A Mn content of 29 wt.% would lead to a theoretical melting point of 800 °C of the alloy. The presence of liquid phases can be fully avoided during heat treatment at 900 °C if the Zn-Mn layer contains at least 40 wt.% Mn.

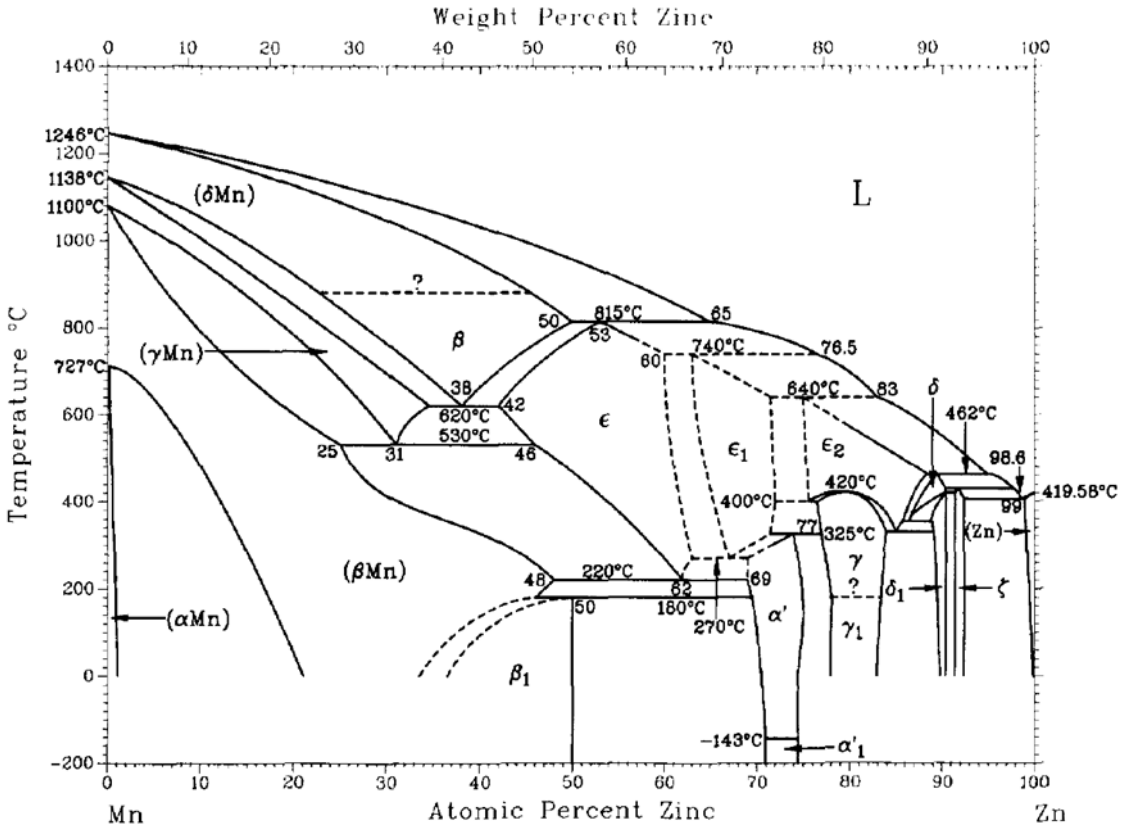

Figure 13: Assessed Mn-Zn equilibrium phase diagram [106].

Since only limited data was found in the literature about the high temperature stability of the Zn-Mn alloys, the present study constitute a novel investigation track. The work of Tsuchiya et al. [107] reported the change in the crystallographic structure of

electrodeposited Zn-Mn alloy coatings with various Mn contents during heating up to 300 °C. However, these results are not directly applicable to the present application, as the temperature is much below the required temperature for hot stamping.

In a similar way to the various coating systems reported in Section 1.5, chemical diffusion is likely to occur between coating and substrate materials, causing the formation of intermetallic phases, such as Zn-Mn-Fe ternary alloys. Very limited information was found in the literature data about phase diagrams of Zn-Mn-Fe alloys [108].

The scarce ternary diagrams found in the literature concern alloy phases formed at temperatures of 450 °C, 625 °C, 720 °C and 1000 °C [108-110]. The experimental Zn-Mn-Fe alloy phase diagram at 450 °C is shown in Appendix 3. The ε_2 Zn-Mn phase can be observed for Mn contents of about 10.2-24.9 wt.%. Moreover, it is interesting to see that this phase provides a very low solubility of Fe at 450 °C. From this observation, it appears that the ε_2 Zn-Mn phase should be preserved after high temperature treatment at 450 °C if no or very low atomic diffusion of Fe or change in the relative Zn and Mn contents occur. The experimental isothermal Zn-Mn-Fe diagrams at 625 °C and 720 °C (Appendix 3) were established on a narrow range of compositions, namely only for Fe-rich and Zn-rich regions.

Two methods were used for studying the different zones of the ternary diagrams [108]. The first method concerns the galvanizing of Fe and Fe-Mn samples before carrying out annealing at 450 °C for a few days. In the second method, Zn was deposited on Fe-Mn alloys from a vapor phase, which permitted to study the Zn poor areas of the ternary diagrams. In the present work, different experimental conditions were used, namely short heating times to mentioned temperatures followed by a quenching of the microstructural and crystallographic properties obtained at high temperatures, which means that the Zn-Mn-Fe phases may not be thermodynamically stable. Moreover, no direct comparison can be made between experimental results and literature data, since different temperatures were reported in the literature compared to the present work. Furthermore, only some areas of the diagrams were studied at high temperature. All these particularities induce challenges in the comprehension of the phase transformations occurring at high temperature.

It is important to note that oxidation of the coating materials can take place at high temperature, inducing changes in the initial coating composition and a loss of a part of the coating. According to the Ellingham diagram presented in Appendix 4, the standard free energy (Gibbs energy) required for the formation of MnO oxide is lower than that for the formation of ZnO, regardless of the temperature considered. This observation indicates that in presence of an oxidizing atmosphere, a preferential oxidation of Mn into MnO takes place compared to Zn, due to its higher oxygen affinity. On the basis of these results, it appears that the use of Zn-Mn coatings for high temperature applications may induce issues due to oxidation, as a loss of Mn is likely to occur during heat treatment. A decrease of the Mn content in the coating may reduce the melting temperature of the alloy and increase the susceptibility to LME appearance during direct hot stamping. In order to avoid or at least to reduce oxidation of the coating materials, upcoming investigations will be carried out in a furnace under a protective atmosphere, namely Argon gas.

A recent work of Baumgart and Sanders [111] reported the behavior of Zn-Mn coatings after heat treatment in an oxidizing atmosphere for the hot stamping application. A Mn-rich oxide layer was observed at the surface of the coating, which could require a surface treatment for providing good compatibility for subsequent joining and painting processes. Moreover, the authors reported the presence of two metallic layers in the coating, namely a Zn-Fe alloy at the coating/steel interface and a Zn-based layer with a low Mn content, presumably due to preferential oxidation of Mn during heat treatment. In a similar way, Zoestbergen et al. stated that after annealing of Zn-Mn alloy coatings with a thickness of 3 µm at 900 °C for 6 minutes in a nitrogen-containing atmosphere, a FeZn layer and a Mn-oxide scale were observed in the coatings, while during annealing in air, all Zn and Mn were found to oxidize [112]. However, very limited information was provided in both last works about the microstructural, crystallographic and forming properties of the as-deposited and heat treated coatings.

In a similar way to the use of Al in galvanized coatings (Section 1.5.1), the alloying of Zn with an element with high affinity to oxygen such as Mn may permit to form an oxide layer on the surface of the heat treated coating and reduce the loss of Zn by oxidation or evaporation and thereby increase the amount of metallic Zn in the coating beneficial for corrosion protection [113].

Anticorrosive properties

Zn-Mn coating were reported to provide higher corrosion protection than pure Zn coatings. By using Manganese, sacrificial corrosion protection can be increased since Mn^{2+}/Mn couple has a lower electrochemical potential (-1.18 V) than both Zn^{2+}/Zn and Fe^{2+}/Fe couples (-0.76 V and -0.44 V respectively). The presence of $Zn_5(OH)_8Cl_2.H_2O$ (ZHC) corrosion products in chloride corrosive medium on electrodeposited Zn-Mn coatings was reported by Ortiz et al. [114]. Boshkov et al. [115, 116] observed the formation of ZHC in similar conditions and explained the role of Mn in its formation. Since Mn is electrically more negative than Zn, it dissolves first as Mn^{2+} ions, causing evolution of hydrogen and consequently a slight increase of the pH value. After the total dissolution of Mn from the surface layer of the coating, the dissolution process continues with the dissolution of Zn. Because of the higher pH value in the near-surface region, Zn^{2+} ions react immediately with the medium and form zinc hydroxide chloride. Manganese oxides and zinc hydroxide sulfates (ZHS) such as $Zn_4(OH)_6SO_4.4H_2O$ were formed in the case of Zn-Mn coatings studied in a sulfate containing medium [117]. These corrosion products were found to promote the formation of a compact and stable passivation layer with a low rate of dissolution, increasing the protective capacity of the layer [115-117]. Moreover, the corrosion products inhibit the activity for the cathodic oxygen reduction, increasing the anticorrosive properties of Zn-Mn coatings [118]. Thus, the use of Zn-Mn coatings provides a double-protective action by forming an insoluble protective oxide surface on the coating, combined with the anodic protection of steel provided by zinc and manganese [97, 116, 119, 120]. This observation resulted in the lowest corrosion rate and the lowest passivation current value for Zn-Mn coatings among the other electroplated layers.

1.6.3 Deposition process of Zn-Mn coatings

Deposition technique

Zn-Mn coatings were reported to be deposited by means of hot-dip galvanizing or electroplating. Hot-dipping of Zn-Mn coatings with a Mn content of up to 0.1 wt.% was reported by Bakthiari [121]. Zhang et al. studied the effect of small additions of 0.4 wt.% of Mn on the corrosion behavior of Zn coatings [122]. However, no higher Mn content was reported in the literature. This can be related to the fact that hot-dipping of Zn-Mn coatings induces challenges due to the high melting point of the alloy when high Mn contents are used. In fact, high energy costs can be expected by the use of high temperature molten baths. Moreover, an annealing effect could be induced on the steel substrate during deposition process, modifying the mechanical properties of the parts. In order to avoid or at least reduce the susceptibility of the coated products to LME mechanisms, a melting point of at least 800 °C should be obtained, which means that the temperature of the molten bath should be even higher for allowing deposition.

The main deposition process for Zn-Mn coatings found in the literature is electroplating. Compared to the hot-dipping process, electroplating reduces the costs related to the amount of raw materials required, since an electrolyte with dissolved cations is used. Moreover, good energy efficiency is achieved, as deposition takes place at room temperature. The adjustment of various plating parameters such as deposition potential or current, chemical composition of the electrolyte or the configuration of the plating cell require comprehensive studies in order to obtain sufficient knowledge about the electrochemical systems and the associated reduction mechanisms. Different aqueous media, such as alkaline pyrosphosphate, acidic sulfate and acidic chloride baths as well as various additives and tensioactives have been investigated in the literature in order to improve current efficiency, control alloy composition or materials properties.

The goal of the present study is to deposit compact and smooth Zn-Mn layers having high Mn contents of up to 40 wt.% corresponding to a theoretical melting temperature of 900 °C (Figure 13).

Electroplating baths for Zn-Mn deposition

The main plating baths used for the deposition of Zn-Mn coatings at the laboratory scale are the alkaline pyrophosphate, acidic sulfate and chloride baths. Some studies [123-125] in sulfate baths reported an increase in manganese content to the detriment of current efficiency. Indeed, Crousier et al. [126] stated that a rather unstable solution and a low compatibility with industrial processes were observed when Mn contents higher than 12 wt.% were obtained, due to a low current efficiency during deposition. Moreover, Bučko et al. stated that Zn-Mn coatings deposited from sulfate baths were heterogeneous as current density increased [127].

Investigations carried out by Bučko et al. on Zn-Mn coatings deposited from alkaline pyrophosphate solutions established a substantial influence of the applied deposition

current density on the corrosion behavior [118]. Coatings deposited at 80 mA cm^{-2} and containing 9.9 wt.% Mn led to the formation of a porous layer of ZHC corrosion product providing a lower protective effect compared to coatings deposited at lower current densities and containing a lower Mn amount. Sylla et al. studied the influence of several additives in alkaline pyrophosphate electrolytes and reported a Mn content of 21 wt.% for very low current efficiencies of about 10 % [128]. Generally, it appears that Zn-Mn coatings obtained from pyrophosphate baths are non-homogeneous and are leading to higher corrosion rates compared to chloride and sulfate media [123]. On the contrary, coatings obtained from chloride baths proved to be compact, smooth and showed a better corrosion behavior in chloride medium compared to other plating baths. Bučko et al. reported a wider process window in terms of suitable deposition current densities and higher current efficiency in presence of chloride electrolytes in comparison to sulfate electrolytes [127]. In the present work, acidic chloride baths were consequently selected for depositing Zn-Mn coatings.

Alloy electrodeposition was reported by Losey and Kelly [129] to depend on the equilibrium potentials of the metals and the ion concentration in the electrolyte. In fact, when the resulting ratio of the metals in the alloy is that expected according to the equilibrium potentials and concentrations and when equilibrium potentials fall close together, normal codeposition takes place and the full range of alloy composition can be obtained. However, if the equilibrium potentials of alloy metals differ significantly, abnormal codeposition takes place, which means that a preferential deposition of the less noble metal occurs. This latter particularity was reported by several researchers to be a significant challenge for electroplating Zn-Mn alloys, since standard electrode potentials of Zn^{2+}/Zn and Mn^{2+}/Mn couples in acidic medium differ significantly. Among other methods, the use of various additives and the optimization of ionic concentrations of the metal ions can permit to reduce the activity of the more noble metal and increase codeposition.

In the literature data, several additives were used to study the possibility of increasing Mn deposition in chloride medium, improving current efficiency during electrodeposition and reducing hydrogen evolution reaction. Various additives, such as sodium benzoate, β-naphtol or sodium diisopropylnaphtalene sulfonate were investigated in chloride electrolytes in order to bring deposition potentials of Zn^{2+}/Zn and Mn^{2+}/Mn couples closer [130]. However, limited information regarding the composition, microstructural properties and anticorrosive properties of the deposited coatings was presented. Further commercial additives were investigated by Sylla et al. in acidic and alkaline baths [131]. The authors observed a significant increase in manganese content and a considerable modification of the coatings morphology in chloride electrolytes, from a cauliflower morphology to an assembly of pyramidal crystals in presence of additives. Moreover, the layers deposited from the acidic chloride bath in presence of the commercial additive were composed of a single ε-Zn-Mn phase and contained up to 22 wt.% Mn. However, no information regarding the nature of the additive used was provided by the authors. Polyethylene Glycol (PEG) was also investigated in different concentrations as an additive and led to a decrease in Mn content

and the presence of several crystallographic phases [132]. Sodium gluconate as a complexing agent [133] was stated to increase overvoltage for Zn deposition as well as to inhibit hydrogen evolution reaction. However, the layers were reported to have a flower-like morphology.

Ammonium thiocyanate NH_4SCN was reported as additive in deposition of Mn coatings to avoid adsorption and precipitation of Mn hydroxides and provide stable manganese phases [134, 135]. Moreover, the influence of NH_4SCN in chloride electrolytes on the morphology, composition and corrosion resistance of Zn-Mn coatings was studied by Díaz-Arista et al. [134] and showed an increase in the Mn content. Other interesting alternative additives are the derivatives of benzaldehyde, which were stated to inhibit hydrogen evolution reaction at high current densities [136, 137]. Consequently, Bučko et al. [138] observed higher Mn contents as well as a reduction of the porosity of the layers when 4-Hydroxybenzaldehyde (4-HB) was used.

2 Aim and experimental approach of the present work [EN + FR]

Nowadays, several coating products are available for the hot stamping application for automotive body parts. Corrosion, high temperature oxidation and decarburization of bare components can thereby be considerably reduced. However, it appears that each coating system implies challenges in terms of manufacturability, processability or product performance. Among the two main coating products, aluminized steels provide a good hot formability and allow the use of direct hot forming. However, no sacrificial corrosion protection can be obtained. On the contrary, a sacrifical effect is obtained in the case of galvanized steels, while a more costly manufacturing process is required due to LME during hot forming. Further coating systems reported in the literature did not result in a serial production, mostly due to technical limits in the processing of coating materials.

The present work is dedicated to the study of alternative coating systems for press-hardened steel parts with the aim of improving performance of state of the art coating products. On the basis of a comprehensive literature research study on currently available products, as well as on the product requirements of coating materials for hot forming, promising protective coatings were defined. A significant benefit of the use of Zn-Mn alloy coatings was found in terms of anticorrosive properties and high temperature behavior. Therefore, the present work is dedicated to the study of the latter system. The experimental approach of the present work is presented in Figure 14.

First of all, a comprehensive study of the electroplating baths, electrolytic and electric parameters will be carried out on 22MnB5 steel plates with surfaces of up to 17 cm^2 to understand electrochemical mechanisms associated to the deposition of Zn-Mn layers. In order to study the materials properties as well as the thermal and mechanical behavior of coatings deposited on 200*200 mm wide steel plates, an electroplating cell was designed for this study. Electrodeposition on large-scale panels will be assessed with regard to the stability of the plating baths, to the reproducibility of the deposits and to the homogeneity of the properties of the layers over the surface of the plates. The as-deposited Zn-Mn layers will be characterized for studying their microstructural, crystallographic and corrosion properties.

The suitability of the protective coatings for high temperature applications will be assessed at various temperatures and dwell times in order to understand chemical diffusion, oxidation and evaporation processes occurring at high temperature. A protective atmosphere containing argon gas will be used for reducing the amount of oxide particles formed on the surface of the coatings. A systematic correlation between the properties of the deposits prior to and post to heat treatment will be done.

Finally, the suitability of alternative Zn-Mn alloy coatings for the direct hot stamping application will be studied on the basis of hot press forming experiments with tools specifically designed, manufactured and started up for this work after computer-aided

design construction and hot forming simulation and correlated to the behavior of current GI products, with the aim of determining the possible benefits of the use of zinc alloys compared to pure Zn coatings, in particular with regard to LME.

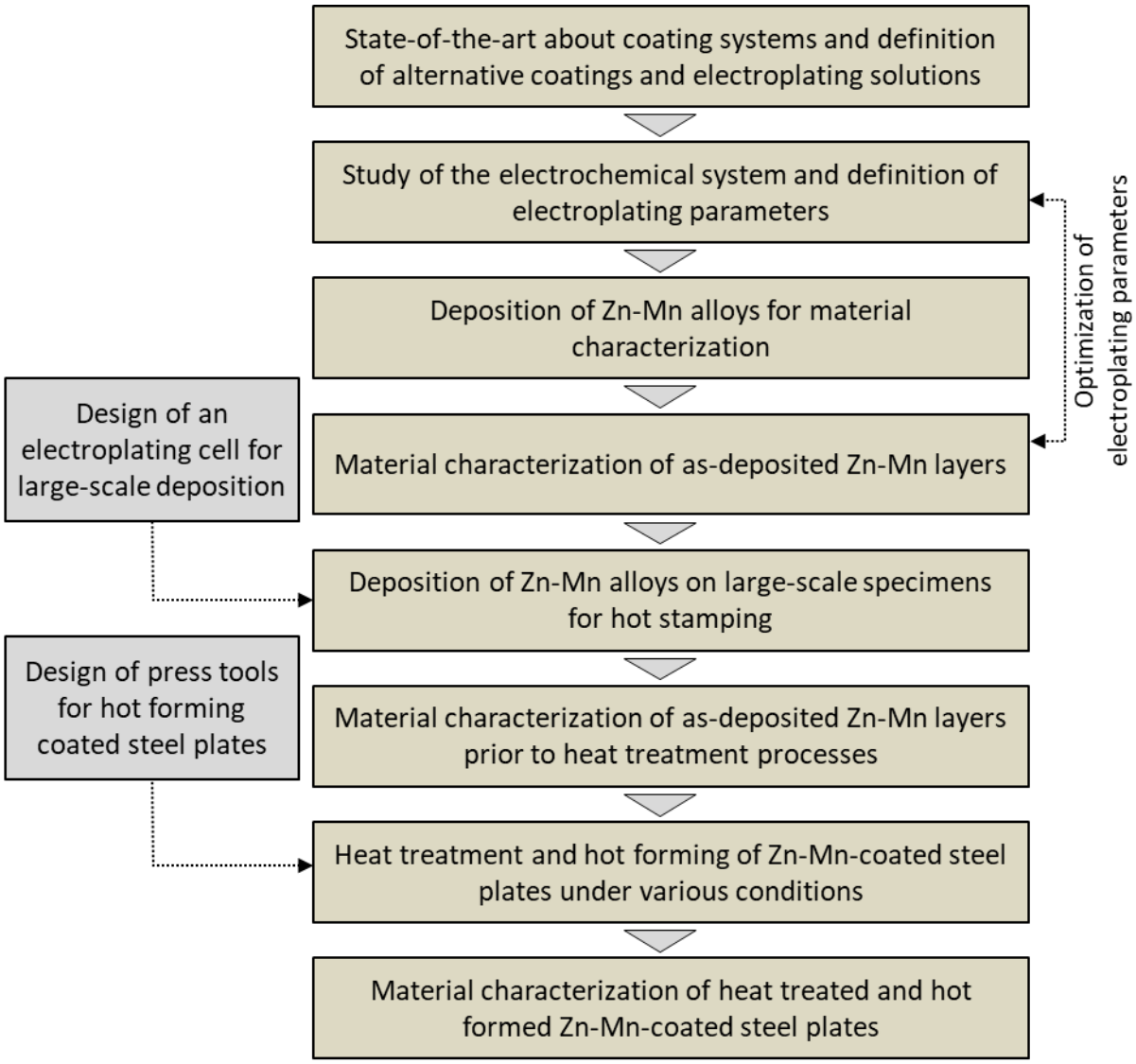

Figure 14: Experimental approach of the study of alternative Zn-Mn coating systems for hot formed steel parts.

Objectif et approche expérimentale de ce travail [FR]

Plusieurs types de revêtements protecteurs sont actuellement disponibles pour l'application de l'emboutissage à chaud de pièces de carrosseries automobiles. De par l'utilisation de revêtements, la corrosion, l'oxydation et la décarburation à haute température d'aciers nus peuvent être considérablement réduites. Cependant, il apparaît que chaque système de revêtements implique des limites en termes de conditions de fabrication, de transformation ou de performances lors de son utilisation. Parmi les deux produits principaux, les aciers aluminiés fournissent une bonne aptitude à la mise en forme à chaud et permettent d'utiliser la mise en forme à chaud de manière directe. Cependant, aucune protection cathodique n'est obtenue avec ce produit.

Au contraire, alors qu'un effet sacrificiel est obtenu dans le cas d'aciers galvanisés, un procédé de fabrication plus coûteux est nécessaire à cause de la formation de fissures par fissuration par métaux liquides pendant la mise en forme à chaud par la méthode directe. D'autres systèmes de revêtements ont été reportés dans la littérature, mais n'ont pas connu d'entrée dans la production en série de pièces de carrosserie, notamment du fait de limites techniques dans les différentes étapes de transformation des revêtements.

Ce travail est dédié à l'étude de nouveaux systèmes de revêtements pour des aciers emboutis à chaud et trempés avec l'objectif d'améliorer les performances des revêtements actuellement proposés par l'industrie automobile et les sidérurgistes. Des matériaux prometteurs ont été sélectionnés sur la base d'une importante étude de la littérature sur les produits commerciaux et sur le cahier des charges des matériaux de revêtements pour la mise en forme à chaud. Un avantage intéressant fut trouvé pour l'utilisation d'alliages Zn-Mn en termes de propriétés anticorrosives et de comportement à haute température. Par conséquent, le travail actuel est dédié à l'étude de ces alliages pour la mise en forme à chaud. L'approche expérimentale considérée lors de ce travail est présentée en Figure 15.

*Tout d'abord, une étude exhaustive des bains électrolytiques ainsi que des paramètres électrolytiques et électriques a été menée sur des plaques d'acier 22MnB5 avec des surfaces de moins de 17 cm² pour comprendre les mécanismes électrochimiques associés à la déposition de couches de Zn-Mn. Afin d'étudier les propriétés des matériaux obtenus ainsi que les comportements thermiques et mécaniques des revêtements déposés sur de grandes plaques d'acier de dimensions 200*200 mm, une cellule électrolytique a été conçue pour cette étude. L'électrodéposition sur des plaques de grandes dimensions sera ensuite évaluée concernant la stabilité des bains èlectrolytiques, la reproductibilité des dépôts et l'homogénéité des propriétés des revêtements obtenus sur toute la surface des plaques. Les dépôts de Zn-Mn seront caractérisés pour étudier leurs propriétés microstructurales, cristallographiques et anticorrosives.*

La compatibilité des couches protectrices pour des applications à haute température sera évaluée à de nombreuses températures et durées de chauffe afin de comprendre la diffusion chimique, l'oxydation et l'évaporation se produisant à haute température. Une atmosphère protectrice contenant de l'argon sera utilisée pour réduire la quantité de particules d'oxydes formées sur la surface des revêtements. Une corrélation systématique entre les propriétés des couches avant et après traitement thermique sera effectuée.

Enfin, la compatibilité des nouveaux revêtements Zn-Mn pour l'application de l'emboutissage à chaud direct sera étudiée sur la base d'essais de mise en forme à chaud avec des outils de presse conçus spécialement pour ce travail avec des outils informatiques de construction et de simulation d'emboutissage à chaud et sera corrélée avec le comportement de produits galvanisés commerciaux avec l'objectif de déterminer les avantages éventuels de l'utilisation d'alliages de Zn comparé à des couches de Zn pu, en particulier concernant la fissuration par métaux liquides.

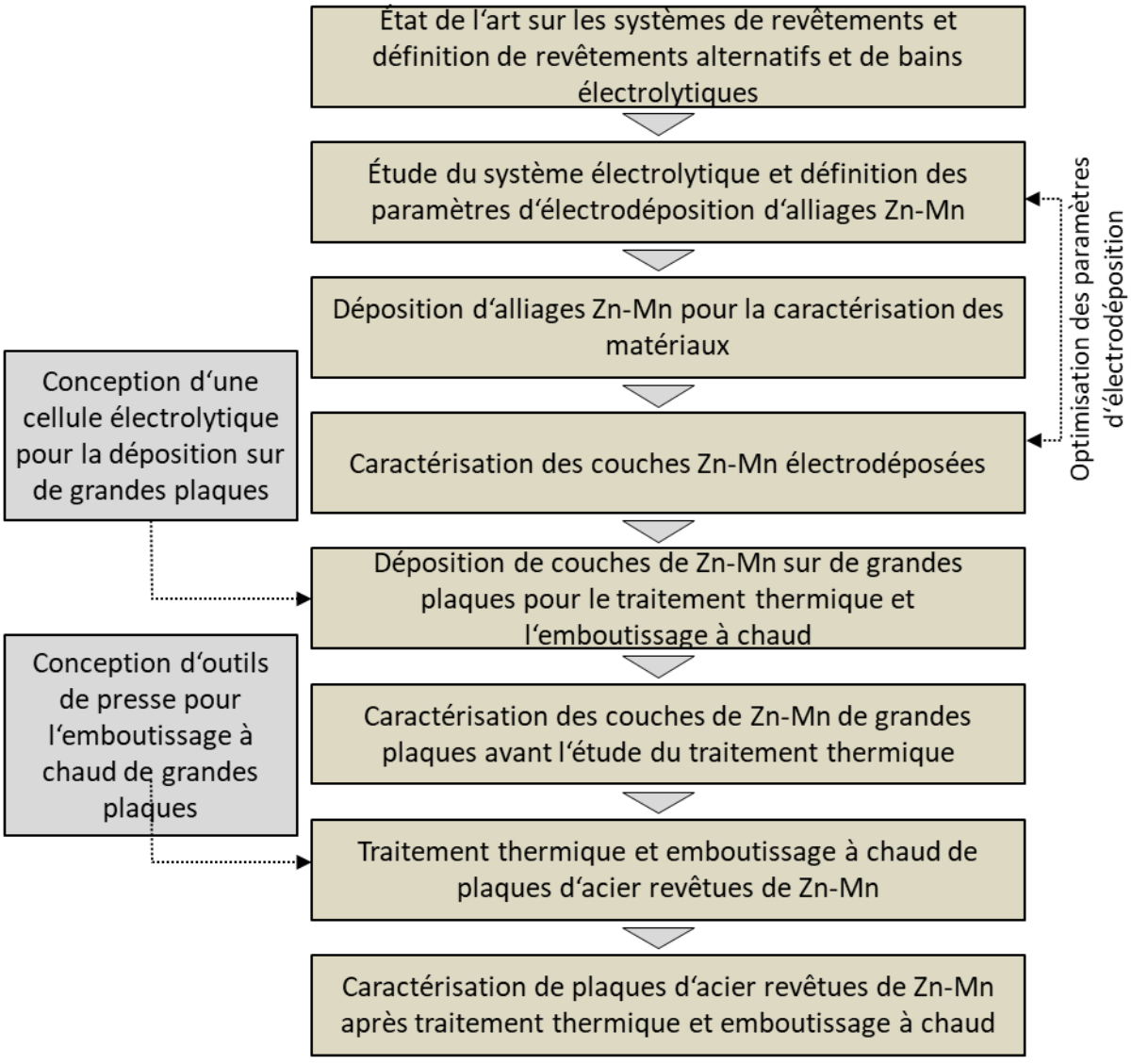

Figure 15: Approche expérimentale de l'étude de nouveaux revêtements Zn-Mn pour des pièces de carrosseries mises en forme à chaud considérée dans le cadre de ce travail.

3 Materials and experimental methods

In this section, essential information regarding the different bare and coated 22MnB5 commercial products used, the experimental conditions considered for the study of electroplating of Zn-Mn alloy coatings as well as the electrodeposition of Zn-Mn coatings on steel plates with various surfaces is reported. In addition, background information and the parameters used for the various characterization techniques utilized in the present work for the investigation of the microstructural, the crystallographic and the anticorrosive properties of Zn-Mn alloy coatings will be presented. Finally, the experimental conditions considered for the study of heat treatment and hot forming behavior are presented.

3.1 Steel products investigated

The behavior of current coated products during direct hot stamping with press tools specifically designed for this study was carried out on aluminized (Usibor 1500P – AS150, ArcelorMittal) and galvanized (phs-ultraform, voestalpine GmbH) steels. These coating systems are reported in Section 1.5. Zn-Mn coatings were deposited on bare 22MnB5 (MBW 1500, ThyssenKrupp Steel Europe AG) steel plates. This steel grade was used as substrate for Cyclic Voltammetry (CV) studies. Spectral analyses were carried out on the bare 22MnB5 steel by means of Optical Emission Spectrometry for determining its chemical composition (Table 5). It should be noted that all steel products used in the present work have a blank thickness of 1.5 mm.

Table 5: Composition of bare 22MnB5 steel (MBW 1500, ThyssenKrupp Steel Europe AG) used in the present work for the deposition of Zn-Mn coatings; in wt.% (rest of Fe); determined by means of Optical Emission Spectrometry.

Bare 22MnB5 steel											
C	**Si**	**Mn**	**Al**	**P**	**S**	**Cr**	**Ni**	**Mo**	**V**	**Ti**	**Nb**
0.198	0.241	1.210	0.026	0.011	0.001	0.135	0.016	0.001	0.003	0.025	0.001
W	**B**	**N**	**Pb**	**Cu**	**Sn**	**As**	**Co**	**Zr**	**Ca**	**Mg**	**Zn**
0.003	0.002	0.007	0.001	0.015	0.004	0.001	0.004	0.001	0.001	0.001	0.001

Confocal microscopy analyses were performed on bare 22MnB5 steel product to study the surface on which Zn-Mn coatings will be deposited. Representative data of the surface topography of 22MnB5 steel is presented in Figure 16.

Mean roughness values of S_a = 1.86 µm and S_a = 1.18 µm were obtained on measurement areas of 636.61 x 477.25 µm² and 84.88 x 63.63 µm², respectively. As coating deposition strongly depends on the initial surface state of surfaces [139], these values will be taken into account during the study of the roughness of Zn-Mn coatings (Section 4.3.2).

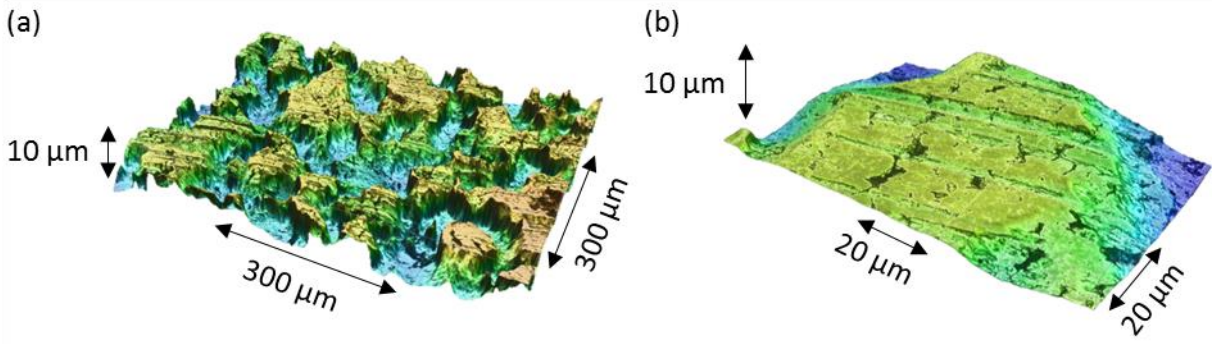

Figure 16: Representative surface topography of bare 22MnB5 steel used for the deposition of Zn-Mn coatings by means of confocal microscopy; measurement areas of 636.61 x 477.25 µm² (a) and 84.88 x 63.63 µm² (b).

Electron Backscatter Diffraction (EBSD) maps (Section 3.3.8) were carried out on the surface and on a cross-section of bare 22MnB5 steel for determining the orientation and the size of the grains of the steel substrate. This preliminary study is necessary to investigate the materials properties of Zn-Mn alloy coatings as the orientation of the crystals of substrate materials was reported to have an influence on that of electrodeposited layers [139].

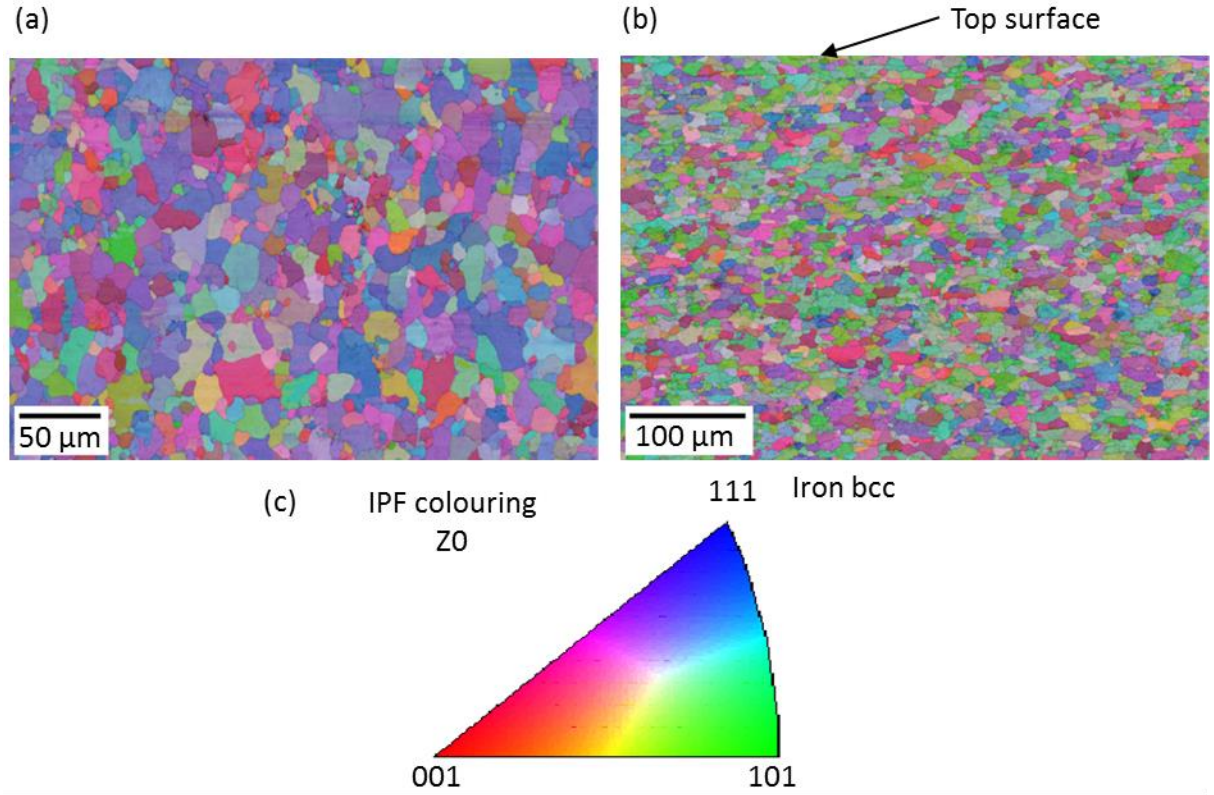

Figure 17: Electron Backscatter Diffraction (EBSD) maps with the grain orientation of 22MnB5 after measurements on the surface (a) and in cross-section (b); orientation triangle of the corresponding maps (c).

In the cross-sectional view of Figure 17 b), the grains appear to be elongated and parallel to the steel surface. This observation can be linked to the rolling process used for manufacturing steel, as confirmed by Geiger et al. [140]. No preferential orientation can be

observed. The mean grain size was determined on the basis of the EBSD orientation maps shown in Figure 17. Values of 8.1 ± 6.4 µm and 7.3 ± 4.7 µm were obtained from analyses on the surface and on cross-sections, respectively. The higher mean grain size observed on the surface can also be linked to the rolling process. It should be noted that the high standard deviation of these measurements is related to a significant heterogeneity of the size of the grains.

3.2 Study of the electrodeposition of alternative Zn-Mn coatings

This section is focused on the review of experimental conditions for the electrodeposition of Zn-Mn alloy coatings. On the basis of the literature data, promising electrolytes and additives will be defined for the present work. In addition, electrochemical methods used for the study of the electroplating systems and the definition of optimal deposition parameters will be presented. Finally, the experimental setups and parameters used for depositing Zn-Mn layers on 22MnB5 steel plates with various surfaces will be presented.

3.2.1 Electrodeposition of metallic coatings

Electrodeposition of metallic coatings involves the reduction of metal ions contained in aqueous, organic or fused-salt electrolytes, generally by the use of an external power supply in order to monitor redox reactions [139]. In the present study, Zn-Mn coatings were deposited from aqueous electrolytes. Electrodeposition process and material properties were reported by Sotto et al. [141] to be based on various variables such as the electrolyte composition, the presence of additives, the properties of the working electrode or the electric parameters applied during deposition, as presented in Figure 18.

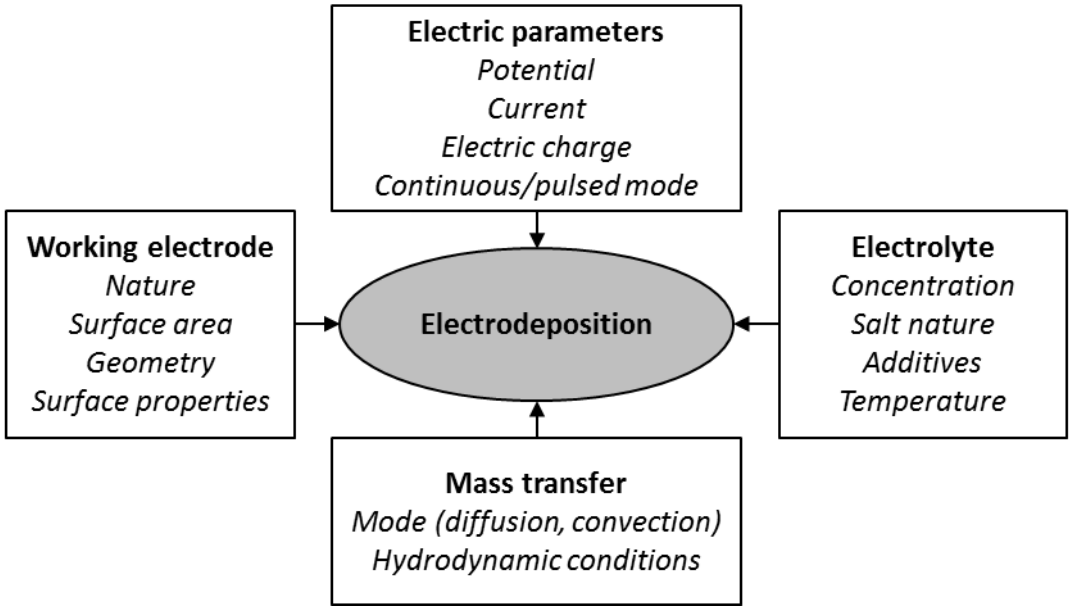

Figure 18: Main variables controlling electrodeposition process and properties of coating materials; from [141].

3.2.2 Cyclic Voltammetry combined with Electrochemical Quartz Crystal Microbalance studies

CV and EQCM methods

Cyclic Voltammetry (CV) permits to study electrochemical oxidation or reduction reactions taking place at the interface between an electrode and a solution in a defined range of potentials. The solution generally consists of a solvent containing the dissolved material investigated and a supporting electrolyte salt to improve electrical conductivity and obtain diffusion-controlled reactions [142]. The evolution of the current during a potential sweep is recorded and permits to obtain a potential-current curve called voltammogram, as illustrated in Figure 19.

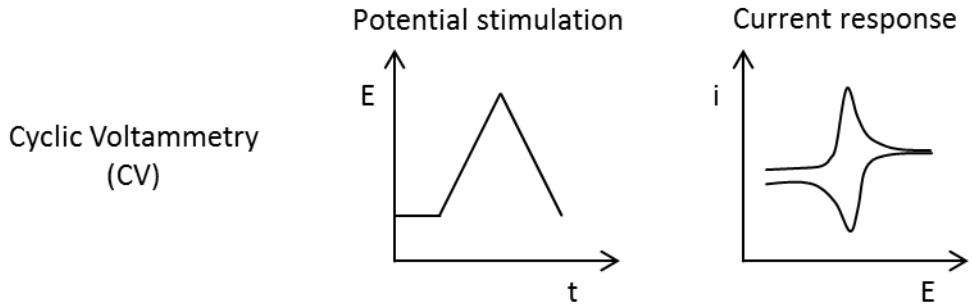

Figure 19: Plots of the potential stimulation and the resulting current response during Cyclic Voltammetry (CV) studies.

This process starts with a scan in one direction, starting at the initial potential and going through a potential domain for which reduction or oxidation of the studied material takes place. The potential scan is then switched at a reverse potential, permitting to visualize the product of the electron transfer reaction of the forward scan a second time [143]. This method is particularly beneficial for studying the composition of electrolytes, the influence of additives on the electrochemical behavior of the electrolytic systems and the interesting potential domains for which reduction or oxidation reactions take place [143]. In this work, the CV studies were carried out in various potential ranges in order to monitor cathodic and anodic signals and improve understanding of the electrochemical system.

Electrochemical Quartz Crystal Microbalance (EQCM) permits to record gravimetric response (mass loss and mass gain) taking place at the electrolyte/electrode during electrochemical processes, generally with the simultaneous use of CV studies. This technique is based on the use of a quartz crystal working electrode, whose resonance frequency varies according to the deposition or dissolution of material on the quartz surface. The plot of the rate of mass change on the quartz crystal surface versus the potential, along with the CV data, permits to differentiate mass changes linked to deposition or dissolution processes accompanied by charge transfer at the electrode surface (Faradaic processes) from processes not associated with charge transfer processes (non-Faradaic processes) [134].

CV and EQCM experimental setups

Electrogravimetric studies were performed by an Electrochemical Quartz Crystal Microbalance (EQCM) with a dedicated potentiostat (Autolab PGSTAT 128N). All measurements were performed with the NOVA software. A platinum-coated quartz electrode with a fundamental resonance frequency of the AT-cut quartz of 6 MHz and with an active surface of 0.361 cm^2 were immerged in an electrolyte volume of about 5 cm^3 and were used at room temperature (22 °C). All the EQCM experiments were conducted with a platinum counter electrode in a cell purged with Ar for limiting oxygen reduction signals. An Ag/AgCl/KCl(sat.) reference electrode was used. All the potentials mentioned in this study are with respect to this reference electrode, except galvanostatic dissolution tests which were carried out with a Saturated Calomel Electrode (SCE).

Prior to each EQCM study, the quartz surface was electrochemically activated in a 0.5 M H_2SO_4 solution by cycling 50 times between -0.25 and +1.40 V at a scan rate of 10 mV/s until current and frequency signals were reproducible in order to obtain impurity-free system and to release any stress from the near-surface region [144].

Calibration of the EQCM is necessary for accurately assigning mass changes to the electrochemical processes involved. Since galvanostatic copper electrodeposition in acidic medium was reported by Broch et al. [144] to be reversible and to have a deposition efficiency of almost 100 %, calibration process was carried out in the same conditions in an electrolyte containing 8.5 x 10^{-2} M $CuSO_4$ and 5.0 x 10^{-1} M H_2SO_4. A cathodic current density of 0.2 mA cm^{-2} was applied for 210 s during deposition, whereas the copper films were removed by applying an anodic potential of 100 mV until the quartz frequency reached the initial value corresponding to the initial surface state. Ten successive deposition/stripping cycles were performed for calibrating gravimetric sensors and the experimental constant of Sauerbrey K was calculated from each deposition step on the basis of the equations reported by the work of Broch et al. [144]. The constant K was calculated by considering a faradic efficiency of 100 %. The results exhibited a constant value of K = 192.93 ± 5.85 Hz μg^{-1}, which is close to the theoretical value K = 225.76 Hz μg^{-1}.

The CV and EQCM studies were carried out with a scan rate of 10 mV/s in baths prepared using deionized water and containing 2.8 M KCl, 0.6 M $MnCl_2$ and 0.32 M H_3BO_3. Concentrations of 0.1, 0.075, 0.06 and 0.05 M were used for $ZnCl_2$. With the aim of increasing Mn deposition, 6.5 mM NH_4SCN and 4.1 mM 4-HB additives were added to the electrolyte. CV and EQCM studies were carried out in electrolytes where cations and additives concentrations were diluted by a factor of ten, in order to obtain well-defined peaks of current and resonance frequency. Boric acid was reported to inhibit both hydrogen formation and zinc deposition by limiting pH evolution at the electrode surface during electrodeposition and therefore blocking the active centers for proton reduction [120, 132]. This mechanism resulted in smoother deposits and higher current efficiencies for metal reduction [127]. Representative CV and EQCM data are shown in the present work and are based on sets of at least 3 measurements.

3.2.3 Electroplating cells and experimental parameters

The influence of the electrolyte composition and the applied cathodic potentials on the Mn content of deposits was studied in a classical three-electrode cell using a Radiometer PGZ 100 potentiostat/galvanostat interfaced with a computer. These experiments on small-scale samples permitted to study the electrochemical system and define the optimal electrolyte composition and electric parameters. 22MnB5 steel plates with various active areas comprised between 2 and 17 cm² were used for deposition. The deposition duration was ruled by an electric charge of 44.56 Q cm^{-2} corresponding to a coating thickness of about 20 µm.

In order to investigate the behavior of the coating materials during heat treatment and hot forming and to evaluate the influence of heat treatment on anticorrosive properties of the alloys, electroplating of Zn-Mn alloys on specimens with larger dimensions was required. A geometry of 200 x 200 mm and a blank thickness of 1.5 mm were defined on the basis of the requirements for the construction of press tools for hot forming. An overview of the electroplating setup is presented in Figure 20. The VersaSTAT 3 potentiostat/galvanostat coupled with a current booster (Princeton Applied Research) were used for deposition. The electroplating cell which was designed for this study consists of four modules assembled with a threaded rod. All modules are separated with seals in order to prevent electrolyte leakage. A more detailed view of the electroplating cell during service is shown in Figure 21. The electroplating cell contains an electrolyte volume of about 2000 ml, in which the working electrodes is vertically immersed. The electric contact is provided with a steel plier insulated with a PVC layer.

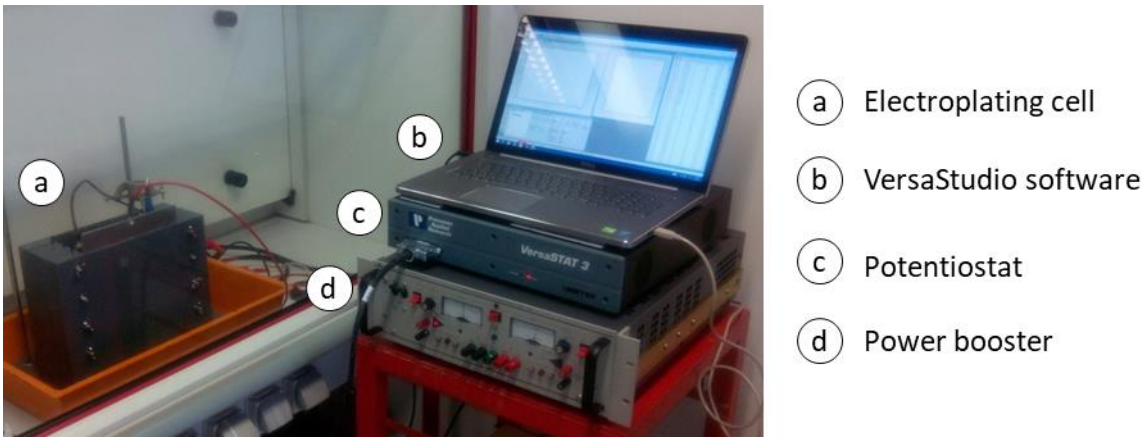

Figure 20: Experimental setup for the deposition of Zn-Mn coatings on large-scale specimens.

The steel substrates were degreased by acetone and rinsed thoroughly with distilled water prior to deposition. Before each experiment, the zinc counter electrode was chemically etched in a 6 M HCl solution for removing oxide scale. A pure Zn plate (99.95 +% purity zinc) with the same area as the working electrode and placed in front of the latter is used as counter electrode. The use of the zinc electrode as soluble anode during electrodeposition

experiments not only allows stabilizing the zinc cation content in the bath but also avoids oxidation of Mn cations to higher oxidation states.

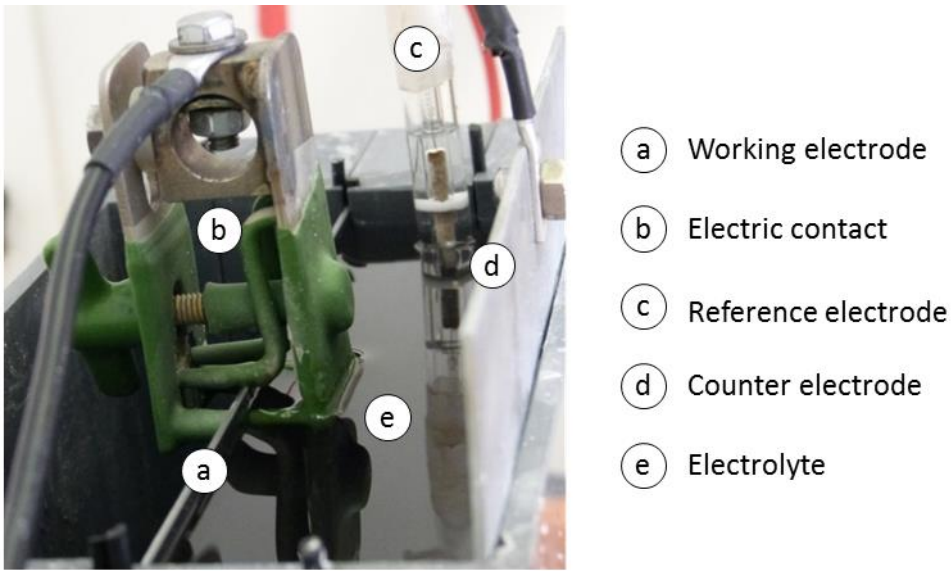

Figure 21: Electroplating cell used for the deposition of Zn-Mn coatings on large-scale specimens.

Several works reported that the temperature of the electrolyte affects the composition and the properties of Zn-Mn electrodeposits. As stated by Müller et al. [124], an increase of the bath temperature leads a decrease of the Mn content in the layer, along with an enhancement of the brightness of the coating [120]. The relative intensity of the XRD peaks was also stated to change by increased temperatures [133]. Therefore, electrodeposition was carried out at room temperature. The initial pH of the solution was approximately 4.3. No stirring and no adjustment of the electrolyte pH were carried out during deposition. The electrolyte was renewed for all deposited coatings. Electrodeposition was carried out with a deposition potential of -1.62 V in electrolytic baths in presence and in absence of additives. After growth, Zn-Mn coatings were rinsed with distilled water to remove chloride salts from the surface of the films, washed with ethanol and finally dried.

A constant $ZnCl_2$ concentration of 0.075 M was used for electrodeposition on large-scale plates. This concentration was fixed after preliminary CV and EQCM studies of electrodeplating baths and Zn-Mn coatings deposited under various conditions.

Moreover, pure zinc layers were deposited from the electrolyte in presence of additives in order to compare the anticorrosive properties of electrodeposited Zn and Zn-Mn alloys by means of potentiodynamic polarization measurements and to possibly identify performance input of the use of Mn alloying element. CV and EQCM studies presented in Section 4.1.1 permitted to define a potential of -1.2 V for which only Zn reduction occurs in the electroplating bath for Zn-Mn alloy deposition.

Strips with area of approximately 60 x 45 mm^2 with homogeneous surface morphology and coating composition and located on the upper part of the coated plates were cut out for material characterization prior to and post to heat treatment and for corrosion experiments.

3.3 Materials characterization

3.3.1 Global procedure

Various complementary characterization techniques, summarized in Figure 22, are used in the present work for determining microstructural, crystallographic and anticorrosive properties of alternative Zn-Mn coatings prior to and post to high temperature processes. The corresponding investigations and characterization methods will be discussed in the next parts.

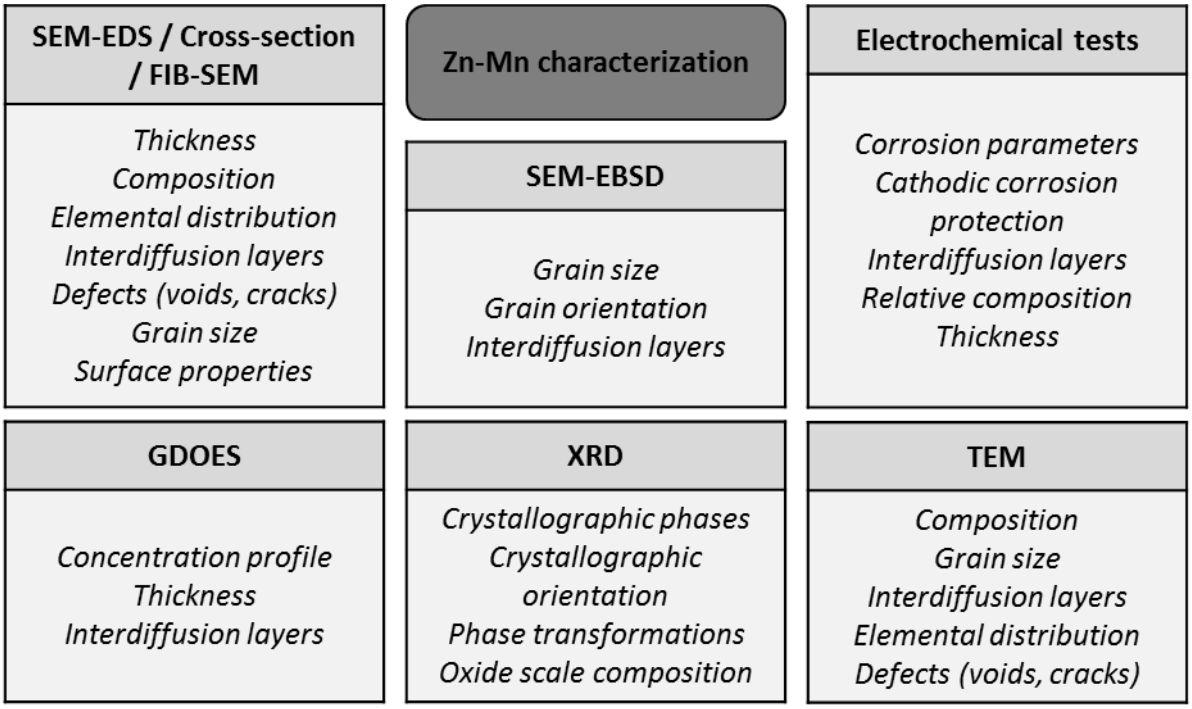

Figure 22: Coating properties investigated by the different complementary characterization methods used in the present work.

3.3.2 Metallographic characterization

The specimens were cut with a Discotom cut-off machine and mounted with a „Struers CitoPress 20“ equipment with EpoMet or PolyFast mounting resins. The mounted cross-sections were mecanically polished with SiC papers up to 1200 µm on a type Struers TegraPol-31 machine, followed by a polish of 12, 3 and 1 µm in a diamond suspension with an alcohol-based solution. The specimens were finally rinsed with ethanol. Galvanized parts were partly etched in an ethanol solution with 3 % nitric acid for revealing the interface between coating and substrate materials and grain boundaries in substrate steel. The thickness, the formability and the microstructure of commercial products and Zn-Mn coatings were studied with a Leica Leitz DM RM optical microscope with magnifications of up to 1000 X. The thickness values presented in this work are based on sets of at least 6 measurements.

3.3.3 Crystallographic characterization

X-rays are high-energy electromagnetic radiations which are produced in a X-ray tube in which electrons generated by a cathode collide with a target anode at very high velocity. The X-ray wave passes through a beryllium (Be) window and strikes the sample, which is mounted on a goniometer. If the incident electron has sufficient energy to eject an inner-shell electron, the hole is filled by an electron from an outer sheel, generating an x-ray photon with an energy equal to the difference in the electron energy levels. This energy is characteristic of the target material. Due to the presence of subshells in the L shell, the characteristic K-radiation emission from typical X-ray tube anode materials contains Kα1, Kα2 and Kβ radiations. Monochromators or Ni filters are often used to filter the undesirable Kβ diffraction lines and obtain an experimental pattern from a single wavelength [145, 146].

In the case of the Bragg-Brentano diffraction system, the incident beam hits the sample with an angle θ with the surface, while the diffracted beam has an angle of 2θ versus the incident beam. There are two main geometrical setups for X-ray Diffraction (XRD) measurements. Either the source remains fixed while the sample is rotated around θ and the detector moves by 2θ (θ/2θ configuration), or the sample is fixed while both the X-ray source and the detector rotate by θ simultaneously, but clockwise and anticlockwise, respectively (θ/θ configuration) [147]. The resulting data, namely diffraction intensity versus degrees, are called diffractograms or diffraction patterns. X-ray diffraction is based on Bragg's law which reveals that each unique inter planar spacing diffracts different wavelengths at their own unique diffraction angles [148]. Each diffraction peak formed on the patterns corresponds to X-rays diffracted from a specific set of planes in the sample. The study of the positions of the peaks, the relative intensities of the peaks, the relative differences in their integrated intensity provides important crystallographic properties of the sample materials, such as the lattice parameters or the type of unit cell. This information permits to identify the crystallographic phases, determine the orientation of the crystals, the average crystallites sizes or measure defects and stresses, among other properties [149]. Besides, in the present work, the cell parameters of the ε_2–Zn-Mn crystallographic phase were fitted to permit the identification of the XRD diffraction lines.

The crystallographic structure of the Zn-Mn deposits was investigated by XRD measurements (Bruker D8Advance) with Cu Kα radiation (λ = 1.5406 Å) at 40 kV and 40 mA and in the Bragg-Brentano θ/θ configuration. The crystallographic phases were identified on the basis of reference data from the Joint Committee on Powder Diffraction Standards (JCPDS) database with the software EVA 3.1.

The crystallographic texture of Zn-Mn coatings deposited with and without additives was determined by XRD pole figure measurements on a homemade diffractometer using Cu Kα radiation. The goniometer was equipped with a curved sensitive detector INEL CPS 120 having 120° angular aperture and configured to record simultaneously pole figures and their background. This method is called multi-pole figure measurement. Pole figures were analysed and plotted with a homemade software (JTEX®) [150].

3.3.4 Scanning Electron Microscopy SEM

In Scanning Electron Microscopy, a finely focused electron beam irradiates a surface or a microvolume with primary electrons, which leads to the emission of secondary electrons, backscattered electrons, auger electrons, x-rays and other photons of various energies. These signals can be used for studying various material properties such as topography, crystallography or composition. Secondary electrons enhance topographic contrast, contrary to material contrast for backscattered electrons. The analysis of the x-radiations permits to provide qualitative identification and accurate quantitative elemental information about volumes of about 1 μm^3. This technique is called Energy Dispersive X-ray Spectroscopy (EDS) and is generally coupled to SEM for chemical analyses. A considerable advantage of this technique for the present work is the possibility of obtaining elemental distributions on surface maps, in particular for cross-sectional studies of Zn-Mn coatings post to heat treatment [151, 152].

The morphology and the composition of the surface of the coatings prior to and post to heat treatment were investigated by means of SEM (VEGA3, Tescan) and coupled to an EDS analyser (Nano, Bruker) for chemical composition analyses. The chemical compositions were determined on the basis of sets of at least 3 measurements. An accelerating voltage of 20-30 kV was used.

The study of the microstructure and the composition of Zn-Mn coatings on cross-sections post to heat treatment was carried out on a Field Emission Gun Scanning Electron Microscope (FEG-SEM) (MIRA3, Tescan) coupled to an EDS analyser (Nano, Bruker). The mean values of the chemical composition of Zn-Mn coatings in cross-sections were determined on the basis of sets of at least 6 values. An accelerating voltage of 15 kV was used. Semi-quantitative values were obtained after Phi-Rho-Z correction for chemical analyses.

3.3.5 Atomic Absorption Spectroscopy AAS

Atomic Absorption Spectroscopy (AAS) permits to determine the concentration of elements dissolved in a solution. In this technique, a source of radiation produces a beam which is passed across the path of an elongated burner. A fine mist of the analytical sample is produced by the burner atomizer and is then burned for analysis. The atoms generated during burning absorb the beam of the radiation source, leading to a decrease in energy measured as a per cent absorption. This value is finally translated into concentration on the basis of calibration curves obtained by measuring the absorbance of standard solutions containining known concentrations of the elements [153]. The main advantage of this technique is the fact that a global composition of the coating can be obtained after dissolution of the coating, compared to SEM analyses which provide local information about the surface analysed.

The AAS (Varian AA240 FS) analyses were carried out on as-deposited Zn-Mn layers after complete dissolution of the coating with a solution containing 5 M HCl and a corrosion

inhibitor for steel corrosion, namely 2 % Hexamethylenetetramine (HMTA) [154]. The calibration solutions were prepared by dilution of standard solutions of Mn (1000 mg l^{-1}, 77036, Fluka Analytical) and of Zn (1000 mg l^{-1}, 18827, Fluka Analytical). The AAS data were evaluated on the basis of sets of up to 5 samples.

3.3.6 Focused Ion Beam FIB

Focused Ion Beam (FIB) microscopy consists in rastering a beam of positively charged ions over a sample surface and analysing the resulting signals to form an image. The FIB column is generally coupled to a SEM column in order to proceed sample preparation and imaging simultaneously. This technique permits to prepare cuts or cross-sections by milling the material with a very wide range of geometries from less than 1 µm to up to 200 µm and with a resolution of 5 nm [151].

In the framework of this study, FIB was used for cross-section imaging of Zn-Mn coatings prior to and post to hot stamping in order to study various characteristics such as the grain size, voids, cracks, interdiffusion layers or the chemical distribution in the layers. This method permits to obtain a higher surface quality for cross-sections compared to mechanical surface preparations, as voids and fragile features are less damaged by the fine polishing.

The FIB preparations were conducted on a Crossbeam FIB-SEM Zeiss Auriga 40 equipped with the Gemini-type electronic column and the Orsay Physics Cobra ionic column. A Liquid-Metal Ion Source (LMIS) of Gallium ions was used for the primary beam. The FIB column and the samples are inclinated at 54° with the SEM column for simultaneous FIB sample preparation and SEM imaging. A gas injection system was used for depositing carbon on the surface to be cut in order to improve quality of the cross-section images and level the coating roughness. Specimens with dimensions of 1 cm^2 were laser cut out of representative areas of large samples and were used for this study.

3.3.7 Transmission Electron Microscopy TEM

In Transmission Electron Microscopy (TEM), a beam of electrons is transmitted through a ultra-thin specimen, which permits to obtain an image from the interaction with the materials. The electron beam is generally accelerated with a potential of 40 to 200 kV. The resulting spatial resolution of 0.02 nm permits to observe atoms in solid materials, contrary to the SEM technique whose resolution is generally comprised between 1 nm and 20 nm [155]. The specimen thickness in TEM is limited by the decrease of transmission through the objective aperture used and by the loss of energy [152].

A TEM lamella of the Zn-Mn coating was prepared by FIB milling to provide further details on the structure and microstructure of the layer after heat treatment at 700 °C compared to SEM-EDS analyses on cross-sections. STEM mappings and composition measurements were performed using an ARM-200 F FEG TEM. The sample was soldered to a TEM grid.

3.3.8 Electron Backscatter Diffraction EBSD

Electron Backscatter Diffraction (EBSD), which is generally coupled to SEM, provides quantitative microstructural information about the crystallographic nature of most inorganic crystalline materials and permits to reveal grain size, grain boundaries, grain orientation, texture, and to identify the crystallographic phases. In EBSD, a highly polished sample is placed at a shallow angle, generally 70° to the incident electron beam. The interaction of the primary beam with the crystal lattice generates low energy loss backscattered electrons, which permit to obtain diffraction patterns, called Kikuchi patterns with the use of an EBSD detector. Each Kikuchi band formed corresponds to each of the lattice diffracting crystal planes. Moreover, a color mapping of the crystallographic orientation of the grains can be obtained when the primary beam is scanned over the specimen surface. Accelerating voltages of up to 30 kV and incident beam currents of 1-50 nA are generally used. The spatial resolution of EBSD is related to that of SEM [156].

In the present work, a Zeiss Supra 40 SEM coupled with a TKD Bruker Optimus EBSD detector were used for EBSD measurements.

3.3.9 Glow Discharge Optical Emission Spectroscopy GDOES

In Glow Discharge Optical Emission Spectroscopy (GDOES), the samples are sputtered with Ar^+ ions with very low energy of 50 eV and generated by a glow discharge device [157]. The resulting plasma permits to atomize and excitate the sample material. The intensity of element-specific spectral lines is then measured as a function of sputtering time for depth profiling, which permits to obtain quantitative depth distribution of elements in bulk or coating materials for depths comprised between a few nanometres and approximately one hundred of micrometres [158]. Most of the elements from the periodic table can be detected. A polychromator is generally used for quantifying several elements simultaneously [158]. An average concentration is obtained over the crater surface, which generally has a diameter of 4 mm [157]. The composition of the analysed material during depth profiling is determined after calibration with reference materials of known composition and sputtering rates [158]. A significant loss of resolution with depth was reported to occur during GDOES analysis [159]. The depth resolution mainly depends on the uniformity of the sputtering rate over the craters, on the micro-roughening induced during sputtering, on the atomic mixing due to collisions of Ar^+ ions and on the grain texture. Convex and concave craters were found to form for non-optimal Ar pressures. Moreover, an edge effect was observed on the periphery of the crater, mostly due to a non-uniform sputtering rate in this region [157].

GDOES analyses were carried out on Zn-Mn coatings prior to and post to heat treatment in order to measure the chemical composition of the layers and to study the influence of heat treatment on interdiffusion mechanisms. The analyses were carried out on a GDOES GDA750 (Spectruma) with direct current. Sets of at least 3 measurements were carried out. Representative curves are shown in the present work. Additionnal cross-sections and SEM-EDS chemical analyses were performed in order to verify the thickness and the composition of the coating and calibrate the concentration-depth curves.

3.3.10 Raman Spectroscopy

Raman spectroscopy is based on the phenomenon of a change of frequency when light is scattered by molecules. The magnitude of the frequency shift between incident and scattered lights is referred to the Raman frequency. This value is generally given as a wave number, expressed in the number of waves per centimeter. The set of Raman frequencies of the scattering materials constitutes its Raman spectrum. The Raman frequencies are independent of the exciting frequency and are characteristic of the materials studied [160]. In fact, during light scattering, each material provides its own characteristic vibrational Raman spectrum, which can be used for its qualitative identification. Moreover, since the intensity of a characteristic Raman line can be considered to be proportional to the volume concentration of the material in question, Raman measurements give the possibility to obtain quantitative information, as reported by Szymanski [160].

Raman spectroscopy was used for characterizing the oxide layer formed on Zn-Mn coatings during heat treatment under oxidizing atmosphere. The analyses were carried out at room temperature using a RXN2 spectrometer (Kaiser Optical Systems) equipped with a 785 nm laser line and a spectral resolution of 2 cm^{-1}. The laser power was set to 100 mW and a lens with a focal distance of 10 mm was used. The Raman spectrum obtained was the accumulation of 40 scans with an exposure of 3 seconds per scan.

3.3.11 Anticorrosive properties

In a similar way to galvanized coatings, anticorrosive properties of Zn-Mn coatings are likely to have a strong dependency on the heat treatment conditions due to chemical diffusion between substrate and coating materials. Corrosion protection of as-deposited Zn-Mn coatings deposited from electrolytes with and without additives will be studied by means of potentiodynamic polarization curves and compared to pure electrodeposited Zn coatings for understanding the input of the use of Mn as alloying element to anticorrosive performance. Sacrificial protection will be studied by means of galvanostatic dissolution measurements prior and post to heat treatment. Similar analyses will be carried out on the commercial galvanized product in order to evaluate the performance of the novel alloys.

Galvanostatic dissolution

As reported in Section 1.4.3, cathodic corrosion protection of Zn-based coatings is generally studied by means of galvanostatic dissolution [47]. The main advantage of this technique is that the electrochemical potential of the coating can be gradually determined during dissolution, which provides essential information regarding interdiffusion layers formed during heat treatment. Indeed, the electrochemical potential of the layers, key information about the number, the composition and the relative amount of the interdiffusion layers formed during heat treatment can be provided by this method, as stated in Section 1.4.3.

Galvanostatic dissolution measurements were carried out on Zn-Mn coatings prior to and post to high temperature treatment in the conditions established for the approval of press-

hardened components for the automotive industry [161]. A Gamry ParaCell electrochemical cell containing an electrolyte composed of 100 g l^{-1} $ZnSO_4 \cdot 7H_2O$ and 200 g l^{-1} NaCl was used. A Saturated Calomel Electrode (SCE) was used as a reference electrode and was placed in a Luggin capillary. A current density of i = 10 mA cm^{-2} was applied on a surface of 1 cm^2 with a Gamry Instruments Potentiostat/Galvanostat – Model Reference 3000. A Platinum counter electrode was placed in front of the working electrode. The temperature was held at 24 °C and the electrolyte was aerated. Sets of at least 3 measurements were carried out on Zn-Mn layers prior to and post to heat treatment. Representative curves are presented in this work. The electrolyte was renewed every three measurements.

Potentiodynamic polarization test

Potentiodynamic polarization measurements are based on current-potential relations under controlled conditions and can provide significant information on corrosion rates, passivity and pitting tendencies of coating materials [162]. A schematic of the current-potential curves during anodic potentiodynamic polarization measurements is presented in Figure 23.

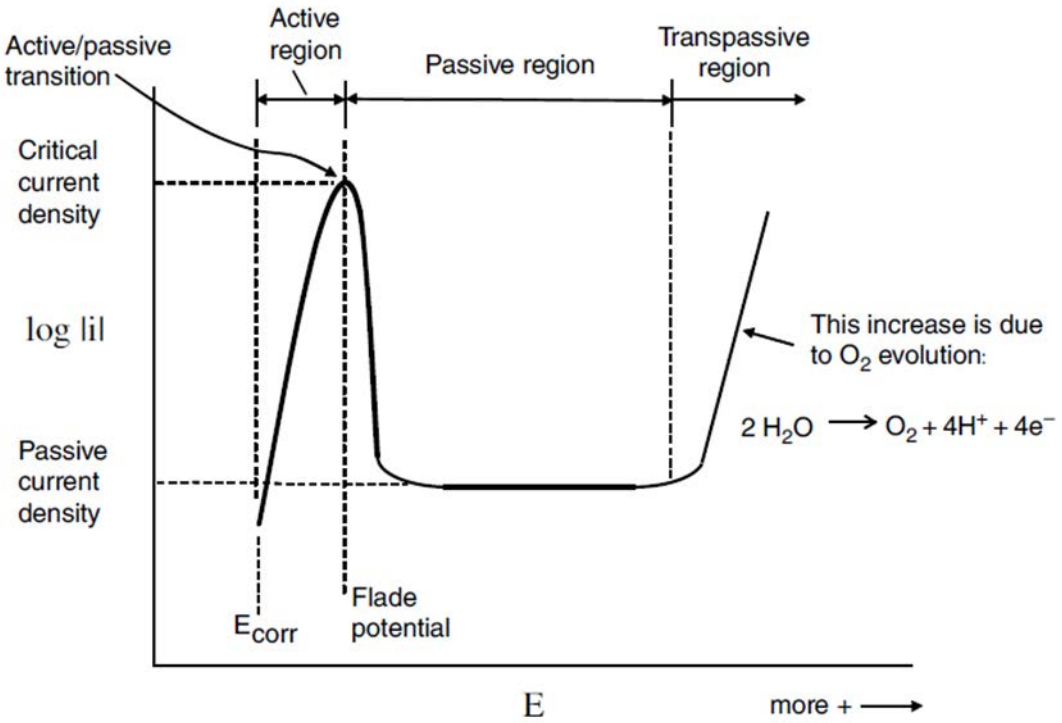

Figure 23: Schematic of an anodic polarization curve showing a passivation region [163].

As reported by McCafferty [163], the polarization measurement start at the open-circuit corrosion potential (E_{corr}) and is moved to the anodic direction. A region with active corrosion is observed and can provide the open-circuit corrosion rate on the basis of the Tafel extrapolation method. It should be noted that an additional anodic polarization step is often carried out at potentials lower than the corrosion potential for determining Tafel slopes. At a certain potential called the Flade potential, further increase in potential causes a decrease in the anodic current density. This is linked to the formation of a passive film on the metal surface. The current density in the passive region is called the passive current

density. For higher potential values, the current increases in a zone called transpassive region due to the evolution of oxygen.

In the present work, potentiodynamic polarization measurements were carried out on as-deposited Zn-Mn and Zn coatings. Mean values of the corrosion potential, corrosion current density and of the polarization resistance were obtained on the basis of five measurements carried out on each coating after an ageing time of three months in air. The measurements were carried out in a dedicated three-electrode cell (Princeton Applied Research model K0235) interfaced with a computer using the VoltaMaster4 software. A defined measurement area of 1 cm^2 was set. An Ag/AgCl/KCl(sat.) reference electrode and a platinum counter electrode were used. The potential scan was performed from a potential 150 mV more cathodic than the previously determined Open Circuit Potential (OCP) in the anodic direction with a polarization step of 0.2 mV/s. A NaCl solution (0.5 M) was used as corrosive medium for corrosion experiments and no stirring was used during the tests. The Tafel extrapolation method was used for determining corrosion rate of the Zn-based coatings on the basis of the data from polarization curves.

3.4 High temperature processes

In order to define heat treatment parameters and study the process-window of coating systems at high temperature, temperature profiles of the samples were recorded during heat treatment. The temperatures were monitored by a 1.1 mm-thick K-type thermocouple connected with the edge of blank of coated 22MnB5 steel specimens. The maximal specimen temperature was set by adjusting the furnace temperature. The dwell time during heat treatment was defined after reaching a specimen temperature of 860 °C, which corresponds to the obtaining of a full martensitic structure in 22MnB5 steel. As reported by Ademaj et al. [39], heating curves of bare and coated steels for hot forming vary significantly, mostly due to the different compositions and therefore different emissivities within the coating variants. Moreover, a different heating behavior of coated steels may occur due to the varying composition of steel, thereby affecting the heating rate and the time for achieving target temperatures. Therefore, the heating curves of all steel products were recorded with preliminary studies for defining heat treatment parameters. Very high cooling rates of more than 300 °C/s were observed during hot stamping experiments on all coated steel specimens.

Heat treatment studies were carried out on commercial and alternative coating materials in air and in presence of inert gas, with the aim of reducing oxidation mechanisms taking place at high temperature. Both experimental setups are presented in the next parts.

3.4.1 Heat treatment in air

The startup of the press tools with commercial products, namely aluminized and galvanized steels, was carried out in a type ME 45/13 furnace (Rohde, Prutting) with a power of 13 kW at a voltage of 400 V and placed beside the press. Temperatures of up to 1300 °C can be

achieved in the latter furnace with a volume of 44 liters. This furnace was also used for preliminary studies with Zn-Mn-coated specimens with various dimensions in order to evaluate the behavior of the coating alloys for high temperature treatments (Appendix 2). The parameters used will be reported in the corresponding parts.

3.4.2 Heat treatment under protective atmosphere

In order to avoid or at least to reduce oxidation of coating materials during heat treatment, a type ME 17/13 furnace (Rohde, Prutting) with a protective gas connection was used for heat treatment under less oxidizing conditions. The setup is presented in Figure 24 a) and features a chamber furnace with an internal volume of 17 litres and is suitable for temperatures of up to 1300 °C.

Before carrying out heat treatment of the samples, the oven is flooded with Argon for about 15 minutes to obtain a homogeneous distribution of protective gas. An Argon flow of 21 L/min was used for all experiments. In order to determine the effective oxygen content in the furnace during argon flow, in-situ oxygen content measurements were carried out on a type OxyP (Pro-Chem Analytik) portable unit, as presented in Figure 24 b). A steel pipe was fixed in the center of the furnace and connected to the analyser equipped with a gas pump in order to extract the gas with a sufficient air flow and cool it down prior to analysis.

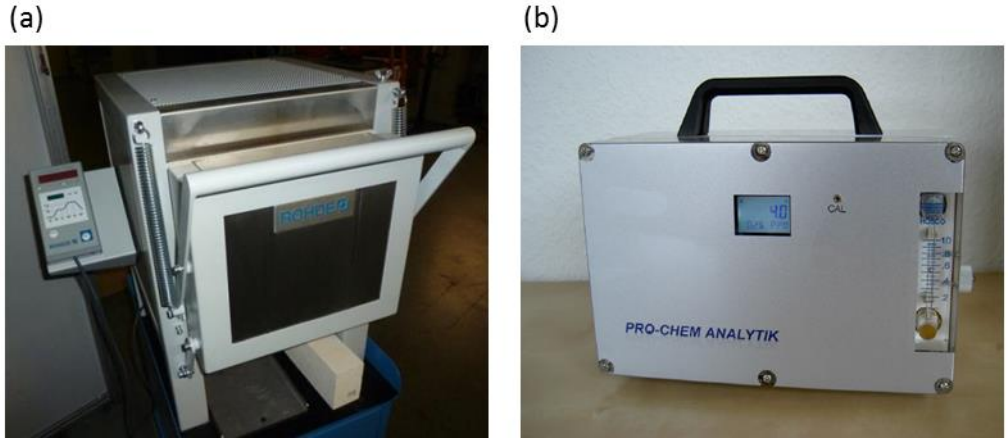

Figure 24: Furnace equipment with inert gas connection (a) and portable oxygen analyser (b) for measuring the O_2 content in the furnace during heat treatment.

In order to determine the effect of the opening of the furnace on the composition of the Argon-containing atmosphere, a preconditioning stage of the furnace with Argon was done. In addition, simultaneous recording of the O_2 content and of the temperature of heated Zn-Mn-coated specimens was carried out after the opening of the door and the insertion of the specimen into the furnace. Representative curves of a set of 5 measurements are presented in Figure 25. It should be noted that the protective atmosphere of the furnace was in contact with the oxygen-containing surrounding atmosphere for at most 4 seconds during the door opening.

Although a brief increase of the oxygen content occurs due to the door opening, the amount of O_2 in the furnace during heat treatment of Zn-Mn coatings can be considerably reduced

by the use of the inert gas flow. In fact, an O_2 content of less than 1 % is achieved in 40 seconds after insertion of the sample into the furnace, which corresponds to a sample temperature of 400 °C. This means that a significant part of the heating process, namely from 400 °C on, takes place under a protective atmosphere. It should be noted that oxidation of Zn-Mn coatings cannot be fully avoided in the present studies, since Zn-Mn coatings are exposed to an oxygen-containing atmosphere during transfer and hot stamping. However, most of the heat treatment stage is carried out in a furnace with reducing atmosphere.

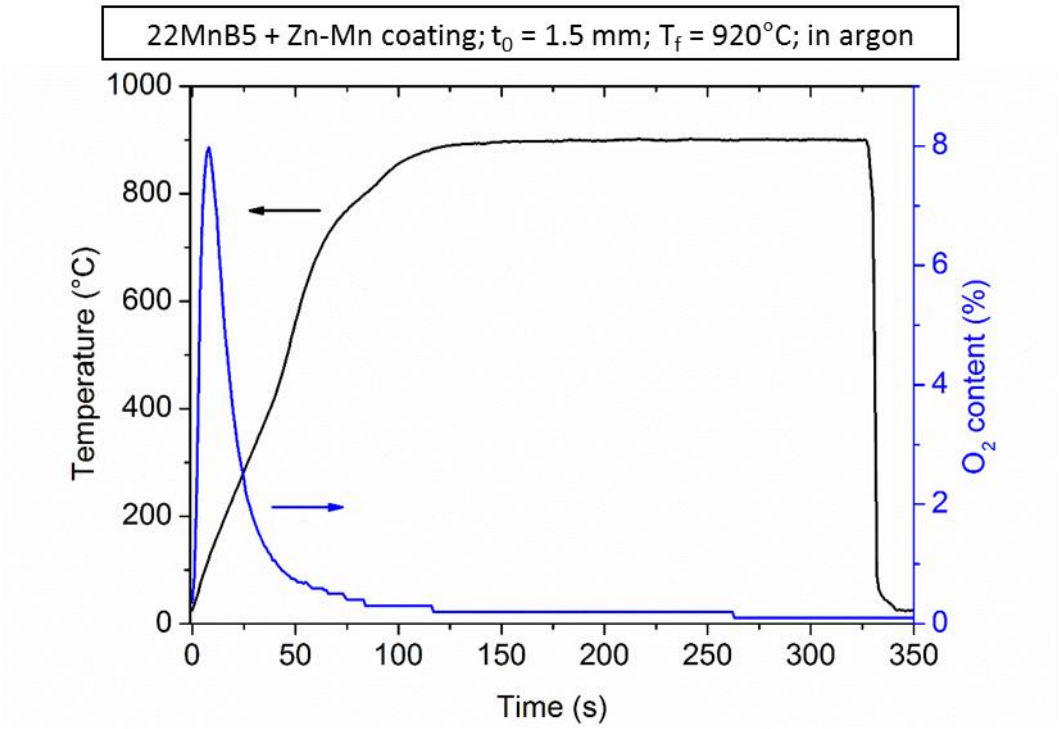

Figure 25: Evolution of the temperature of a Zn-Mn-coated 22MnB5 steel specimen (black curve) during heat treatment in a furnace with a temperature of T_f = 920 °C in presence of argon and of the O_2 content in the furnace (blue curve) after opening the door (about 4 seconds) and insertion of the sample.

3.4.3 Experimental conditions during hot stamping

With the aim of investigating the hot formability of current and alternative coating systems, press tools were specifically designed for the present study. The geometries selected permit to study the adhesion of the deposited layers with the substrate, the possible formation of defects such as micro and macro-cracks, the peeling or flaking of the coatings and to evaluate the process-window of coated products during direct hot forming process. The geometries of the press tools as well as the results from hot stamping experiments will be presented in Section 6.1.1.

In order to determine the most appropriate geometries of the press tools for achieving specific range of thinning values, hot forming simulations were carried out with Autoform plus R3.1 WIN 64 with the solver Afthermo.solver_R3.1_HOT after the construction of the respective tools with Catia V5 software. The modeling of the forming behavior of 22MnB5

was based on temperature-dependent flow curves. The temperature of the press tools was set to 20 °C and the transfer time of the blank from the furnace to the press unit was set to 7 s and included heat transfer by emission and convection. The closing time was set to 10 s for sufficient cooling of the specimens. The Heat Transfer Coefficient (HTC) was defined in dependency of the contact pressure applied by the press tools and a friction coefficient of 0.35 was used, in good accordance with the literature data [2, 14, 29, 32].

Direct hot stamping of conventional and alternative coated products was performed on a type TSP 100SO hydraulic press (Lasco, Coburg) with a force of 1,000 kN. The press unit comprises a punch and a die cooled down with an 18 °C tap water flow. Heated blanks were transferred manually to the press unit for about 5 seconds and quenched subsequently with a constant closing speed and a contact pressure of 12.5 MPa. The specimens were held in the press tools for 10 seconds.

The blank thickness and the forming behavior of the coating materials were investigated by means of cross-sectional optical microscope measurements and by optical 3D scanning (GOM ATOS Core 300) for defining the requirements of alternative coating materials. The parameters used for heat treatment will be reported in the corresponding parts.

4 Deposition and characterization of as-deposited Zn-Mn coatings

As reported in Section 1.6, Zn-Mn alloys were identified as the most promising single layer coatings for the purpose of the present study. In order to deposit layers with tailored composition, properties and behavior for the hot stamping application, it is important to understand and control the deposition process and select the most appropriate parameters. First of all, the electrolytic system for the deposition of Zn-Mn alloy coatings will be studied in Section 4.1 on the basis of small scale experiments with different plating baths in order to determine the behavior of the plating bath. The main objective of this part is to obtain compact Zn-Mn alloy layers with high Mn contents in order to increase the melting temperature of the coating. In addition, the achievement of a good surface quality with a low roughness are of interest for corrosion protection and subsequent processing. A part of the results obtained in this section were published in the Surface and Coatings Technology journal [164].

As the purpose of the present work is to assess the suitability of the coating materials for the hot forming application, it is necessary to dispose of coated specimens with large dimensions. Therefore, optimal parameters determined from the study on small samples will be used and applied for depositing Zn-Mn coatings on large-scale plates in Section 4.2. As numerous plates will be required to investigate the properties in various conditions at high temperature, the stability of the deposition process and the reproducibility of the properties of the deposits will be assessed.

Finally, Section 4.3 will be dedicated to the comprehensive materials characterization of the alloys in terms of microstructure, composition, crystallographic and anticorrosive properties. In addition to the understanding of the influence of the experimental conditions and of the electroplating system on the composition and the properties of the coatings, this study will permit to better understand the influence of heat treatment and hot stamping on the behavior and the properties of the coatings, which will be investigated in Section 5 and Section 6, respectively.

4.1 Study of the Zn-Mn electroplating system

As seen previously, various types of electrolytes and additives can be used for the deposition of Zn-Mn alloy coatings. A high current efficiency and noteworthy surface and microstructural properties were found to be obtained when a chloride electrolyte was used. In addition, the separate use of NH_4SCN and 4-HB additives was found to increase the incorporation of Mn and to reduce hydrogen evolution reaction. As reported by Nayana and Venkatesha, the combination of different additives may generate a synergetic effect on the coating properties and the performance of Zn electroplating baths [165]. Therefore, the present study is based on the investigation of Zn-Mn coatings deposited in simultaneous presence of both additives 4-HB and NH_4SCN. Comparative studies will be carried out in

absence of additives in order to evaluate the influence of the latter on the electrodeposition process and on the material properties of the layers.

In this part, the influence of the composition of different electroplating baths on the deposition process will be investigated by means of combined CV and EQCM experiments in Section 4.1.1. In addition, the influence of the deposition potential and the Zn and Mn metallic ions concentration ratio on the properties of Zn-Mn alloy coatings will be studied to define optimal conditions (Section 4.1.2) for the deposition of Zn-Mn alloys with high and reproducible Mn contents. These conditions will be used for large-scale electroplating (Section 4.2).

4.1.1 CV and EQCM studies for Zn-Mn deposition

CV studies combined with EQCM studies, as well as the definition of the optimal deposition potential were performed in a base electrolyte containing 2.8 M KCl, 0.6 M $MnCl_2$, 0.32 M H_3BO_3 and 0.1 M $ZnCl_2$, as well as in an electrolyte containing 6.5 mM NH_4SCN and 4.1 mM 4-HB additives in addition to the base composition, as reported in Section 3.2.2. The $[Mn^{2+}]/[Zn^{2+}]$ ratio of 6 was previously optimized by Bučko et al. for Zn-Mn electroplating [138]. Higher ratios of up to 12 will be studied in Section 4.1.2 for further increasing Mn content in the coatings. Electrogravimetry studies were carried out in both electroplating baths in order to understand redox mechanisms occurring during cathodic and anodic scan. Representative data are presented in Figure 26.

During CV scan to the negative direction, two reduction peaks appear at approximately -1.1 V (E_{pc1}) and -1.6 V (E_{pc2}) for respectively Zn and Mn reduction for both electrolytes. A light shift of the Zn peak to the more negative direction as well as a light shift of the Mn peak to more positive potentials can be observed for the electrolyte in presence of additives compared to the additive-free electrolyte. In the case of codeposition of two metals with different standard potentials, deposition of the less noble metal and increase of its content in the alloy will be facilitated if a shift of the reduction potential to the negative values is achieved [138]. It can therefore be assumed that higher Mn contents would be obtained in presence of additives since reduction potentials of Zn and Mn are getting closer. Alternatively, the deposition of Zn-Mn coatings at slighty lower cathodic potentials can be expected. It should be noted that the cathodic scan was reversed at -1.70 V in the case of the additive-free electrolyte for reducing hydrogen evolution reaction.

The cathodic part of the positive return path was found to be below the curve obtained during the cathodic-going scan for both voltammograms. As stated by Sylla et al. [19], this observation can be linked to the roughness of the coating, leading to more important active surface and to the associated current densities. In the present study, a transition from a dendritic to a smooth coating morphology was observed with the use of additives (see section 4.3.2) and could not be correlated with the difference between the negative and positive scans in the cathodic part of the voltammograms. Moreover, the difference in chemical nature of the underlying materials was stated to possibly affect the interaction during cathodic and anodic scans.

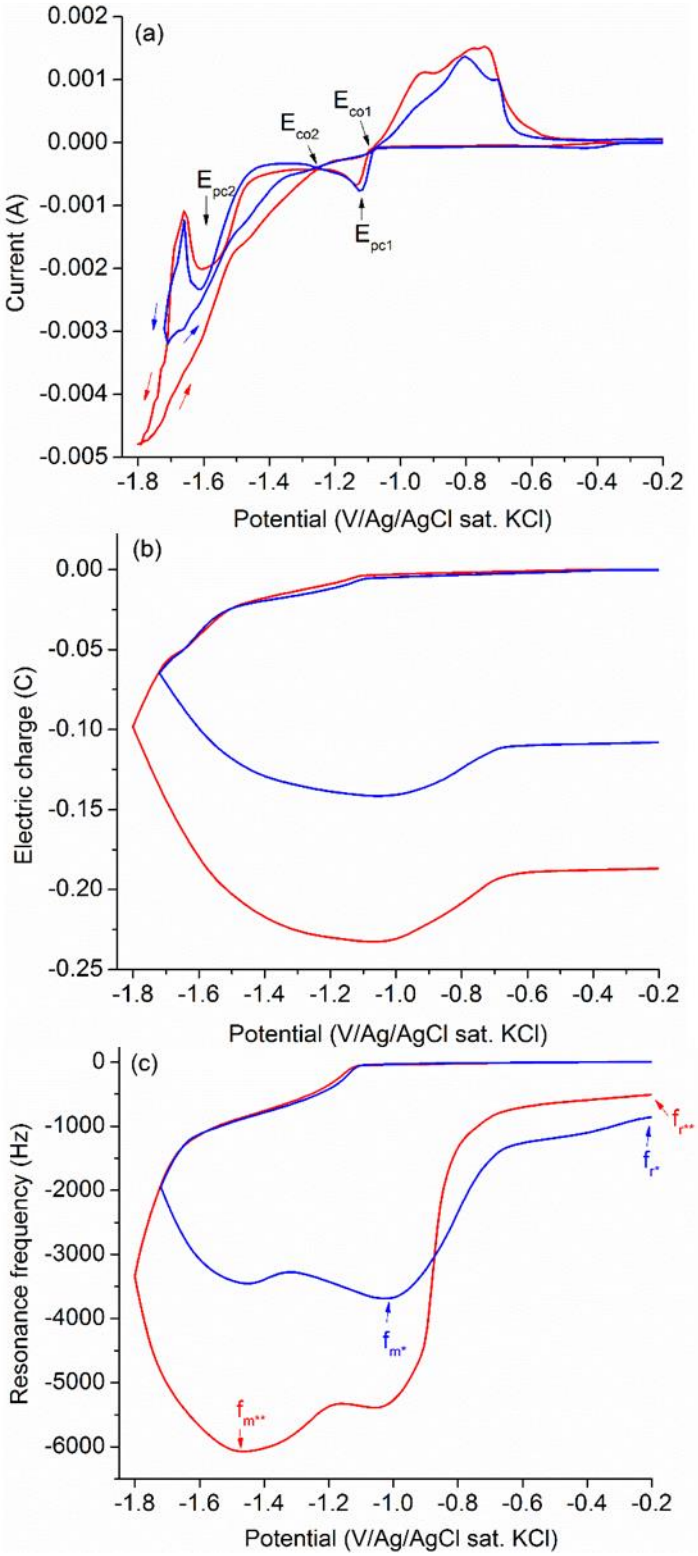

Figure 26: Cyclic voltammogram (a), electric charge (b) and quartz resonance frequency (c) of the EQCM electrode obtained during cathodic and anodic scans carried out in electrolytes (0.28 M KCl + 0.06 M $MnCl_2$ + 0.32 M H_3BO_3 + 0.01 M $ZnCl_2$) without additives (blue curve) and in presence of additives (red curve) (4.1 mM 4-HB + 0.65 mM NH_4SCN) at a scan rate of 10 mV/s; fm and fm** the maximal frequencies of solutions respectively without and with additives and f_{r*} and f_{r**} the residual frequencies of solutions respectively without and with additives.*

During anodic scan, up to four positive peaks can be identified for both electrolytes, indicating that the deposited coating may be multiphasic. Similar observations were made by Sylla et al. [131] in pyrophosphate baths and were stated to be linked to the dissolution of zinc deposited at high potentials and Zn-Mn phases at lower potentials during cathodic scan.

Although peaks formed during anodic scan may provide significant information regarding the phases deposited during cathodic scan, the present work is focused on the study of the cathodic part. On switching the direction of the potential scan to the positive direction, two cross-overs appear, indicating that new phases are formed in the system. A first cross-over appears at potentials of E_{co1**} = -1.096 V for the electrolyte with additives and at E_{co1*} = -1.085 V for the additive-free electrolyte. A similar cross-over potential at E_{co} = -1.051 V was reported by Díaz-Arista et al. [134] to be presumably associated with the equilibrium potential of the metallic ion/metal system $ZnCl_4^{2-}$/Zn(0) ($E_{ZnCl_4^{2-}/\,Zn(0)}$ = -1.053 V [166]), indicating that the formation of complexes with SCN^- is not likely to occur. A second cross-over appears at E_{co2} = -1.255 V for both electrolytes. This value is far from the value of $E_{Mn(Cl)_4^{2-}/Mn} = -1.446$ V reported in the literature [167], which means that a Zn-Mn phase is likely to deposit during cathodic scan.

The evolution of the electric charge transferred during cathodic and anodic scans in both electrolytes is presented in Figure 26 (b). Whatever the electrolyte used, the results show a residual electric charge. The higher amount of electric charge involved in the electrolyte in presence of additives can be explained by the lower reverse scan potential. By comparing the coulometric ratio between the anodic and the cathodic evolution Qa/Qc, it appears that the presence of additives decreases this ratio from 23.7 % to 19.7 %, which can be related to the wider potential range used in presence of additives, promoting hydrogen evolution reaction. In order to confirm the presence of parasite hydrogen evolution reaction and determine if the coating was completely dissolved during anodic scan, resonance frequencies of the EQCM were measured and are presented in Figure 26 (c).

The non-reversible frequency cycles indicate that coatings deposited from both electrolytes are not entirely dissolved during anodic scan, even after scanning to more anodic potentials. From these data, the ratio r_f was calculated between the residual final frequency f_r versus the observed maximum frequency f_m (see Figure 26 (c)). Thus, a decrease of r_f from 23.5 % to 9.5 % is observed when using both 4-HB and NH_4SCN additives, which corresponds to a better reversible dissolution process. A possible explanation is the growth of layers with different morphology, homogeneity and composition. Deposition and characterization investigations reported further in this work show that very smooth coatings are deposited from electrolytes with additives, whereas additive-free electrolytes lead to rough layers.

A drop of the resonance frequency can be observed for potentials more cathodic than -1.1 V, indicating that a mass uptake is occurring. This result can be explained by the presence of zinc reduction, as confirmed by the E_{pc1} reduction peak presented in Figure 26 (a). Furthermore, a frequency gain is observed after reaching the maximal frequency value located at around -1.458 V for both electrolytes, although negative current values were

obtained during CV studies in this potential range. A stronger gain occurs in the case of the electrolyte with additives. Sylla et al. [132] stated that manganese deposits were not stable and tended to dissolve in acidic media. Díaz-Arista et al. [167] studied manganese deposition from chloride electrolytes and reported that a dissolution of two different manganese species following a non-faradaic process due to the absence of oxidation current occurs during the potential scan in the positive direction.

The analytical approach of the gravimetric study was based on the following considerations. As stated by Zimmer et al. [168], the evolution of the quantity of electricity Q and the resonance frequency Δf during deposition stage can be connected by the Faraday's law (assuming 100 % current efficiency) and the Sauerbrey equation to obtain the molar mass M of the electrodeposited Zn-Mn alloy in the overall reaction (Eq. (1)):

$$(1-x)\ Zn^{2+} + x\ Mn^{2+} + 2\ e^{-} = Zn_{1-x}Mn_{x} \qquad (1)$$

where x is the molar content of Mn in the alloy. This method results in the following equation Eq. (2) for determining M ratio:

$$M_{Zn_{1-x}Mn_{x}} = 2.\frac{-\Delta f \cdot F}{K \cdot Q} \qquad (2)$$

The evolution of the molar mass of the alloys during CV study can provide significant information regarding reduction mechanisms and the influence of the use of additives on the electrochemical system. Thus, the molar mass of the metals deposited during cathodic scan between potentials of -1.0 V and -1.8 V was calculated and representative curves are presented in Figure 27.

The results show a significant increase of the molar mass of the deposit for cathodic potentials higher than -1.1 V. This value corresponds to the starting potential for zinc reduction reaction, in accordance with the presence of the Zn reduction peak observed during CV studies and reported in Figure 26. The increase of the molar mass in the case of the electrolyte with additives was found to appear at potentials slightly lower than in the case of the additive-free electrolyte. This can be explained by the light shift of zinc reduction peak to more cathodic potentials in presence of additives, as discussed in Figure 26. A maximal molar mass value of around 60 g/mol was reached for a potential of about -1.2 V, that is assigned to the formation of Zn (65.4 g/mol).

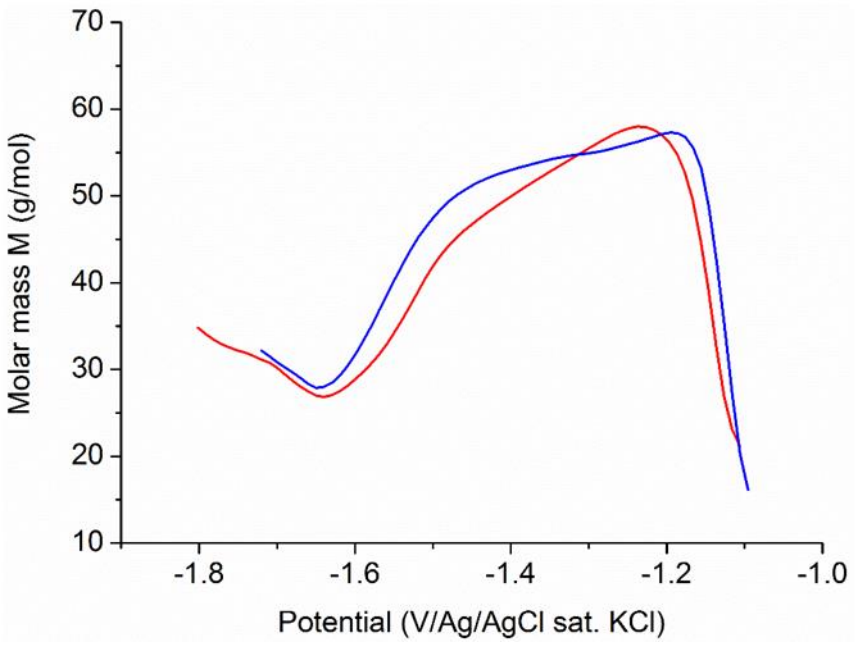

Figure 27: Evolution of molar mass on quartz electrode calculated from EQCM data during cathodic scan in electrolytes without additives (blue curve) and in presence of additives (red curve) at a scan rate of 10 mV/s; experimental conditions of Figure 26.

During scan to more cathodic potentials, the molar mass was found to decrease until a minimum value at a potential of around -1.62 V for both electrolytes. Since the molar mass of manganese is lower than that of zinc, this result can be associated with the deposition of a Zn-Mn alloy with increasing Mn content during scan to negative direction. However, the calculated molar mass decreases to values which are considerably inferior to the possible values for Zn-Mn alloys (molar mass of Mn 54.9 g/mol). The electric charge Q is overestimated due to hydrogen evolution and thus induces a reduction of the molar mass calculated from the Equation 2. A potential of -1.62 V with the lowest molar mass value would theoretically lead to the highest Mn content in the coating.

By further scanning to the cathodic direction, molar mass was found to increase whatever the electrolyte. A possible explanation for this result is an increase of the electrolyte pH in the vicinity of the working electrode due to the substantial hydrogen evolution reaction observed during CV scan at high cathodic potentials. This pH increase could induce the formation of hydroxides in the plating baths and lead to the deposition of metallic hydroxides on the quartz surface. Bučko et al. [138] reported that the buffering effect of boric acid and the complexation with Cl^- ions can prevent hydroxide formation only to a limited extent and can induce the formation of $Zn(OH)_2$ and $Mn(OH)_2$ at sufficiently high pH values. Furthermore, hydroxide species were stated to be likely to incorporate into the layer when high reduction rates occur. Moreover, a modification of the surface properties and of the stability of the quartz surface due to the formation of hydrogen bubbles may be responsible for the increase of the molar mass beyond -1.62 V.

Conclusion

From this analytic and gravimetric study, Zn and Mn peaks were found to become closer in presence of additives, leading to a possible increase in the Mn content in the coating. Moreover, deposition of Zn-Mn alloys seems to take place for potentials inferior to -1,2 V with an increasing Mn content for more cathodic potentials.

4.1.2 Definition of optimal electroplating solutions and electric parameters

In the previous section, it was shown by means of EQCM analyses that the cathodic potential applied on the electrolytic system strongly influences the molar mass and thereby the composition of the alloys. It is now important to verify the potential range for which Zn-Mn alloys can be deposited and determine the potentials for which high Mn contents can be obtained. Therefore, Zn-Mn coatings were deposited at several cathodic potentials between -1.2 V and -1.8 V from the electrolyte with both additives. The potentials were defined on the basis of the interesting potentials observed during the EQCM studies. AAS analyses were carried out on dissolved coatings for determining their chemical composition (Figure 28).

The data plotted in Figure 28 confirm the trend observed in the electrogravimetric studies. Pure zinc coatings are deposited at $E_{Deposition}$ = -1.2 V. No significant Mn content is noticed up to -1.4 V and this content increases significantly towards the more negative potentials.

A low reproducibility of the Mn content is observed when a potential of -1.76 V is used. Moreover, potentials of -1.76 V and -1.67 V provided mat coatings with a heterogeneous surface, whereas layers deposited at more positive potentials were bright and smooth. Similar observations were made by Savall et al. [120]. These particularities can be associated with the hydrogen evolution reaction causing the formation of pores and spongy layers and limiting alloy deposition. The deposition potential $E_{Deposition}$ = -1.62 V permits to obtain reproducible Mn contents of about 18 wt.% and will therefore be used for further investigations.

As reported by Bucko et al. [138], the amount of Mn incorporated into the deposits can be increased by increasing the concentration of Mn salt in the electrolyte. Therefore, coatings deposited from acidic chloride electroplating baths with higher $[Mn^{2+}]/[Zn^{2+}]$ concentration ratios than those studied in the literature were characterized by AAS in order to evaluate the possibility of further increasing Mn reduction. A constant concentration of Mn^{2+} ions of 0.6 M and $[Mn^{2+}]/[Zn^{2+}]$ ratios of 8, 10 and 12 were used in the electrolyte and deposition was carried out at a potential of $E_{Deposition}$ = -1.62 V.

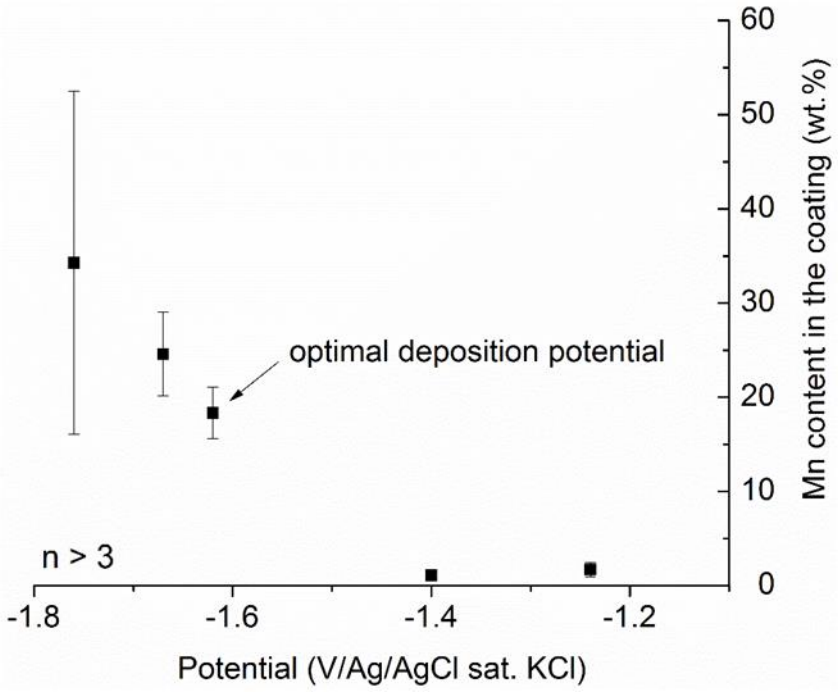

Figure 28: Influence of the cathodic deposition potential on the Mn content in coatings deposited in an electrolyte with a $[Mn^{2+}]/[Zn^{2+}]$ ratio of 6 and in presence of additives (2.8 M KCl + 0.6 M $MnCl_2$ + 0.32 M H_3BO_3 + 0.1 M $ZnCl_2$ + 4.1 mM 4-HB + 6.5 mM NH_4SCN); values determined by AAS analyses.

On the basis of the results presented in Figure 29, a significant increase in the Mn content can be observed for the tested higher $[Mn^{2+}]/[Zn^{2+}]$ ratios. However, a low reproducibility of the Mn content occurs for ratios equal or superior to 10, while coatings with reproducible Mn contents of 18 and 21 wt.% were successively obtained for ratios of 6 and 8. In a similar way, high Mn^{2+} concentrations in chloride plating baths in absence of additives were reported by Bučko et al. [138] to promote hydrogen evolution during galvanostatic deposition, to decrease current efficiency for metal reduction and to increase porosity of the layers. Ganesan et al. studied Zn-Mn coatings deposited from chloride electrolytes at -1.755 V in presence of sodium gluconate with various $[Mn^{2+}]/[Zn^{2+}]$ concentration ratios and observed a substantial increase in the Mn content in the coatings and a reduction of hydrogen evolution reaction by increasing Mn^{2+} concentration [133]. Moreover, a transition from smooth and uniform layers to non-uniform and powdery Zn-Mn coatings was observed by successively increasing Mn^{2+} concentration in the electrolyte.

A partial detachment of the Zn-Mn alloy in the form of fine powder was reported to possibly occur during deposition, reducing cathodic current efficiency. In the present work, no significant change in the coating morphology was observed for the various concentration ratios, namely no powdery coating was obtained, even at high concentration ratios. However, a transition from light gray to dark gray color was induced by the increase of the Mn^{2+} concentration. A concentration ratio of 8 leading to Zn-Mn coatings with a Mn content of up to 21 wt.% was selected as the optimal condition for further investigating and characterizing Zn-Mn coatings.

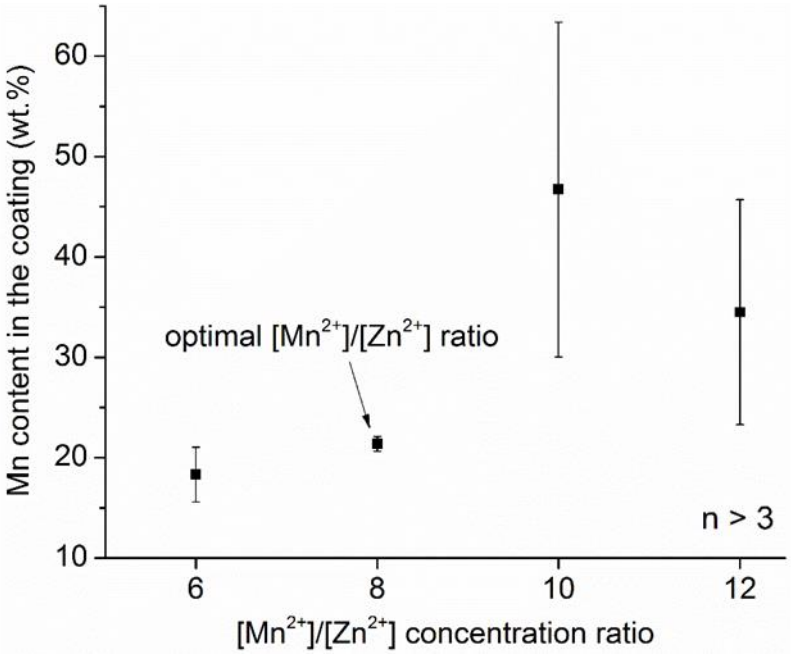

Figure 29: Influence of the $[Mn^{2+}]/[Zn^{2+}]$ ions concentration ratio of an electrolyte with additives (2.8 M KCl + 0.6 M $MnCl_2$ + 0.32 M H_3BO_3 + 4.1 mM 4-HB + 6.5 mM NH_4SCN + various concentrations of $ZnCl_2$) on the Mn content in the layers deposited on steel at a cathodic potential of $E_{Deposition}$ = -1.62 V; values determined by AAS analyses.

Conclusion

To sum up, several electroplating solutions and deposition parameters were studied and permitted to define optimal conditions. The simultaneous presence of both 4-HB and NH_4SCN additives in the electrolyte appears to promote codeposition of Mn. A deposition potential of -1.62 V and a $[Mn^{2+}]/[Zn^{2+}]$ ions concentration ratio of 8 were found to provide high and reproducible Mn contents of up to 21 wt.%.

Microstructural, crystallographic and anticorrosive properties of Zn-Mn coatings deposited with the above-mentioned parameters from electrolytes with and without additives will be studied in order to study the role of the additives on the materials properties of the layers. Zn-Mn coatings deposited with additives will be used for heat treatment and hot stamping. The composition of the electrolytes is shown in Table 6.

Table 6: Composition of the electroplating baths without and with additives used for the present work.

Electrolyte	KCl	H_3BO_3	$ZnCl_2$	$MnCl_2$	NH_4SCN	4-Hydroxybenzaldehyde
Without additives	2.8 M	0.32 M	0.075 M	0.6 M	-	-
With additives	2.8 M	0.32 M	0.075 M	0.6 M	6.5 mM	4.1 mM

4.2 Deposition of Zn-Mn coatings on large-scale plates

The present part is dedicated to the study of the electrolytic system and the experimental setup used for the deposition of Zn-Mn alloy coatings on large-scale plates. The Zn-Mn alloys were deposited from the electrolytes with the compositions listed in Table 6 and with the experimental setup presented in Section 3.2.3.

First of all, the analyses presented in Section 4.2.1 will be focused on the assessment of the homogeneity of the properties of the deposits obtained with the experimental conditions used regarding the morphology, the microstructure, the thickness, the composition and the crystallographic properties of the alloys.

The experimental procedure during electroplating of the layers on large-scale plates with the experimental setup used will be studied in Section 4.2.2 in order to define optimal parameters to obtain coated plates with reproducible compositions and properties.

On the basis of this study, it will be possible to ensure the deposition of layers with reproducible properties and to dispose of sufficient amount of coated plates for upcoming studies, in particular for heat treatment and hot forming experiments.

4.2.1 Homogeneity of Zn-Mn coatings deposited on large-scale plates

Surface morphology and composition of Zn-Mn coatings from large-scale plates

In this part, Zn-Mn alloys deposited with and without additives were characterized on various positions on the large-scale plates in order to evaluate the homogeneity of the coatings and to define interesting areas for heat treatment and characterization studies. The plates were divided into three columns and three rows, as presented in Figure 30.

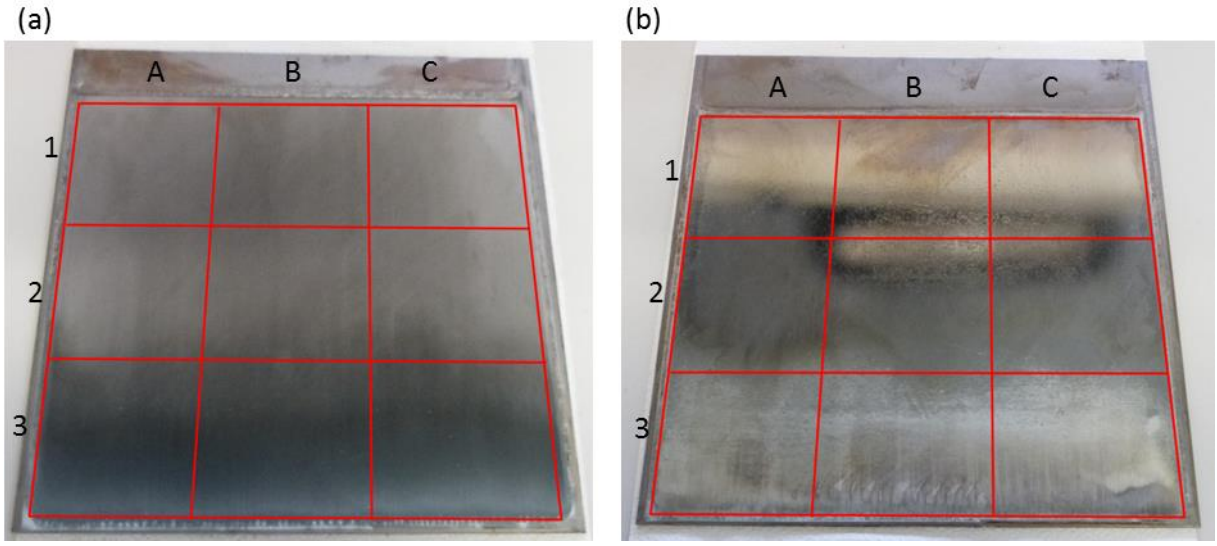

Figure 30: Large-scale steel samples coated with Zn-Mn layers deposited from electrolytes in absence (a) and in presence (b) of additives; position of the specimens cut out of the large samples for materials characterization: rows 1, 2 and 3 and columns A, B and C.

The coatings deposited on large-scale plates appear to have a heterogeneous surface appearance, in particular in the height of the plates. In presence of additives, the coating is bright in the two upper thirds of the plates, while the lower part is mat. In absence of additives, the entire coating is mat, with a light gray color on the upper two thirds of the plates, while the lower area is dark gray.

In order to link the appearance with the surface state of the coatings, the surface morphology of specimens located on rows 1, 2 and 3 (Figure 30) and deposited from both electrolytes was studied by means of SEM analyses (Figure 31).

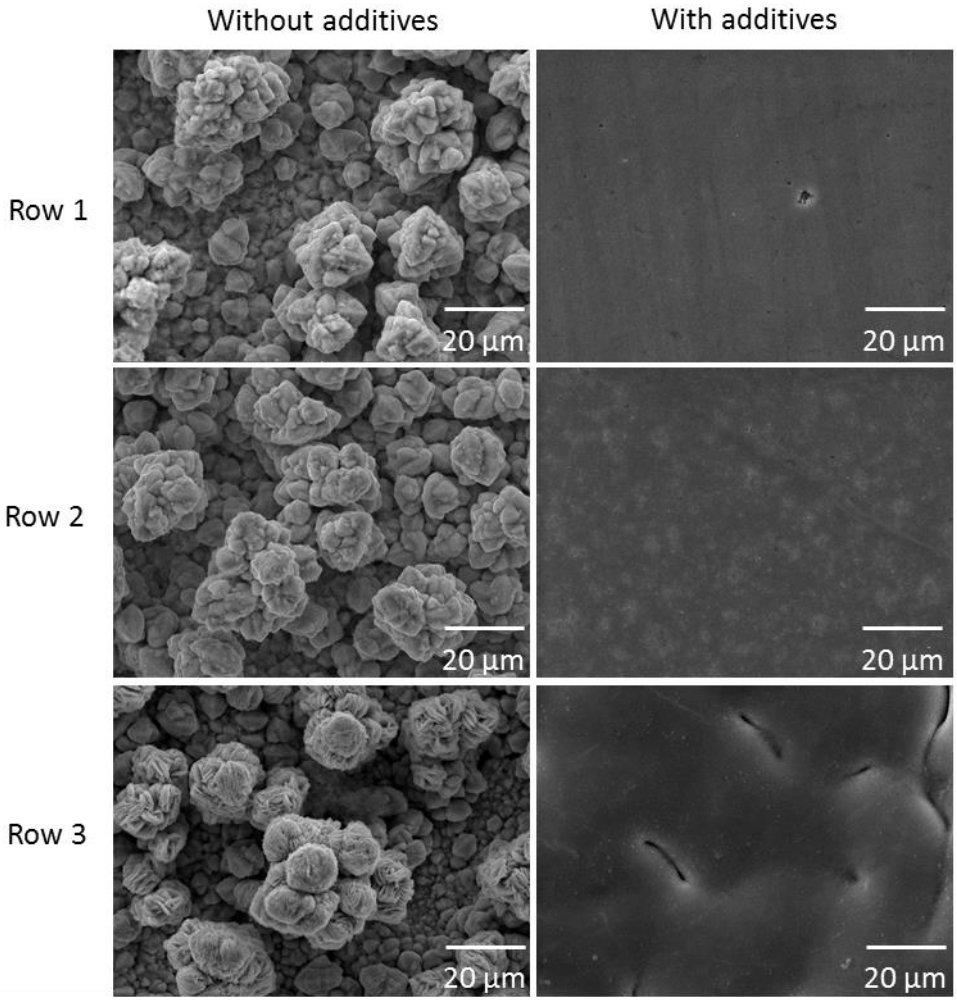

Figure 31: SEM micrographs of the surface morphology of Zn-Mn coatings deposited on steel from electrolytes in absence and in presence of additives at a magnification of 2000x; specimens cut out of large-scale plates and located on column A and rows 1, 2 and 3 (Figure 30).

It can be observed that the morphology of the coating deposited in presence of additives varies in the height. In fact, the lower area of the coating was found to be slightly rougher compared to the upper part, which is very smooth. In the case of Zn-Mn coatings deposited in absence of additives, a non-regular cauliflower-like dendritic morphology is uniformly distributed over the specimens surface. No significant difference in the coating morphology

could be observed between the upper and the lower parts of the plates. More information regarding the surface properties of both layers will be reported in Section 4.3.2.

Crystallographic characterization of Zn-Mn coatings from large-scale plates

XRD analyses were carried out on Zn-Mn coatings deposited with and without additives on rows 1, 2 and 3 of the large-scale plates (Figure 30). The corresponding patterns, presented in Figure 32, were superimposed for evaluating the heterogeneity of the crystallographic properties of the layers along the height of the plates. The two upper rows of the coating deposited in presence of additives consist of the ε_2-Zn-Mn phase. For the specimen located in the third row of the large-scale plates, the layer consists of a pure hexagonal Zn phase. The coating deposited in absence of additives (Figure 32 b)) consists of the ε_2-Zn-Mn phase with low signals of pure Zn for the first row. On the second row, the signals of the pure Zn phase increase. The third row mainly consists of signals from the Zn phase and some diffraction lines of the ε_2-Zn-Mn phase. A more detailed study of the crystallographic properties of the coatings deposited in presence and in absence of additives will be reported in Section 4.3.3.

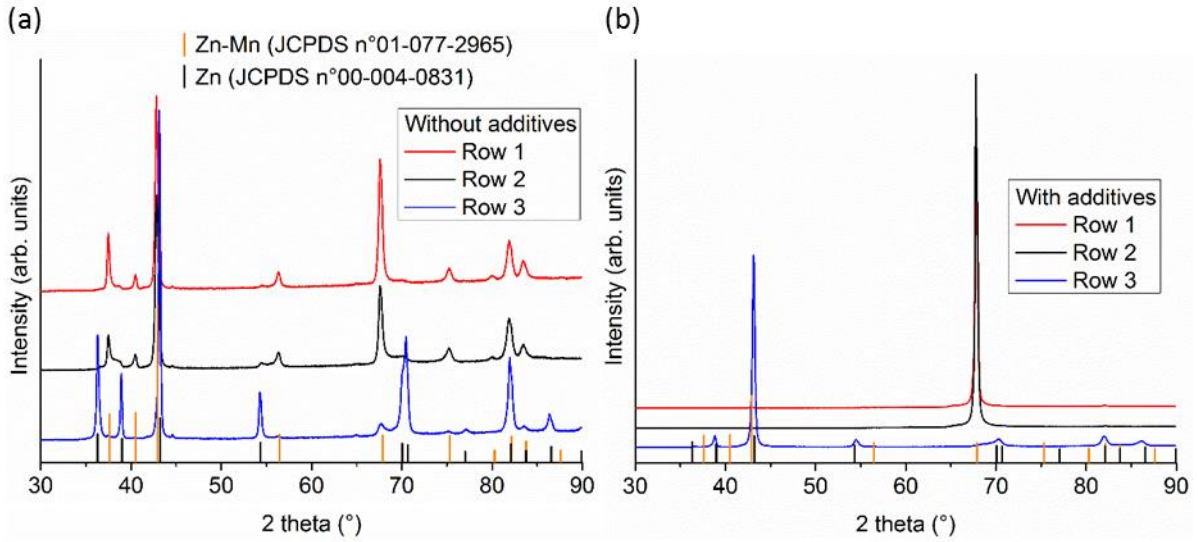

Figure 32: XRD patterns of Zn-Mn coatings located on the first (red), second (black) and third (blue) rows (Figure 30) of coatings deposited on large-scale plates from electrolytes in absence (a) and in presence (b) of additives; patterns of the identity cards JCPDS n°01-077-2965 (orange columns) of Zn-Mn and JCPDS n°00-004-0831 (black columns) of Zn.

To sum up, both Zn-Mn layers have heterogeneous crystallographic properties along the height of the large specimens. The lower part of the large plates was found to consist of a hexagonal Zn phase, while the upper part consists of a single-phase ε_2-Zn-Mn layer.

Thickness and composition of Zn-Mn coatings from large-scale plates

In order to identify a possible inhomogeneity of the composition of the layers over the surface of large-scale specimens, SEM-EDS measurements were carried out on the surface of the coating deposited in presence of both additives on several positions along the height. In

a similar way, microscope analyses were carried out on cross-sections to measure the thickness of the coating. The evolution of the Mn content in the coating and the thickness of the layer in dependency of the distance from the upper edge of the plate is presented in Table 7. The Mn content and the coating thickness values were obtained on the basis of sets of 4 and at least 50 values, respectively.

As shown in Table 7, a relatively constant coating thickness is obtained along the height of the large specimens. The high standard deviation values for the coating thickness may be related to a difference in the roughness of steel substrate and coating. More information will be reported later (Section 4.3.2).

Mn contents comprised between 14.7 and 17.3 wt.% were obtained on the upper part of the plates, namely at a distance of at most 16 cm from the upper edge of the specimen. The lower area of the coating has a much lower Mn content of at most 4.3 wt.% and corresponds to the mat area of the coating.

Table 7: Composition and thickness of a Zn-Mn coating deposited on a large-scale plate from the electrolyte with additives in dependency of the distance from the upper edge by means of SEM-EDS surface analyses and cross-sectional measurements.

Distance from the upper edge (cm)	Mn content (wt.%)	Coating thickness (µm)
4	14.7 ± 0.3	14.9 ± 1.8
8	16.8 ± 0.4	16.3 ± 3.2
12	17.3 ± 0.7	16.0 ± 2.4
16	14.8 ± 0.6	17.5 ± 2.0
18	4.3 ± 0.3	16.9 ± 2.6
19	0.1 ± 0.1	-

The heterogeneity of the properties of electrodeposited Zn-Mn coatings was already reported in the case of layers deposited from sulfate-citrate electrolytes [169]. Bučko et al. found that heterogeneous coatings were obtained in sulfate electrolytes when high current densities were applied [127]. Moreover, Fels and al. stated that the use of very cathodic potentials induced burns on the coating, which is likely to be the case for the present coatings, in particular in the bottom of the plates [170]. The authors proposed that the narrow potential range for Zn-Mn deposition, along with a fluctuation of the deposition potential during plating may induce heterogeneous Mn distribution. According to the work of Chung et al. [171], Zn-Mn coatings deposited from ionic liquids were found to be darker when high cathodic potentials were used, with the presence of a black color at the edges of the specimens. This observation was assumed to be related either to manganese deposition or “burnt” zinc after reaching the limiting current density for Zn deposition, leading to poor deposits.

In order to verify the homogeneity of the potential applied during electrodeposition over the entire working surface during electrodeposition, measurements (not shown in this work)

were carried out during electroplating. No difference was observed between the upper and the lower parts of the large-scale specimens. Stirring of the solution permitted to reduce the heterogeneity in coating morphology, but did not permit to avoid the loss of Mn on the lower part of the plates. No clear explanation could be found and would require more investigations for understanding and improving the electroplating conditions.

From the previous investigations, it appears that Zn-Mn alloy coatings located on the upper part of the large-scale plates were found to have similar crystallographic properties, high Mn contents and similar surface state, while rougher layers with a lower Mn content were obtained on the lower part of the plates. Therefore, it was chosen to use the upper part of the large-scale plates for materials characterization of Zn-Mn alloy coatings prior to and post to heat treatment and hot stamping. The study of the heat treatment behavior of Zn-Mn alloys was carried out on 60 x 45 mm wide specimens (A, B and C) laser cut out of the upper part of large-scale specimens, as presented in Figure 33.

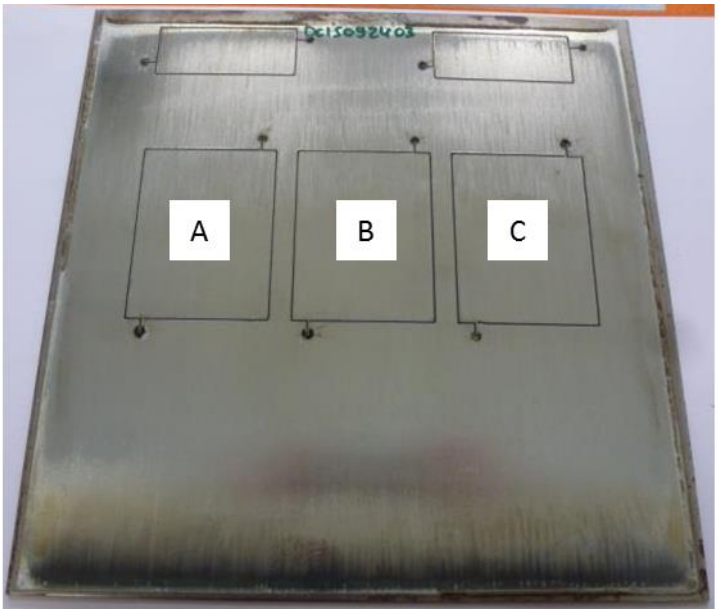

Figure 33: Position and designation of the 60 x 45 mm wide specimens laser cut out of large-scale plates and used for the study of heat treatment behavior.

In order to verify the homogeneity of the crystallographic properties Zn-Mn alloys located on the upper part of the large-scale plates and ensure a good traceability of the properties of Zn-Mn coatings prior to and post to heat treatment, XRD measurements were carried out on several positions (A, B and C) of the same plate, as presented in Figure 34.

The results show very similar diffraction patterns, which means that the crystallographic properties of the layer located on the upper part of the large-scale plates are sensibly the same. The same observation was made for all large-scale coated plates used for this study.

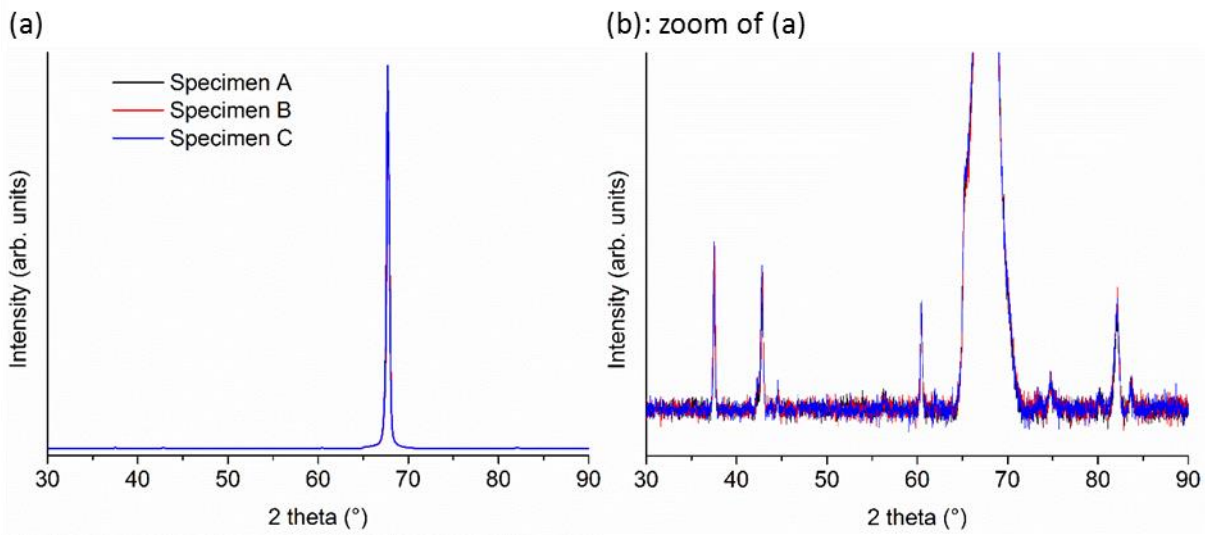

Figure 34: XRD patterns of Zn-Mn-coated specimens A, B and C (see Figure 33) cut out from a large-scale plate; complete view (a) and zoom (b) of the diffraction pattern; the intensity scale of the XRD pattern (b) was restricted to 0.8 % of the highest (110) line intensity.

4.2.2 Deposition of Zn-Mn alloy coatings on large-scale plates

In this part, the experimental conditions of the deposition of Zn-Mn coatings on large-scale plates are studied with the aim of optimizing the experimental procedure. First of all, the behavior of the electroplating bath will be studied in order to determine how many layers can be deposited with a same bath without affecting the composition and the properties of the layers. In addition, the reproducibility of the deposition process, in particular the reproducibility of the composition of the deposits obtained will be assessed by means of materials characterization of coatings deposited on several large-scale plates from new electrolytes.

Evolution of the electroplating baths

In this part, the evolution of the electroplating bath composition after several successive deposition processes of Zn-Mn coatings on large-scale panels was studied with an electrolyte in presence of both additives. AAS studies were carried out on the electrolyte after successive depositions for determining the remaining Zn and Mn contents and thereby identify any loss or enrichment of cations in the electrolyte. The initial Zn and Mn concentrations in the electrolyte were 5 g l^{-1} and 33 g l^{-1}, respectively. After each deposition process ruled by an electric charge of 44.56 Q cm^{-2}, a sample of the used electrolyte was taken and was diluted by a factor of 10000 and 50000 for AAS analysis of respectively Zn and Mn for obtaining concentrations comprised in the calibration range. Moreover, the pH of the electrolyte was adjusted to 4.3 with a 12 M HCl solution prior to each deposition.

Calibration solutions were prepared with [Zn^{2+}] and [Mn^{2+}] concentrations comprised between 0.25 and 4.00 mg l^{-1} for determining the calibration slopes of each element. The corresponding solutions were prepared by dilution of a standard solution of Mn

(1000 mg/l ± 5 mg l^{-1}; Fluka Analytical, Ref. 77036) and a standard solution of Zn (1000 mg l^{-1} ± 4 mg l^{-1}; Fluka Analytical, Ref. 18827).

The evolution of the Zn and Mn concentrations determined by AAS measurements on the diluted electrolytes in dependency of the electric charge applied during electrodeposition is presented in Figure 35. It should be noted that the evolution of Zn and Mn concentrations versus the electric charge is calculated by considering a faradic efficiency of 100 %. However, a lower current efficiency is obtained due to hydrogen evolution taking place at the working electrode during deposition. This point will be discussed later.

The reduction reaction of Equation 1 is expected to occur at the working electrode during electrodeposition, which means that a consumption of Zn^{2+} and Mn^{2+} cations from the electrolyte takes place. However, the Zn concentration in the electrolyte appears to increase during successive deposition of Zn-Mn coatings. This result can be explained by the dissolution of Zn from the counter electrode according to the following oxidation reaction:

$$Zn = Zn^{2+} + 2e^{-} \qquad \text{(Equation 3)}$$

According to the data from Figure 35, a slight decrease of the concentration of Mn occurs for electric charge values of up to 45000 C, which is linked to Mn deposition. The loss is however not significant, as a high $MnCl_2$ salt concentration is used. The higher Mn concentration values for higher electric charge values could not be explained.

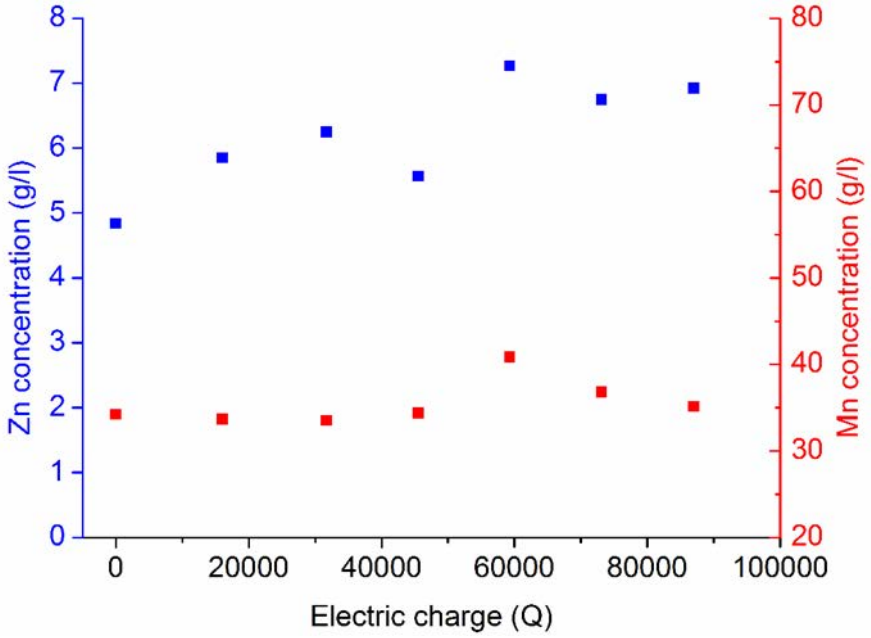

Figure 35: Evolution of Zn (blue plot) and Mn concentrations (red plot) in the electrolyte after subsequent electrodeposition of Zn-Mn coatings on large-scale plates in dependency of the applied electric charge; values determined by means of AAS analyses.

This study permitted to ascertain that the Mn concentration in the electrolyte during electrodeposition of a Zn-Mn layer on large-scale panels can be considered to remain stable, while a significant increase of the Zn content occurs. This effect could modify the relative Zn^{2+} and Mn^{2+} ions concentrations in the electrolyte and thereby influence the composition

of the deposited coatings, as discussed in the last section. The evolution of the ions concentration ratio versus the electric charge applied during successive deposition stages is presented in Figure 36. The study was conducted on three electrolytes, including that used for Figure 35. It appears that the ratio decreases as the electrolyte is reused, presumably due to the increase of the Zn content in the electrolyte. In fact, the value of the ratio decreases from 8 to approximately 7 and 6 after one and two deposition processes in all three electrolytes, respectively.

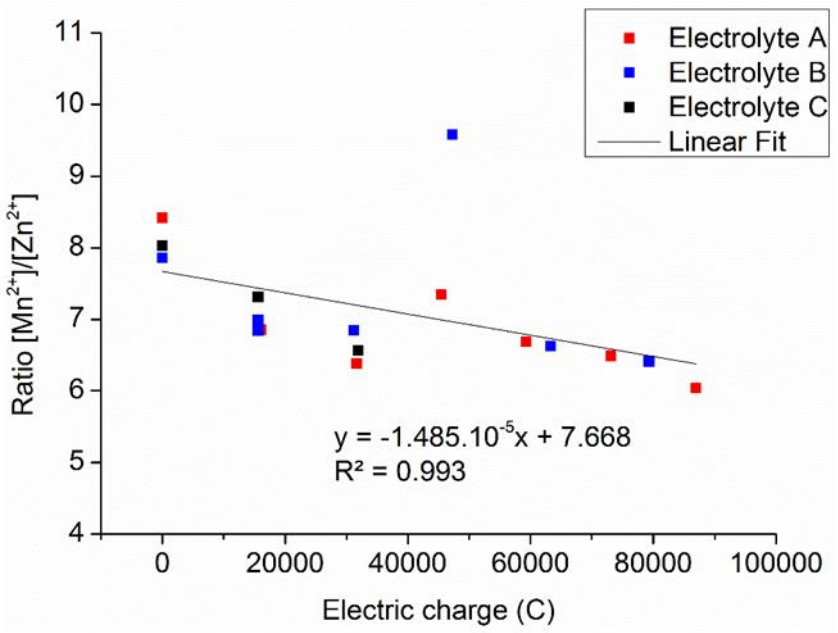

Figure 36: Evolution of the $[Mn^{2+}]/[Zn^{2+}]$ cations concentration ratio of three electrolytes (A, B and C) in dependency of the electric charge applied during successive electrodeposition processes of Zn-Mn coatings on large-scale panels; linear fit of the data (black line) with the corresponding slope; the electrolyte A was used in Figure 35.

In addition, an increase of 1.5 of the pH value of the solution was observed after each deposition process, which is likely to affect the behavior of the electroplating bath and influence the properties of the layers, such as their composition, their crystallographic or anticorrosive properties if reused. This result could be related to the hydrogen evolution reaction taking place at the working electrode during deposition, inducing a progressive increase of the electrolyte pH.

It can be concluded that a unique utilization of the electrolyte permits to maintain a constant relative concentration ratio of Zn and Mn cations with reproducible pH values and thereby to ensure a good stability of the deposition process. Therefore, the electrolyte was renewed after each deposition stage.

Reproducibility of the Zn-Mn deposits

In order to verify the stability and the reproducibility of the deposition process, several steel plates were coated with Zn-Mn layers with the electrolyte in presence of additives. A new electrolyte was used for each panel. The same experimental procedure was used for all

specimens. Chronoamperograms of the corresponding deposits are presented in Figure 37 (a). The current densities applied on the several large-scale plates were found to vary significantly, with values comprised between 11 and 21 mA cm^{-2}. As the electroplating conditions used were strictly the same for all coatings, the variations observed could be linked to the kinetics of Zn and Mn codeposition. It should be noted that the current values presented in Figure 37 depict the cathodic current applied on the entire large-scale plates and may be heterogeneous over the coating surface.

A representative cathodic current-time transient observed at the initial stage of deposition of the data shown in Figure 37 a) is presented in Figure 37 (b) and illustrates nucleation and growth mechanisms involved in Zn-Mn alloy deposition, according to Paunovic and Schlesinger [139].

After the formation of a sharp peak associated to the charging current of the double layer during the first seconds of the process, a rising current appears. This increase can be related to the nucleation and the growth of independent nuclei. A maximal value (i_A) is reached as the growth centers begin to overlap, followed by a decrease in the cathodic current when the diffusion zones around the nuclei overlap, leading to a decrease in the effective electrode surface area [139]. The cathodic current was then found to reach a minimum value (i_B) before increasing linearly until the end of the deposition process. This increase could not be explained by an increase of the electrode surface area, since very smooth layers were obtained. From these observations, the formation of a multilayer coating is likely to take place during electrodeposition under the above-mentionned conditions, as two current-time transients are formed in the first stage of deposition.

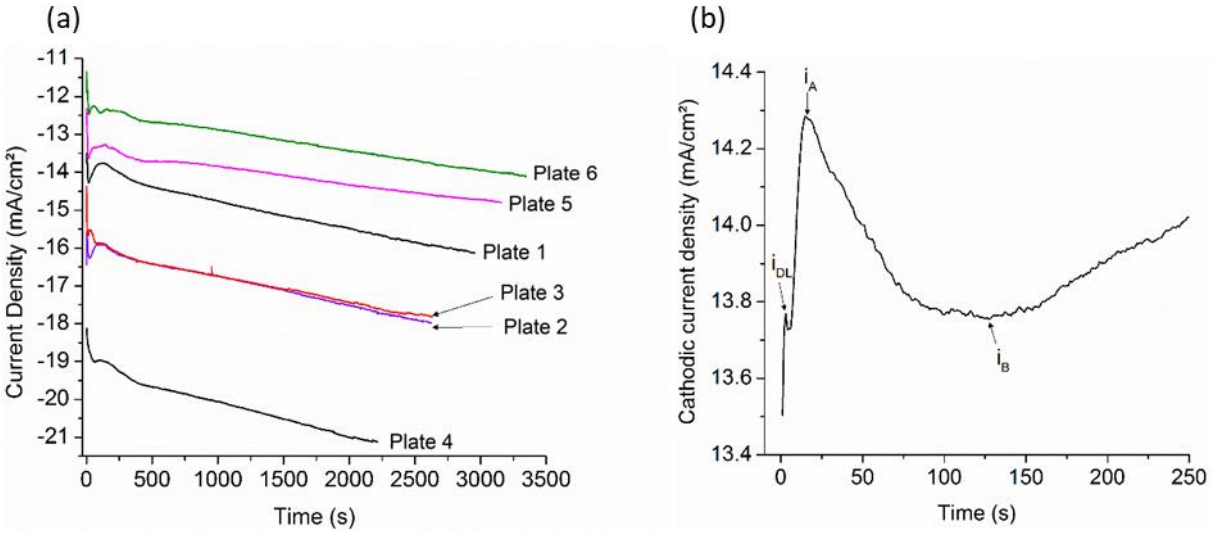

Figure 37: Chronoamperometric current-time transients of several Zn-Mn coatings deposited on large-scale specimens at a potential of -1.62 V in presence of additives (a) and representative curve for initial times of current transient (b);

SEM-EDS and XRD characterization studies were carried out on specimens laser cut out of the upper area of the same large plates (Figure 33), namely on specimen B. Semi-quantitative values of the composition of the Zn-Mn layers were obtained on the basis of sets of at least four values (Table 8). It can be seen that the Zn-Mn coatings located on the upper part of several large-scale plates have a relatively constant Mn content comprised between 14.0 and 17.4 wt.%. It is important to note that the various Mn contents could not be linked to the current densities applied for Zn-Mn electrodeposition and reported in Figure 37 a).

Table 8: Mn content of Zn-Mn coatings deposited from new electrolytes in presence of additives measured by means of SEM-EDS analyses on the surface of specimens B (Figure 33) from several large-scale plates.

Large-scale plates	Mn content (wt.%)
1	16.9 ± 0.4
2	15.9 ± 0.3
3	17.4 ± 0.2
4	16.2 ± 0.2
5	14.0 ± 0.2
6	14.4 ± 0.1

As reported earlier, specimens located on the upper part of the same plate were found to have the same crystallographic properties (Figure 34). In order to study the reproducibility of the crystallographic properties of the coatings during consecutive deposition processes, XRD measurements were carried out on specimens from several plates on the same position (Figure 38).

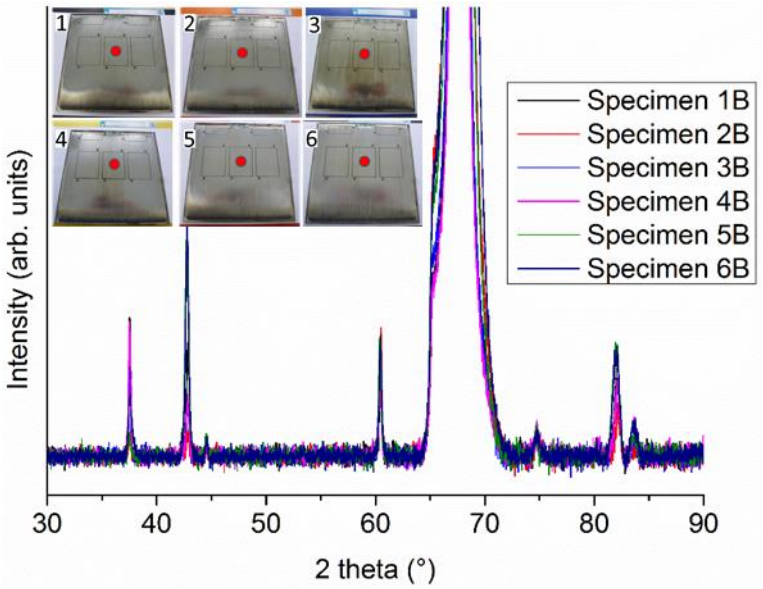

Figure 38: XRD patterns of Zn-Mn-coated specimens cut out from 6 different large-scale plates; analyses carried out on position B (Figure 33); the intensity scale of the XRD pattern was restricted to 0.8 % of the highest (110) line intensity.

The results show identic diffraction patterns, regardless of the large-scale panels. Along with the observation made from Figure 34, it can be concluded that the crystallographic properties of all specimens laser cut out of the upper part of the large-scale plates are very similar and that the experimental procedure for electrodepositing Zn-Mn coatings with the above-mentioned plating cell provides coatings with reproducible properties.

4.3 Materials characterization of as-deposited Zn-Mn coatings

This part is focused on a comprehensive materials characterization of the properties of Zn-Mn alloy coatings deposited on large-scale specimens.

First of all, the chemical composition and the microstructure of Zn-Mn layers deposited with and without additives will be investigated in Section 4.3.1 and Section 4.3.2 respectively in order to understand the influence of the use of additives on the deposition process and on the resulting materials properties. The crystallographic properties of the deposits will be studied in Section 4.3.3 by means of XRD analyses which will permit to determine the orientation of the grains and to identify the phases formed in the deposits.

Finaly, the anticorrosive properties of Zn-Mn coatings deposited with and without additives as well as pure Zn coatings will be assessed in Section 4.3.4 by means of electrochemical measurements in order to determine the influence of the presence of Mn and of the Mn content on the anticorrosive behavior of Zn-based coatings.

As the properties of the deposits were found to vary over the surface of the large-scale plates, it was chosen to carry out these investigations on the upper part of the large-scale coated plates, namely on rows 1 and 2 according to Figure 30. It is important to note that the results presented in this section describe the properties of the layers used for the study of the heat treatment behavior. On the basis of these results, it will then be possible to assess the evolution of the coating systems after heat treatment processes.

4.3.1 Chemical composition of Zn-Mn coatings

In order to determine the composition of Zn-Mn coatings deposited with and without additives, semi-quantitative analyses were carried out by means of SEM-EDS measurements on the surface of the coatings. The results are presented in Table 9.

Table 9: Zn and Mn relative contents in coatings deposited at $E_{Deposition}$ = -1.62 V in presence and in absence of additives (wt.%); values determined by SEM-EDS analyses.

Electrolyte	Mn (wt.%)	Zn (wt.%)
With additives	17 ± 1	83 ± 1
Without additives	11 ± 1	89 ± 1

The results clearly show an increase of the Mn content in the coatings by the use of additives. The additive-free bath provided deposits with a Mn content of 11 wt.%, while deposits with 17 wt.% Mn were obtained in the presence of additives.

It should be noted that the Mn content is inferior to the value of 21 wt.% obtained from the preliminary study (Section 4.1.1) on smaller surface areas. As both values were determined with two different methods, namely by AAS and SEM-EDS analyses, additional measurements were carried out on several samples with both methods in order to verify the consistency of the results (Appendix 5). Very similar Mn contents were provided by the two characterization techniques, which means that the difference in the values of the Mn content is not related to the characterization methods used. This difference can however be explained by the transition to electrodeposition under large-scale conditions.

In the case of Zn-Mn coatings deposited from electrolytes without additives, only signals from Zn and Mn elements were detected, whereas small traces of further elements such as S, C and O could be observed on Zn-Mn coatings deposited in electrolytes in presence of additives. The presence of S in Zn-Mn coatings was reported by Ortiz et al. to occur due to the use of NH_4SCN in the electroplating bath and more specifically due to the occlusion of sulfur during reduction of $Mn(SCN)_4^{2-}$ complex [114]. Furthermore, a Pourbaix-type diagram of various Mn cations was constructed from thermodynamic constants associated with the formation of complexes with Cl^-, SCN^- and NH_3 and studied through electrochemical studies by Díaz-Arista et al. [167]. The authors reported that in presence of NH_4SCN, the reduction of Mn(II) involves the species $Mn(SCN)_4^{2-}$ in the pH range 0-10. This theory was not considered as a persuasive explanation of Mn complexes formation due to the very low amount of thiocyanate anions in the electrolyte compared to available Mn^{2+} cations. Moreover, no reduction peak nor cross-over for the corresponding reduction reaction appeared during cathodic scan in the cyclic voltammetry study. As reported by Ortiz et al. [114], the presence of C, O and N in the films can be linked to the growth rate of the coatings that is greater than the rate of desorption and diffusion of the additives into the bulk solution. It can be assumed that the loss of sulfur by incorporation into the Zn-Mn layers may induce changes in the behavior of the electrolytic bath during electrodeposition.

In order to evaluate the homogeneity of the composition of Zn-Mn coatings deposited in presence of additives, depth profile analyses were carried out by means of GDOES (Figure 39). The Mn amount appears to be constant along the thickness of the coating. Moreover, the presence of O, S and C could be identified, in agreement with the SEM-EDS data.

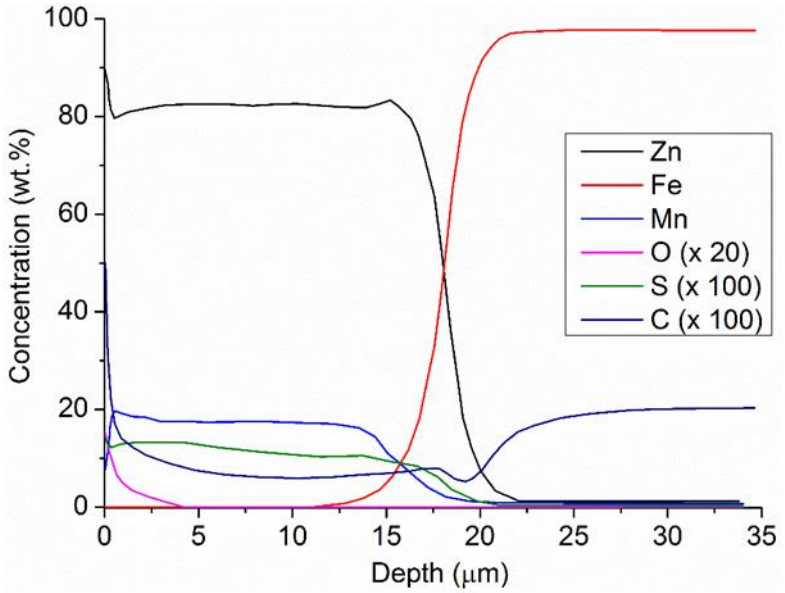

Figure 39: Representative GDOES elemental concentration profiles of a Zn-Mn coating deposited in presence of additives in dependency of the analysis depth.

It should be noted that GDOES measurements carried out on coatings deposited without additives did not provide relevant and reproducible results, most probably due to the fact that the surface is very rough and induces issues for the generation of the plasma.

4.3.2 Microstructural properties of Zn-Mn coatings

SEM analyses were carried out on the surface of Zn-Mn coatings deposited in presence and in absence of additives and located on the upper part of the large-scale plates to study the influence of the electrolyte composition on the coating morphology. Micrographs of the corresponding layers are presented in Figure 40.

Zn-Mn coatings deposited from the electrolyte without additives have a non-regular cauliflower-like dendritic morphology which is uniformly distributed over the surface (Figure 40 (a) and (b)). Similar coating morphology was reported by Bučko et al. [138] for 20 µm-thick Zn-Mn layers deposited in chloride electrolytes in presence of 4-HB at a current density of 300 mA cm^{-2}. It should be noted that in the present work, deposition current densities of 15-20 mA cm^{-2} were recorded during potentiostatic deposition for both electrolytes.

The surface of Zn-Mn coatings deposited in presence of additives is very smooth without well-defined geometric characteristics, as shown in Figure 40 (c) and (d). In addition, some pin holes are randomly observed on the coating surface, presumably due to the formation of hydrogen bubbles during deposition. It should be noted that the coatings have a good adhesion to steel surface and are not powdery. The change in the morphology of the layers deposited in presence of additives indicates a change in the nucleation and growth of crystals.

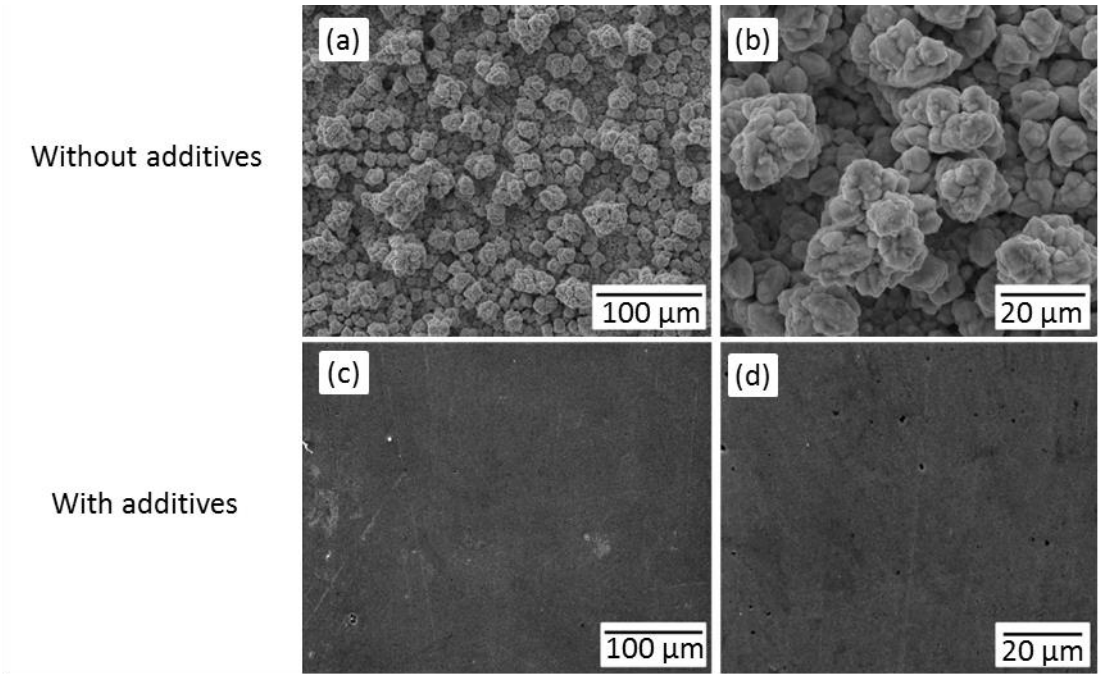

Figure 40: SEM micrographs of the surface of Zn-Mn coatings deposited on steel at $E_{Deposition}$ = -1.62 V in an electrolyte without additives at two different magnifications of 500x (a) and 2000x (b) and with additives at two different magnifications of 500x (c) and 2000x (d).

Confocal microscopy analyses were carried out on both coating systems in order to study their topography and determine their roughness. The results are presented in Figure 41.

Mean roughness values of S_a = 9.01 µm and S_a = 76.46 nm were obtained for coatings deposited respectively in absence and in presence of additives on areas of 84.88 x 63.63 µm² located on the upper part of the plates. To the best knowledge of the author, such an outstanding surface state was not described in the literature.

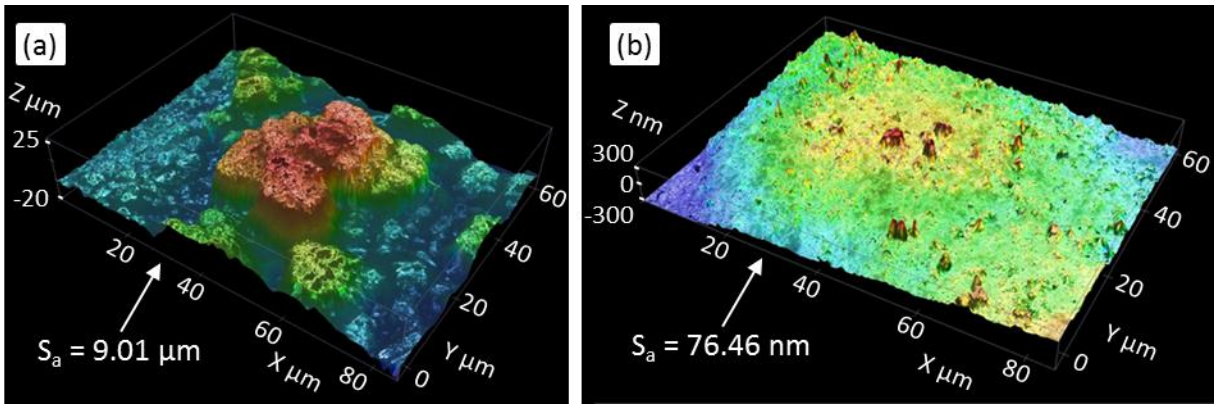

Figure 41: Surface topography and mean roughness (S_a) values of coatings deposited in absence (a) and in presence of additives (b) by means of confocal microscopy on surface areas of 84.88 x 63.63 µm².

Cross-sections were performed on Zn-Mn coatings in order to determine the thickness of the layers and evaluate the microstructure of the coatings. Representative micrographs of the corresponding cross-sections are presented in Figure 42. It should be noted that a dark

interface appears between steel substrate and coating and is due to the presence of mounting material used for the surface preparation of the specimens.

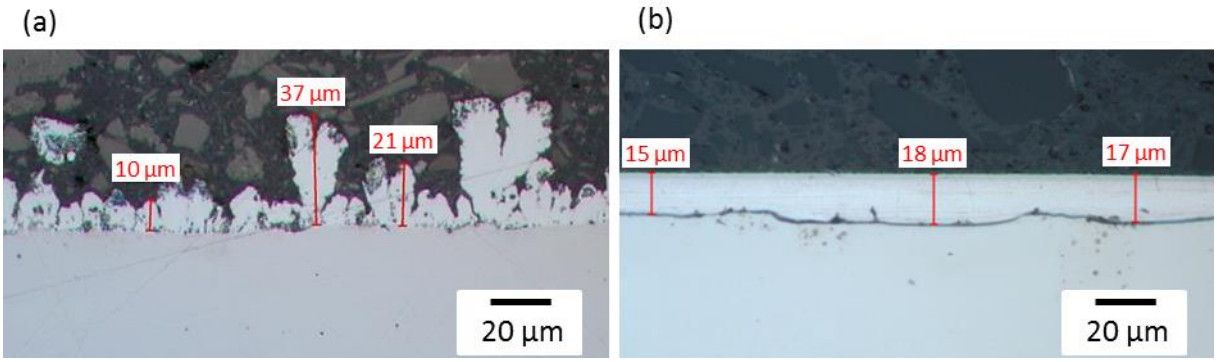

Figure 42: Cross-sectional micrographs of Zn-Mn layers deposited on steel at $E_{Deposition}$ = -1.62 V without (a) and with additives (b).

The results unambiguously show the benefit of the use of both additives, leading to compact and smooth layers. The coating appears to provide a leveling effect to the substrate roughness. In the case of Zn-Mn coatings deposited from the electrolyte free of additives, a discontinuous layer with a rough surface and compact globules was formed. An effective thickness (e) of e = 16.69 ± 1.98 µm was obtained in the case of layers deposited in presence of additives. The current efficiency η for the latter deposit containing 17 wt.% Mn (Table 9) was then calculated on the basis of redox reaction (Eq. (1)) and Faraday's law (Eq. 3)):

$$\eta\,(\%) = \frac{\rho \cdot e \cdot S \cdot z \cdot F}{Q \cdot M_{Zn_xMn_y}} \times 100 \qquad (3)$$

where ρ is the volumic mass of 7.104 g cm^{-3} of the alloy (JCPDS n°01-077-2965), e the thickness of the layer, S the surface of the coated area, z the number of electrons exchanged during metal-ion reduction, F the Faraday's constant and Q the electric charge applied during electrodeposition. A current efficiency of 81.1 % was obtained under these conditions. It should be noted that this value depicts the behavior of the complete large-scale plates and does not take the heterogeneities of the properties of the layers into consideration. Similar current efficiencies were reported by Bučko et al. [138] for Zn-Mn coatings deposited galvanostatically from chloride electrolytes containing 4-HB as additive. Since layers obtained from the electrolyte without additives were found to have a considerably rough surface, it was chosen not to measure any mean coating thickness in order to avoid inaccuracies in the calculation of the current efficiency from Equation 3.

SEM-FIB analyses were carried out on a Zn-Mn layer deposited in presence of additives for further studying the microstructure of the coating. The specimens with a surface of 1 cm^2 were laser cut out of the upper part of large-scale plates for good compatibility with the experimental setup. Representative micrographs are presented in Figure 43 and were obtained with the Secondary Electrons Secondary Ions (SESI) detector, which provides images with metallographic details such as grain orientation contrast. A carbon layer was deposited on the coating surface in order to improve image quality and stability of the ion beam.

It should be noted that a „curtain effect“ inducing light vertical lines across the layer and parallel to the incident ion beam is visible in the micrographs. This particularity was stated to occur due to insufficient FIB carbon deposition and improper milling parameters [172, 173]. Reducing the ion beam current or its acceleration voltage permits to increase surface quality, but induces a considerable increase of milling and polishing times, in particular for such large cross-sections. In the present case, this effect was most probably related to the presence of pores and cracks in the coating, which may have resulted in the instability of the ion beam.

Two layers can be observed in the coating presented in Figure 43. The first layer located on the surface of the substrate steel is likely to consist of equiaxed grains with a low size of approximately 50 nm and contains a significant amount of voids. This porosity may be related to hydrogen evolution reaction during Zn-Mn codeposition.

The second layer located in the upper part of the coating has horizontal sublayers in the form of strata with a thickness of up to 100 nm. As no variation of the cathodic current with time is observed in the chronoamperograms during deposition (Figure 37) and as the cathodic potential applied does not vary, the strata do not seem to form due to electric processes. However, the periodical formation of closely spaced parallel lines was reported to be related to variations of the overpotential and to the interruption of the growth, corresponding to the so-called banded structure [174]. This structure was already observed for Ni-P alloy coatings and was presumably induced by cyclic depletion and enrichment of metal ions in the diffusion layer [175]. According to the same authors, higher hydrogen evolution takes place in the event of an increase of the overpotential, leading to an increase of the pH and thereby to a variation in the composition of the coating. Therefore, it is possible that a slight change in the composition of the coating takes place on these areas. It should be noted that no variation of the coating composition was observed during GDOES analyses, presumably due to the low thickness of the strata. Convection and pulse plating were stated to stabilize the amount of metal ions concentrations and of the pH at the deposit surface [175]. A lower amount of voids can be observed (Figure 43 b)) in the second layer compared with the first layer, possibly due to a transition in the growth mechanisms from fine grains to columnar grains, along with a reduction of hydrogen evolution during deposition.

A possible explanation of the presence of cracks in the second layer is the handling and the surface preparation of the specimens, or a possible presence of residual stresses in the coating. Moreover, cracks could be linked to the presence of discontinuities in terms of current density distribution during electroplating [139]. Vertical stripes can be observed in the second layer, which evidence the formation of elongated grains towards the growth direction of the deposit. This layer can be considered to have a columnar structure.

No difference could be observed between the composition of both layers during GDOES and SEM-EDS analyses on cross sections. Therefore, it can be considered that only a change of the microstructure and of the crystallography occurs during electrodeposition under these conditions.

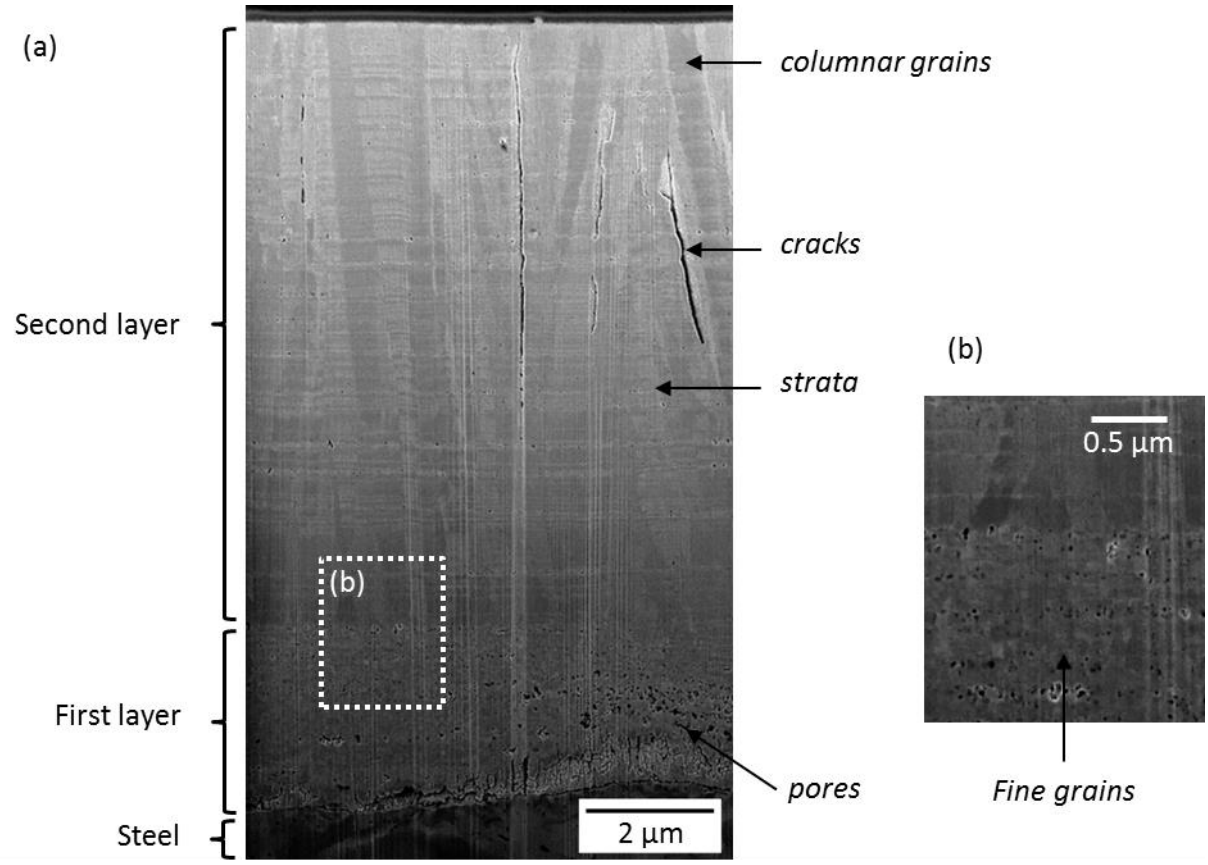

Figure 43: Cross-sectional micrographs of an as-deposited Zn-Mn coating after SEM-FIB milling and polishing; overview of the coating (a) and magnification of the interface between the first and the second layers (b).

The first layer observed in Figure 43 can be considered to have a fine-grained or equiaxed structure, typically consisting of grains with a size of 10 to 100 nm and generally obtained under conditions with high current densities and hydrated oxides [139]. Metallic deposits with a columnar structure, such as the second layer of the Zn-Mn coating (Figure 43) have a low strength and hardness but possess a high degree of ductility and are generally obtained under low current densities. This structure is common for compact thin films and results from preferred growth in certain crystal directions [139]. Thus, a transition from a fine grain size near the substrate to a coarse columnar grain size is likely to take place for the Zn-Mn coatings deposited in the current work.

The successive formation of two layers during electrodeposition was already reported in the literature. Blonde et al. reported the transition from an equiaxed structure to a structure with elongated nanograins for copper coatings electrodeposited using a pulsed-current [176]. As reported by Paunovic and Schlesinger, the development of a columnar microstructure can be explained by the growth competition between adjacent grains. Low-surface-energy grains grow faster than high-energy grains, which results in an increase in mean grain size with increased coating thickness [139]. In addition, it can be assumed that a change in the stability of the plating process, namely local variations of the pH, of the temperature or of the composition of the electrolyte may have induced a transition in the growth mechanisms.

4.3.3 Crystallographic properties of Zn-Mn coatings

XRD analyses were carried out on Zn-Mn coatings deposited with and without additives in order to investigate their crystallographic properties. The corresponding XRD patterns are presented in Figure 44.

It is important to note that both experimental XRD patterns of Zn-Mn alloys correspond to the hexagonal close-packed ε_2–Zn-Mn phase (JCPDS n° 01-077-2965) presented in Figure 44 c), irrespective of the electrolyte used for electrodeposition and of the Mn content. The latter crystallographic phase was reported by Okamoto et al. to form in a Mn content range of 8.8 and 21.9 wt.% and to belong to the ε-phase field, thermodynamically stable between 220 °C and 815 °C [106]. The inner areas of the ε-phase domain were found to differ in the literature data, leading to inconsistencies about the crystallographic properties of the latter phase. Some works proposed the presence of three similar regions called ε, ε_1 and ε_2, while other authors reported the presence of a unique wide ε domain [106].

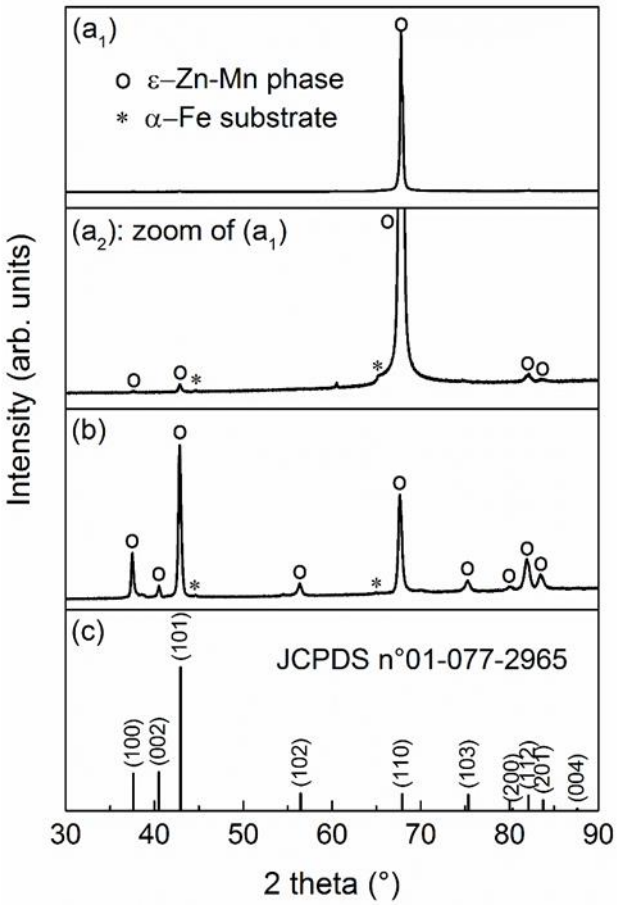

Figure 44: X-ray Diffraction (XRD) patterns of Zn-Mn coatings electrodeposited at $E_{Deposition}$ = -1.62 V from electrolytes with ((a_1) and (a_2)) and without (b) additives and columns (c) of the identity card JCPDS n°01-077-2965; the intensity scale of the XRD pattern of the Zn-Mn coatings deposited in presence of additives (a_2) was restricted to 10 % of the (110) line intensity and is based on the data from pattern (a_1).

In the present case, the cell parameters of the ε_2–Zn-Mn phase were fitted with a = b = 2.76200 Å and c = 4.46087 Å. The lattice parameters were reported by the latter authors to depend on the composition of the alloy, as shown in Figure 45. According to the literature data, a Mn content of 17.4 wt.% can be expected for the above-mentioned value of the cell parameter a [106]. This result is close to the experimental value of 17 wt.% obtained in Table 3.

From these investigations, it appears that a metastable phase was formed by electrodeposition under the considered conditions. Various work reported the same results for electrodeposited Zn-Mn coatings, as presented in Table 10.

On the basis of the phase diagram presented in Figure 13 and by considering a Mn content of 17 wt.%, a melting temperature of about 725 °C is obtained for the Zn-Mn alloy. Thus, a significant increase of the melting temperature of the coating can be achieved by the alloying of Zn with Mn, compared to the melting point of 419.6 °C of pure Zn [106]. As reported in Section 1.6, this particularity may permit to reduce or suppress LME during hot press forming. However, chemical diffusion is likely to take place during heat austenitizing, leading to a modification of the relative Zn and Mn content in the alloy, in addition to the presence of Fe in the layer parameters.

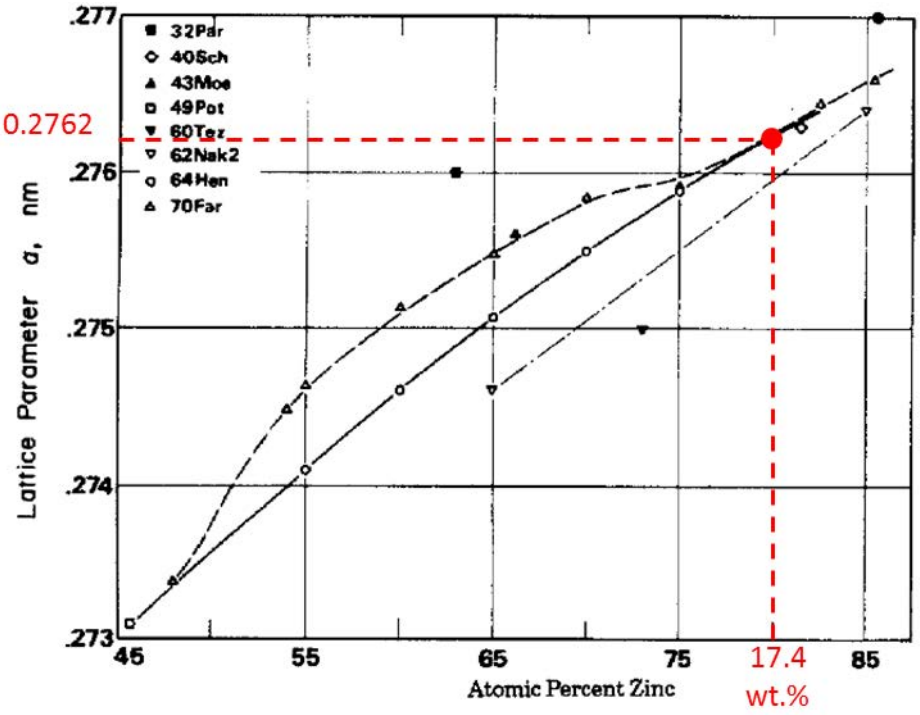

Figure 45: Relation between lattice parameter a and Mn content of the ε-Zn-Mn phase from the literature data [106]; Mn content corresponding to the experimental value of a obtained for the Zn-Mn alloy coating deposited with additives in the present work (red).

In the case of coatings electroplated with additives, the (110) intense and main diffraction line suggests that the ε–Zn-Mn crystals are preferentially oriented with their basal plane perpendicular to the steel substrate. In order to further investigate this change in the

microstructure by the use of additives, comparative pole figures were calculated from specific diffraction experiments with a home made software JTEX [150]. The (110) and the (002) pole figures obtained from the XRD measurements are presented in Figure 46.

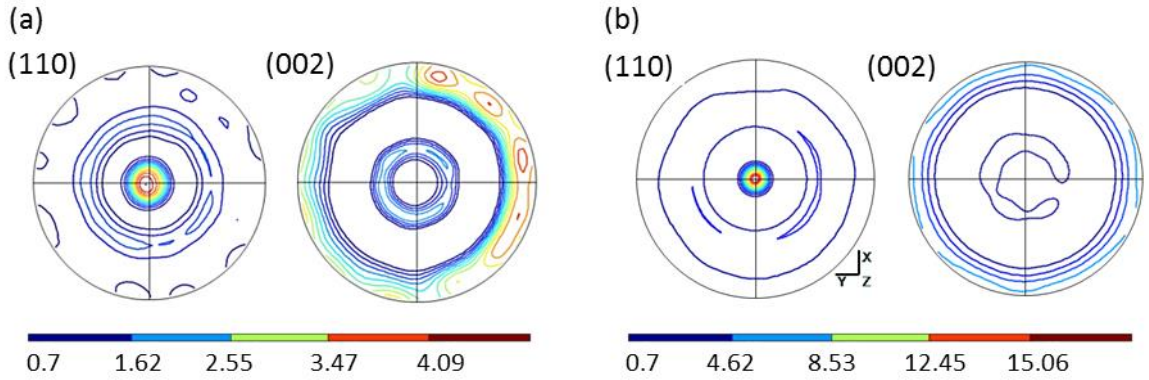

Figure 46: (110) and (002) pole figures of Zn-Mn coatings deposited from electrolytes without (a) and with (b) additives, calculated from JTEX software [150].

The results confirm the preferential crystallographic orientation along the <110> direction for Zn-Mn layers deposited in presence of additives, with a texture intensity of 15. Such a texture is commonly known as a fiber texture. A <110> fiber texture also appears for deposits obtained in absence of additives, but with a lower texture intensity of 4. The concentric circle in the (110) pole figure presented in Figure 46 (a) is larger than the one shown in Figure 46 (b), indicating a slight dispersion of the fiber texture.

The texture of electrodeposited films was reported by Paunovic and Schlesinger [139] to depend on electrochemical parameters and not on substrate properties when a deposit thickness of more than 1 µm is used, which is the case in the present study. In fact, the texture is influenced by the deposition current density, the bath pH, the potential, the bath composition, the temperature and many other parameters [139, 177]. Besides, additional factors may be the plastic deformation caused by the internal stresses in the deposit during growth as well as the overvoltage during deposition [177]. The presence of a texture influences various properties such as corrosion resistance, hardness, magnetic properties or contact resistance [139, 178]. In addition, mechanical, anticorrosive, thermal and forming properties of the Zn-Mn deposits may be affected. Therefore, the fiber texture obtained in presence of additives should be considered during characterization studies.

The preferential orientation along the <110> direction was observed in several works for monophasic ε-Zn-Mn coatings deposited in chloride electrolytes and containing about 20 wt.% Mn (Table 10). However, no or only partial information regarding the composition of the electrolytes used was reported in the literature data. Moreover, no texture intensity was calculated in the corresponding works. The present work permitted to quantify the importance of the presence of both additives on the crystallographic texture of the coatings on the basis of pole figure measurements.

It should be noted that these XRD analyses may not provide crystallographic information of the entire coating, as an attenuation of intensity of X-rays is caused by their absorption

[147]. In order to evaluate the limits of detection during XRD measurements, the penetration depth of the X-ray beam was determined using the AbsorbDX software.

Table 10: Electroplating conditions and crystallographic properties of Zn-Mn coatings in the literature data.

Electrolyte	Additive	wt.% Mn	Zn-Mn phase	Preferential orientation	Reference
Pyrophosphate	-	16	ε	<002>	Sylla et al. [128]
Pyrophosphate	Not provided	21	ε, γ	-	Sylla et al. [128]
Citrate	EDTA	17	γ, ε	-	Müller et al. [124]
Citrate	EDTA	25	ε, γ	-	Müller et al. [124]
Citrate	EDTA	30	ε	-	Müller et al. [124]
Chloride	NH_4SCN	6.2	ε, α	ε <002>, α <111>	Díaz-Arista et al. [134]
Chloride	Fra 700 (McDermid), Brightener(not provided)	20	ε	<110>	Savall et al. [120]
Chloride	-	11	ε	-	Sylla et al. [132]
Chloride	Not provided	19.2	ε	<110>	Sylla et al. [131]
Chloride	Not provided	10.3	ε	-	Sylla et al. [131]
Chloride	-	10	ε	<101>	Bučko et al. [127]
Chloride	NH_4SCN, 4-HB	17	ε	<110> (high)	Present work
Chloride	-	11	ε	<110> (low)	Present work

The calculated angle-dependent penetration depth is presented in Figure 47.

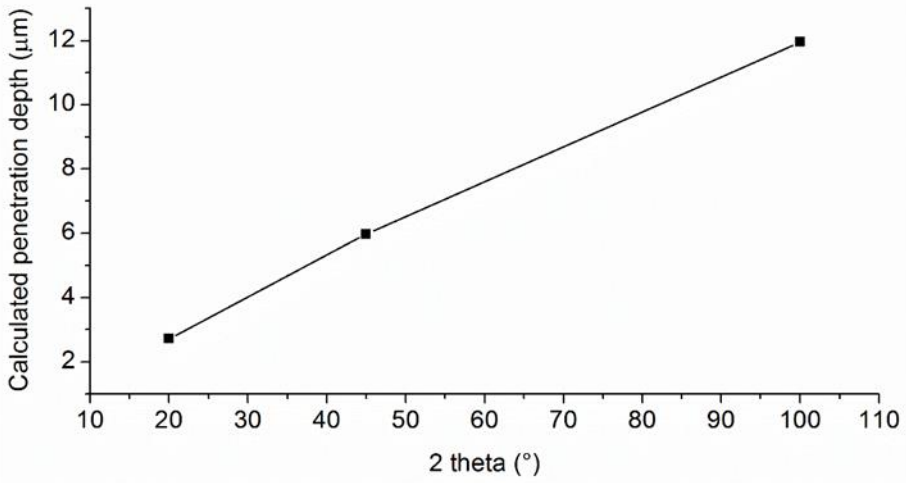

Figure 47: X-ray penetration depth in a Zn-Mn coating calculated using the AbsorbDX software and by considering a density of 7.104 g/cm³ (JCPDS n°01-077-2965), a wavelength of 1.5406 Å, a contribution of 90 % to the diffracted beam and in the Bragg condition.

A penetration depth of at most 12 µm is obtained at 90° with a contribution of 90 % to the diffracted beam. As the Zn-Mn layers have a thickness of approximately 17 µm, the diffraction data may describe predominantly the properties of the upper layer of the coating.

EBSD measurements were carried out on the surface of Zn-Mn coatings deposited in presence of additives in order to study the microstructure of the coating surface, as well as the orientation, the size and the number of grains. The positions of the atoms of the coating were set on the basis of the identity card of the ε_2–Zn-Mn (JCPDS n°01-077-2965).

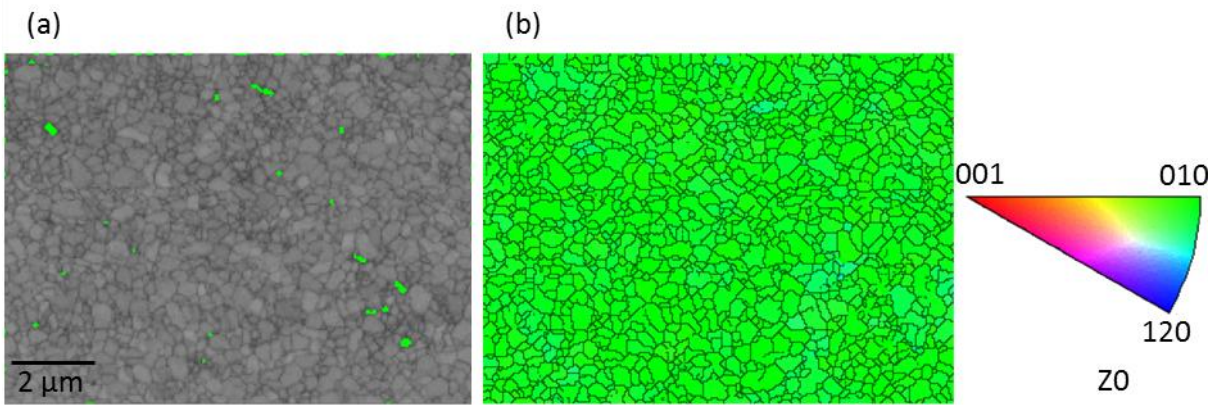

Figure 48: Band contrast (BC) map (a) and inverse pole figure (IPF) map of the orientation mapping (b) of the surface of a Zn-Mn coating deposited in presence of additives; measurement steps of 0.05 µm; sample direction along the y axis.

The gray-scaled Band Contrast (BC) map shown in Figure 48 a) provides image-like maps showing the coating microstructure in a qualitative way, in a similar way to SEM or light microscope [156]. The coating appears to principally consist of fine grains with a mean diameter of 0.268 ± 0.138 µm and an average surface of 0.071 ± 0.074 µm². Several grains, shown in green, could not be indexed, presumably due to a concave or convexe surface.

Inverse Pole Figures (IPF) orientation maps are generally used for studying materials with strong fiber textures and for understanding preferred orientation parallel to a given sample direction [156]. The IPF map shown in Figure 48 b) shows a unique color for all grains, which proves the presence of a significant preferential orientation of the grains. On the basis of the stereographic unit triangle (Figure 48 b)) showing the crystal directions that are parallel to the specimen direction, it is clear that the grains are oriented along the <110> direction.

In order to confirm the presence of the preferential orientation of the grains and to further investigate the microstructure of as-deposited Zn-Mn coatings, EBSD measurements were carried out on cross-sections (Figure 49). The results show that the first micrometers of the coating close to the substrate (Region 1) could not be indexed due to the absence of kikuchi bands, which could be explained by the formation of an intermediary layer with very fine grains at the early stages of the deposition process, as reported in Figure 44. On top of this thin layer, the coating consists of very fine grains elongated towards the growth direction of the deposit with lengths of up to several micrometers.

In good accordance with the results reported in the previous investigations, the as-deposited Zn-Mn coatings appear to have a preferential orientation along the <110> direction, as proved by the representation of most of the grains in blue (Figure 49 b)). As visible in Figure 49 (Region 2), it appears that a rupture of the microstructure of the coating occurs in the form of sublayers. The formation of intermediary layers during electrodeposit growth was already observed during SEM-FIB studies (Figure 44) and could be explained by a variation of the pH or the ionic concentrations of the electroplating bath at the vicinity of the working electrode during deposition, modifying the crystallographic properties of the resulting alloy.

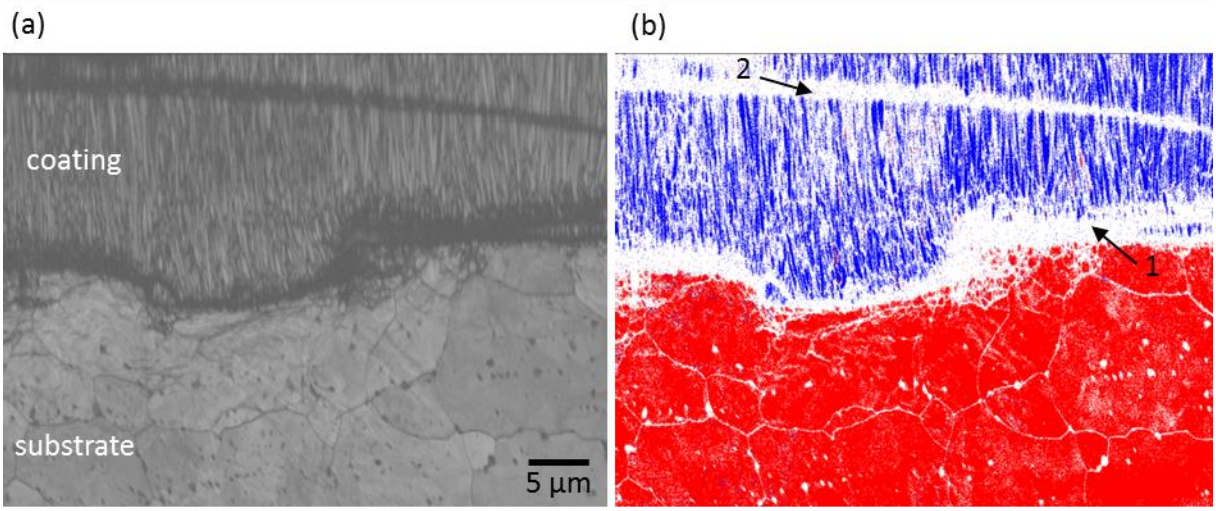

Figure 49: Band contrast (BC) map (a) and orientation mapping (b) of a cross-section of an as-deposited Zn-Mn coating; color representation of iron (red) and of the ε_2–Zn-Mn phase of the coating (JCPDS n°01-077-2965) (blue); measurement steps of 0.05 µm.

4.3.4 Anticorrosive properties of Zn-Mn coatings

Electrochemical corrosion behavior of Zn-Mn coatings in chloride environment

In order to investigate the corrosion behavior of Zn-Mn coatings deposited from electrolytes with and without additives, potentiodynamic polarization (Tafel) measurements were performed in a 0.5 M NaCl solution, which is appropriate for activating corrosion mechanisms due to chloride ions. In addition, electroplated Zn coatings were used for evaluating protective effect of the alloying with Mn. Figure 50 shows typical Tafel polarization curves.

Whatever the analysed coatings, the shapes of the curves are similar. A plateau is observed in the cathodic part of the potential scan and is characteristic of processes controlled by diffusion. This potential range is associated with the reduction of dissolved oxygen in the electrolyte [114].

Moreover, the anodic part of all curves exhibits a potential domain around -0.4 V where the current density drops. This drop appears to take place at potentials slightly more cathodic for the Zn-Mn layers. This observation was reported in several works to be linked to the formation of more compact passive layers made of Zn salts and various Mn oxides, inducing

changes in the catalytic activity for cathodic oxygen reduction [133]. However, in the present work, the current density in this potential domain is around 10 mA/cm², which is relatively too important to be considered as a passive current. Further surface analysis should be performed in order to have a better understanding of the origin of this current transient.

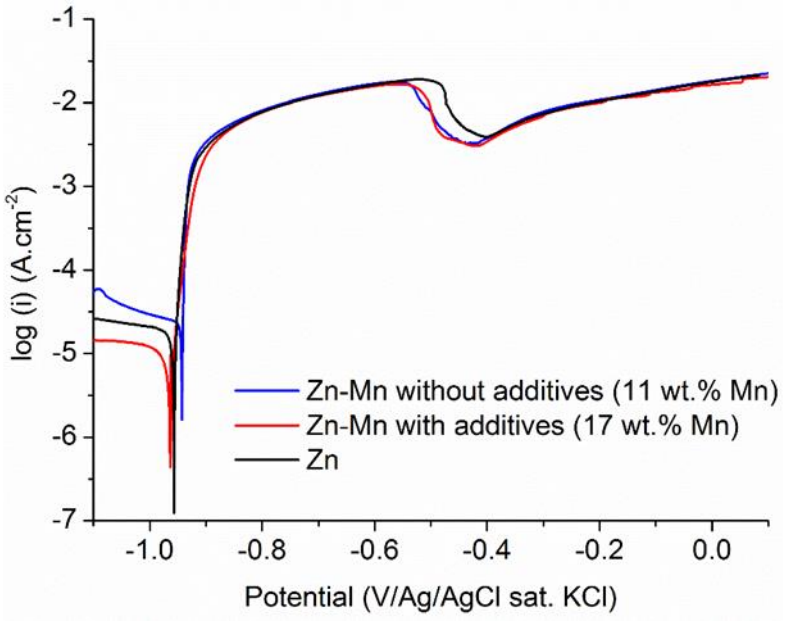

Figure 50: Linear polarization curves of pure Zn (black curve) and Zn-Mn alloys deposited at a potential of $E_{Deposition}$ = -1.62 V in presence (red curve) and in absence (blue curve) of additives.

The corrosion potential (E_{corr}), corrosion current (i_{corr}) and polarization resistance (R_p) were determined from potentiodynamic polarization plot extrapolation according to the Tafel approach. The average data, evaluated on the basis of sets of 3 to 5 samples, are presented in Figure 51. It should be noted that the method used is not strictly appropriate in the case of these measurements. In fact, a plateau was observed in the cathodic part of the scan which is related to a diffusion limited current. This particularity is in contradiction with the Tafel hypothesis for which electrochemical phenomena are controlled by charge transfer. However, tendencies can be observed between the different materials studied.

Several works [114, 123] stated that the use of Mn leads to a decrease of the corrosion potential compared to pure Zn layers, due to the more negative potential of Mn. In the present study, a slight negative shift of the E_{corr} value of Zn-Mn alloys deposited in presence of additives is observed compared to that of coatings synthesized in the additive-free electrolyte, accordingly to the increase of the Mn content. However the E_{corr} mean value of Zn-Mn coatings with the largest content of Mn is surprisingly closer to that of the Zn layer.

As would be expected, the use of additives results in the decrease of corrosion current density by comparison with Zn layers. However, Zn-Mn coatings deposited without additives have a higher corrosion current density than pure Zn coatings, indicating that the presence of Mn in the coating is not sufficient for improving corrosion protection of Zn layers. Similar observations were reported in the work of Bučko et al. [127] in which Zn-Mn coatings with

higher Mn contents did not provide higher corrosion protection. In the present study, the high corrosion current density for Zn-Mn deposited without additives can be explained by the dendritic morphology of the coating. A significant increase in the polarization resistance of Zn-Mn coatings by a factor of two was obtained by using additives. In presence of additives, the Zn-Mn layers provide a higher polarization resistance than pure Zn coatings, which can be explained by their smooth surface, their high Mn content and their texture.

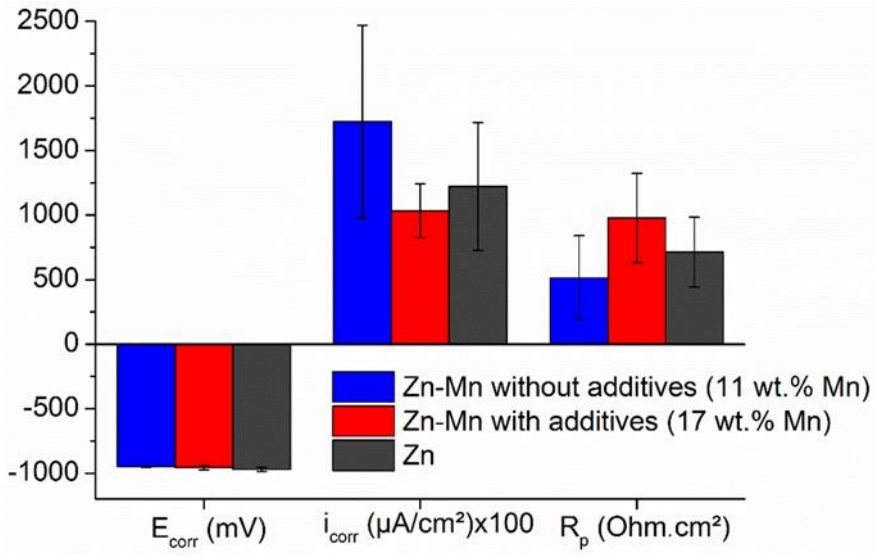

Figure 51: Corrosion parameters E_{corr}, i_{corr} and R_p in a 0.5 M NaCl solution of electrodeposited Zn (black columns) and Zn-Mn alloy coatings deposited from electrolytes with (red columns) and without additives (blue columns); results obtained from potentiodynamic polarization studies.

According to the works of Ganesan et al. [133] and Sylla et al. [131], alloy coatings consisting of the ε-Zn-Mn phase provide the best corrosion protection. On the basis of the results reported in the current work, the presence of an ε-Zn-Mn phase is not sufficient to provide better corrosion protection than Zn coatings, since Zn-Mn layers deposited from the additive-free electrolyte and consisting of a pure ε-Zn-Mn phase were found to have a higher corrosion current density and a lower polarization resistance than pure Zn layers. It appears that the benefit of Mn in Zn layers is suppressed if the surface state is dentritic with high density of pores and open porosity, as observed in Figure 42 a).

Galvanostatic dissolution of as-deposited Zn-Mn coatings

As reported in Section 3.3.11, galvanostatic dissolution of Zn-based coatings permits to determine essential information regarding the number, the relative amount and the electrochemical potential of intermetallic phases formed during heat treatment. This method permits thereby to evaluate the process window of coating materials in terms of corrosion resistance after high temperature processes.

Galvanostatic dissolution measurements were carried out on various locations on the upper part of large plates coated in presence of additives in order to study the electrochemical properties of the coatings and to verify the reproducibility of the electrodeposition process.

The evolution of the electrochemical potential of the Zn-Mn coatings deposited in presence of additives in dependency of the dissolution time is presented in Figure 52. In all, 18 measurements were carried out on four plates with the aim of providing statistic data regarding the coating behavior. The average values of the potentials of Zn-Mn and steel materials, as well as the total duration for coating dissolution are presented in Figure 52 b).

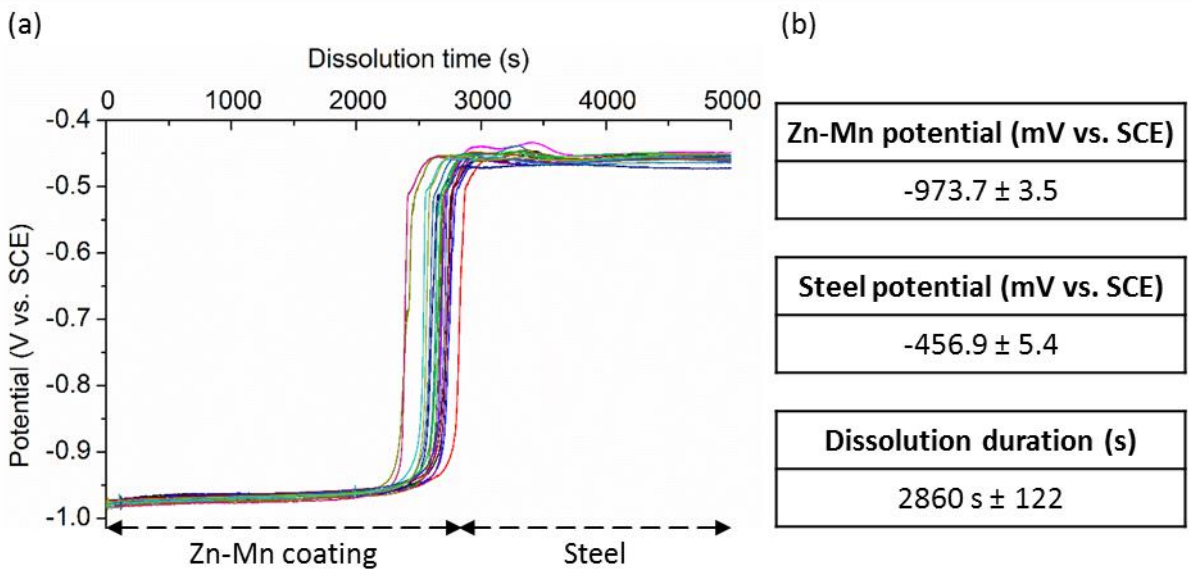

Figure 52: Evolution of the electrochemical potential of Zn-Mn-coated steel in dependency of the dissolution time by means of galvanostatic dissolution measurements carried out on the upper part of plates coated with Zn-Mn layers deposited in presence of additives (a); mean values of the potential of steel and Zn-Mn materials and total duration of dissolution of the coatings (b).

From these results, it can be observed that a relatively constant duration of 2860 s is required for the dissolution of the electrodeposited Zn-Mn coatings (Figure 52 b)), which means that the thickness of the coating is sensibly the same. Moreover, the electrochemical potential of Zn-Mn coatings and steel were found to be very similar for all measurements, regardless of the position of the analyses. Furthermore, it can be observed that the Zn-Mn coating provides sacrificial protection to steel, as the layer has an electrochemical potential more than 500 mV lower than that of steel. These results will permit to study the influence of heat treatment on the anticorrosive properties of Zn-Mn coatings (Section 5.3).

4.3.5 Overview of the materials properties of electrodeposited Zn-Mn alloys [EN + FR]

In this section, comprehensive studies were carried out to determine the microstructural, the crystallographic and the anticorrosive properties of Zn-Mn alloy coatings electrodeposited on large-scale plates with the electrolytic deposition conditions reported in Section 4.1 and with the experimental procedure defined in Section 4.2. The following main conclusions can be drawn on the basis of the results obtained in this section.

First of all, a Mn content of 17 wt.% was obtained by the simultaneous use of both 4-HB and NH_4SCN additive and was found to be constant across the thickness of the deposits. Although this value is much lower than that desired in the framework of this study in order to increase the melting temperature of the alloys, it is important to note that the deposition of layers with higher Mn contents could be achieved but was found to lead to a degradation of the surface properties of the coatings and to a low reproducibility. The presence of traces of sulfur observed in the layers could be explained by the incorporation of NH_4SCN additive during deposition. This result may induce changes in the behavior of the electroplating system. In addition, an outstanding surface state with a very low roughness could be achieved along with a clear leveling effect for the substrate roughness. Cross-sectional studies permitted to observe that a transition in the microstructure of the layers takes place during deposition, namely from an equiaxed structure with very fine grains for the first micrometers of the deposits to a columnar microstructure for the upper part of the coating. The coatings were found to be compact and to have a light gray and bright appearance.

On the other hand, rough deposits with a non-regular cauliflower-like dendritic morphology were obtained from electrolytes without additives. Such a surface state is likely to have negative effects on the anticorrosive behavior of the layers. Besides, lower Mn contents of about 11 wt.% were obtained in comparison with Zn-Mn alloys deposited with additives. On the basis of these results, it appears that the use of both additives permits to provide deposits with more interesting microstructural properties and composition, in good accordance with the observations reported in Section 4.1.

In presence of additives, deposits are composed of a ε_2-Zn-Mn-HCP single phase. According to the composition of the layers and to the binary phase diagram of Zn-Mn alloys, a melting temperature of approximately 725 °C can be obtained in these conditions. This value is much higher than that of pure Zn coatings and may be beneficial for the behavior of the coatings for the hot stamping application. A strong fiber texture along the <110> direction is observed in presence of additives, indicating that the crystals are well oriented with their basal plane normal to the surface. Such a preferential orientation was not found in the literature and may influence the thermal stability, the formability and the anticorrosive behavior of the layers.

Finally, it was found that Zn-Mn coatings deposited in presence of additives provide better anticorrosive behavior than pure Zn deposits and Zn-Mn layers deposited without additives. This result can be associated with the high Mn content, the smooth surface of the layers and the preferential crystallographic orientation which could decrease the dissolution rate of the alloy. Due to the presence of an electrochemical potential more than 500 mV lower than that of steel, a significant sacrificial effect is obtained with the considered layers.

The studies carried out in this part permitted to determine a wide range of properties of the Zn-Mn alloys deposited in the conditions considered for this work. On the basis of the results obtained, it will be possible to investigate the influence of heat treatment and hot stamping on the properties and on the performance of the coatings in the next parts.

Bilan des propriétés des alliages Zn-Mn électrodéposés

Dans cette partie, de nombreuses études de caractérisation ont été menées afin de déterminer les propriétés microstructurales, cristallographiques et anticorrosives d'alliages Zn-Mn électrodéposés sur de larges plaques d'acier avec les conditions d'électrodéposition fixées dans le Chapitre 4.1 et avec la procédure expérimentale définie dans la Section 4.2. Les conclusions suivantes peuvent être établies à partir des résultats obtenus dans cette partie.

Tout d'abord, une teneur massique en Mn de 17 % a été obtenue par l'utilisation simultanée des additifs 4-HB et NH_4SCN. Cette valeur est constante sur toute l'épaisseur des revêtements. Même si cette teneur est beaucoup plus faible que le domaine de compositions souhaité dans le cadre de cette étude afin d'augmenter suffisamment la température de fusion des alliages, il est important de préciser que des revêtements avec de plus fortes teneurs en Mn ont pu être obtenus mais ont été sujets à de mauvaises qualités de surface et une mauvaise reproductibilité. La présence de traces de soufre dans les couches déposées peut être expliquée par l'incorporation de l'additif NH_4SCN pendant la déposition. Il se peut que ce résultat ait une influence sur le comportement du système électrolytique.

En outre, un état de surface remarquable avec une très faible rugosité ainsi qu'un effet nivelant de la rugosité du substrat a pu être obtenu avec les conditions d'élaboration choisies. Les analyses effectuées en coupe ont permis d'observer qu'une transition intervient dans la microstructure des revêtements lors de la déposition avec la formation d'une structure équi-axe avec des grains très fins pour les premiers micromètres de la couche suivie de la formation d'une microstructure colonnaire pour la partie supérieure du revêtement. Les couches obtenues sont compactes, ont une couleur gris clair et sont brillantes. En revanche, les revêtements déposés à partir de bains sans additifs possèdent une morphologie dendritique irrégulière de type chou-fleurs. Il est fort probable qu'un tel état de surface ait des effets négatifs sur le comportement anticorrosion des revêtements. De plus, des teneurs en Mn plus faibles d'environ 11 % ont été obtenues comparé aux alliages Zn-Mn déposés en présence d'additifs. D'après ces résultats, il apparait que l'utilisation des deux additifs permet d'obtenir des revêtements avec des propriétés microstructurales et des compositions plus intéressantes, conformément aux observations faites dans le Chapitre 4.1.

En présence d'additifs, les revêtements sont composés d'une seule phase cristallographique ε_2-Zn-Mn de type hexagonal. D'après la composition des revêtements et du diagramme de phases binaire des alliages Zn-Mn, une température de fusion d'approximativement 725 °C est susceptible d'être atteinte dans les conditions utilisées. Cette valeur est nettement supérieure à celle du zinc pur et peut être bénéfique pour le comportement des revêtements pendant l'emboutissage à chaud.

Une texture de fibre selon la direction <110> est observée pour les couches élaborées en présence d'additifs, ce qui indique que les cristaux sont bien orientés avec leur plan basal perpendiculaire à la surface. Une telle orientation préférentielle n'a pas été trouvée dans la littérature et peut avoir une influence sur la stabilité thermique, l'aptitude à la mise en forme

et le comportement de protection contre la corrosion des revêtements. Enfin, les couches déposées en présence d'additifs présentent une meilleure résistance contre la corrosion comparé à des couches de Zn pur et des alliages Zn-Mn déposés sans additifs. Ce résultat peut être associé à la présence d'une forte teneur en Mn, d'une surface très lisse et d'une orientation préférentielle qui pourraient réduire la vitesse de dissolution de l'alliage. Un effet d'anode sacrificielle est obtenu pour les revêtements considérés grâce à la présence d'un potentiel électrochimique d'au moins 500 mV plus bas que celui de l'acier.

Les études menées dans cette partie ont permis de déterminer une vaste gamme de propriétés des alliages élaborés dans les conditions considérées dans ce travail. Sur la base des résultats obtenus, il sera possible d'étudier l'influence du traitement thermique et de la mise en forme à chaud sur les propriétés et sur les performances des revêtements dans les prochains chapitres.

5 Characterization of Zn-Mn coatings post to heat treatment

The previous chapter was dedicated to the study of the electrolytic system for the deposition of Zn-Mn alloy coatings and to the comprehensive characterization of the crystallographic, microstructural and anticorrosive properties of the as-deposited layers. From the investigations carried out in Section 4, it was proved that Zn-Mn alloy deposits with reproducible properties could be obtained with the electroplating bath and the experimental procedure used. On the basis of the results obtained, it is now possible to investigate the behavior of the coating materials at high temperature.

First of all, the experimental approach used for the study of the behavior of the deposited coatings during high temperature treatments will be reported in Section 5.1. Section 5.2 will be focused on the evolution of the properties of deposits heat treated to various temperatures and dwell times in a furnace heated in air, while more comprehensive experiments will be carried out in presence of a protective atmosphere in Section 5.3. Finally, the results obtained will be summarized in Section 5.4 in order to evaluate the process-window of the coating materials in the considered conditions and determine the suitability of the alternative alloy layers for the hot stamping application.

5.1 Methodical and experimental procedure

As reported earlier (Section 1.5), heat treatment of coated steel for the hot stamping application enables significant changes in the microstructure and the properties of the layers. According to Section 1.6.2, no scientific publications were found in the literature data regarding the behavior of Zn-Mn coatings at high temperature. In fact, only very few information reported the formation of a Mn-rich oxide layer on the surface of Zn-Mn deposits during hot forming. No further details on the microstructure and on the properties of the coatings were reported. In order to better understand the evolution of the coating properties at high temperature, comprehensive microstructural, crystallographic and anticorrosive studies were carried out in the present work on Zn-Mn deposits after high temperature treatment in various conditions.

First of all, the use of different atmospheres will permit to assess the processability of Zn-Mn alloy coatings. Zn-Mn coated specimens will be first heated in an oxidizing atmosphere, which is generally used in the industrial hot stamping process. On the basis of these investigations, it will be possible to evaluate the behavior of the coating with regard to oxidation, assess the data provided in the literature and determine the composition and the properties of the coatings. According to the literature data and to preliminary studies carried out in this work (Appendix 2), it appears that the loss of Mn by oxidation is likely to affect the initial motivation of the use of Mn as alloying element for Zn, namely the increase of the melting temperature of the coating in order to improve hot formability of the coated products. Therefore, a more comprehensive study of the evolution of the coating properties

after heat treatment in a protective atmosphere will be carried out under argon. Information about the experimental conditions and the protective atmosphere used are reported in Section 3.4.2.

In order to evaluate the suitability of the Zn-Mn alloys for the hot stamping application, it is important to study the influence of the austenitizing treatment prior to hot stamping on the composition and the properties of Zn-Mn-coated steels. Therefore, it was chosen to heat coated specimens to different temperatures with regular intervals comprised between 300 °C and conventional temperatures reported for serial production.

The main focus of this work is dedicated to the study of the behavior of Zn-Mn coatings after heat treatment to 300 °C, 500 °C, 700 °C, 800 °C and 900 °C under argon. As significant changes were observed regarding the composition and the microstructure of the coatings above 700 °C, comparative studies were carried out at 700 °C and 900 °C in a furnace under air to assess the influence of the atmosphere on the behavior of the coatings. The same furnace temperature will be used for all specimens to ensure constant heating rates and the heating path will be interrupted after reaching the latter blank temperatures. This methodic permits to simulate the evolution of the coated system during austenitizing treatment and to assess approximate temperature ranges for which changes such as interdiffusion, oxidation or phase transformations take place.

Austenitizing treatment used by steelmakers to produce press-hardened parts is generally carried out for several minutes after reaching the austenitizing temperature of 22MnB5 steel, as reported in Section 1.3. This duration is mostly related to the manufacturing route of the components and to the flexibility of the process. In order to study the process window of the coating materials and evaluate their suitability for conventional austenitizing parameters, heat treatments with blank temperatures of 900 °C and 920 °C and dwell times of up to 120 s after reaching 860 °C will be used.

In order to illustrate the thermal treatment applied on Zn-Mn coating studied in this section, a representative heating curve of the specimens is presented in Figure 53 with the different temperatures and dwell times to which the plates were heated prior to cooling in press tools. The corresponding parameters used are listed in Table 11. The specimens with dimensions of 60 x 45 mm² were inserted into the furnace and removed manually with pliers and cooled down without deformation in the flat areas of cooled press tools after reaching the reference heating durations. The duration of the heat treatments required to reach the target temperatures for the above-mentioned studies were defined on the basis of sets of at least 3 calibration curves obtained by thermocouples fixed on the edge of Zn-Mn-coated specimens.

Three specimens were used for each heat treatment parameter studied in this part and were cut out of the upper part of coated large-scale plates (Figure 33) for which reproducible properties and Mn contents were obtained, as reported in Section 4.2.2. Only one side of the blanks was coated with a Zn-Mn layer. Blanks with a thickness of 1.5 mm were used. The furnace was set to temperatures of 920 °C and 940 °C to heat blanks up to 900 °C and

920 °C, respectively. The difference in furnace and blank temperatures can be explained by heat loss due to the experimental setup and to the distribution of the temperatures within the furnace. The presence of a non-linear heating curve can be explained by phase transformations taking place in steel during austenitizing treatment as well as by the endothermic diffusion processes occurring between coating and substrate materials, which influence the heating behavior of coated steel. Optimal ranges of heating rates are recommended by steelmakers for their products, depending on various parameters such as the type of heating facilities, the sheet thickness or the type of coatings. In fact, melting of the coatings may occur at too high heating rates and induce a contamination of the furnace rollers and the loss of protective coating material. Sufficiently low heating rates may be required to enable diffusion processes and provide good surface, anticorrosive and forming properties to the products, whereas too low heating rates are likely to reduce process efficiency [2].

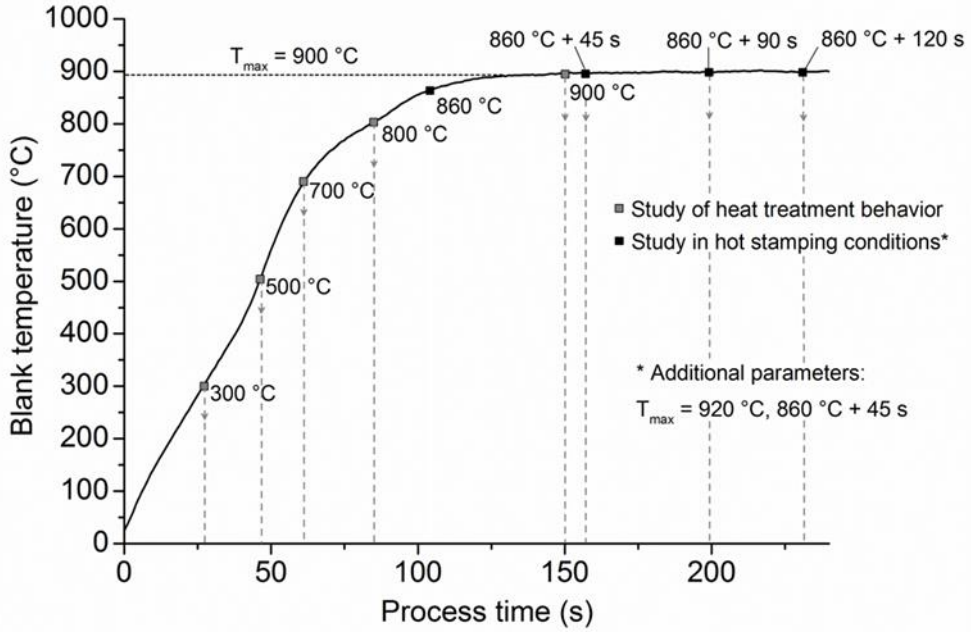

Figure 53: Representative heating curve of a Zn-Mn-coated 22MnB5 steel sample (dimensions of 60 x 45 mm² and thickness of 1.5 mm) with the parameters used for the study of the behavior of Zn-Mn coatings during heat treatment at various temperatures and dwell times in presence of argon.

In order to investigate the influence of heat treatment under the above-mentioned conditions on the properties of Zn-Mn alloy coatings, the coating materials will be characterized regarding the composition, the distribution and the properties of the phases formed at high temperature, in particular due to chemical interdiffusion between coating and steel substrate.

Phase transformations taking place at high temperature in the coating will provide information about the high temperature stability of the coating materials and possible structural changes. High temperature oxidation will be taken into account, in particular the composition of the oxides formed and their temperature dependency. In fact, this phenomenon may lead to a loss of metallic Zn and Mn and affect anticorrosive performance,

to a variation of the melting point of the coatings as well as to the formation of an oxide scale which may induce challenges in terms of weldability and paintability, in a similar way to galvanized steels.

Table 11: Parameters used for heat treatment of Zn-Mn coatings in a furnace under air and under protective atmosphere (Argon).

Blank temperature T_{max}(°C)	**Furnace temperature T_f (°C)**	**Austenitization time t_{aust} (s)**	**Heating duration (s)**	**Atmosphere**
Study of heat treatment behavior in air				
700 °C	920 °C	-	62 s	Air
900 °C	920 °C	-	150 s	Air
Study of heat treatment behavior in Argon				
300 °C	920 °C	-	27 s	Argon
500 °C	920 °C	-	45 s	Argon
700 °C	920 °C	-	62 s	Argon
800 °C	920 °C	-	90 s	Argon
900 °C	920 °C	-	150 s	Argon
Study of heat treatment with relevant industrial process parameters in Argon				
900 °C	920 °C	860 °C + 45 s	155 s	Argon
900 °C	920 °C	860 °C + 90 s	200 s	Argon
900 °C	920 °C	860 °C + 120 s	230 s	Argon
920 °C	940 °C	860 °C + 45 s	155 s	Argon

Furthermore, the study of the microstructure of the coatings after heat treatment will permit to evaluate the occurrence of evaporation on Zn-Mn alloys. On the basis of these results, it will be possible to evaluate the suitability of Zn-Mn-coated steel sheet for manufacturing processes with regard to the austenitizing conditions, to the process window at high temperature and to post-processing of the coated components by painting and joining. In addition, anticorrosive properties will be determined and provide information about the advantages of the use of Zn-Mn coating for this application.

XRD measurements will permit to study the influence of heat treatment on the properties of the initial ε-Zn-Mn phase, to identify phase transformations and to identify additional crystallographic phases formed in the coating during heat treatment. The surface morphology of the coatings will be studied by means of SEM. GDOES will be used to investigate the formation and the relative amount of interdiffusion phases and oxide scales during heat treatment. The evolution of the electrochemical potential during galvanostatic dissolution measurements will be correlated to the GDOES measurements, as the results permit to reveal interdiffusion phases with different compositions and estimate the thickness of the coating, in addition to the assessment of anticorrosion performance with regard to sacrificial corrosion protection. In addition, SEM-EDS and FIB-SEM analyses on will be performed on cross-sections to visualize the microstructure, the elemental distribution and the composition of the coatings post to heat treatment. TEM analyses will be used for

the same purpose, with however a much higher resolution than SEM-EDS analyses. More details regarding the characterization methods are reported in Section 3.3.

5.2 Characterization of Zn-Mn coatings post to heat treatment in air

This part is dedicated to the study of the behavior of Zn-Mn coatings during heat treatment in a conventional atmosphere, namely in a furnace in presence of air. The composition, the phase distribution and the microstructural properties of Zn-Mn coatings heat treated to 700 °C and 900 °C will be reported and will permit to evaluate the suitability of the coating materials for heat treatment in an oxidizing atmosphere. The results obtained will be compared with the studies carried out under argon in order to assess the influence of the atmosphere on the coating properties.

5.2.1 Heat treatment to 700 °C in air

In order to study the microstructure and the composition of Zn-Mn coatings heat treated to temperatures of up to 700 °C in air, SEM-EDS cross-sectional analyses were carried out on different positions of 2 specimens. A representative cross-sectional SEM micrograph is presented in Figure 54. The coating consists of a superficial layer (Layer 1) with a thickness of 0.8 ± 0.1 µm from 10 measurements, an upper layer (Layer 2) with a high density of defects such as pores and precipitates with a thickness of 11.4 ± 3.0 µm measured from 10 measurements and a compact layer (Layer 3) located at the interface with steel. The latter was found to have a mean thickness of 6.6 ± 2.5 µm on the basis of 14 measurements on two specimens. Layer 3 appears to be almost parallel to steel surface, which indicates that a planar interdiffusion front forms during heat treatment.

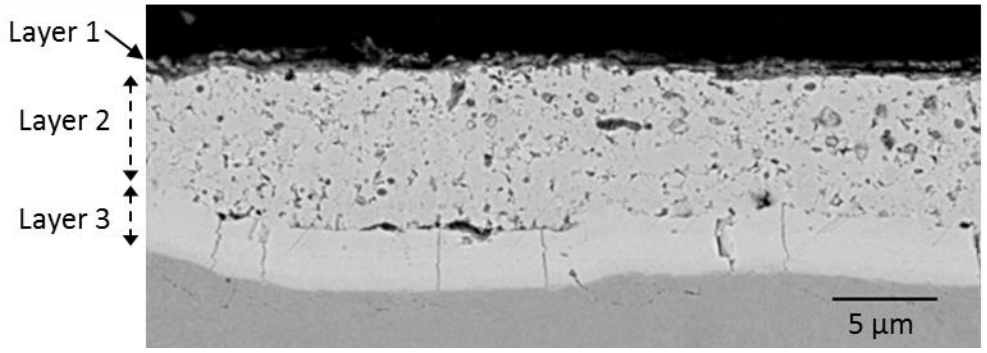

Figure 54: Cross-sectional SEM micrograph (BSE mode) of a Zn-Mn coating heat treated to 700 °C in a furnace heated in air.

Cross-sectional SEM-EDS analyses were carried out on the corresponding coatings of two specimens. According to the representative EDS mapping shown in Figure 55, the Zn content appears to be relatively constant along the coating thickness, while a higher amount of sulfur is present in the upper layer. The same observation was made in the case of Zn-Mn coatings heated to 700 °C in argon and will be reported in detail in the next section. According to the signals shown in Mn and O elemental mappings, the superficial layer (Layer 1) clearly consists of Mn oxides.

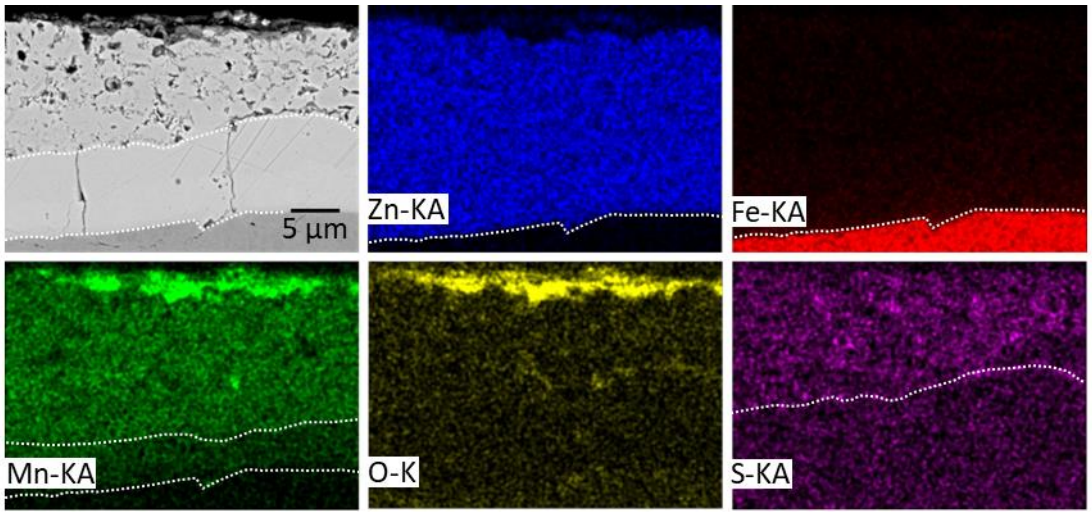

Figure 55: Cross-sectional SEM micrograph (BSE mode) and SEM-EDS elemental mapping of Zn-Mn coatings heat treated to 700 °C in a furnace heated in air.

Further SEM investigations were carried out on the lower part of the coating in order to study the microstructure and the composition of Layer 3. Representative cross-sectional SEM-EDS elemental mappings of the lower region of Layer 2 and of the complete Layer 3 are presented in Figure 56. In addition, the chemical composition of the coating including the sublayers was determined on the basis of sets of at least 10 SEM-EDS measurements listed in Table 12.

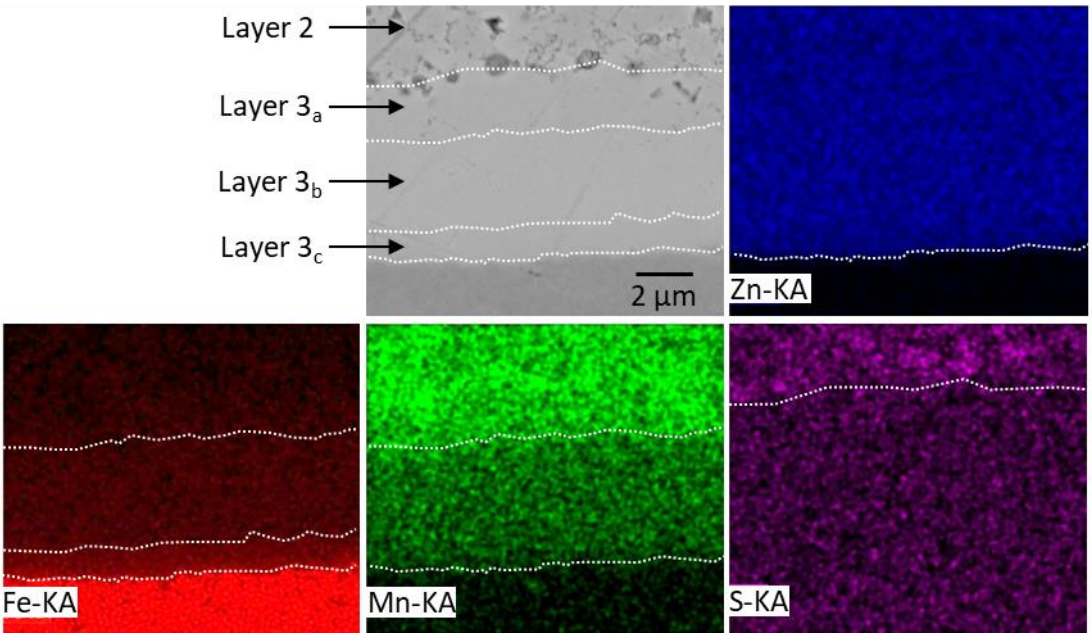

Figure 56: Cross-sectional SEM micrograph (BSE mode) and SEM-EDS elemental mapping of the lower region of Layer 2 and of the complete Layer 3 (Figure 54) of Zn-Mn coatings heat treated to 700 °C in a furnace heated in air.

On the basis of these results, it appears that Layer 3 consists of three sublayers (Layers $3_{a\text{-}c}$) with different compositions. As observed in Figure 55, the signals related to the presence of S were mainly found in Layer 2, which contains approximately 0.5 wt.% S.

According to Figure 56, Layer 3_a contains a Mn content similar to that of the lower part of Layer 2. Differences in the Mn content of Layer 2 and Layer 3_a reported in Table 12 can be explained by the fact that the measurements for Layer 2 were carried out in the entire layer, whereas the results shown in Figure 56 depict only the lower region of Layer 2. It is interesting to note that the amount of Zn remains relatively high above 70.0 wt.% in the entire coating, which indicates that a sacrificial protection to steel is likely to be achieved. The amount of Fe gradually decreases towards the top surface of the coating, with the presence of approximately 1.1 wt.% Fe in Layer 2, while a Fe content of up to 26.6 wt.% is obtained in the sublayers of Layer 3. The Mn content of approximately 16.8 wt.% observed in Layer 2 is similar to that of the as-deposited coating.

Table 12: Chemical composition of different layers (Figure 56) observed in Zn-Mn coatings heat treated to 700 °C in a furnace heated in air, determined by semi-quantitative EDS analyses.

Analyzed area	Composition (wt.%)			
	Zn	Mn	Fe	S
Layer 2 (entire)	81.5 ± 1.2	16.8 ± 0.6	1.1 ± 1.3	0.5 ± 0.4
Layer 3_a	80.7 ± 0.7	13.8 ± 0.6	5.5 ± 0.4	-
Layer 3_b	82.8 ± 0.5	7.4 ± 0.7	9.8 ± 0.8	-
Layer 3_c	70.0 ± 1.0	3.4 ± 0.3	26.6 ± 1.1	-

In order to determine the electrochemical properties of the coatings, galvanostatic measurements were carried out. Representative curves of the evolution of the electrochemical potentials of coating and substrate materials prior to and post to heat treatment to 700 °C in air are presented in Figure 57 and are based on 4 measurements on 2 specimens.

These potential curves describe the phase distribution shown in the above-mentioned SEM-EDS studies. The presence of an initial dissolution stage of approximately 2000 s with a potential similar to that of the as-deposited coating can be explained by a low Fe content and can be attributed to Layer 2 of the coatings (Table 12). Above 2000 s, three stages comprised between the potentials of Layer 2 and the base material can be observed and most likely correspond to the sublayers reported in Figure 56. A short stage with a duration of about 200 s and an electrochemical potential approximately 50 mV higher than that of Layer 2 can be most likely attributed to Layer 3_a. In addition, a difference of approximately 200 mV can be observed for the electrochemical potentials of Layer 2 and Layer 3_b (Figure 57). Although Layer 2, Layer 3_a and Layer 3_b were found to contain very similar Zn contents (Table 12), the increase of the electrochemical potential is most likely related to the successive increase of the Fe content towards steel.

The coating provides significant sacrificial corrosion protection to steel, with the exception of Layer 3_c which appears to have an electrochemical potential similar to that of steel. Given the fact that a high Zn content of 70.0 wt.% (Table 12) was observed for the latter layer, it is very likely that the potential measured does not depict the behavior of Layer 3_c. This result could not be explained.

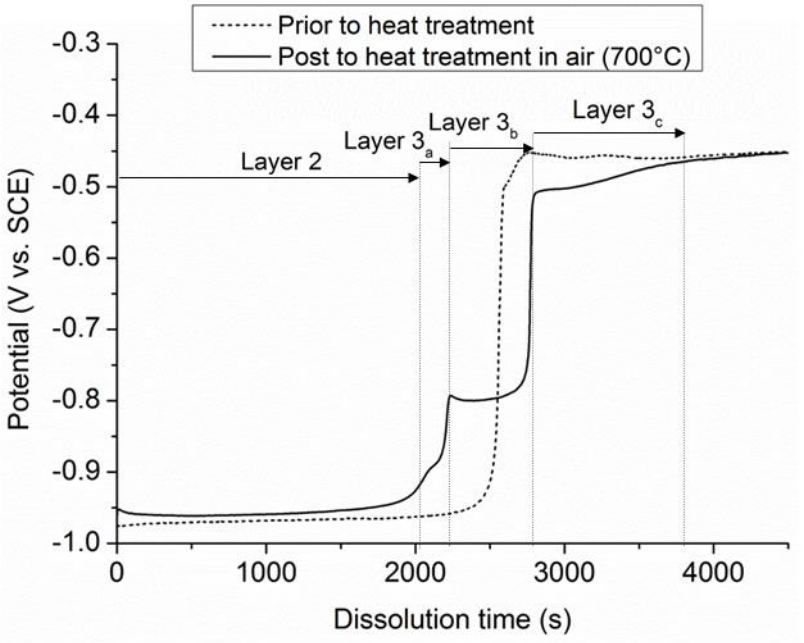

Figure 57: Evolution of the electrochemical potential of coating and substrate materials during galvanostatic dissolution prior to and post to heat treatment to 700 °C in a furnace heated in air vs. SCE.

According to Figure 54, cracks can form in the lower compact layers (Layers 3_{a-c}) of the coatings, as confirmed by the more detailed micrographs presented in Figure 58. The cracks were found to propagate into steel substrate on some positions, as shown in Figure 58 a) or to stop at the interface with steel (Figure 58 b) and c)). As reported in Section 1.5.1, cracks with a depth of at most 10 µm in the base material are generally considered to have no significant influence on the functional properties of the products. No cracks were found to exceed this value.

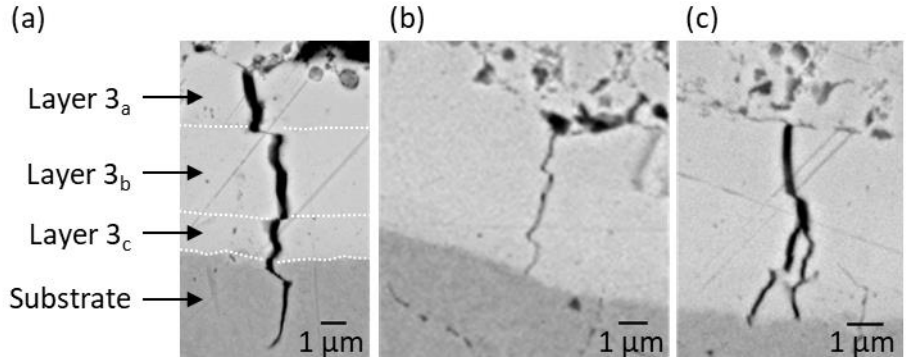

Figure 58: Cross-sectional SEM micrographs (BSE mode) of cracks formed in Layer 3 (Figure 54) of Zn-Mn coatings heat treated to 700 °C in a furnace heated in air.

It is interesting to note from Figure 58 that the profile of the cracks is not straight through the above-mentioned sublayers. Since no deformation was applied on the coated specimens, it can be assumed that these cracks did not appear due to forming, but could be related to a difference in the relative expansion coefficients of the coating layers and of steel, in a similar

way to aluminized steel (Section 1.5.2). An alternative explanation could be the presence of crystallographic transformations at high temperature.

Besides, it is very likely that the presence of microstructural defects such as pores and precipitates observed in Layer 2 (Figure 54) facilitate the initiation and the propagation of cracks. It is not clear if the cracks propagate along the grain boundaries or through the grains of the considered layers, which could provide information about a possible brittle behavior of the coating.

Conclusion

From this study, it appears that heat treatment of Zn-Mn coatings to a temperature of 700 °C in air induces the formation of an oxide layer on the top surface, mostly consisting of Mn oxides. The upper part of the coating appears to contain a high amount of defects such as pores and contains a Mn content similar to that of as-deposited layers. In addition, a thick interdiffusion layer was observed at the interface with steel, with the presence of a composition gradient with a higher Fe content towards steel as well as a Mn content lower than in the upper part of the coating.

5.2.2 Heat treatment to 900 °C in air

As presented in Figure 59, the surface of Zn-Mn coatings heat treated to 900 °C in air is non-homogeneous and mostly consists of brownish particles in which gray areas are visible. Besides, spots consisting of white particles (white areas in Figure 59) can be observed.

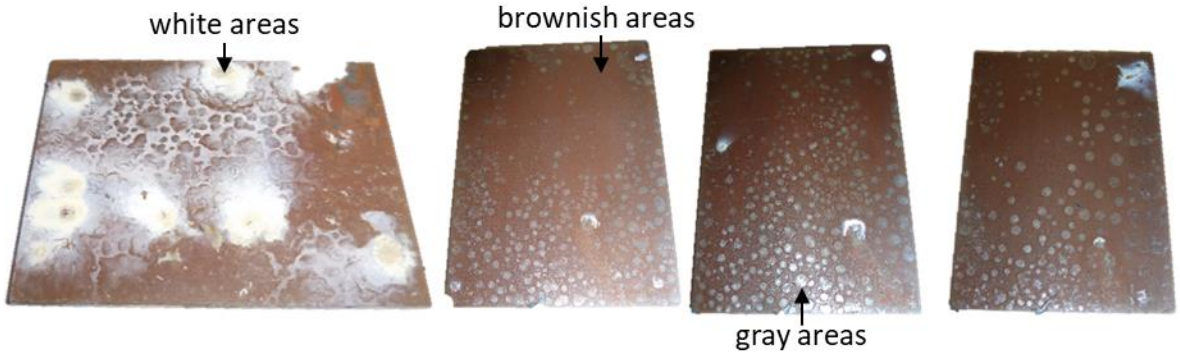

Figure 59: Surface appearance of Zn-Mn coatings after heat treatment to 900 °C in a furnace heated in air.

Characterization studies of both white and brownish regions of the coatings will be reported in the next parts in order to determine the microstructure and the composition of the coatings.

Characterization of brownish areas of the coatings

Cross-sectional SEM-EDS investigations were carried out on the brownish areas of two specimens shown in Figure 59. Representative micrographs are presented in Figure 60. The coating consists of two different layers. A superficial layer (Layer 1) consisting of loose particles and a high amount of voids can be observed on the top surface of the coating

(Figure 60 a) and b)) and appears have a high overall thickness of more than 20 µm. The effective thickness of this layer, that is to say the thickness of the oxide particles without considering the porosities was measured on regular positions on 6 cross-sectional views from 2 specimens. A thickness of 12.5 ± 6.3 µm was obtained from 35 measurements. The high standard deviation observed can be explained by the non-homogeneous distribution of this layer and to the presence of an accumulation of oxide particles. This oxide scale was not present on some areas of the sample (Figure 60 c)), presumably due to a low adhesion with the underlying layer during press-hardening. It can be assumed that these oxide-free regions correspond to the gray areas visible on the top surface of the coatings in Figure 59. A compact layer (Layer 2) with a thickness of 8.5 ± 2.2 µm determined from 50 measurements was observed in the lower region of the coating and appears to provide good adhesion with steel, as no defects such as voids can be observed at the interface. Cracks can be observed in the coating but were not found to propagate beyond the interface with steel.

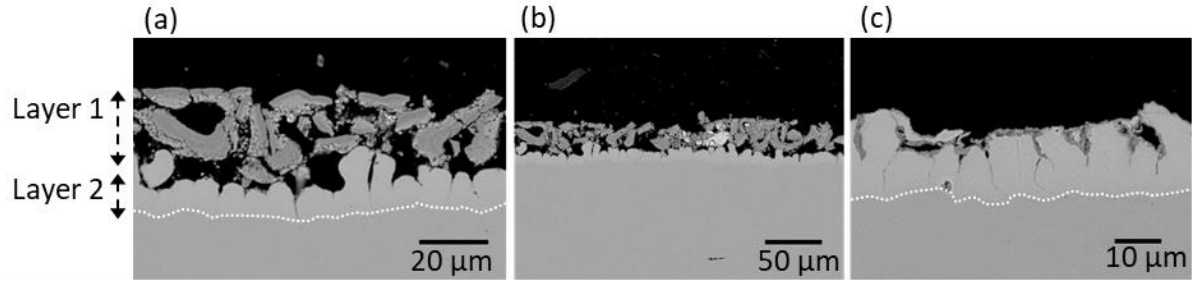

Figure 60: Cross-sectional SEM micrographs (BSE mode) of Zn-Mn coatings heat treated to 900 °C in a furnace heated in air; microstructures with superficial layer ((a) and (b)) and without superficial layer (c); cross-sections carried out on brownish areas of the specimens (Figure 59).

Further microstructures were observed during cross-sectional SEM-EDS analyses, with the presence of an additional phase (light regions) located at the interface between the compact lower layer and the oxide scale, as well as between the oxide particles. Representative cross-sectional micrographs of the corresponding areas obtained from analyses on 2 specimens are presented in Figure 61.

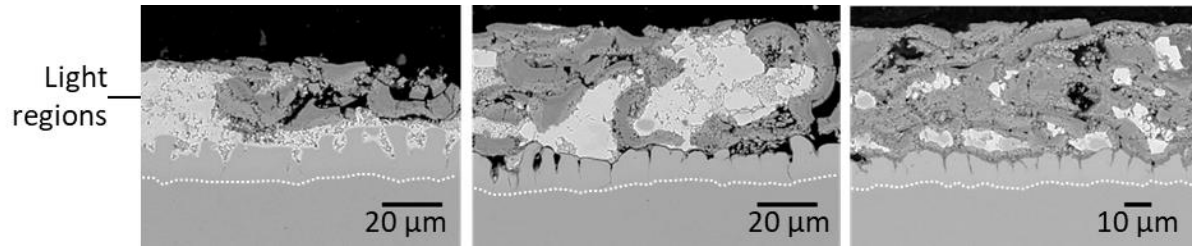

Figure 61: Cross-sectional SEM micrographs (BSE mode) of Zn-Mn coatings heat treated to 900 °C in a furnace heated in air; presence of additional phases (light areas) compared to Figure 60; cross-sections carried out on brownish areas of the specimens (Figure 59).

The compact layer in contact with the substrate was found to have a thickness of 12.2 ± 3.2 µm determined on the basis of 35 measurements. This value is higher than that

obtained in the case of coatings containing no light regions (Figure 60). A possible explanation for this result is that the absence of Zn-rich regions in the case of coatings presented in Figure 60 prevents the growth of the interdiffusion layer (Layer 2), contrary to the case of Zn-rich-containing coatings shown in Figure 61.

As visible in Figure 61, the distribution of the light regions and the oxide scale is irregular, as no clear layered structure is observed. This particularity is induced by the significant oxidation of the coatings in the above-mentioned conditions. The thickness of both regions was determined by measuring the thickness of the corresponding areas along regular vertical positions of 7 cross-sectional views from 2 specimens. Mean thicknesses of 10.6 ± 9.0 µm and 14.8 ± 8.3 µm were respectively obtained for the light regions and for the superficial oxide scale on the basis of sets of 35 measurements. The high standard deviation values illustrate the non-homogeneous microstructure observed in Figure 61.

In order to determine the relative composition of the different areas visible in Figure 61, cross-sectional SEM-EDS elemental mappings were carried out on several positions of two coated specimens. Representative mappings are presented in Figure 62. In addition, semi-quantitative EDS analyses of the compositions of the different regions identified were carried out on the basis of sets of at least 20 measurements (Table 13).

According to the results, Region A is a Fe-rich phase containing 68.8 ± 4.3 wt.% Fe, whereas Region B of the coatings is composed of a Zn-rich phase containing approximately 91.3 ± 3.1 wt.% Zn. It is important to note that both regions A and B contain a low Mn content of 0.7 wt.% Mn. This result indicates that heat treatment in air up to 900 °C induces a significant loss of metallic Mn by oxidation, which was found to form the thick and porous layer of particles visible in Figure 62 (region C).

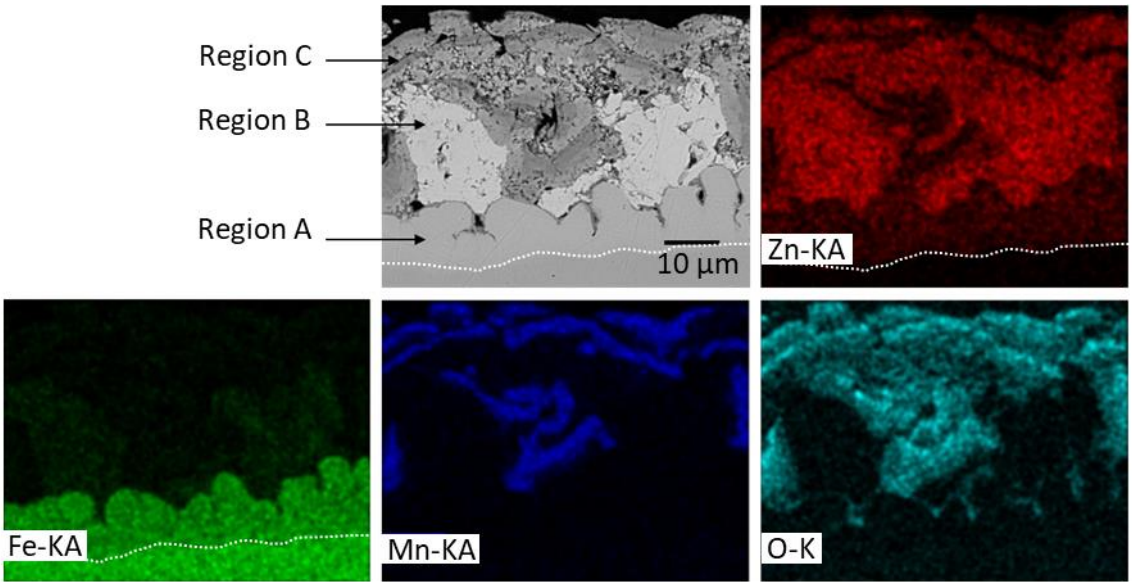

Figure 62: Cross-sectional SEM micrograph (BSE mode) and SEM-EDS elemental mapping of Zn-Mn coatings heat treated to 900 °C in a furnace heated in air; cross-sections carried out on brownish areas of the specimens (Figure 59).

It can be assumed that the Zn-rich phases observed in Figure 61 may have disappeared due to high temperature evaporation, which could explain the presence of the microstructure shown in Figure 60 and consisting only of a Fe-rich phase. It is interesting to note that the superficial oxide layer (Region C) also contains Zn oxides.

Given the low amount of Mn in both layers, it can be assumed that they consist of Zn-Fe alloys with Mn in solid solution. In fact, according to the mean composition values (Table 13) and to the Zn-Fe binary diagram presented in Figure 10, the lower layer most likely corresponds to the α-Fe phase with Zn in solid solution, while the Zn-rich layer may be constituted by a mixture of δ- and ζ-Zn-Fe intermetallic phases.

Table 13: Chemical composition of regions A and B observed in Zn-Mn coatings heat treated to 900 °C in a furnace heated in air, determined by semi-quantitative EDS analyses.

	Composition (wt.%)		
	Zn	Mn	Fe
Region A	30.5 ± 4.2	0.7 ± 0.2	68.8 ± 4.3
Region B	91.3 ± 3.1	0.7 ± 0.3	7.9 ± 2.9

Galvanostatic dissolution measurements were carried out on the brownish areas of Zn-Mn coatings heat treated to 900 °C in air on the basis of 4 measurements in order to identify any beneficial effect of the presence of Zn-rich phases in the deposits.

First of all, it can be observed that two types of curves are obtained, presumably due to the non-homogeneous microstructure of the coating, as mentioned earlier. Some curves appear to have an electrochemical potential significantly lower than that of steel (Type 1 in Figure 63) and are most probably related to the presence of Region B observed in Figure 62 and consisting of a Zn-rich phase, which provides a cathodic protection of at least 350 mV to steel during the first 1000 s of dissolution.

An increase of the total duration of dissolution of the coating can be observed compared to the as-deposited coating, most probably because of the increase of the coating thickness due to the formation of an interdiffusion layer at the interface between coating and steel (Region A in Figure 62). It should be noted that the transition time between stages with different potentials was found to vary, which can be explained by different relative amounts of the phases present in the coatings.

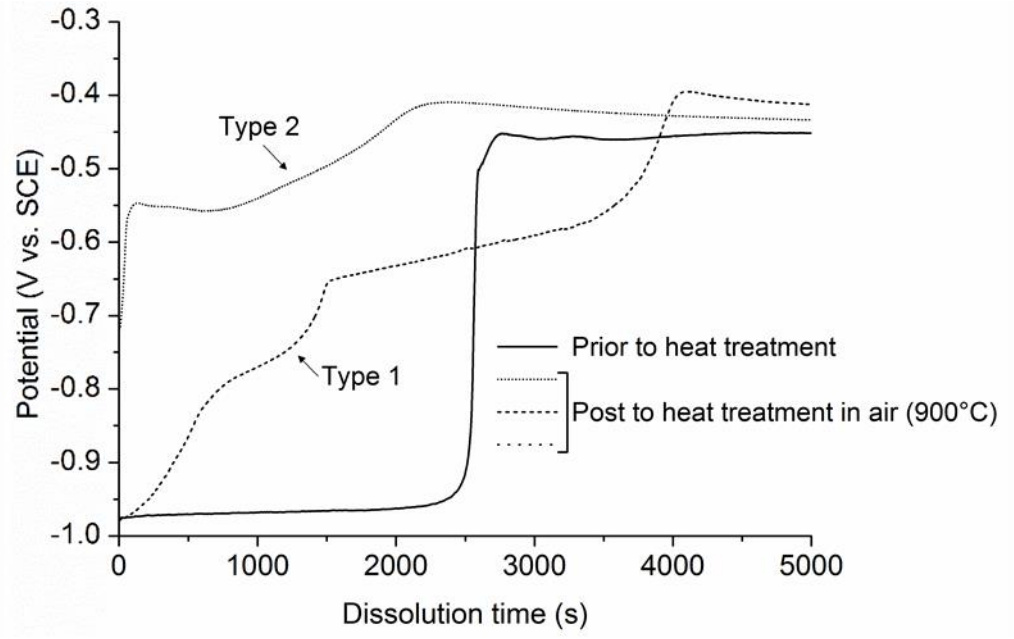

Figure 63: Evolution of the electrochemical potential of coating and substrate materials during galvanostatic dissolution prior to and post to heat treatment to 900 °C in a furnace heated in air vs. SCE.

It is very likely that Type 2 curves describe the electrochemical behavior of layers containing no or almost no Zn-rich regions and presented in Figure 60. In this case, a more moderate potential difference of about 200 mV for 2000 s (Type 2 in Figure 63) is provided with steel.

Characterization of white areas of the coatings

The white areas observed in Figure 59 were studied by means of cross-sectional SEM analyses on two coated specimens. Representative SEM micrographs are presented in Figure 64 and show that the coatings mostly consist of a thick superficial layer containing a high amount of loose particles and fractured layers. In addition, a compact layer with a thickness of 9.8 ± 1.6 µm determined on the basis of 15 measurements can be observed at the interface with the steel substrate. A representative elemental EDS mapping of the corresponding coatings is presented in Figure 65.

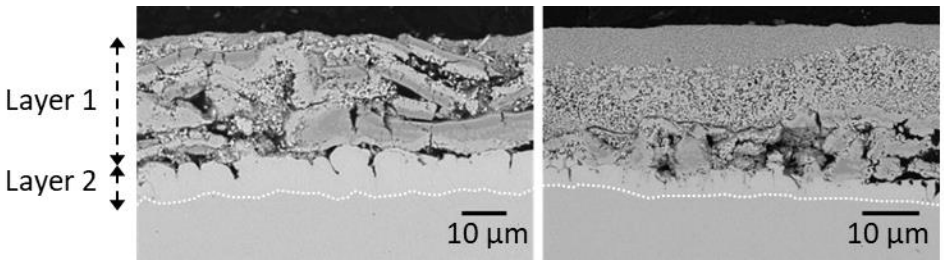

Figure 64: Cross-sectional SEM micrographs of Zn-Mn coatings heat treated to 900 °C in a furnace heated in air; cross-sections carried out on white areas of the specimens (Figure 59).

The results clearly indicate that the amount of loose particles and fractured layers observed in Figure 64 in the upper part of the coating (Layer 1) mainly consists of oxides, in particular

of Zn oxides. On the one hand, the local formation of a Zn-rich oxide scale on the surface of the coatings is not likely to be related to heterogeneous microstructures and compositions or to the presence of local defects in the microstructure of as-deposited layers.

On the other hand, these areas are likely to correspond to the defects reported in the case of galvanized steel (Section 1.5.1) for which zinc blisters or burn-offs take place at the top surface of the coatings due to the manual handling of the blanks, the presence of contaminants on the blanks or to the use of high temperatures in the furnace.

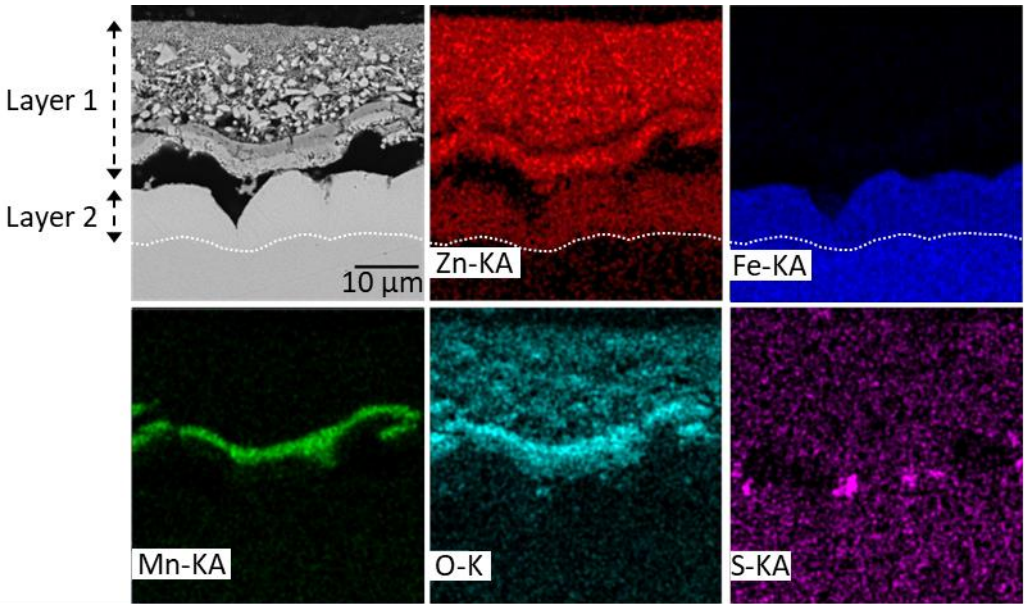

Figure 65: Cross-sectional SEM micrograph (BSE mode) and SEM-EDS elemental mapping of Zn-Mn coatings heat treated to 900 °C in a furnace heated in air; cross-sections carried out on white areas of the specimens (Figure 59).

The composition of Layer 2 was assessed by means of EDS on the basis of 6 measurements (Table 14). The interdiffusion layer appears to contain a high Fe content of about 75.1 wt.% and a very low Mn content of approximately 0.9 wt.%. This value is very similar to that observed in the brownish areas of the coatings (Table 13).

Table 14: Chemical composition of Layer 2 (Figure 65) observed in the white areas of Zn-Mn coatings heat treated to 900 °C in a furnace heated in air, determined by semi-quantitative EDS analyses.

	Composition (wt.%)		
	Zn	Mn	Fe
Layer 2	23.9 ± 1.6	0.9 ± 0.1	75.1 ± 1.6

Conclusion

The results obtained in this study permitted to confirm the scarce results found in the literature and reported in Section 1.6.2, namely that annealing of Zn-Mn coatings up to 900 °C in air leads to the loss of Mn from the coating due to severe high temperature oxidation, which results in the formation of a thick and non-homogeneous oxide layer consisting of loose particles on the surface of the coatings. Two layers, namely a Fe-rich and

a Zn-rich layer with very low Mn contents of about 0.7 wt.% were observed below the oxide layer, in good accordance with the observations of Baumgartner and Sanders [179]. Both layers were found to provide good sacrifical protection to steel after heat treatment. However, the Zn-rich layer was found to have a non-regular distribution across the coatings and to be partly embedded in the oxide scale. It can be considered that evaporation of this phase takes place at temperatures of up to 900 °C, as it was absent on some parts of the coatings. It is interesting to note that some defects, namely white spots related to significant oxidation of Zn were observed on the surface of the heat treated samples, indicating that a loss of metallic Zn and a degradation of the surface state of the coatings could be induced. These areas are likely to correspond to zinc blisters and burn-offs reported in the case of galvanized steel (Section 1.5.1).

According to Section 1.6.2, a decrease of the Mn content in the alloys is likely to induce a reduction of the melting temperature of the coating, and thereby affect the protection against LME mechanisms during direct hot forming. Besides, it is most probable that a surface treatment such as abrasive blasting is required to remove the thick oxide scale formed on the surface of the coated parts and to achieve good paintability of the press-hardened components. For these reasons, the behavior of Zn-Mn coatings in a protective atmosphere will be studied in the next investigations of heat treatment and hot stamping.

5.3 Characterization of Zn-Mn coatings post to heat treatment in a protective atmosphere

This part is dedicated to the study of microstructural, crystallographic and anticorrosive properties of Zn-Mn coatings after heat treatment in order to understand the phase transformations and interdiffusion layers formed at high temperature and evaluate the suitability of the deposits for heat treatment prior to hot stamping. A protective atmosphere containing argon was used. A description of the experimental setup used is reported in Section 3.4.2.

The surface appearance of the corresponding coatings after heat treatment to temperatures of 300 °C, 500 °C, 700 °C and 900 °C is shown in Figure 66. The appearance of specimens heat treated to 300 °C is very similar to that of the as-deposited coating. A light colored surface can be observed at 500 °C, while a brownish color appears for temperatures higher than 700 °C. The latter color is most probably related to the appearance of Mn oxides, as confirmed by the preliminary study shown in Appendix 2. In contrast to Zn-Mn coatings heat treated to 900 °C in air, no white spots were observed for layers heated to 900 °C in argon, which most likely indicates a lower occurrence of Zn oxidation by the use of protective gas. In addition, lower amounts of loose particles were observed after heat treatment in argon.

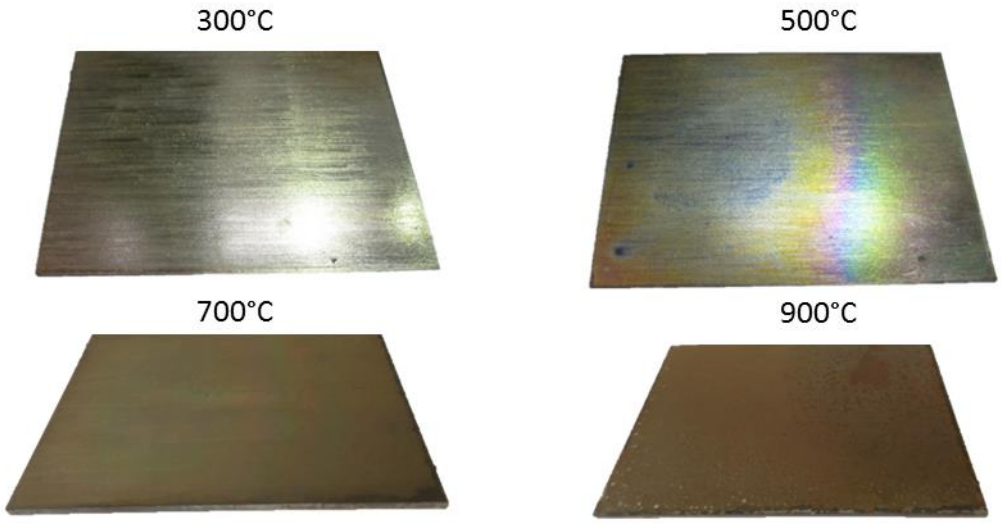

Figure 66: Surface appearance of Zn-Mn coatings post to heat treatment to temperatures of 300 °C, 500 °C, 700 °C and 900 °C in a furnace heated in argon.

5.3.1 Crystallographic properties of Zn-Mn coatings post to heat treatment in a protective atmosphere

XRD measurements were carried out on Zn-Mn coatings prior to and post to heat treatment to various temperatures in order to study the evolution of the crystallographic properties of the as-deposited layers at high temperature, identify phase transformations and oxides formation. Representative results are shown in Figure 67.

The intensity scales of the XRD patterns (a)—(e) were restricted to 10 % of the (110) line intensity located at approximately 2θ = 67.6° and corresponding to the preferential crystallographic orientation mentioned in Section 4.3.3.

Prior to heat treatment (Figure 67 a)), the coating consists of a single ε_2-Zn-Mn phase, in good accordance with the results presented in Figure 44. After heat treatment to 300 °C, the pattern is very similar to that of the as-deposited coating. A few additional diffraction lines corresponding to MnO oxide appear. Very similar diffraction patterns were obtained at a temperature of 500 °C.

At 700 °C, a noteworthy increase of the intensity of the lines related to Mn oxides can be observed. In addition, a considerable increase of the intensity of the peaks of the ε_2-Zn-Mn phase appears, notably at 2θ = 37.7° and 2θ = 43.0°. As mentioned earlier, a metastable ε_2-Zn-Mn phase with a preferential orientation was deposited in the considered electroplating conditions. Heat treatment of the coating at a temperature of 700 °C may induce a reorientation of the crystals, as the relative intensity of the diffraction line corresponding to the (110) plane decreases. The presence of diffraction lines corresponding to Fe_2O_3 may be related to impurities on the coating surface or to the oxidation of substrate steel on areas of the specimens without coating due to surface preparation.

A considerable change in the diffraction patterns can be observed at a temperature of 800 °C, with the disappearance of all diffraction lines of the ε_2-Zn-Mn phase, even for the (110) diffraction line which is characteristic of the preferential orientation of the crystals. This observation may be related to the melting of the coating at temperatures comprised between 700 °C and 800 °C. The diffraction pattern mainly consists of diffraction lines corresponding to Γ-Fe_3Zn_{10} and ζ-$FeZn_{10.98}$ phases. The latter phases were reported to contain 73.1-84.2 wt.% Zn and 88.5-93 wt.% Zn, respectively [180]. The $Zn_{0.988}Mn_{0.012}$ phase could also be detected. Finally, the presence of MnO can be observed, in a similar way to lower temperatures.

At a temperature of 900 °C, the most intense peaks are associated to Mn_3O_4 and MnO oxides. Several peaks corresponding to the Γ-Fe_3Zn_{10} phase can be observed (Figure 67 f)). It should be noted that the diffraction patterns reported in Figure 67 may depict only a part of the crystallographic properties of the coatings, since the penetration depth of the X-ray beam was found to vary during analysis (Section 4.3.3). Thus, it is likely that further crystallographic phases form at high temperature, in particular interdiffusion layers at the steel/coating interface. Besides, a very limited amount of information was reported regarding Zn-Mn-Fe phases formed in Zn-Mn-coated steel during heating, which implies that further phases could not be evidenced on the basis of XRD measurements. Further characterization studies are required to fully understand the behavior of the Zn-Mn coating during heat treatment.

From this study, it appears that Zn-Mn coatings are likely to melt at temperatures comprised between 700 °C and 800 °C. Although this result is in good agreement with the theoretical melting point according to the binary phase diagram (Section 4.3.3), further studies are required to precise the value of the melting point of the alloy, for instance by using the differential scanning calorimetry technique. It appears that the use of a protective atmosphere during heat treatment investigations does not permit to fully avoid oxidation mechanisms, since the presence of MnO was detected, in particular for temperatures higher than 700 °C. The thickness of this layer and its evolution during heat treatment will be reported later. It is interesting to note that no diffraction lines corresponding to ZnO could be observed, which can be explained by the higher oxygen affinity for Mn compared to Zn (Section 1.6.2). The next part will be dedicated to the microstructural and anticorrosive properties of the Zn-Mn coatings after heat treatment in the above-mentioned conditions.

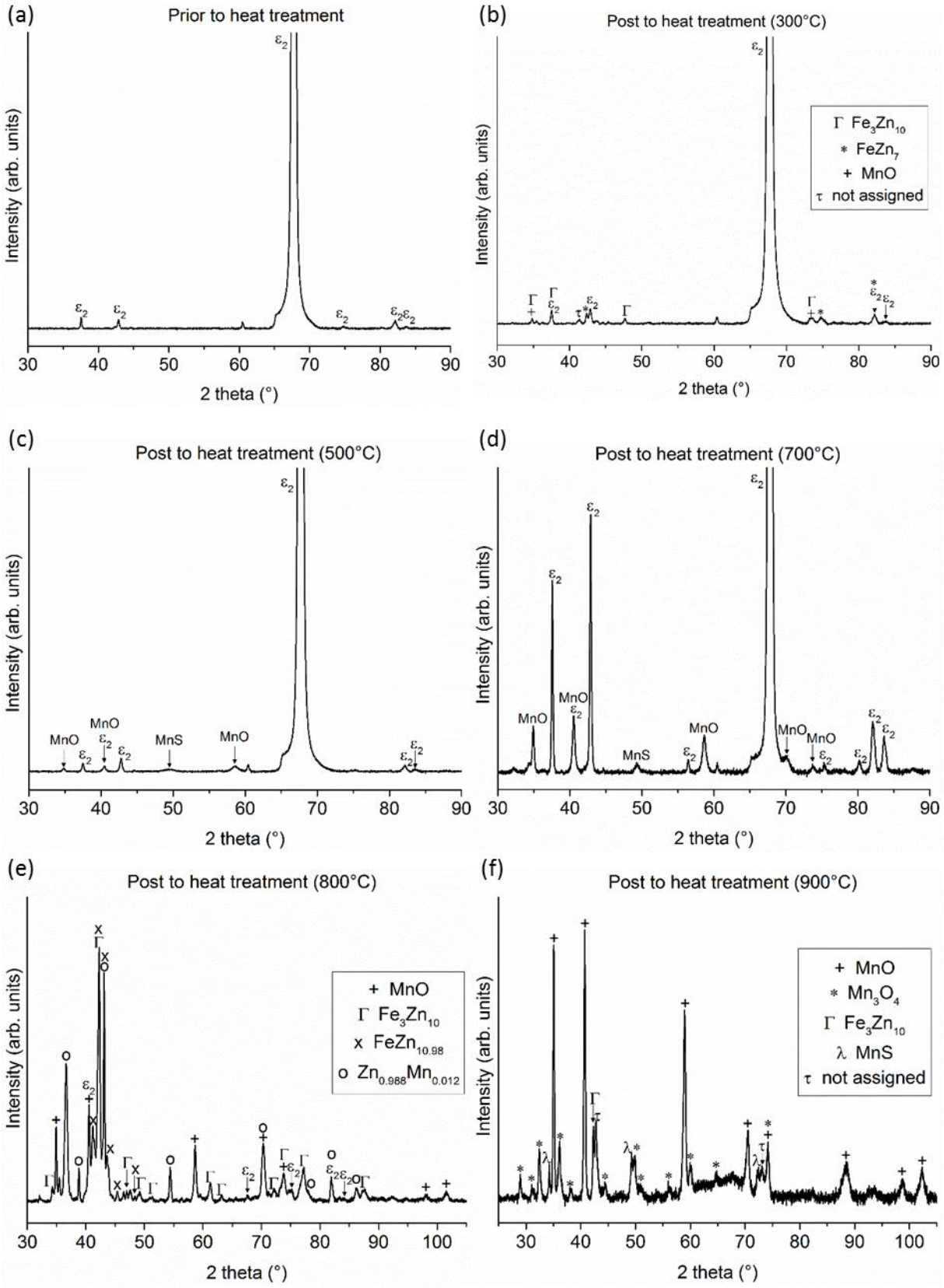

Figure 67: X-ray Diffraction (XRD) patterns of Zn-Mn coatings prior to (a) and post to heat treatment to temperatures of 300 °C (b), 500 °C (c), 700 °C (d), 800 °C (e) and 900 °C (f) in a furnace heated in argon; the intensity scale of the XRD patterns (a)-(d) was restricted to 10 % of the (110) line intensity of the ε_2-Zn-Mn-phase at approximately $2\vartheta = 67.6°$.

5.3.2 Surface morphology of Zn-Mn coatings post to heat treatment in a protective atmosphere

In this part, SEM analyses were carried out on the surface of heat treated specimens in order to study the influence of heat treatment on the morphology of the deposits. Sets of at least 5 surface analyses were used for this study. Representative micrographs of the surface of Zn-Mn coatings prior to and post to heat treatment at various temperatures are presented in Figure 68.

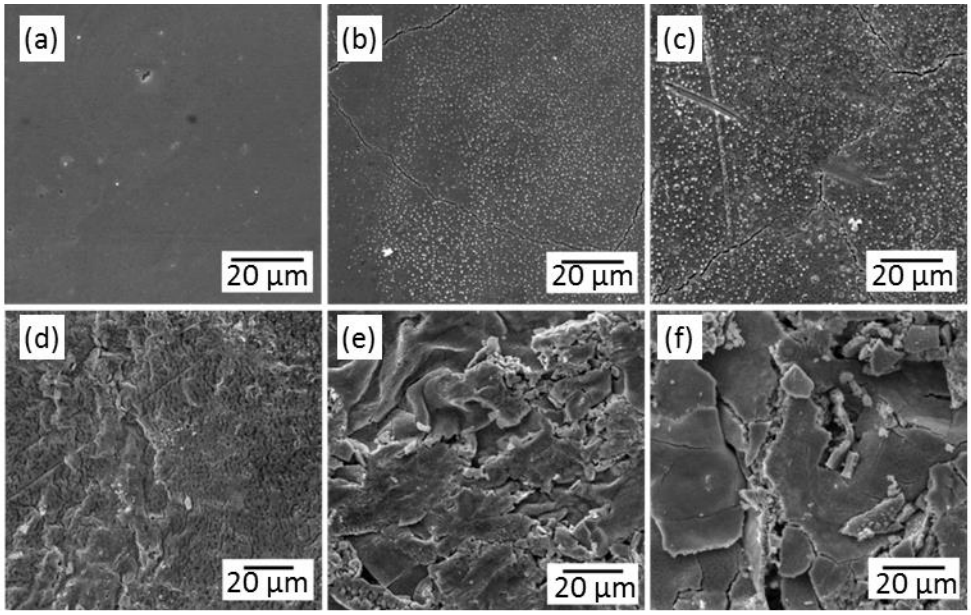

Figure 68: SEM micrographs of the surface of Zn-Mn coatings prior to (a) and post to heat treatment to temperatures of 300 °C (b), 500 °C (c), 700 °C (d), 800 °C (e) and 900 °C (f) in a furnace heated in argon.

After heat treatment up to 300 °C, the topography of the coating does not change significantly compared to the as-deposited coating. Particles with a diameter of up to 500 nm appear on the surface and may be related to oxidation of the coating materials or to the adhesion of particles during quenching in the press tools. A higher density of the latter particles was observed on the surface of specimens heat treated to 500 °C. The formation of cracks for coatings heat treated at 300 °C and 500 °C may be related to a difference in the thermal expansion coefficient of coating and substrate materials, as reported in the case of the aluminized coating (Section 1.5.2). Moreover, a release of residual stresses may have taken place during heating.

After heating to 700 °C, the surface of the coating appears to be more rough, whereas for temperatures higher than 800 °C, loose particles as well as a breakup of a superficial layer can be observed. As XRD signals of MnO oxide were found to increase by increasing temperature (Figure 67), it is likely that the amount of MnO formed in the coating increases and forms a superficial layer. On the basis of these results, it appears that coatings heat treated up to 700 °C are relatively smooth, whereas the surface rugosity and the presence of loose particles for coatings heated to 800 °C and 900 °C may have a negative impact on the

subsequent processing of the press-hardened components, in particular for painting. In fact, the fractured and porous surface of the heat treated coatings may induce the formation of non-homogeneous phosphate and electrophoretic coatings. Besides, the presence of loose particles is likely to induce a contamination of the electrophoretic bath and to lead to a delamination of painting layers. In addition, the presence of a thick superficial layer consisting of oxides is likely to imply challenges in terms of weldability due to an increase of the electrical contact resistance for RSW, in a similar way to galvanized steel (Section 1.5.1).

5.3.3 Microstructural and anticorrosive properties of Zn-Mn coatings post to heat treatment in a protective atmosphere

The present part is focused on the study of microstructural and anticorrosive properties of Zn-Mn coatings post to heat treatment at different temperatures in a protective atmosphere on the basis of various characterization techniques presented in Section 3.3. A particular interest will be given to the phase evolution during heating, which will provide essential information about the suitability of the coatings for the hot stamping process.

Heat treatment to 300 °C and 500 °C in a protective atmosphere

Galvanostatic dissolution analyses were carried out on specimens prior to and post to heat treatment to 300 °C in argon. Representative curves are presented in Figure 69 a) and are based on 3 measurements on one specimen. The potential of the coated steel system was found to be identical to that of an as-deposited Zn-Mn coating (Figure 69 a)), which means that the composition of the coating is likely not to be influence by the heating process. A significant sacrificial effect of approximately 500 mV is provided to steel, in good accordance with the results obtained on as-deposited layers (Section 4.3.4). Moreover, the transition of coating and steel potentials is abrupt, which indicates that no interdiffusion phases are likely to form in the considered conditions. Diffraction analyses showed that no change in the crystallographic properties of the Zn-Mn coating occurs after heat treatment. In addition, no change in the duration of dissolution could be observed compared to the data obtained on as-deposited layers, which indicates that the thickness of the coating does not vary due to heat treatment. A thickness of 17.7 ± 2.3 µm was determined on the basis of 15 cross-sectional microscope measurements carried out on two specimens.

From the GDOES measurements shown in Figure 69 b), it appears that the concentrations of Zn, Mn, O, S and C are relatively constant along the coating thickness, in a similar way to the results reported for the measurements carried out on the coatings prior to heat treatment (Figure 39). Semi-quantitative SEM-EDS analyses carried out on 3 specimens and based on 35 measurements revealed that the coatings contain 17.5 ± 2.6 wt.% Mn. A discontinuous evolution of the elemental concentrations appears at about 22 µm before reaching the substrate. The most probable explanation for this result is the transition between coating and substrate materials during measurement due to the roughness of the base material. A further explanation for this transition can be the presence of a thin interdiffusion layer at the interface, although no intermediary stage between steel and coating electrochemical

potentials was observed during galvanostatic measurements. Moreover, this result may be induced by the presence of a Zn-Mn layer with very small grain size and high density of pores in the proximity of the substrate, as discussed in Section 4.3.2. It can be assumed that the variation of the elemental concentrations at the coating surface, in particular of Zn and Mn, is related to the time required for establishing a plasma and was already observed on the as-deposited coating (Figure 39).

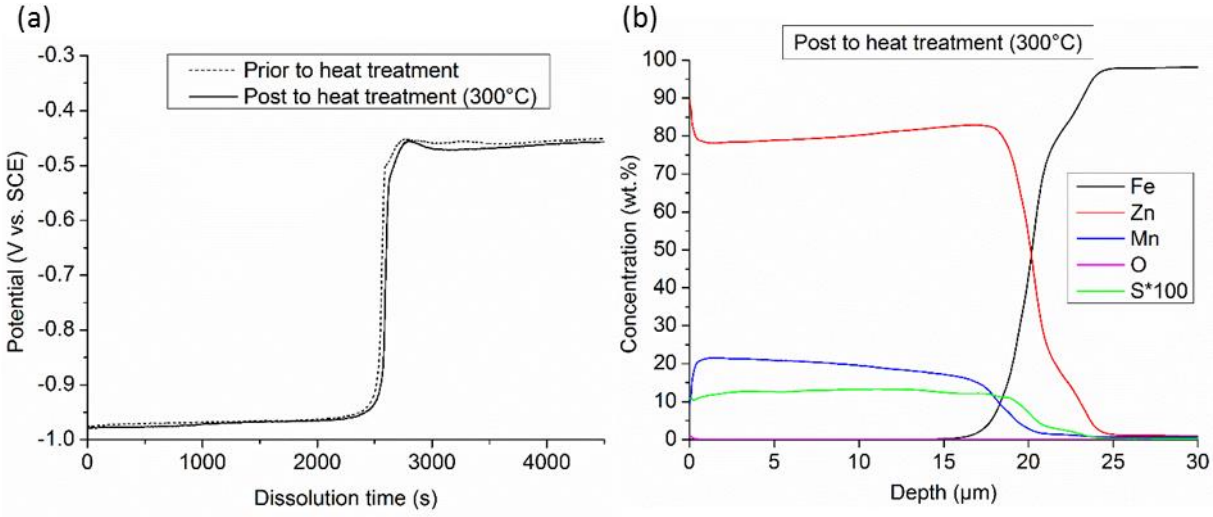

Figure 69: Evolution of the electrochemical potential of coating and substrate materials during galvanostatic dissolution prior to and post to heat treatment to 300 °C vs. SCE (a); Glow Discharge Optical Emission Spectroscopy (GDOES) concentration profile of the corresponding layer; heat treatment carried out in a furnace heated in argon.

Representative curves of galvanostatic dissolution of Zn-Mn coatings prior to and post to heating to a temperature of 500 °C are presented in Figure 70 and are based on 3 measurements.

It appears that the layers have an electrochemical potential similar to that of the as-deposited coatings (Figure 70) and approximately 500 mV lower than that of steel. The transition at the coating/steel interface appears to be discontinuous, which could be attributed to the formation of a thin interdiffusion layer at the interface coating/steel with an intermediary Fe content. The increase of the duration for the complete dissolution of the coating compared to the as-deposited layer can be mainly attributed to a slight variation of the thickness of the as-deposited coating and by the formation of an additional interdiffusion layer.

In order to study the microstructure of Zn-Mn coatings after heat treament to 500 °C, SEM-EDS analyses were carried out on cross-sections on several positions of two coated specimens. Representative elemental mappings are presented in Figure 71 a). The results indicate that homogeneous Zn and Mn contents are obtained over the entire coating thickness. The vertical stripes visible on the upper area of the SEM micrograph of Figure 71 a) may be associated to the cracks observed on the surface of the corresponding layer (Figure 68 c)). These cracks did not form along the entire thickness of the coating. Dark

spots visible in the SEM micrograph are most likely linked to the presence of pores in the coating, in a similar way to the results discussed in Section 4.3.2 for as-deposited coatings. A coating thickness of 16.7 ± 1.4 µm was obtained from a set of 17 measurements.

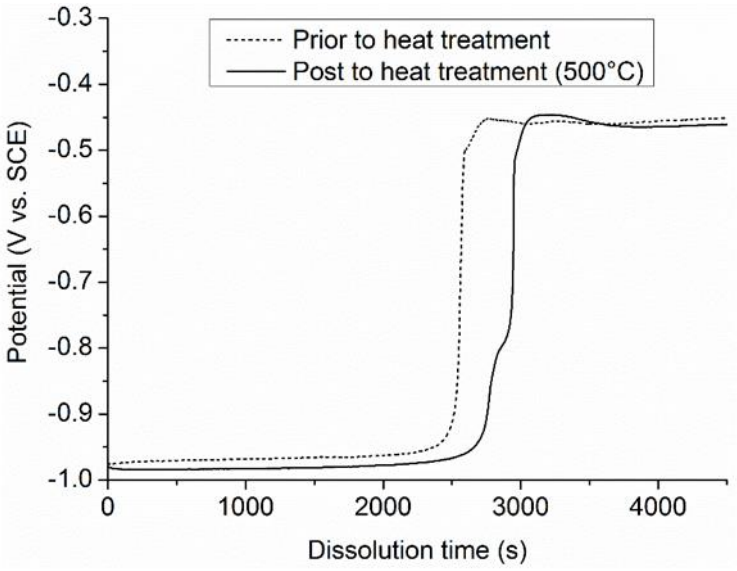

Figure 70: Evolution of the electrochemical potential of coating and substrate materials during galvanostatic dissolution prior to and post to heat treatment to 500 °C vs. SCE; heat treatment carried out in a furnace heated in argon.

In order to evidence the presence of an interdiffusion layer observed in the electrochemical measurements and determine its composition, more detailed SEM-EDS analyses were carried out at the coating/steel interface. Representative results from 5 cross-sectional analyses carried out on two coated specimens are presented in Figure 71 b). The coating appears to be constituted by a thick layer (Layer 1 in Figure 71 b)) visible in Figure 71 a) and separated fom the substrate by a thin intermediary layer (Layer 2 of Figure 71 b)). It is important to note that only the lower part of Layer 1 is visible on the elemental mapping presented in Figure 71 b). Layer 2 has a thickness of approximately 1.1 ± 0.2 µm and mainly consists of Zn and Fe, with a Mn content much lower than that of the upper layer. The decrease of the relative Mn content in the latter region of the coating may indicate that interdiffusion coefficient of Zn and Fe are higher than those of Mn and Fe. This particularity induces a preferential formation of Zn-Fe alloys during atomic diffusion. The presence of such an interdiffusion layer along with the absence of pores is an indication of a good adhesion of the coating with substrate steel.

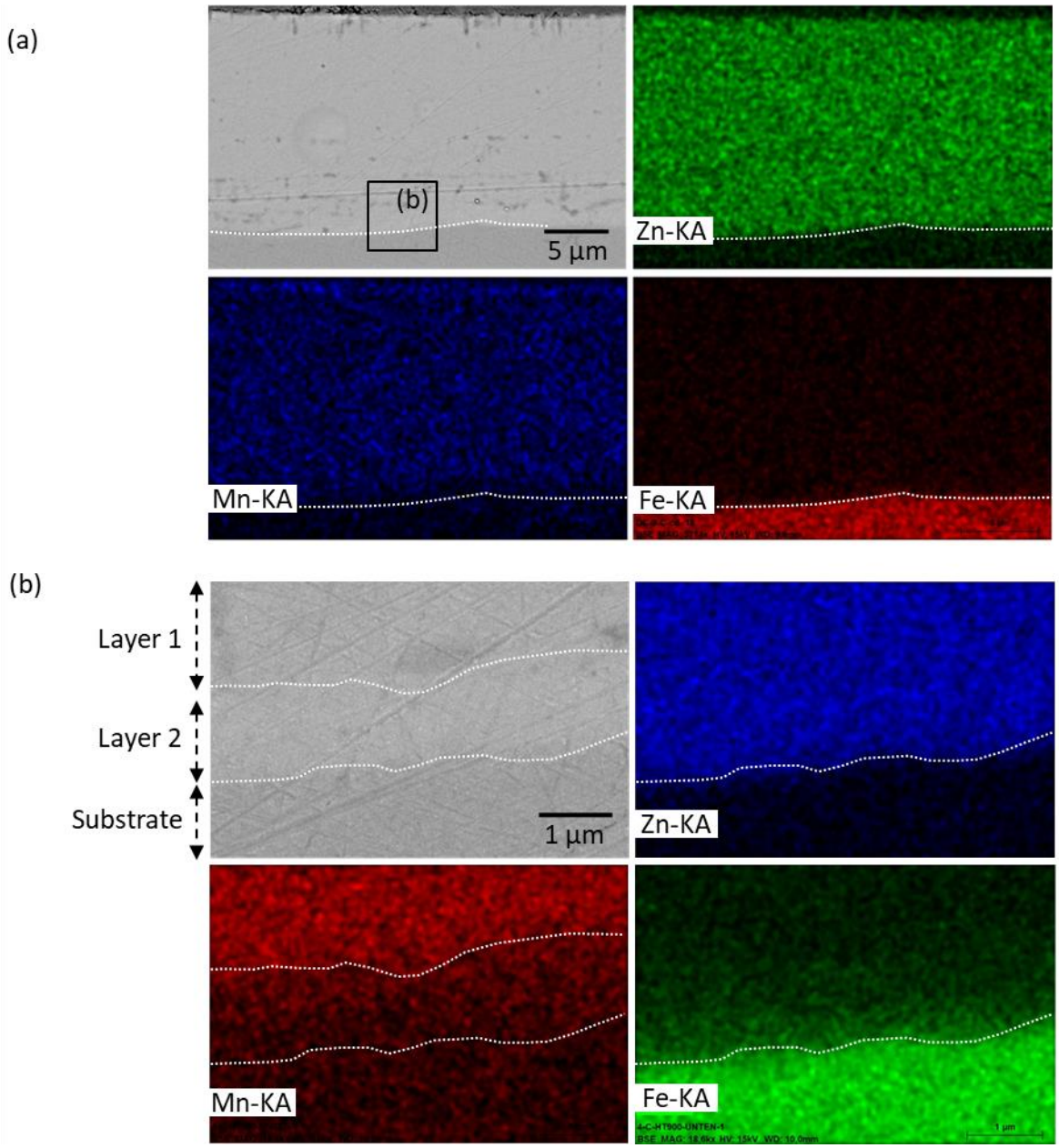

Figure 71: Cross-sectional SEM micrographs (BSE mode) and SEM-EDS elemental mapping of a complete Zn-Mn coating heat treated to 500 °C in a furnace heated in argon (a) and of the lower region of the coating with two identified layers 1-2 (b).

The chemical composition of both layers was determined by cross-sectional SEM-EDS analyses from sets of at least 10 measurements and is listed in Table 15. It should be noted that very little traces of iron were found in the lower part of Layer 1, that is to say in the region in contact with Layer 2. However, Fe was not taken into account in the quantification of the chemical composition of the complete Layer 1 due to the low intensity of the signals obtained.

It appears that the upper layer is a Zn-Mn alloy with a Mn content of 17.2 wt.%, which is very similar to the composition of the as-deposited coating. The initial ε_2-Zn-Mn phase is still present after heat treatment to 500 °C according to the XRD analyses (Figure 67). Given the

fact that the intermediary layer contains about 14.4 wt.% Fe, it appears that heat treatment up to 500 °C induces atomic diffusion mostly on the 1.1 µm-thick region below the coating.

The identification of the crystallographic phase formed in the interdiffusion layer is challenging, as XRD measurements are likely not to provide information regarding Layer 2 due to its depth. In addition, no literature data was found for Zn-Mn-Fe alloys formed at 500 °C. However, according to the scarce ternary phase diagrams (Appendix 3) of Zn-Mn-Fe alloys formed at 450 °C (Figure 112) and on the basis of the composition of Layer 2 (Table 25), the latter is likely to consist of a Γ_1 crystallographic phase which differs from the initial ε_2-Zn-Mn phase. This particularity could mean that a phase transformation occurs for the lower part of the coating during heat treatment.

Table 15: Zn, Mn and Fe relative contents (wt.%) in Layers 1 and 2 (Figure 71 b)) of Zn-Mn coatings heat treated at 500 °C in a furnace heated in argon, determined by semi-quantitative EDS analyses.

Analyzed area	Composition (wt.%)		
	Zn	Mn	Fe
Layer 1	82.8 ± 1.1	17.2 ± 1.1	-
Layer 2	78.2 ± 2.4	5.7 ± 1.8	16.1 ± 3.7

Conclusion

From these results, it appears that heat treatment of Zn-Mn coatings at temperatures of up to 300 °C does not influence the chemical composition, the crystallographic properties and corrosion resistance of the layers. However, after heating to a temperature of 500 °C, atomic diffusion processes take place between steel and Zn-Mn coatings, leading to the formation of a thin interdiffusion layer which was found to mainly consist of a mixture of Zn and Fe. The microstructural and anticorrosive properties as well as the chemical composition of the upper part of the coating are very similar to those of as-deposited layers.

Heat treatment to 700 °C in a protective atmosphere

A significant change in the microstructure and in the composition of Zn-Mn coatings takes place after reaching a temperature of 700 °C. A representative cross-sectional SEM micrograph of the corresponding Zn-Mn coatings is presented in Figure 72.

The coating appears to be composed of three layers, namely a thin superficial layer (Layer 1), a porous and inhomogeneous layer (Layer 2) and a compact layer located at the interface with steel (Layer 3). In the case of Layer 2, a thickness of 14.7 ± 2.8 was measured from 10 measurements. The high standard variation can be explained by the leveling effect of the as-deposited coating reported in Section 4.3.2, along with the high roughness of the substrate. However, it is interesting to note that a relatively constant thickness of 5.2 ± 0.5 µm was observed for Layer 3 on the basis of at 20 measurements on several cross-sections, which indicates that the interdiffusion front moves parallelly to the substrate surface during heat treatment.

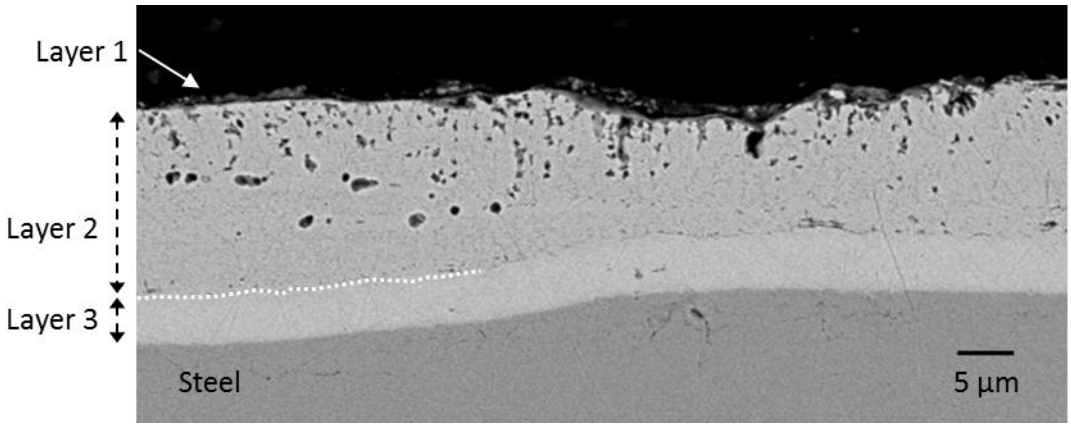

Figure 72: Cross-sectional SEM micrograph (BSE mode) of a Zn-Mn coating heat treated to 700 °C in a furnace heated in argon with three identified layers 1-3.

Representative SEM-EDS elemental distribution mappings presented in Figure 73 a) show that Layer 1 mainly contains Mn and O. On the basis of this observation and according to the XRD results (Figure 67), this layer most probably consists of MnO oxide. The Mn content appears to be higher in Layer 2 compared to Layer 3, while Layer 3 contains more iron than Layer 2. The Zn content is similar in both layers.

In order to understand chemical interdiffusion taking place at the interface with steel, more detailed SEM-EDS elemental mappings analyses were carried out in the lower part of Layer 2 and in Layer 3 (Figure 73 b)). From the results, it appears that the Fe content in Layer 3 is higher than that of Layer 2, in particular at the interface with substrate steel, as shown with the white arrow in the Fe mapping. A homogeneous Zn content can be observed in the lower part of Layer 2 and in Layer 3. The interface between Layer 2 and Layer 3 is porous (white arrow in the SEM micrograph) and contains higher oxygen and manganese contents than the rest of the area, as shown by the white arrow in the Mn mapping. It is interesting to note that Zn-Mn coatings heat treated to 700 °C in air have a similar microstructure (Section 5.2), with the exception of the presence of sublayers in the interdiffusion layer.

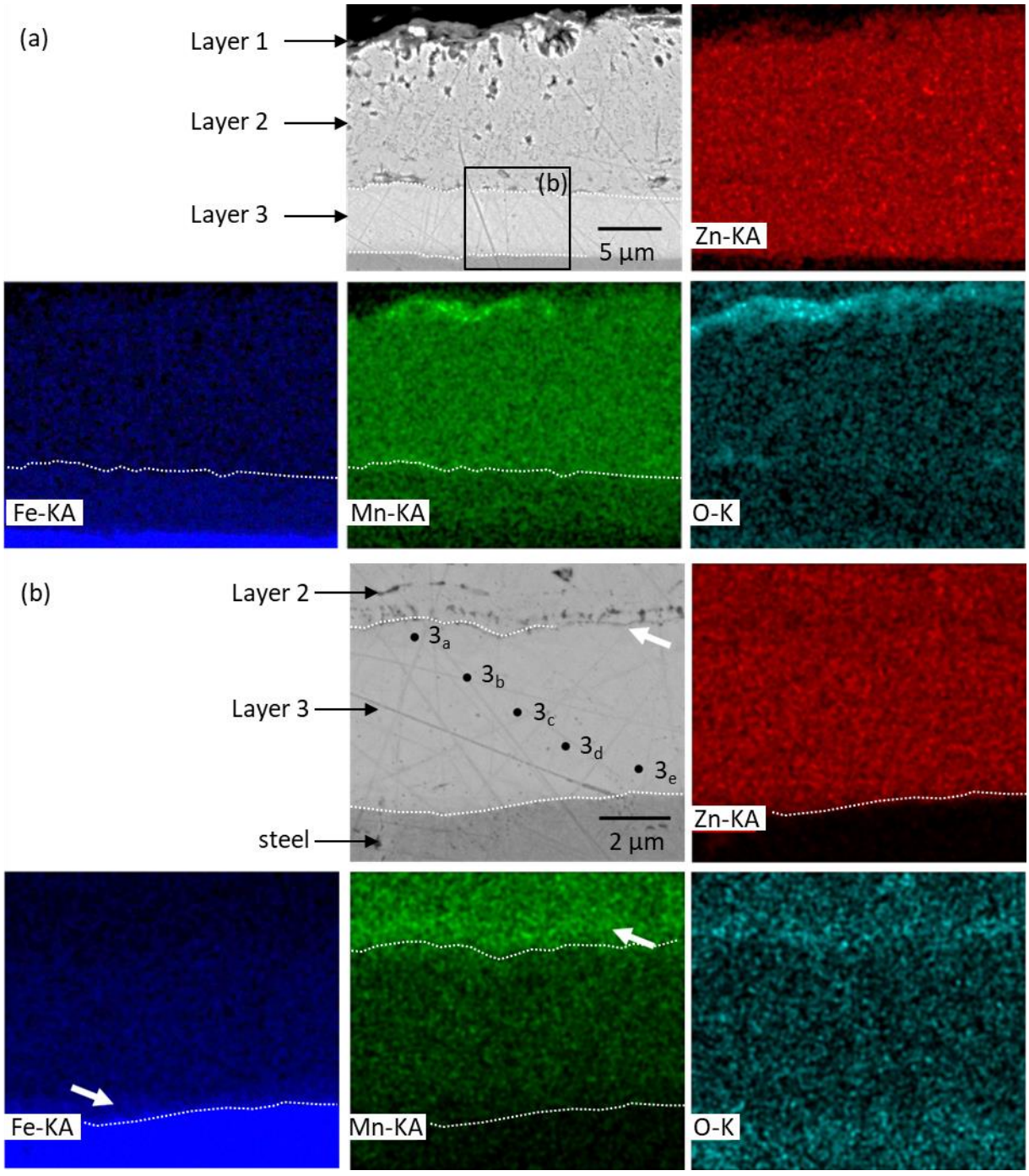

Figure 73: Cross-sectional SEM micrographs (BSE mode) and SEM-EDS elemental mappings of a Zn-Mn coating heat treated to 700 °C in a furnace heated in argon with three identified layers (1-3) (a) and of the lower region of Layer 2, Layer 3 and the substrate (b) with the positions (3_{a-e}) of semi-quantitative SEM-EDS measurements of the composition (Table 16) of Layer 3.

Semi-quantitative SEM-EDS measurements (Table 16) were carried out on the entire Layer 2 as well as on several positions of Layer 3 shown in Figure 73 b) in order to determine the composition of the coating. Layer 2 contains approximately 17.9 wt.% Mn, which is very similar to that of the as-deposited coating. This layer most probably consists of the initial ε_2-Zn-Mn phase observed in the XRD analyses in Section 5.3.1, although a small amount of Fe is present. It appears from Table 16 that Layer 2 contains about 0.5 wt.% S, contrary to Layer 3

which does not contain sulfur. This point will be discussed later. Layer 3 was found to have a composition gradient with an increasing Fe content and a decreasing Mn content towards the substrate, in good accordance with the results reported in Figure 73. The amount of Zn is relatively constant with approximately 83.6 wt.%.

As reported in Figure 67, the ε_2-Zn-Mn phase is still present after heating to 700 °C and may be present in Layer 2 of the coating, in good accordance with the chemical composition of the latter. The crystallographic properties of Layer 3 of the coating heated to 700 °C cannot be determined with certitude, as only the upper part of the coating is likely to be analyzed by XRD, as stated in Section 4.3.3.

On the basis of the compositions observed for Layer 3 (Table 16) and of the Zn-Mn-Fe alloy diagrams obtained at 625 °C and 720 °C presented in Appendix 3 (Figure 113), the identification of the crystallographic phases formed in the interdiffusion layer (Layer 3) is challenging. In fact, only very limited composition ranges were reported in the literature. It is important to note that the literature data regarding the crystalloraphic phases formed at high temperature is obtained in thermodynamically stable conditions, which is not the case in this study, as the phases are formed during heat treatment and are quenched to room temperature. Therefore, further investigations are required to identify the crystallographic properties of the interdiffusion phases formed at this temperature.

Table 16: Zn, Mn, Fe and S relative contents (wt.%) in Layer 2 and Layer 3 (Figure 72) of Zn-Mn coatings heat treated to 700 °C in a furnace heated in argon determined by semi-quantitative EDS analyses; positions 3_{a-e} are shown in Figure 73 b).

Analyzed area	Composition (wt.%)			
	Zn	Mn	Fe	S
Layer 2 (n=6)	79.8 ± 1.5	17.9 ± 1.0	1.9 ± 0.3	0.5 ± 0.3
Layer 3 - Position 3_a	82.1	12.9	5.1	-
Layer 3 - Position 3_b	85.1	7.5	7.3	-
Layer 3 - Position 3_c	84.8	6.8	8.4	-
Layer 3 - Position 3_d	82.0	6.9	11.2	-
Layer 3 - Position 3_e	80.0	4.9	15.1	-
Layer 3 (average contents)	83.6 ± 1.2	7.9 ± 2.0	8.5 ± 1.8	-

The evolution of the electrochemical potential of coating and substrate materials is presented in Figure 74 a) and is based on 6 measurements on 2 specimens. In addition, representative curves of concentration profiles are shown in Figure 74 b) and are based on analyses carried out on 2 specimens. The electrochemical potential of the coating is similar to that of the initial deposit, which means that the low Fe content reported in Table 16 for Layer 2 does not influence the electrochemical potential of the deposit. A stage with intermediary potential values appears at the coating/steel interface, which most probably corresponds to Layer 3 observed in Figure 73.

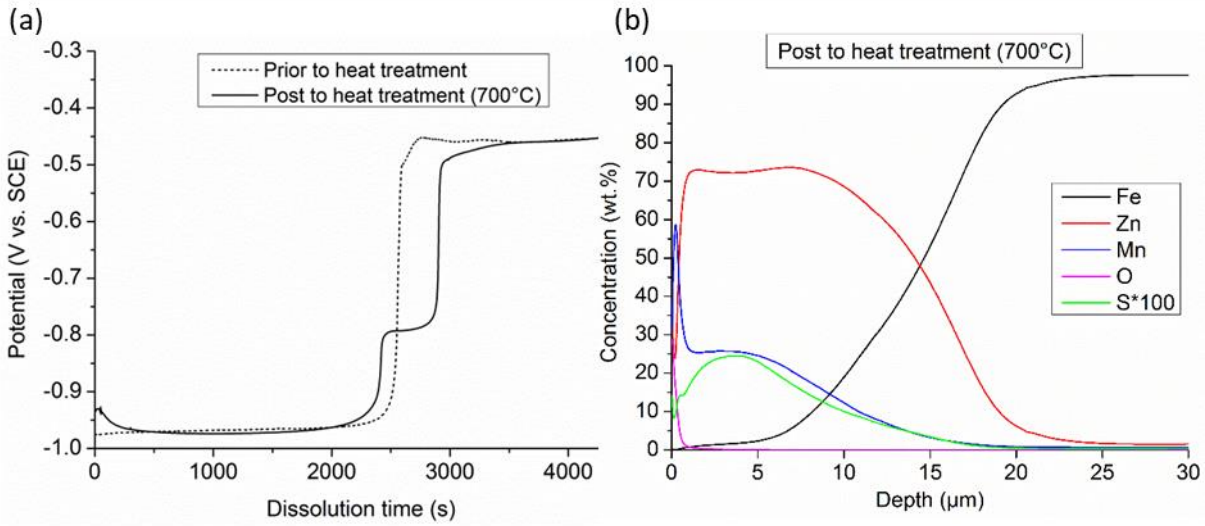

Figure 74: Evolution of the electrochemical potential of coating and substrate materials during galvanostatic dissolution prior to and post to heat treatment to 700 °C in a furnace heated in argon, vs. SCE (a); Glow Discharge Optical Emission Spectroscopy (GDOES) concentration profile of the corresponding layer (b).

It should be noted that the total dissolution time of the coating is slightly higher than that of the as-deposited coating. This particularity can be explained by the formation of an interdiffusion layer (Layer 3), thereby increasing the thickness of the coating. Stages with similar potentials and durations were observed in the case of Zn-Mn coatings heat treated to 700 °C under air (Figure 57), with the exception of the presence of sublayers in the interdiffusion layer. The gradual increase of the Fe content in the coating towards steel observed in the GDOES concentration profiles (Figure 74 b)) can be explained by the presence of Fe-containing interdiffusion layers or by the variation of the thickness of the coating and the resulting short time required to detect the presence of Fe. The high Mn and O content values observed in the first stage of GDOES measurements are most probably related to the presence of Mn oxides in the superficial layer of the coating, as confirmed by the signals corresponding to MnO observed in XRD analyses (Figure 67). It is interesting to note the presence of traces of S in the upper part of the coating, which confirms the above-mentioned results from the cross-sectional SEM-EDS analyses.

In order to further study the microstructure and the phase distribution in Zn-Mn coatings heat treated to 700 °C, cross-sectional SEM-FIB analyses were carried out on two positions of one specimen with dimensions of 1 cm². Representative micrographs are presented in Figure 75. A decohesion of the coating took place in the lower region of the layer. Such a defect was not observed during SEM-EDS cross sectional analyses and is very likely to result from the specimen preparation by mechanical cutting prior to FIB preparation. A thin carbon layer was deposited on the coating for improving surface state of the cross-sectional views and is visible on the top surface of the micrograph.

The three layers identified in the previous analyses can be observed (Figure 75 a)). The thickness of the oxide layer (Layer 1) is 0.6 ± 0.1 µm and was determined on the basis of

12 measurements. The latter appears to be homogeneously distributed on the top surface of the coating.

It is important to note that the columnar structure reported in Section 4.3.2 for the as-deposited Zn-Mn coatings is not observed after heat treatment up to 700 °C. Instead, large grains with not well-defined geometries and sizes of at most 3 µm can be observed in Layer 2 (Figure 75 a)). Thin dark spots with a diameter of approximately 100 nm and accompanied with a high density of pores are formed at the interface between Layer 2 and Layer 3 (Figure 75 b)) and at the grain boundaries of Layer 2 (Figure 75 c)). The pores observed may be related to the Kirkendall effect, as reported in the case of the aluminized coating (Section 1.5.2) and based on the difference in the diffusivity of Fe, Mn and Zn metals in the coating. Moreover, a coalescence of the pores formed during electrodeposition and visible in Figure 43 may take place at high temperature. The chemical composition of these areas could not be determined due to the limited resolution of SEM-EDS technique, along with the low size of the details.

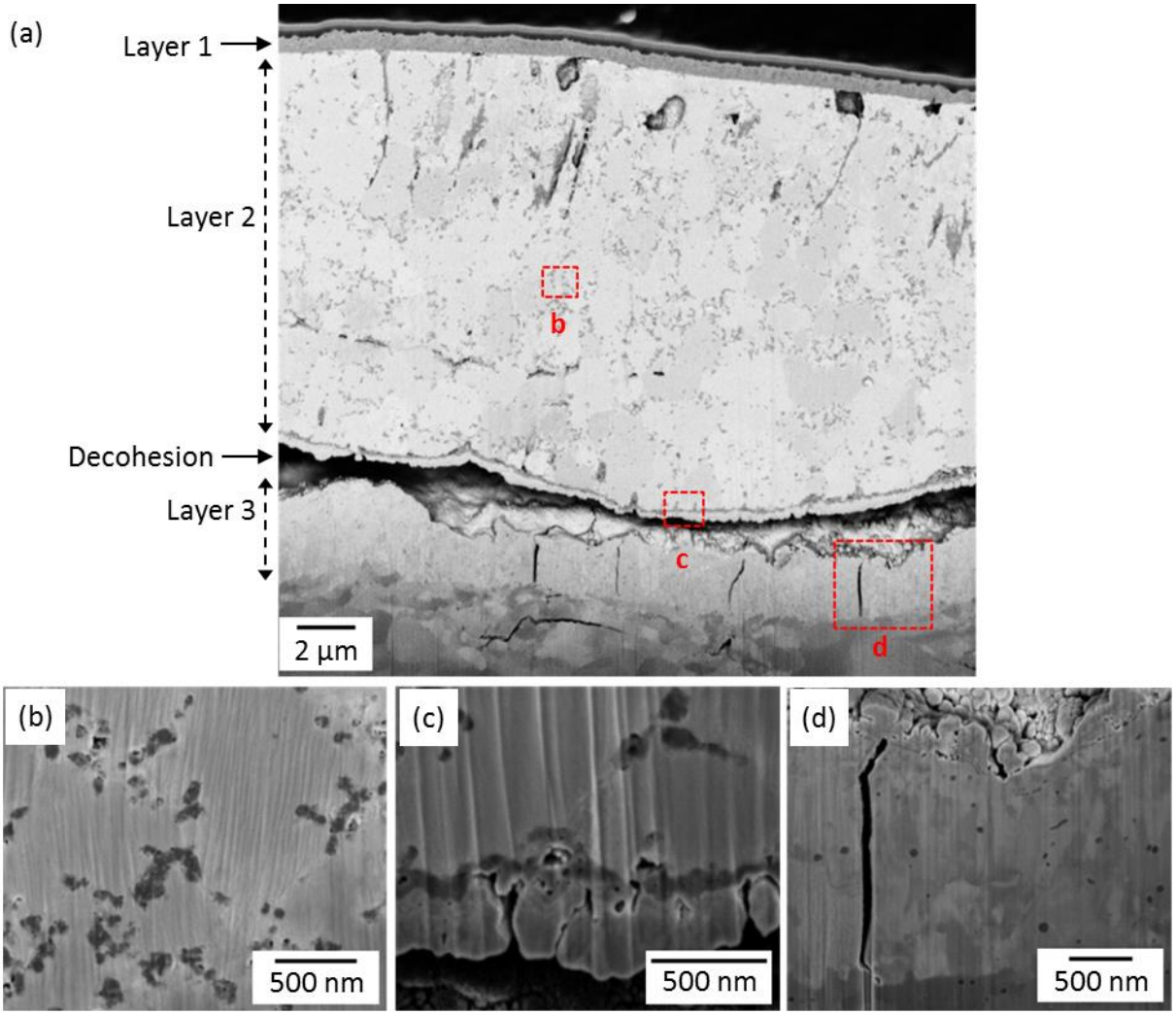

Figure 75: Cross-sectional SEM-FIB micrographs of a Zn-Mn coating after heat treatment to 700 °C in a furnace heated in argon; enlargements of characteristic areas b, c and d.

The interdiffusion layer (Layer 3) is compact and contains cracks which stop at the coating/steel interface (Figure 75 d)). These cracks were not observed during cross-sectional SEM-EDS analyses and may have been induced by the mechanical preparation of the specimens required for SEM-FIB milling. A further possible explanation for this observation is a difference in the expansion coefficient of steel and coating materials during heating and quenching. It is interesting to note that these cracks are straight, in contrast to the discontinuous cracks observed in Zn-Mn alloys heated to 700 °C in air, which may be related to the composition gradient observed in Layer 3.

In order to explain the presence of the dark spots observed in Layer 2 and to determine the composition of the different layers of the coating, Scanning Transmission Electron Microscopy (STEM) elemental mappings (Figure 76) were carried out on two areas of a lamella prepared by means of FIB milling and with a thickness of at most 250 nm. It should be noted that the thickness of the lamella was found to vary in the coating, most probably due to the presence of layers with different compositions and hardness and providing different behaviors during ion beam preparation. In agreement with the SEM-FIB analyses performed on cross sections (Figure 75), Layer 2 mainly consists of compact grains separated with areas with defects such as pores or precipitates (Figure 76 a)). The same areas were reported in the case of Zn-Mn coatings heat treated to 700 °C in air (Figure 54). It is noteworthy that the dark spots contain higher Mn and S content than the compact areas corresponding to the grains (arrows in Mn and S mappings of Figure 76 b)). As discussed in Section 4.3.1, the presence of sulfur can be explained by the use of ammonium thiocyanate in the electroplating bath. According to the diffraction pattern obtained at this temperature (Figure 67 d)), these areas are likely to contain manganese sulfur (MnS).

In addition, oxygen appears to be partly present on the dark areas, which indicates that oxides such as MnO may be present. As the compact grains and Layer 3 do not seem to contain sulfur, it can be assumed that S segregates in these regions during heat treatment.

The pores observed in SEM-FIB analyses were not visible from STEM mappings, presumably due to their relatively low size compared to the thickness of the lamella used for STEM analyses. It is interesting to note that the dark spots located at the interface between Layer 2 and Layer 3 contain high Mn and O contents compared to the rest of the area. These spots partly contain Fe and S, as shown by the arrows in the corresponding Fe and S mappings of Figure 76 b). Their presence could not be explained. Layer 2 and Layer 3 appear to contain similar Mn and Zn contents, irrespective of the dark spots. The iron content appears to be much higher in Layer 3 and increases towards steel, which confirms GDOES and cross-sectional SEM-EDS results mentioned earlier.

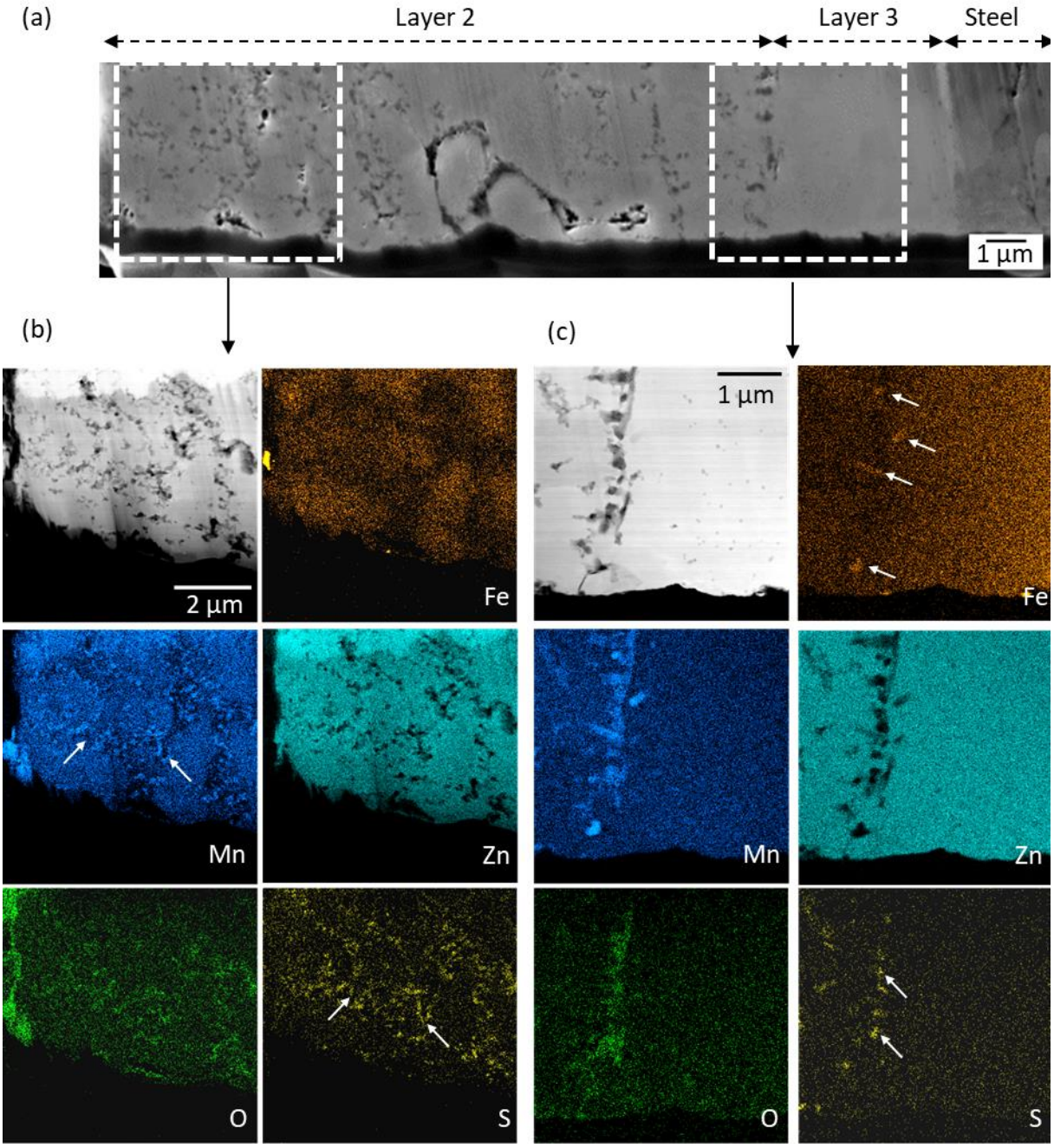

Figure 76: Cross-sectional SEM-FIB micrograph of the lamella (a) used for Scanning Transmission Electron Microscopy (STEM) analyses and prepared by means of FIB milling; STEM elemental mapping of Fe, Mn, Zn, O and S elements on Layer 2 (b) and Layer 3 (c) of a Zn-Mn coating heat treated to 700 °C in a furnace heated in argon.

Conclusion

It can be concluded that a significant change in the microstructure of Zn-Mn coatings is observed after reaching a temperature of 700 °C in a furnace in presence of argon. An oxide scale mostly consisting of MnO was observed on the top surface of the coating, despite the use of a protective atmosphere during heating. At this temperature, atomic diffusion of Fe takes place into the entire deposit. The microstructure with columnar grains observed prior

to heat treatment was found to disappear. Instead, globular grains were observed on the upper part of the coating (Layer 2), which appear to consist of the ε_2-Zn-Mn phase. Noteworthy defects located at the grain boundaries of the upper layer (Layer 2) and at the interface between Layer 2 and Layer 3 were found by STEM analyses to consist of precipitates with high Mn, S and O contents. The presence of manganese sulfur (MnS) was evidenced by means of XRD measurements, while oxides such as MnO are also assumed to form on these areas. It is important to note that additional investigations are required to precise the temperature at which these microstructural transformations occur, as no study was carried out at intermediary temperatures comprised between 500 °C and 700 °C. A compact interdiffusion layer forms at the interface between coating and steel, with a thickness higher than that observed at a temperature of 500 °C and with increasing and decreasing Fe and Mn contents, respectively. It is interesting to note that similar microstructures and anticorrosive properties were reported in the case of Zn-Mn alloys heat treated to 700 °C under air (Section 5.2), which indicates that the atmosphere used does not have a significant influence on the properties of Zn-Mn coatings below 700 °C.

Heat treatment to 900 °C in a protective atmosphere

Various microstructures were observed after heating Zn-Mn coatings to 900 °C in presence of argon, as shown in Figure 77. In fact, different types of curves of the potential evolution were obtained during galvanostatic dissolution, which indicates the presence of regions with different compositions and phase distributions.

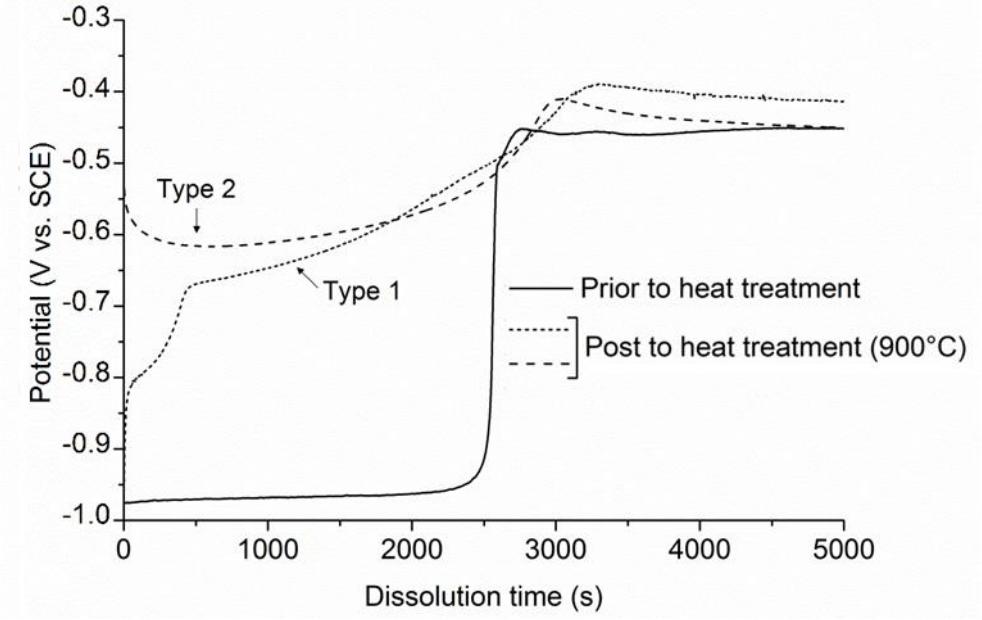

Figure 77: Evolution of the electrochemical potential of coating and substrate materials during galvanostatic dissolution prior to and post to heat treatment to 900 °C in a furnace heated in argon, vs. SCE.

From the set of 7 measurements carried out on two specimens, it appears that two types of coatings can be obtained after heating to 900 °C. Some curves (Type 1 in Figure 77) were found to consist of two stages, namely a first stage with an electrochemical potential about

400 mV lower than that of steel and a second stage with a lower sacrifical effect of 150 mV. This results indicates that the coating most probably consists of two phases with different compositions. It is important to note that the duration required to dissolve both phases was found to vary, which indicates that the relative amounts of the phases in the coatings varies. Other measurements show coatings constituted by a unique phase with a potential difference of approximately 150 mV with steel (Type 2 in Figure 77).

The duration of the complete dissolution of the coatings was found to be similar to that of the as-deposited layers, which indicates that heat treatment does not induce significant changes in the thickness of the coatings. Both types of coatings will be characterized in the next parts in order to understand the behavior of the Zn-Mn alloys at this temperature.

Heat treatment to 900 °C: Type 1 coatings

A representative SEM-EDS elemental mapping of Type 1 Zn-Mn coatings treated to 900 °C in a furnace heated in argon is presented in Figure 78. The composition of both regions was determined from sets of at least 5 measurements by EDS analyses. From the results listed in Table 17, it appears that the Zn-rich phase shown in Figure 78 contains about 85.3 wt.% Zn and 13.7 wt.% Fe, while the Fe-rich phase contains 40 wt.% Zn and 57.6 wt.% Fe. The high standard deviations obtained for Zn and Fe can be related to a gradient in the composition of the coating. The presence of the Zn-rich phase explains the initial stage with low electrochemical potentials observed in galvanostatic dissolution measurements (Type 1 in Figure 77). It is interesting to note that a very low Mn content of at most 2.3 wt.% was observed in the layer after heat treatment. This result can be explained by significant oxidation of Mn, which forms a thick superficial oxide layer, as visible in the Mn and O mappings shown in Figure 78.

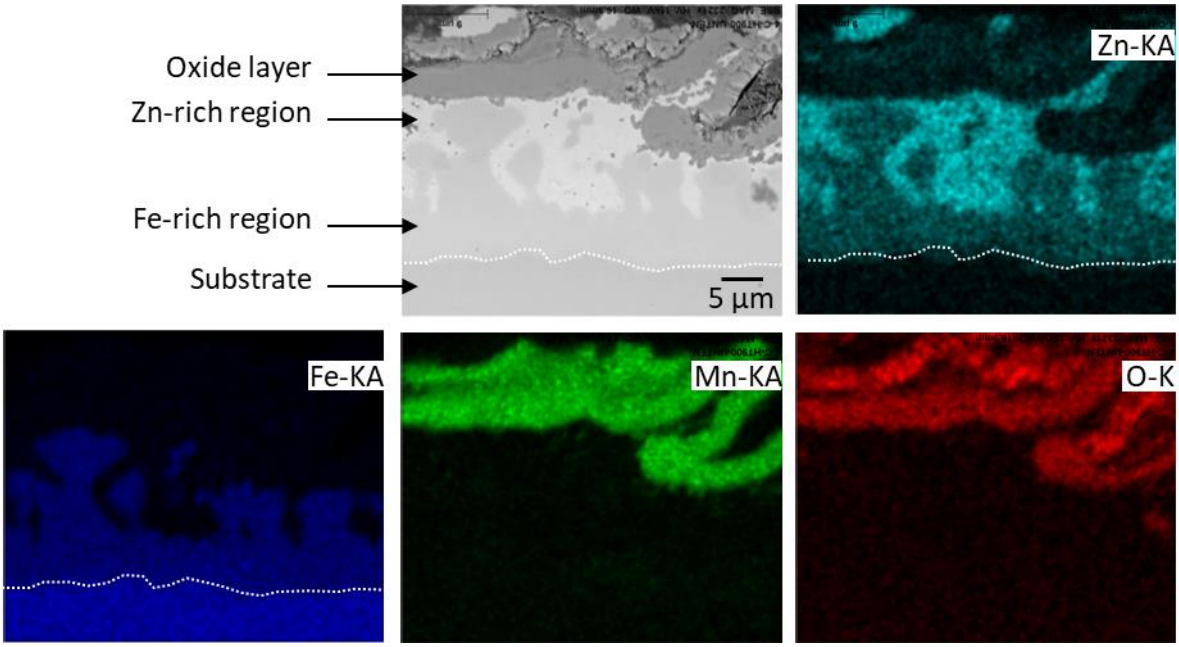

Figure 78: Cross-sectional SEM micrograph (BSE mode) and SEM-EDS elemental mapping of a Zn-Mn coating (Type 1) heat treated to 900 °C in a furnace heated in argon.

Thicknesses of 6.9 ± 6.1 µm and 11.1 ± 3.8 µm were measured for Zn- and Fe-rich regions, respectively, on the basis of sets of 24 measurements on two specimens. The high standard deviation values obtained, in particular in the case of the Zn-rich phase, can be related to the heterogeneous distribution of both phases among the lower part of the coatings, as visible in Figure 78. The superficial oxide layer has a thickness of 4.6 ± 2.7 µm determined from 35 measurements on 2 specimens. This value is much lower than that obtained in the case of Zn-Mn coatings heat treated to 900 °C in air.

The Zn-rich region is likely to partly consist of the Γ-Fe_3Zn_{10} phase for which signals were observed in the XRD patterns of Zn-Mn coatings heat treated to 900 °C in argon (Figure 67 f)). In fact, the Zn content of the Zn-rich region (Table 17) is slightly above the composition range of 73.1-84.2 wt.% Zn of the Fe_3Zn_{10} phase reported in Section 5.3.1. However, it should be considered that the remaining Mn content may induce changes in the composition domains and the properties of the crystallographic phases.

Table 17: Chemical composition of the two phase regions (Figure 78) formed in a Zn-Mn coating (Type 1) treated to 900 °C in a furnace heated in argon, determined by semi-quantitative EDS analyses.

Analyzed area	Composition (wt.%)		
	Zn	Mn	Fe
Zn-rich region	85.3 ± 5.1	1.2 ± 0.3	13.7 ± 5.2
Fe-rich region	40.0 ± 4.9	2.3 ± 1.9	57.6 ± 3.2

Heat treatment to 900 °C: Type 2 coatings

Representative SEM cross-sectional micrographs presented in Figure 79 show Zn-Mn coatings which can be either compact (Figure 79 a)) or porous (Figure 79 b)) and which appear to have a homogeneous composition, as no significant contrast differences are visible in the BSE micrographs. Therefore, it can be presumed that this coating corresponds to the Type 2 layers observed in Figure 77, with the presence of a unique dissolution stage.

A thickness of 15.1 ± 3.5 µm was obtained on the basis of 40 measurements carried out on two coated specimens.

It can be assumed that the porous microstructure observed in Figure 79 b) was induced by evaporation of volatile phases contained in the coating, in particular Zn-rich phases, which are most probably located between Fe-rich grains, in a similar way to the microstructure shown in Figure 78.

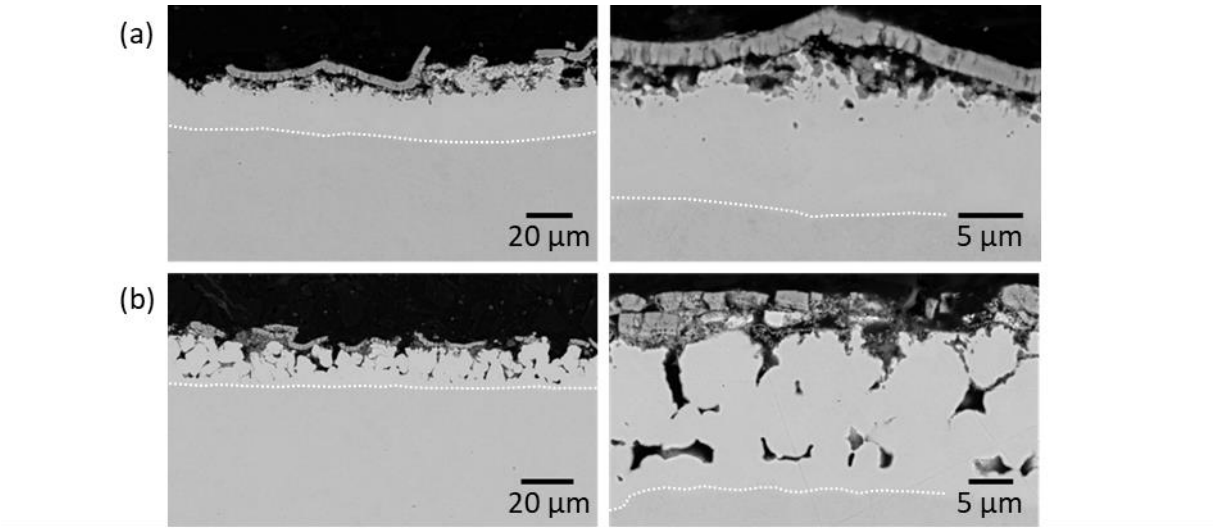

Figure 79: Cross-sectional SEM micrographs (BSE mode) of compact (a) and porous (b) Zn-Mn coatings (Type 2) after heat treatment to 900 °C in a furnace heated in argon.

A superficial oxide layer with a thickness of 1.8 ± 0.3 µm can be observed on the top surface of the coating. It is interesting to note that voids and particles are visible below the oxide scale, indicating that a low adhesion of the latter with the coating takes place.

In order to determine the composition of the different regions observed in the coatings, elemental mappings and composition measurements were carried out on several positions on heat treated specimens by means of SEM-EDS cross-sectional views. Representative mappings are presented in Figure 80.

According to Mn and O mappings shown in Figure 80 and XRD analyses of the corresponding coatings (Figure 67 f)), the superficial layer is mainly constituted by MnO. Traces of Zn can also be observed in the latter area of the coating, and may indicate the formation of Zn oxides. It is interesting to note that the particles formed between the oxide scale and the heat treated deposit are mainly composed of S, Mn and O. It can be assumed that the sulfur-rich areas observed after heating to 700 °C (Figure 76) migrate from the grain boundaries of the coating towards the surface by a further increase of the temperature. This region of the coating may also contain oxides, which could not be identified. From the SEM-EDS mappings, the coating appears to consist of two regions, namely Region 1 and Region 2 for which the interface could not be determined with precision. Both regions appear to contain similar Zn contents but different Fe and Mn contents.

Sets of at least 24 measurements of the elemental composition were carried out by means of EDS analyses on both regions. The results are presented in Table 18. The Zn content appears to be constant in the entire coating. In addition, a higher Fe content and a lower Mn content in Region 2 were obtained compared to Region 1, which indicates that Fe and Mn are diffusing towards the surface of the coating during heat treatment.

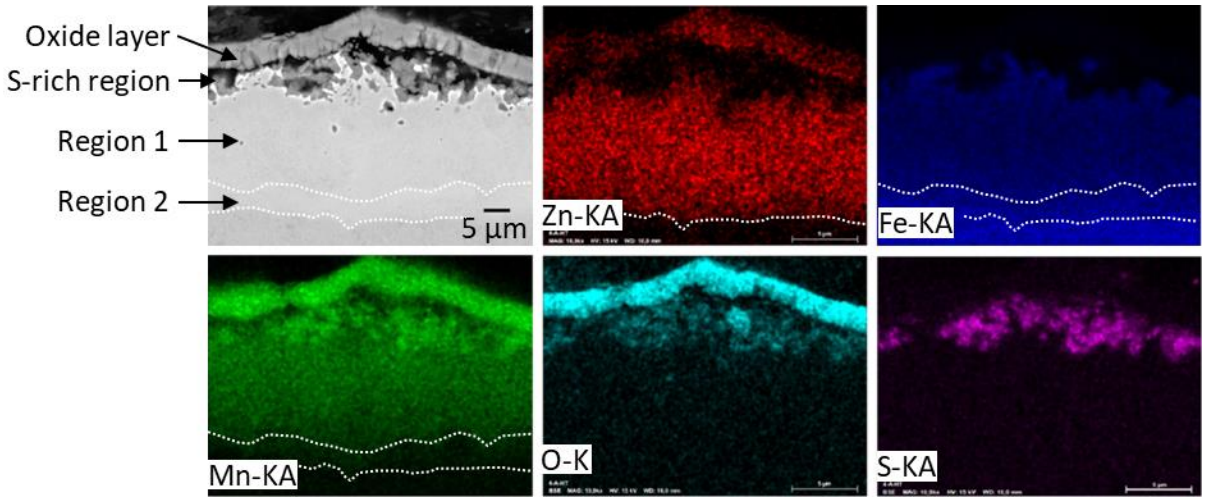

Figure 80: Cross-sectional SEM micrograph (BSE mode) and SEM-EDS elemental mapping of Zn-Mn coatings (Type 2) treated to 900 °C in a furnace heated in argon.

It is important to note that a high Mn content of up to 14.9 wt.% is still present in the coatings after heating to 900 °C. The presence of a high amount of Fe in both regions may explain the presence of a moderate electrochemical potential difference of about 150 mV with steel during galvanostatic measurements (Figure 77). The high standard deviations obtained in these measurements and the absence of clear interface between both regions is very likely related to the presence of a unique layer with a composition gradient. In addition, the presence of two stages with different electrochemical potentials could not be identified in the galvanostatic dissolution measurements (Figure 77).

Table 18: Chemical composition of Layer 1 and Layer 2 (Figure 80) formed in Zn-Mn coatings (Type 2) heat treated to 900 °C in a furnace heated in argon, determined by semi-quantitative EDS analyses.

	Composition (wt.%)		
	Zn	Mn	Fe
Region 1	20.4 ± 2.4	14.9 ± 3.9	64.7 ± 4.5
Region 2	21.1 ± 6.5	6.2 ± 1.5	72.6 ± 6.5

Conclusion

On the basis of the investigations carried out on Zn-Mn coatings heat treated to a temperature of 900 °C in argon, it appears that the use of the considered protective atmosphere and experimental setup is not sufficient to prevent oxidation mechanisms, in particular of Mn. An oxide scale with a thickness of several micrometers forms on the top surface of the coating in the shape of a non-homegeneous and fractured layer with a high amount of loose particles. Contrary to coatings heated to 900 °C in air, it is important to note that high Mn contents could be obtained on some regions of the coatings. The defects containing high amounts of S observed at the grain boundaries of layers heat treated to 700 °C were found to migrate to the top surface of the coating at 900 °C, mainly in the area below the oxide scale. A complex and non well-defined microstructure was observed, presumably due to the partial and localized exposure of the layers to oxidation, leading to a

change in the distribution and in the composition of the phases formed in the coatings. Besides, the presence of porous layers (Figure 79 b)) may be related to the evaporation of Zn-rich phases at high temperature. Furthermore, as Zn-Mn coatings deposited in presence of additives were found to provide a leveling effect of the roughness of the steel substrate (Section 4.2.2), the local variation of the thickness of as-deposited coatings may have induced heterogeneities in terms of phase distribution post to heat treatment. It should be noted that the thickness of the coatings post to heat treatment is similar to that of the as-deposited layers despite the formation of interdiffusion layers, which further points out the loss of metallic Zn and Mn due to oxidation and evaporation.

Heat treatment with relevant industrial process parameters

In order to evaluate the process-window of the coating materials within the austenitization temperature range, specimens were heat treated at conventional austenitizing temperatures of 900 °C and 920 °C in a furnace heated in argon at respectively 920 °C and 940 °C and with dwell times of 45 s, 90 s and 120 s after reaching the temperature of 860 °C and cooled down in the press tools. The parameters used are summarized in Table 11. Sets of at least 3 measurements of galvanostatic dissolution were carried out on the corresponding coated specimens. Representative curves of the evolution of the electrochemical potential of the layers are presented in Figure 81.

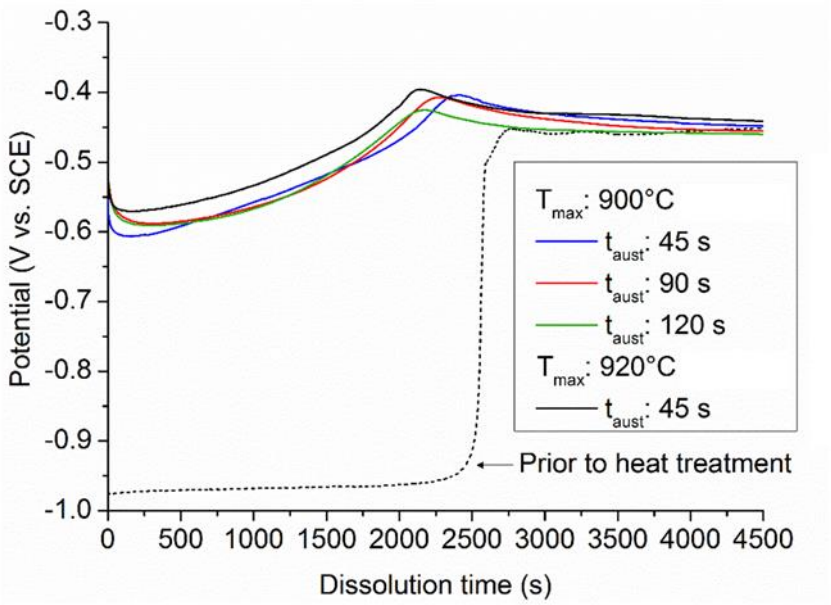

Figure 81: Representative curves of the electrochemical potential of coating and substrate materials during galvanostatic dissolution prior to and post to austenitizing treatment to temperatures of 900 °C and 920 °C with dwell times of 45, 90 and 120 s above 860 °C in a furnace heated in argon, vs. SCE.

It is striking to note that very similar potential values are obtained, regardless of the heat treatment parameters used, which means that in these conditions the dwell time does not influence the anticorrosive properties of the Zn-Mn alloys. A potential difference of approximately 140 mV between steel and coating materials is obtained, which means that the layers provide a moderate sacrificial protection to steel in comparison to the difference

of 500 mV between steel and coating prior to heat treatment. The total duration for coating dissolution appears to be similar for all coatings and is lower than that obtained for the as-deposited coating. In the same way as for Zn-Mn coatings heat treated to 900 °C, this particularity can be explained by the loss of a part of the coating, namely a loss of Mn by high temperature oxidation. In addition, evaporation of a part of the coating is likely to have taken place in the considered conditions, in a similar way to Zn-Mn coatings (Type 2) heat treated to 900 °C under argon and studied in the last section.

In order to study the microstructure and the composition of the above-mentioned coatings, cross-sectional SEM analyses were carried out on two specimens heat treated at 900 °C with a dwell time of 45 s. Representative micrographs are shown in Figure 82. The coatings consist of a compact layer with a good adhesion to steel substrate and a mean thickness of 10.9 ± 2.2 µm as well as a superficial layer with a thickness of 1.8 ± 0.6 µm, determined from sets of at least 17 measurements.

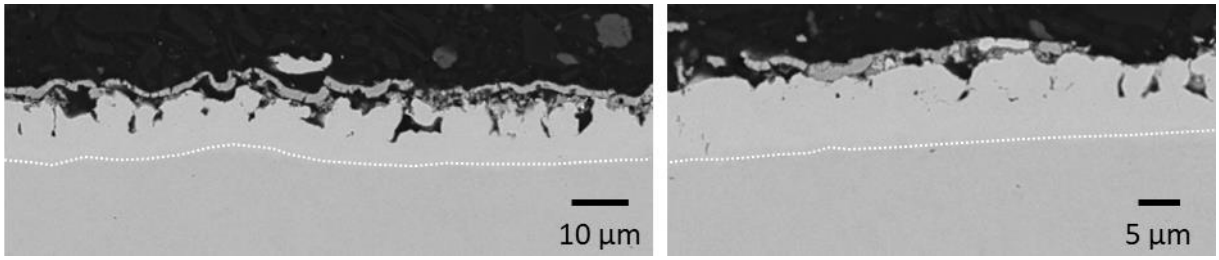

Figure 82: Cross-sectional SEM micrographs (BSE mode) of Zn-Mn coatings austenitized at 900 °C with an austenitizing time of 45 s above 860 °C in a furnace heated in argon.

A representative cross-sectional elemental mapping of the corresponding coatings is presented in Figure 83. From the results, it appears that the oxide layer consists of Zn and Mn oxides. In good accordance with the observations from Figure 80, S-containing particles are found below the superficial layer. The underlying coating appears to be constituted by two compact regions with different compositions, namely Region 1 and Region 2. The compositions of both regions were determined on the basis of sets of at least 15 measurements by means of EDS analyses. The results are listed in Table 19 and prove the presence of similar Zn contents for both layers.

Region 1 contains a much higher Mn content of approximately 15.2 wt.% compared to Region 2. It is important to note that this value is slightly lower than that of the initial Mn content of the coating. Similar compositions were observed in the case of Type 2 coatings heat treated to 900 °C (Table 18), which can be related to the use of similar heat treatment durations.

Cross-sectional analyses were carried out on Zn-Mn coatings heat treated at 900 °C with a longer austenitizing time of 120 s by means of SEM. Representative micrographs are presented in Figure 84 and indicate the formation of a coating with a microstructure similar to that shown in Figure 79 a), namely with the presence of a compact layer with a good adhesion to steel substrate located below a non-adherent oxide layer with a thickness of

1.5 ± 0.6 µm from 15 measurements. A coating thickness of 10.4 ± 2.1 µm was obtained on the basis of 15 measurements, which is very similar to the value obtained for Zn-Mn coatings heat treated with an austenitizing time of 45 s. This result confirms the similar durations required to complete the dissolution of the corresponding coatings in Figure 81.

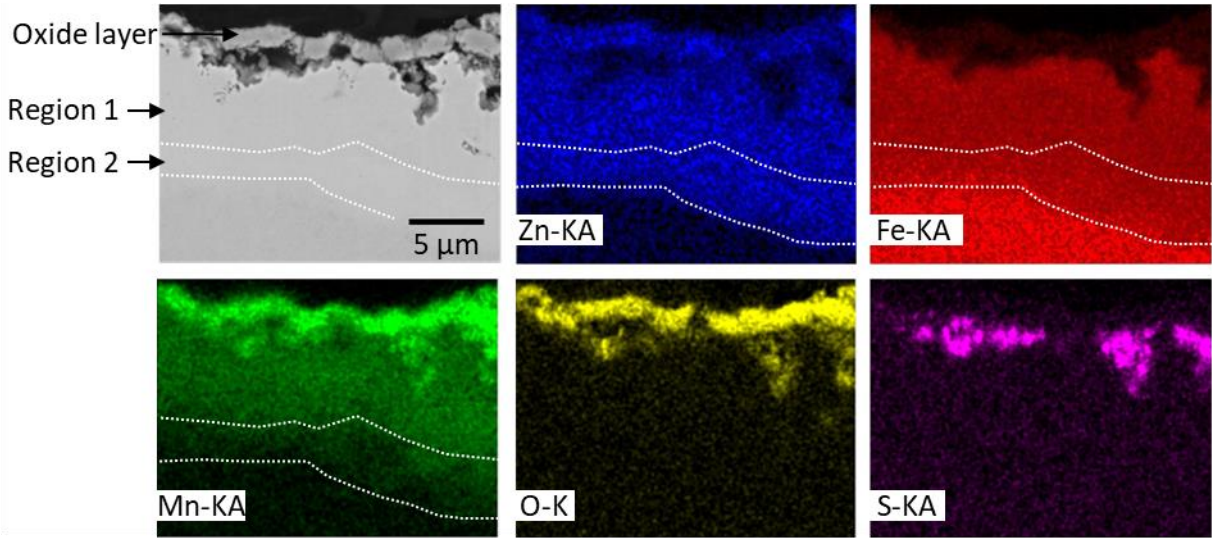

Figure 83: Cross-sectional SEM micrograph (BSE mode) and SEM-EDS elemental mapping of Zn-Mn coatings heat treated to 900 °C with an austenitizing time of 45 s above 860 °C in a furnace heated in argon.

Table 19: Chemical composition of Region 1 and Region 2 observed in Zn-Mn coatings austenitized at 900 °C with an austenitizing time of 45 s above 860 °C in a furnace heated in argon, determined by semi-quantitative EDS analyses.

	Composition (wt.%)		
	Zn	Mn	Fe
Region 1	22.8 ± 3.1	15.2 ± 2.8	62.0 ± 3.0
Region 2	19.1 ± 2.4	5.8 ± 1.0	75.1 ± 3.0
Coating (mean contents)	21.5 ± 3.3	11.9 ± 5.1	68.5 ± 7.0

Compared to the results of the analyses carried out on deposits heat treated with a lower dwell time of 45 s (Figure 83), deposits heat treated at 900 °C with an austenitizing time of 120 s coating appear to consist of a single layer. In order to verify this assumption, the composition of the layers was determined by means of EDS analyses from 40 measurements carried out randomly in the coating thickness (Table 20). According to the results, the deposits have a rather high Fe content of approximately 75.5 wt.%, which could explain the low difference in the electrochemical potentials of the deposits and steel (Figure 81). A moderate Mn content of approximately 8.4 wt.% is observed. It is interesting to note that this value is much lower than that observed for Layer 2 of coatings heated to 900 °C with an austenitizing time of 45 s (Table 19), which may indicate that the use of higher dwell times favors the loss of Mn due to high temperature oxidation.

According to the mean composition of coatings heated with a dwell time of 45 s (Table 19) and 120 s (Table 20), the Zn content of the overall coating was found to decrease along with the increase of the Fe content by the increase of dwell time.

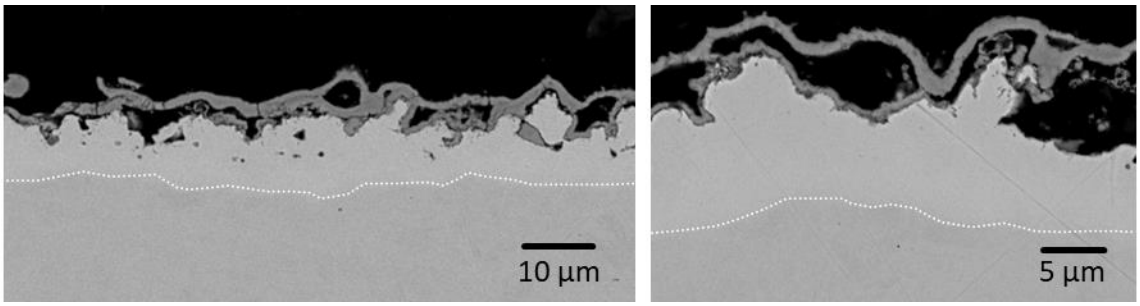

Figure 84: Cross-sectional SEM micrographs (BSE mode) of Zn-Mn coatings austenitized at 900 °C with an austenitizing time of 120 s above 860 °C in a furnace heated in argon.

This particularity is theoretically likely to affect anticorrosion. However, it is striking to note that the variation of Zn and Fe contents in Zn-Mn coatings heat treated to 900 °C for up to 120 s does not have a significant influence on the electrochemical potential of the corresponding coatings, as similar dissolution curves were obtained for all three heat treatment conditions (Figure 81). As the curves corresponding to coatings heat treated to 920 °C for 45 s were found to be above those obtained at 900 °C, it is likely that a lower Zn content and a higher Fe content are present in the coatings.

Table 20: Chemical composition of the layers formed in Zn-Mn coatings austenitized at 900 °C with an austenitizing time of 120 s above 860 °C in a furnace heated in argon, determined by semi-quantitative EDS analyses.

	Composition (wt.%)		
	Zn	Mn	Fe
Coating	16.0 ± 2.2	8.4 ± 1.6	75.5 ± 2.4

Conclusion

From this study, it appears that heat treatment of Zn-Mn coatings in argon with process relevant austenitizing temperatures of 900 °C and 920 °C and different heating times leads to the formation of layers with similar microstructures, compositions and thicknesses regardless of the parameters used. The presence of coatings with a thickness lower than that of the as-deposited coating suggests that a loss of coating materials takes place at high temperature. In fact, oxidation of the coatings could not be completely prevented by the use of argon, as an oxide scale forms on the top surface of the coatings, which results in a decrease of the Mn content in the coatings. It is not clear if the presence of a Mn-rich oxide layer on the top surface of the coatings requires a surface treatment in order to provide good compatibility with subsequent processes such as painting and joining. In addition, it is very likely that evaporation of a part of the coating occurs at temperatures of up to 900 °C in presence of argon, as reported in Section 1.5.1 for galvanized steel. The presence of approximately 75 wt.% Fe in the layers is responsible for the presence of a moderate sacrificial effect of approximately 140 mV of the coatings for steelm which may provide limited interest in terms of anticorrosive resistance for final press-hardened components.

5.4 Suitability of Zn-Mn coatings for high temperature processes in air and in a protective atmosphere [EN + FR]

In the framework of the development of alternative Zn-Mn alloy coating materials and of the study of their suitability for the hot stamping application, it is of great importance to assess the influence of annealing on the coating materials prior to hot forming operations.

On the basis of the characterization studies carried out on as-deposited coatings (Section 4.3), the evolution of microstructural, crystallographic and anticorrosive properties of the Zn-Mn alloy coatings post to heat treatment in various conditions was investigated. The Zn-Mn-coated specimens were first heated up at a constant furnace temperature for various durations corresponding to intermediary target temperatures comprised between 300 °C and standard austenizing conditions, cooled down in press tools and finally analyzed with various complementary characterization techniques. The present section is dedicated to the drawing of the main conclusions established during the investigations.

An overview of the results obtained in this section is presented in Figure 85 and shows the distribution and the thickness of the different layers formed in the coatings post to heat treatment in the above-mentioned conditions. The difference between the potential of the latter layers and of substrate steel are indicated in order to provide information regarding sacrificial corrosion protection of steel.

On the basis of these results, it appears that the microstructure of the initial coating varies after heat treatment above 500 °C with the formation of various Fe-rich layers at the interface with steel, Zn-rich layers in the upper part of the coatings, as well as of superficial oxide layers. Besides, it can be observed that the use of temperatures of up to 900 °C partly leads to coatings with heterogeneous microstructures, which is likely to be related to high temperature oxidation and evaporation. Anticorrosive performance of the coating systems is strongly affected by the microstructural changes, as the overall sacrificial effect disminishes by increasing heat treatment temperature and dwell time, in the same manner as galvanized steel (Section 1.5.1).

The compositions of the corresponding layers presented in Figure 85 are shown in Figure 86.

It is important to note that the use of high heat treatment temperatures and long dwell times induces an increase of the Fe content in the coatings to the detriment of Zn, in particular at the interface with steel due to chemical diffusion between steel and coating materials. This particularity is clearly responsible for the reduction of the sacrificial effect of the coatings. In addition, the Mn content of the coating appears to decrease towards steel, which is related to preferential oxidation of Mn along with the formation of Fe-Zn-based interdiffusion layers. On the basis of the results obtained in Section 5.2 and Section 5.3 as well as on the overview data presented in Figure 85 and Figure 86, the main conclusions drawned by the study of the behavior of Zn-Mn coatings during heat treatment will be reported in the next sections according to two central motivations.

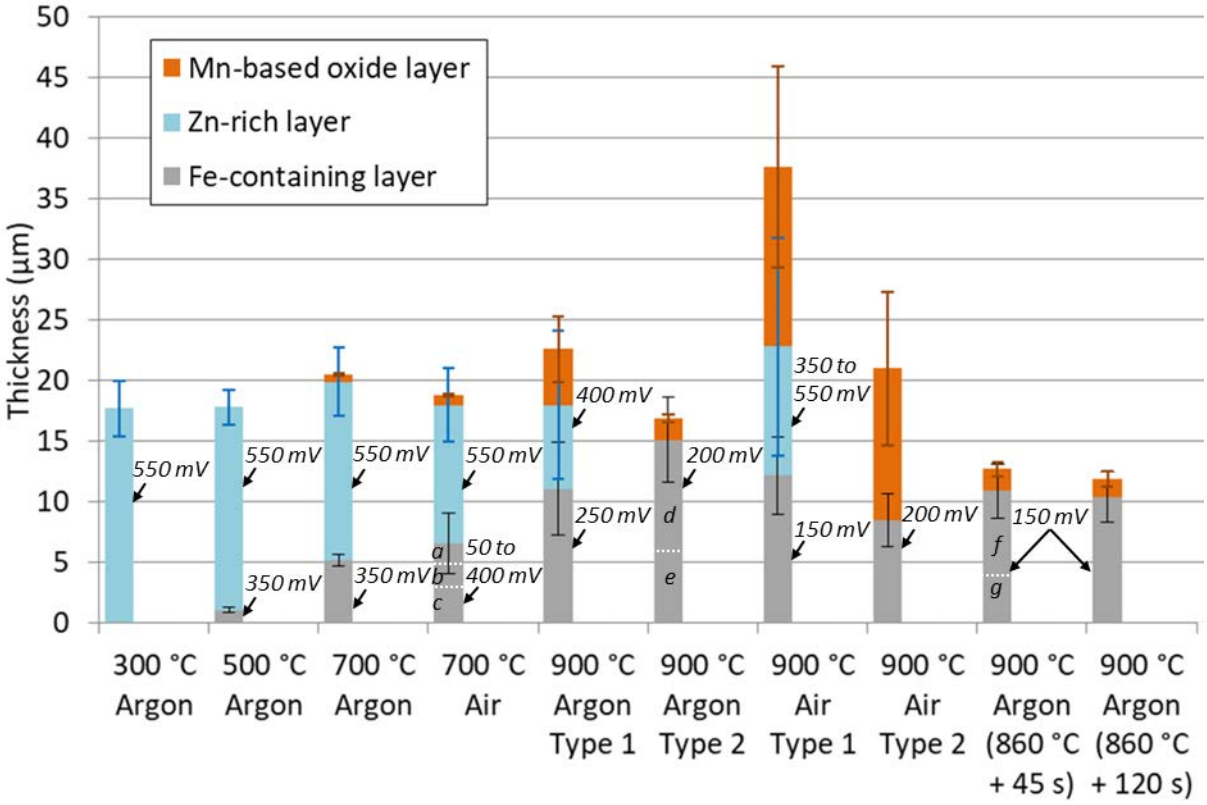

Figure 85: Thickness and electrochemical potential during the dissolution of layers formed in Zn-Mn coatings after heating in a furnace with air and argon to temperatures comprised between 300 °C and 900 °C and dwell times of 45 s and 120 s above 860 °C, determined in Section 5.2 and Section 5.3.

The first aim of this part was focused on the study of the influence of the atmosphere used during austenitization treatment on the properties of the alloy coatings. In addition to the use of a conventional air furnace, an argon-containing atmosphere was used for heating Zn-Mn-coated steel plates in order to assess the behavior of the coating materials with regard to high temperature oxidation, in particular that of Mn. The results obtained are summarized in Section 5.4.1.

The second aim of this section was focused on a comprehensive characterization study of the properties of Zn-Mn alloy coatings heat treated in argon to temperatures comprised between 300 °C and austenitizing temperatures of up to 900 °C in order to assess diffusion, oxidation and evaporation processes taking place during austenitizing treatment. In addition, Zn-Mn-coated specimens were austenitized in process-like conditions with conventional temperatures and dwell times in presence of argon in order to evaluate their suitability for the hot stamping application and determine their process-window. A summary of the conclusions established in this chapter is reported in Section 5.4.2.

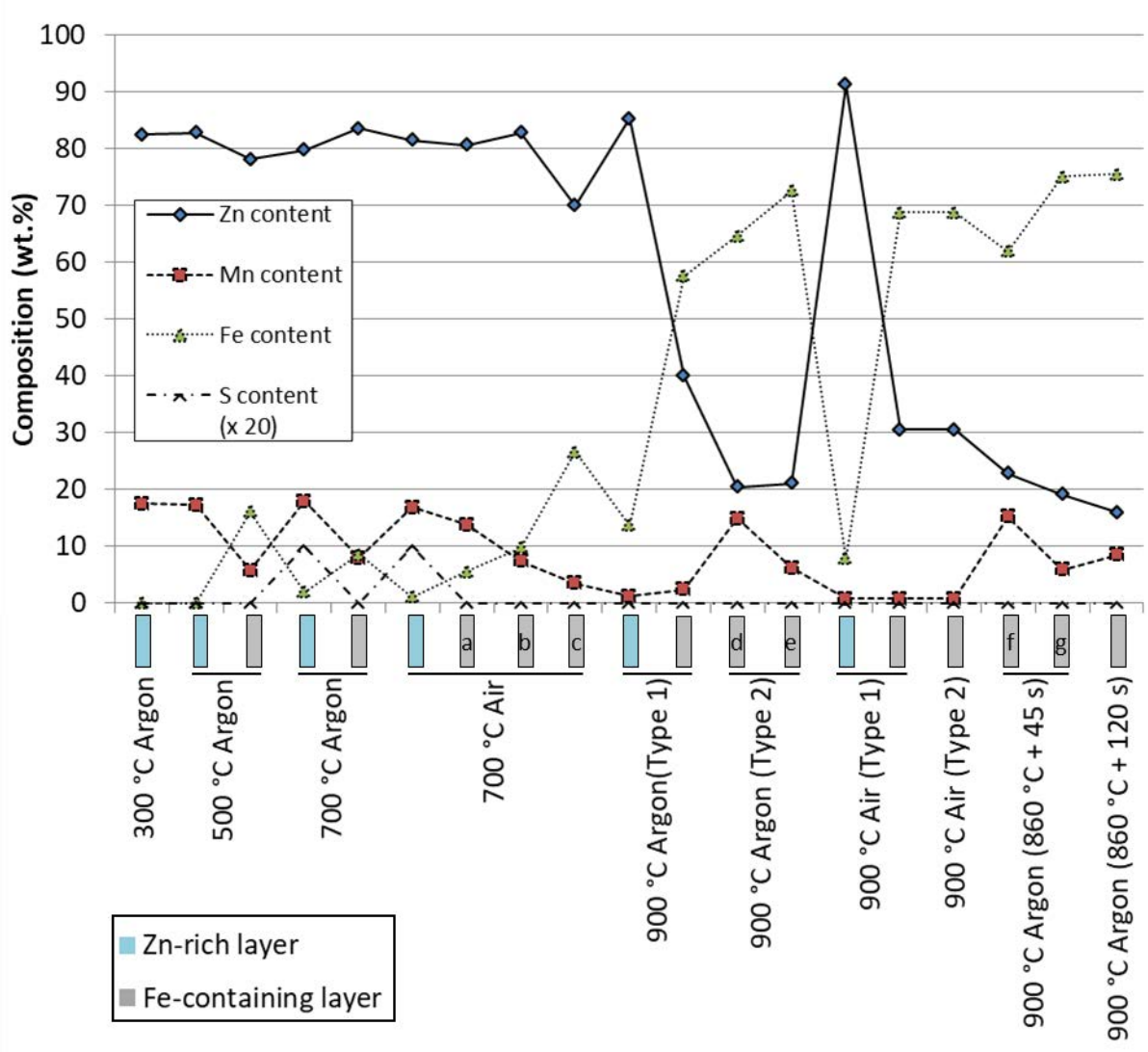

Figure 86: Composition of layers formed in Zn-Mn coatings after heating in a furnace with air and argon to temperatures comprised between 300 °C and 900 °C and dwell times of 45 s and 120 s above 860 °C, determined by means of SEM-EDS analyses on cross-sectional views; layers represented in Figure 85.

5.4.1 Influence of the austenitizing atmosphere on the coating behavior

According to the properties of Zn-Mn layers heat treated to various temperatures in presence of air and argon presented in Figure 85 and Figure 86, it is possible to evaluate the influence of the austenitizing atmosphere on the behavior of the coatings. The type of austenitizing atmosphere does not have a significant influence on the properties of Zn-Mn coatings heated up to 700 °C, as the composition, the microstructure of the coating as well as the thickness of the Mn-rich oxide layer were found to be similar for coatings heat treated in air and in argon up to this temperature. After heating to 900 °C in air, Zn-Mn coatings were found to undergo Mn oxidation, which resulted in a very low Mn content of 0.9 wt.% in the remaining coatings. It is important to note the difference with the as-deposited coatings containing approximately 17 wt.% Mn (Table 9). This loss of Mn induced the formation of a thick oxide layer with a high amount of pores on the top surface of the coatings. The

presence of the latter superficial layer is very likely to be incompatible with subsequent processing such as phosphating or painting as well as with joining processes such as welding due to the high porosity of the oxide scale and the low adhesion with the underlying coating. This particularity points out the necessity of carrying out a surface treatment such as abrasive blasting to reduce the amount of loose particles on the surface and to improve surface quality. Similar conclusions were reported in the scarce literature data regarding annealing of Zn-Mn coatings (Section 1.6.2).

As reported in Section 1.5.1, the use of 0.2 wt.% Al in galvanized steel permits to form an Al_2O_3-based superficial oxide layer, which reduces the occurrence of oxidation and evaporation of the underlying Zn coating. In the same manner, as preferential oxidation of Mn takes place with regard to Zn (Section 1.6.2), it may be assumed that the formation of a superficial Mn oxide layer on Zn-Mn coatings during heat treatment in air permits to reduce the loss of Zn by oxidation and evaporation, which is likely to preserve the amount of metallic Zn for anticorrosion. As some areas of the coatings heat treated to 900 °C in air were found to mainly consist of ZnO, it appears that Zn oxidation could not be fully avoided. In addition, evaporation of a part of the coatings is likely to take place in the considered conditions, regardless of the atmosphere used. In fact, Zn-rich phases were found to be partly absent on some areas of the coatings, which results in the loss of metallic Zn beneficial for cathodic corrosion protection. Therefore, it can be assumed that the presence of a superficial Mn-rich oxide scale is not sufficient to fully prevent high temperature oxidation and evaporation of Zn-containing underlying layers.

As reported in Section 1.6.2, the main aim of the use of Mn as alloying element for Zn is the increase of the melting temperature in comparison with pure Zn deposits in order to reduce the susceptibility of the coated steel to LME phenomenon. Heating to 900 °C in air leads to an almost complete loss of the initial Mn content in the coating. At this stage, the solidification temperature of the alloy coating is therefore lowered, which increases the probability that liquid phases are present in the coating during forming operations and that cracks related to LME form in the hot formed components. In this regard, it is clear that high temperature oxidation should be avoided or at least minimized.

The use of an argon-containing atmosphere during annealing of Zn-Mn-coated steel to 900 °C permitted to reduce the occurrence of oxidation of Mn, as coatings containing up to 15.2 wt.% Mn were obtained in representative conditions used for manufacturing press-hardened components. Besides, the use of a protective atmosphere resulted in a much lower thickness of the oxide scale at 900 °C of only a few micrometers. It is not clear if the oxide scale formed on the top surface of Zn-Mn coatings after heating to 900 °C in presence of argon requires a surface treatment in order to provide good paintability and weldability. In addition to the improvement of the surface quality of the heat treated products, the reduction of the loss of Mn by oxidation is very likely to have a positive effect on the susceptiblity for LME by maintaining a sufficiently high melting temperature of the alloy coatings. Further austenitizing conditions with different atmospheres and industrial

equipments may permit to fully avoid oxidation in order to improve surface quality as well as to maintain a sufficient Mn content in the coating to improve hot formability.

5.4.2 Behavior of Zn-Mn coatings during austenitizing in a protective atmosphere

After heating to 300 °C in an argon-containing atmosphere, the Zn-Mn coatings were found to be similar to as-deposited layers (Figure 85). At a temperature of 500 °C, the first signs of chemical diffusion could be observed with the formation of a thin interdiffusion layer at the interface between coating and steel. A significant change in the microstructure of the coating was observed after reaching a temperature of 700 °C with the presence of a compact interdiffusion layer with a thickness of about 5 µm. It is important to note that both latter interdiffusion layers were found to contain a Mn content lower than that of the upper part of the coatings. The columnar structure observed for as-deposited Zn-Mn alloys (Section 4.3.2) disappears after heating to 700 °C. Instead, large grains without well-defined geometries are formed in the upper part of the coatings. The microstructure was found to be inhomogeneous due to the presence of a high density of pores and precipitates at the grain boundaries. On the basis of STEM elemental studies and XRD measurements, these areas mainly consist of S and Mn, most probably due to the presence of MnS. In fact, sulfur traces reported for as-deposited coatings and induced by the use of S-containing NH_4SCN additive (Section 4.3.1) were found to migrate to grain boundaries after heat treatment to 700 °C. It is interesting to note that the ε_2-Zn-Mn phase of as-deposited coatings and its preferential orientation are still present after heating to 700 °C.

Coatings with non-regular microstructures and phase distributions were observed after heating to 900 °C under argon. This result can be explained by the significant variation of the thickness of as-deposited layers as well as to heterogeneous oxidation of the coatings, in particular of Mn. In fact, in the conditions considered in this study, it appears that oxidation of the coating materials could not be prevented despite the use of an argon-based atmosphere, as traces of Mn oxides were observed for coatings heated above 300 °C. After heating to a temperature of 900 °C conventionally used in the manufacturing process, a Mn-rich oxide scale with a thickness of several micrometers forms on the top surface of the coatings. It is interesting to note that S-rich particles observed at the grain boundaries of the upper layer of the coatings heated to 700 °C were found to migrate to the top surface of the coatings below the Mn-rich oxide scale after heating to 900 °C.

The anticorrosive behavior of heat treated Zn-Mn coated steels was found to vary after heating to temperatures above 300 °C due to chemical diffusion of Fe into the coatings. The progressive formation of interdiffusion layers within the coatings resulted in an increase of the electrochemical potential of the layers and a reduction of the relative amount of Zn-rich phases, in a similar way to galvanized steel (Section 1.5.1). It is noteworthy that all coatings studied in this part provided sacrificial corrosion protection to steel of at least 150 mV after heat treatment. The absence of Zn-rich phases on some areas of Zn-Mn coatings heated to 900 °C and at 900 °C with different dwell times supports the hypothesis of heterogeneous

evaporation of the Zn-rich phases at high temperature in presence of argon. These particularities resulted in different anticorrosive behaviors due to the non-homogeneous presence of Zn-rich phases. The use of higher temperatures and dwell times was found to lead to similar microstructures and moderate sacrificial corrosion protection due to high amounts of Fe in the remaining layers. The achievement of reproducible phase distributions along with sufficient anticorrosive properties could be avoided by using optimized heating conditions such as heating rates, austenitizing atmospheres or controlled temperatures.

It is important to note that a good adhesion and interaction of the Zn-Mn deposits with steel substrates was achieved for all deposits after heat treatment, regardless of the atmosphere used and the temperature. Besides, almost no defects such as pores, peeling or decohesion of the coatings were obtained. This particularity is most likely related to the formation of interdiffusion layers between coating and steel observed above 500 °C and can be considered to have a positive influence on the formability of the coatings at high temperature.

On the basis of XRD measurements carried out on specimens heated under argon to different temperatures, it appears that the considered alloys have a melting temperature above 700 °C, as the ε_2-Zn-Mn phase observed in the as-deposited coatings (Section 4.3.3) was still present after heating to 700 °C. This result proves that alloying of Zn with Mn leads to an increase of the melting temperature of the coating compared to pure Zn layers, in good accordance with the assumptions reported in Section 1.6.2. This result may provide benefits for the hot stamping application, as interdiffusion can be slowed down by the increased melting point and the susceptibility of the austenitized coated steels to LME can be reduced. The next part will be dedicated to the study of the behavior of Zn-Mn-coated steel sheets during direct hot stamping and to the comparison with commercial galvanized steel.

Compatibilité des alliages Zn-Mn pour une application à haute température sous air et dans une atmosphère protectrice [FR]

Dans le cadre du développement de nouveaux alliages Zn-Mn et de l'étude de leur compatibilité pour l'application de l'emboutissage à chaud de pièces de carrosseries, il est important d'évaluer l'influence du traitement thermique sur les propriétés des matériaux des revêtements avant d'étudier les opérations de mise en forme.

Sur la base des résultats obtenus lors des analyses de caractérisation menées sur les revêtements après déposition (Chapitre 4.3), l'évolution des propriétés microstructurales, cristallographiques et anticorrosives des alliages après des traitements thermiques dans de nombreuses conditions a été étudiée en détails dans cette partie. Les échantillons revêtus de couches d'alliages de Zn-Mn ont été chauffés dans un four réglé à une température constante pendant différentes durées correspondant à des températures ciblées comprises entre 300 °C et des conditions d'austénitisation généralement utilisées dans l'industrie, puis refroidies rapidement dans des outils de presse sans déformation. Les échantillons ont enfin été étudiés par de nombreuses techniques de caractérisations complémentaires.

Le bilan des résultats obtenus dans ce chapitre est présenté en Figure 85 et montre la distribution et l'épaisseur des différentes couches formées dans les revêtements après traitement thermique dans les différentes conditions considérées. La différence entre le potentiel de chaque couche et le substrat est indiquée afin de fournir des informations concernant la protection cathodique de l'acier par le revêtement.

Sur la base de ces résultats, il apparaît que la microstructure du revêtement initial varie après le traitement thermique au-delà de 500 °C avec la formation de nombreuses couches riches en Fe à l'interface avec le substrat, des couches riches en Zn dans la partie supérieure des revêtements ainsi que des couches d'oxydes en surface. En outre, il a pu être constaté que l'utilisation de plus hautes températures allant jusqu'à 900 °C conduisent en partie à des revêtements comportant des microstructures hétérogènes, ce qui est vraisemblablement lié à l'oxydation et à l'évaporation à haute température. Les performances anticorrosives des revêtements sont considérablement affectées par les changements microstructuraux, comme le prouve la diminution de l'effet sacrificiel des couches lors de l'augmentation de la température et de la durée de chauffe dans le four, de la même manière que pour les aciers galvanisés commerciaux (Chapitre 1.5.1).

Les compositions des couches présentées en Figure 87 sont résumées en Figure 88. Il est important de noter que l'utilisation de hautes températures de traitement thermique et de longues durées de chauffe dans le four induisent une hausse de la teneur en Fe dans les revêtements au détriment du zinc, en particulier à l'interface avec l'acier dû à la diffusion chimique entre les matériaux du substrat et des revêtements. Cette particularité est responsable de la réduction de l'effet sacrificiel du substrat par le revêtement. De plus, la teneur en Mn du revêtement semble diminuer en direction du substrat, ce qui est lié à

l'oxydation préférentielle du Mn en plus de la formation de couches d'interdiffusion consistant principalement d'alliages Fe-Zn.

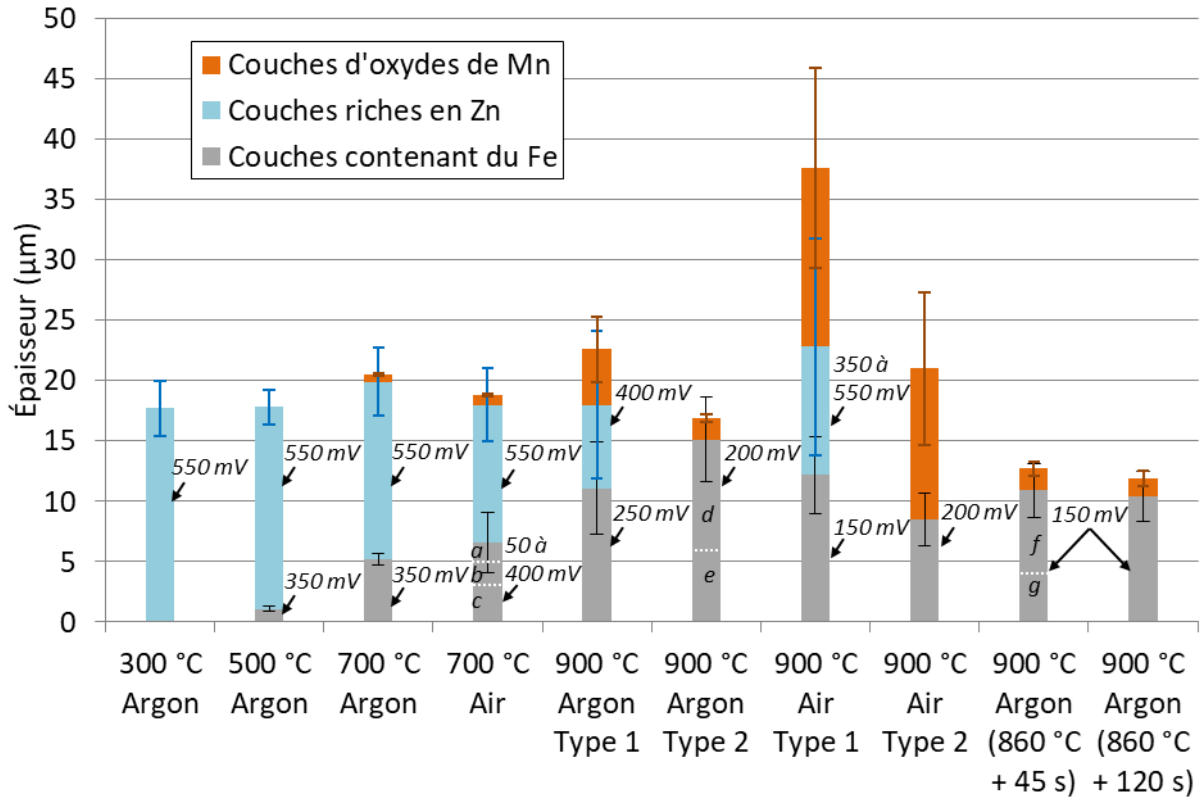

Figure 87: Épaisseur et potentiel électrochimique des couches formées dans les revêtements Zn-Mn après traitement thermique dans un four chauffé sous air et sous argon à des températures comprises entre 300 °C et 900 °C et des durées de chauffe de 45 s et 120 s au delà de 860 °C, déterminées dans les chapitres 5.2 et 5.3.

Sur la base des résultats présentés en Figure 87 et en Figure 88, les conclusions générales obtenues dans l'étude du comportement des revêtements Zn-Mn pendant le traitement thermique seront traitées dans les parties suivantes selon deux axes principaux.

Le premier objectif de cette partie est dédié à l'étude de l'influence de l'atmosphère utilisée pendant le traitement d'austénitisation sur les propriétés des revêtements. En plus d'analyses effectuées après traitement thermique dans un four conventionnel sous air, une enceinte contenant de l'argon a été utilisée pour chauffer les plaques d'acier revêtues de couches de Zn-Mn afin d'évaluer le comportement des matériaux des couches concernant l'oxydation à haute température, en particulier du Manganèse contenu dans les dépôts.

Le deuxième objectif de cette partie est concentré sur la caractérisation exhaustive des propriétés des alliages Zn-Mn chauffés sous argon à des températures comprises entre 300 °C et des températures d'austénitisation allant jusque 900 °C afin d'étudier les phénomènes de diffusion, d'oxydation et d'évaporation ayant lieu pendant le traitement d'austénitisation. De plus, des plaques revêtues de Zn-Mn ont été austénitisées dans des conditions proches du procédé industriel avec des températures et durées de chauffe

conventionnelles en présence d'une atmosphère contenant de l'argon afin d'évaluer la compatibilité des nouveaux matériaux pour l'application de l'emboutissage à chaud et déterminer les limites du procédé.

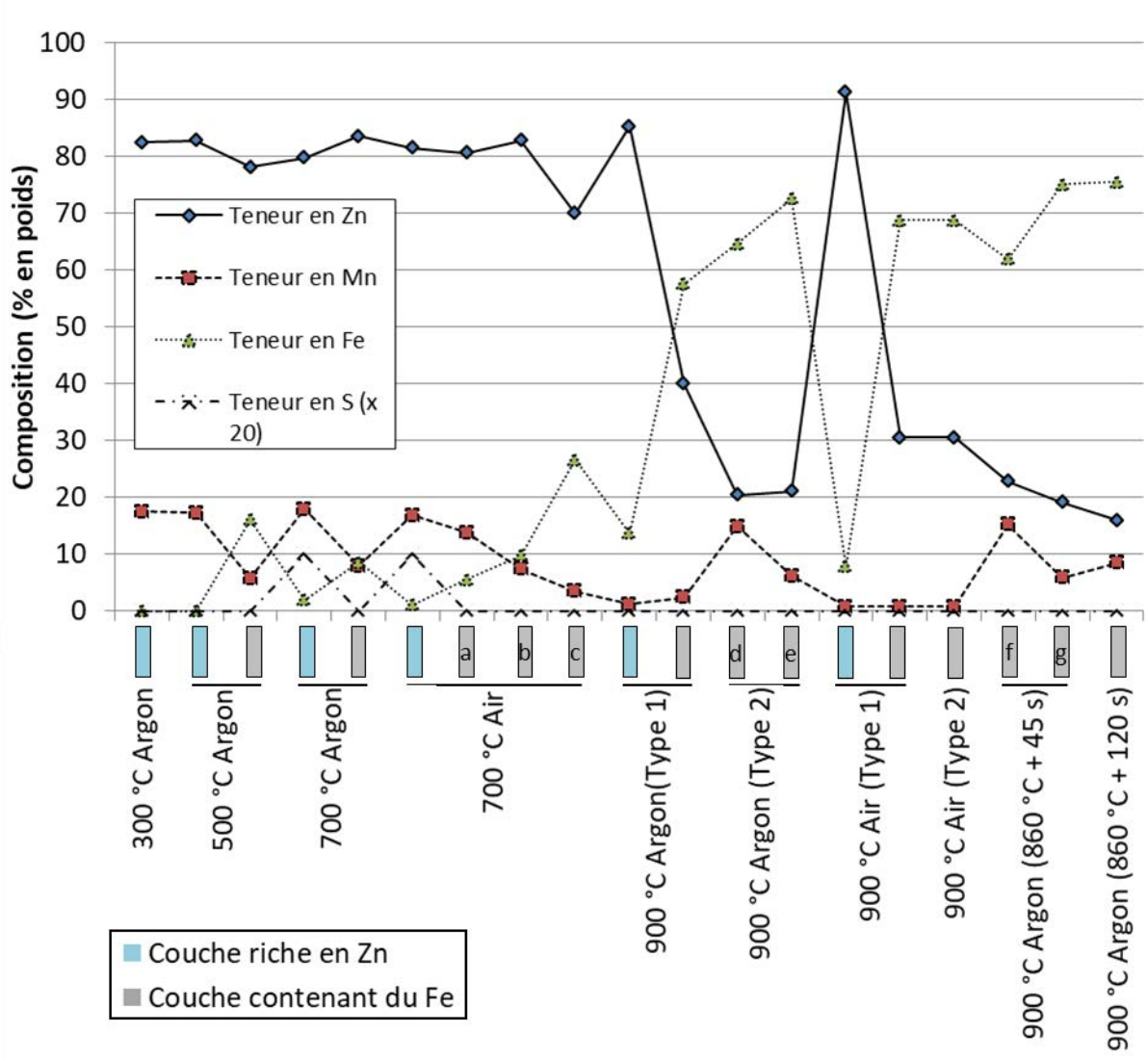

Figure 88: Composition des couches formées dans les revêtements Zn-Mn après traitement thermique dans un four sous air et sous argon à des températures comprises entre 300 °C et 900 °C et des durées de chauffe de 45 s et 120 s au delà de 860 °C, déterminées par des mesures SEM-EDS sur des vues en coupe ; couches représentées en Figure 87.

Influence de l'atmosphère sur le comportement des revêtements pendant l'austénitisation

D'après les propriétés des revêtements Zn-Mn traités thermiquement à différentes températures en présence d'air et d'argon présentées en Figure 87 et Figure 88, il apparaît que le type d'atmosphère n'a pas d'influence significative sur les propriétés des couches chauffées à des températures allant jusqu'à 700 °C étant donné que la composition, la microstructure des couches et l'épaisseur de la couche d'oxydes riche Mn sont similaires pour les plaques chauffées sous air et sous argon à cette température. Après traitement à 900 °C

sous air, l'oxydation d'une grande partie du Manganèse contenu dans les couches de Zn-Mn a pu être observée, ce qui a conduit à la présence d'un faible taux de Mn de 0.9 % massique dans les couches restantes. Il est important de noter la différence avec les revêtements après déposition contenant approximativement 17 % massique (Table 9). Cette perte de Mn induit la formation d'une épaisse couche d'oxydes avec une grande quantité de pores à la surface des revêtements. Il est fort probable que cette couche superficielle est incompatible avec les procédés de transformation ultérieurs tels que la phosphatation, la peinture ainsi qu'avec les procédés d'assemblage tels que le soudage à cause des fortes porosités de la couche d'oxydes et de sa faible adhésion avec les couches inférieures. Cette particularité implique la nécessité d'effectuer un traitement de surface tel que le grenaillage après l'emboutissage afin de réduire la quantité de particules sur la surface et d'améliorer la qualité de surface des aciers revêtus avant leur utilisation. Des conclusions similaires ont été reportées dans la littérature pour les revêtements Zn-Mn (Chapitre 1.6.2).

Comme annoncé dans le chapitre 1.5.1, l'utilisation de 0.2 % massique d'aluminium dans les aciers galvanisés permet de former une couche superficielle d'oxydes constituée de Al_2O_3 qui réduit l'exposition à l'oxydation et à l'évaporation du revêtement de Zn. D'une manière similaire, il peut être supposé que la formation d'une couche d'oxydes de Mn pendant le traitement thermique d'alliages Zn-Mn permet de réduire la perte de Zn par oxydation et par évaporation, ce qui a de fortes chances de préserver la quantité de Zn métallique bénéfique pour la protection contre la corrosion. Comme certaines zones des revêtements traités à 900 °C sous air sont principalement constituées de Zn, il apparaît que l'oxydation du Zn ne peut pas être évitée complètement. De plus, l'évaporation d'une partie des revêtements a vraisemblablement eu lieu dans les conditions considérées dans cette étude, indépendamment de l'atmosphère utilisée. En effet, des phases riches en Zn n'ont été que partiellement observées sur certaines zones des revêtements, ce qui indique qu'une perte de Zn métallique a pu avoir lieu. C'est pourquoi il est probable que la présence d'une couche superficielle d'oxydes de Mn n'est pas suffisante pour éviter complètement l'oxydation et l'évaporation des couches sous-jacentes à haute température.

Comme reporté dans le chapitre 1.6.2, l'objectif principal de l'utilisation du Manganèse en tant qu'élément d'alliage du zinc est d'augmenter la température de fusion du revêtement comparé à des couches de Zn pur afin de réduire la fragilité des aciers revêtus à la fissuration par métaux liquides. Le traitement thermique à 900 °C sous air conduit à une perte quasi-totale de la teneur initiale en Mn dans le revêtement. Dans ce cas, la température de solidification du revêtement est ainsi diminuée, ce qui accroît la probabilité que des phases liquides soient présentes dans le revêtement pendant les opérations de mise en forme et que des fissures appararaissent dans les pièces. C'est pourquoi il est important que l'oxydation à haute température soit évitée ou pour le moins réduite.

L'utilisation d'une atmosphère constituée d'argon pendant le traitement thermique d'aciers revêtus de couches de Zn-Mn à 900 °C a permis de réduire l'exposition des couches à l'oxydation du Mn, comme le prouve la présence de couches contenant des teneurs en Mn allant jusqu'à 15.2 % massique dans des conditions représentatives de la fabrication

industrielle de pièces. De plus, l'utilisation d'une atmosphère protectrice a permis de réduire fortement l'épaisseur de la couche d'oxydes formée à la surface de couches traitées à 900 °C pour atteindre seulement quelques micromètres. Il est encore incertain si la couche superficielle d'oxydes formée à la surface des revêtements après chauffe à 900 °C en présence d'argon implique la nécessité d'effectuer un traitement de surface pour obtenir une bonne compatibilité avec les procédés ultérieurs de peinture et d'assemblage. En plus d'une amélioration de la qualité de surface des produits traités thermiquement, il est fort probable que la réduction de la perte de Mn par oxydation à haute température ait un effet positif sur la fragilité des matériaux à la fissuration par métaux liquides en maintenant une température de fusion du revêtement suffisamment haute. D'autres conditions d'austénitisation avec des atmosphères différentes et des équipements industriels pourraient permettre d'éviter totalement l'oxydation afin d'améliorer l'état de surface des produits et de maintenir une teneur en Mn constante dans le revêtement en vue d'améliorer l'aptitude à la mise en forme à chaud.

Comportement des revêtements Zn-Mn pendant l'austénitisation dans une atmosphère protectrice

Les revêtements Zn-Mn étudiés après traitement thermique à 300 °C sous argon sont similaires aux couches après déposition (Figure 87). À une température de 500 °C, les premiers signes de diffusion chimique ont pu être observés avec la formation d'une fine couche d'interdiffusion à l'interface entre le revêtement et l'acier. Un changement important de la microstructure du revêtement a pu être observée après avoir chauffé les échantillons à 700 °C, avec la présence d'une couche d'interdiffusion avec une épaisseur d'environ 5 µm. Il est important de noter que ces couches d'interdiffusion contiennent une teneur en Mn inférieure au reste du revêtement. La structure colonnaire observée pour les dépôts non traités (Chapitre 4.3.2) disparaît après traitement à 700 °C. À la place, de larges grains sans géométrie particulière se forment dans la partie supérieure des revêtements. La microstructure formée est hétérogène à cause de la présence d'une forte densité de pores et de précipités aux joints de grains. Des analyses de microscopie électronique à balayage par transmission et de diffraction des rayons X ont permis de montrer que ces zones sont vraisemblablement constituées de MnS. D'après cette observation, il apparaît que les traces de soufre reportées dans le cas des couches après déposition et induites par l'utilisation de l'additif NH_4SCN (Chapitre 4.3.1) migrent vers les joints de grains du revêtement après traitement thermique à 700 °C. Il est intéressant de noter que la phase ε_2-Zn-Mn du dépôt initial et son orientation préférentielle sont toujours présentes après traitement à 700 °C.

Des revêtements avec des microstructures et des distributions de phases non régulières ont été observés après chauffe à 900 °C sous argon. Ce résultat peut être expliqué par la variation significative de l'épaisseur des dépôts initiaux ainsi qu'à l'oxydation hétérogène des revêtements et en particulier du Mn. Dans les conditions considérées dans cette étude, il apparaît que l'oxydation des revêtements n'a pu être évitée malgré l'utilisation d'une

atmosphère constituée d'argon, comme le prouvent les traces d'oxydes de Mn observées après traitement à 300 °C.

Après le traitement thermique à une température de 900 °C généralement utilisée dans le procédé industriel, une couche superficielle riche en oxydes de Mn avec une épaisseur de plusieurs micromètres se forme sur la surface du revêtement. Il est important de noter que les particules riches en S observées aux joints de grains de la partie supérieure de revêtements traités à 700 °C ont migré vers la surface du revêtement en dessous de la couche d'oxydes de Mn après traitement à 900 °C.

Il apparaît que le comportement en protection contre la corrosion des alliages Zn-Mn traités thermiquement varie à cause de la diffusion chimique de Fe de l'acier dans le revêtement. La formation progressive de couches d'interdiffusion dans les revêtements conduit à la hausse du potentiel électrochimique du système et à la réduction de la quantité relative de phases riches en Zn, d'une manière similaire aux aciers galvanisés (Chapitre 1.5.1). Il est intéressant de noter que tous les revêtements étudiés dans cette partie présentent une protection cathodique de l'acier d'au moins 150 mV après traitement thermique. L'absence de phases riches en Zn sur certaines zones des alliages Zn-Mn chauffés à 900 °C et à 900 °C avec différentes durées de chauffe appuie l'hypothèse de l'évaporation hétérogène des phases riches en Zn à haute température en présence d'argon. La présence hétérogène de phases riches en Zn a conduit à différents comportements en protection contre la corrosion. Il a pu être observé que l'utilisation de plus hautes températures et de plus longues durées de chauffe conduisent à des microstructures similaires et une protection cathodique moyenne due à une forte teneur en Fe dans les couches restantes. L'utilisation de conditions de chauffe optimisées telles que des vitesses de chauffe contrôlées, des atmosphères différentes ou un four avec des zones de températures contrôlées pourrait permettre d'obtenir une distribution de phases reproductible et homogène ainsi que des propriétés anticorrosives optimales.

Il est important de noter qu'une bonne adhésion et une bonne interaction sont obtenues entre les revêtements et le substrat pour toutes les couches après traitement thermique, indépendamment de l'atmosphère et des températures utilisées. De plus, presque aucun défaut tel que des pores ou une décohésion des couches n'a été observé. Il est fort probable que ce résultat est lié à la formation de couches d'interdiffusion entre les revêtements et l'acier observée pour des températures de 500 °C et plus et peut être considérée comme bénéfique pour l'aptitude à la mise en forme à haute température.

D'après les analyses de diffraction par rayons X effectuées sur les échantillons traités thermiquement sous argon à différentes températures, il apparaît que les alliages Zn-Mn obtenus dans cette étude ont une température de fusion de plus de 700 °C étant donné que la phase ε_2-Zn-Mn observée pour les revêtements après déposition (Chapitre 4.3.3) ainsi que son orientation préférentielle sont toujours présentes après chauffe à 700 °C. Ce résultat prouve que l'alliage du Zn avec du Mn permet effectivement d'augmenter la température de fusion de l'alliage comparé à des couches de Zn pur, conformément aux hypothèses reportées

dans le chapitre 1.6.2. Il est fort probable que cette particularité présente des avantages pour l'application de l'emboutissage à chaud étant donné que l'interdiffusion peut être ralentie par la haute température de fusion de l'alliage et que l'apparition de fissuration par métaux liquides peut être évitée par la suppression de phases liquides. Le chapitre suivant est dédié à l'étude du comportement de plaques d'acier revêtues d'alliages Zn-Mn pendant l'emboutissage à chaud direct comparé à celui d'aciers galvanisés commerciaux.

6 Hot stamping experiments on commercial and alternative Zn-Mn-coated steels

This section is focused on the study of the forming of commercial and alternative coatings on the basis of hot forming experiments with press tools designed specifically for this study.

Section 6.1 will be dedicated to the design, the manufacturing and the startup of press tools with current coated products. On the basis of these investigations, it will be then possible to evaluate the formability of the alternative Zn-Mn alloy coatings and determine their performance in comparison with commercial products.

The behavior of commercial galvanized and alternative Zn-Mn-coated steels during hot stamping will be investigated on the basis of hot forming experiments and materials characterization. The main results will be focused on the study of the microstructural properties of the layers and on the appearance of cracks due to LME. The results will be reported in Section 6.2. At last, Section 6.3 will summarize the results obtained in order to statue about the suitability of the alternative Zn-Mn alloy coatings for the hot forming application and define new investigation tracks which could permit to complete the observations made in the framework of this study.

It is important to note that the experiments presented in this part constitute a preliminary work regarding the assessment of the formability of Zn-Mn coatings during direct hot forming, mainly due to a limited amount of large-scale plates at disposition for hot stamping experiments.

6.1 Design and startup of press tools with current coated products

Press tools were designed and manufactured for the purpose of the study of the behavior of commercial and alternative coating materials during direct hot stamping.

In Section 6.1.1, the key criteria which should be taken into consideration in the study of the hot formability of coated blanks will be discussed and the most appropriate geometries for the press tools will be defined with the help of hot forming simulation tools. After manufacturing of the press tools, preliminary experiments will be carried out with commercial aluminized blanks in order to compare the distribution of the thinning between real specimens and simulation data (Section 6.1.2).

The formability of commercial aluminized and galvanized products was studied by hot stamping experiments with regard to the cracks and local defects forming in the coatings and the results are presented in Section 6.1.3 and in Section 6.1.4, respectively. The investigations were carried out with various heat treatment temperatures and dwell-times in order to understand the properties and the processability of both coatings during direct hot stamping.

6.1.1 Simulation of hot stamping and design of press tools

With the aim of investigating the hot formability of alternative coating systems, press tools were specifically designed for the present study. The main objective in the design of the press tools was to obtain a wide range of thinning of up to 20 % of the blanks on a unique specimen in order to evaluate the limits of the coating materials in terms of formability. The latter thinning value was stated to correspond to the highest value generally encountered for current hot stamped components [94]. The design was processed using computational tools for the simulation of hot forming. A two-part press tool was selected for good compatibility with the experimental press setup, although the absence of blank holders leads to a reduction of the possible configurations and tool geometries.

In addition to the setting of a wide range of thinnings values, it was important to take into account the dimensions of the large-scale plates. On the one hand, it was necessary to dispose of a sufficient surface area to carry out various electrochemical, corrosion and characterization experiments on the hot stamped parts. On the other hand. the use of large dimensions was a limiting parameter in the electrodeposition procedure of alternative coating materials, as high amounts of electrolyte and complicated experimental setup would be involved. Therefore, it was chosen to define suitable dimensions of 200 x 200 mm² for the specimens and press tools, as reported for the deposition of Zn-Mn coatings on large-scale plates. These dimensions were found to be optimal for laboratory-scale investigations.

The design of the press tools and the corresponding hot stamped plates with their relative geometries was carried out on the basis of computational construction with Catia V5. The simulation of hot forming was carried out on Autoform plus R3.1 from which information of interest such as thinning and temperature evolution were obtained. On the basis of these both softwares, numerous concepts and geometries were developed and tested [181].

An overview of several simulations is presented in Figure 89. Intermediary versions of the press tools were based on linear U and V-punches distributed over the entire sample width (Figure 89 a)). As shown in Figure 89, other models based on blanks with several circular cups with different diameters, depths and radii permitted to obtain thinning values comprised in the target range, in particular between 10 % and 20 %. The location and the distribution of the thinning values were assessed for the selection of the optimal model. Finally, the cups were positioned for obtaining sufficient space for material characterization.

The final geometry of the designed specimens is presented in Figure 89 c) and consists of 200 x 200 mm² wide blanks containing three cups with an identical diameter of 35 mm and different depths [182]. The depths of cups A, B and C are 4.25, 5.6 and 8 mm respectively and were defined for achieving maximal thinnings of 10, 15 and 20 % on the punch corner of each cup. Flat areas located around the cups were used for the cooling of small-scale specimens used for the study of the behavior of the Zn-Mn coatings during heat treatment (Section 5). In addition, these areas were used for the study of the electrochemical properties of the layers by means of galvanostatic dissolution.

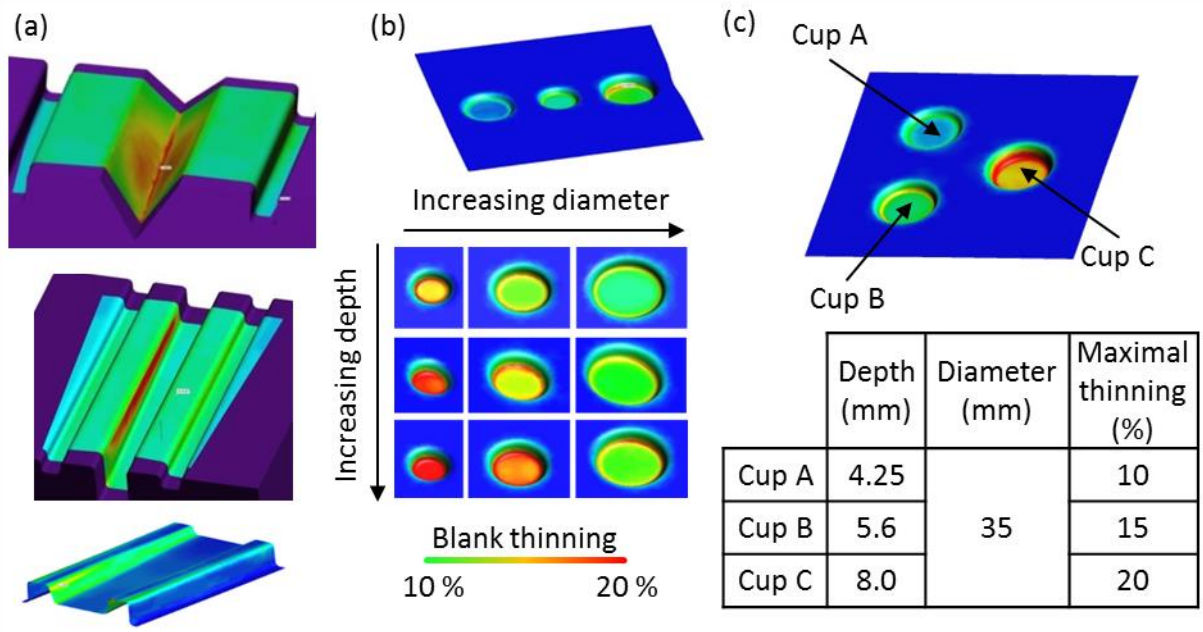

	Depth (mm)	Diameter (mm)	Maximal thinning (%)
Cup A	4.25	35	10
Cup B	5.6		15
Cup C	8.0		20

Figure 89: Linear V and U-punches (a) and circular punches (b) of intermediary models and circular punches of final press tools with the corresponding depths, diameters and blank thinnings of the cups (c) after construction on Catia V5 and hot forming simulation on Autoform R3.1.

6.1.2 Startup of the press tools with real specimens

As said earlier, the design of the press tools and of the resulting press-hardened parts was processed by computational hot forming simulations. In order to be able to study the above-mentioned criteria in terms of formability of current and alternative coating materials, it is necessary to correlate the behavior of real hot formed components with the simulation dada and thereby validate the geometries of the press tools. The distributions of the blank thickness after simulation and after experimental tests on aluminized steel plates are presented in Figure 90 a) and Figure 90 b), respectively.

The results show a similar behavior of the coated materials in the case of cups A and B for simulated and real aluminized specimens, with the maximal thinning located on the punch radius for both cups. However, a different behavior was observed in the case of the cup C. Optical 3D scanning and cross-sectional investigations presented in Figure 90 c) show a maximal thinning located in the middle of the punch depth, contrary to the punch radius in the simulation data. This result could be linked to the resolution of the solver used for hot forming simulation or to differences between the simulation conditions and the experimental conditions applied during heat treatment and hot forming experiments related to the furnace and press facilities. The same location of the maximal thinning was observed for GI and Al/Si blanks, regardless of the austenitizing parameters used.

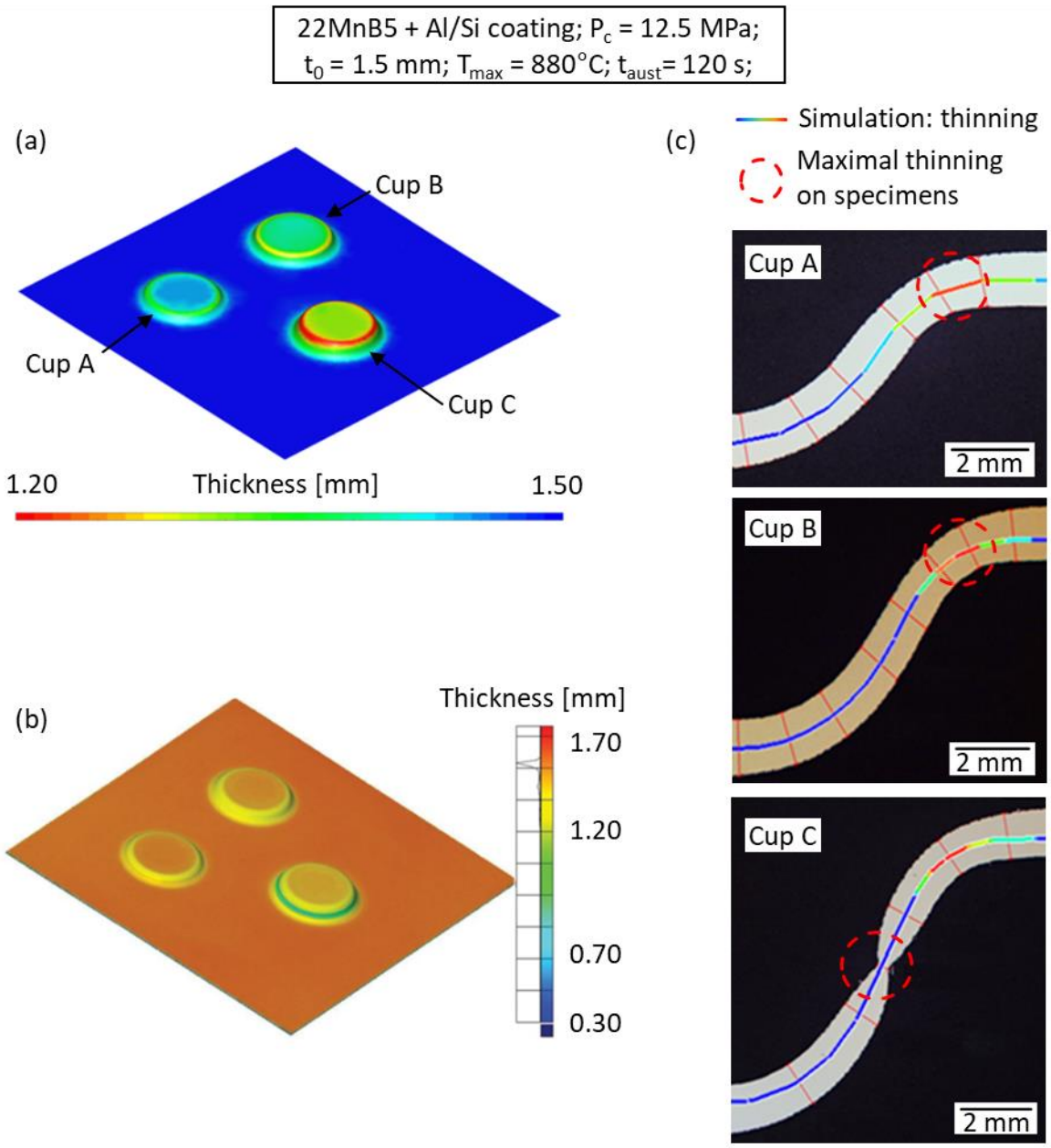

Figure 90: Thinning of aluminized blanks on the basis of Autoform 3.1 simulation data (a) and of 3D scanning of hot stamped blanks (b); cross-sectional micrographs of a hot stamped blank on cups A, B and C with the maximal thinning from the simulation data (colored line) and on real specimens (red circle).

The next sections will be focused on the study of the behavior of commercial aluminized and galvanized coatings during hot stamping experiments with various heat treatment temperatures and dwell times by using the above-mentioned press tools. The main focus will be the assessment of the formation of defects in the coatings, in particular of cracks related to LME in the case of galvanized steel.

6.1.3 Hot forming behavior of aluminized coatings

In this part, aluminized steel plates were austenitized at 950 °C for 120 s in a furnace under air and hot stamped with the above-mentioned press tools. The surface appearance and cross-sectional micrographs of the corresponding coated product are presented in Figure 91. The results indicate that a rupture of the coating occurs on areas undergoing tensile stresses, in particular on the radii of the cups.

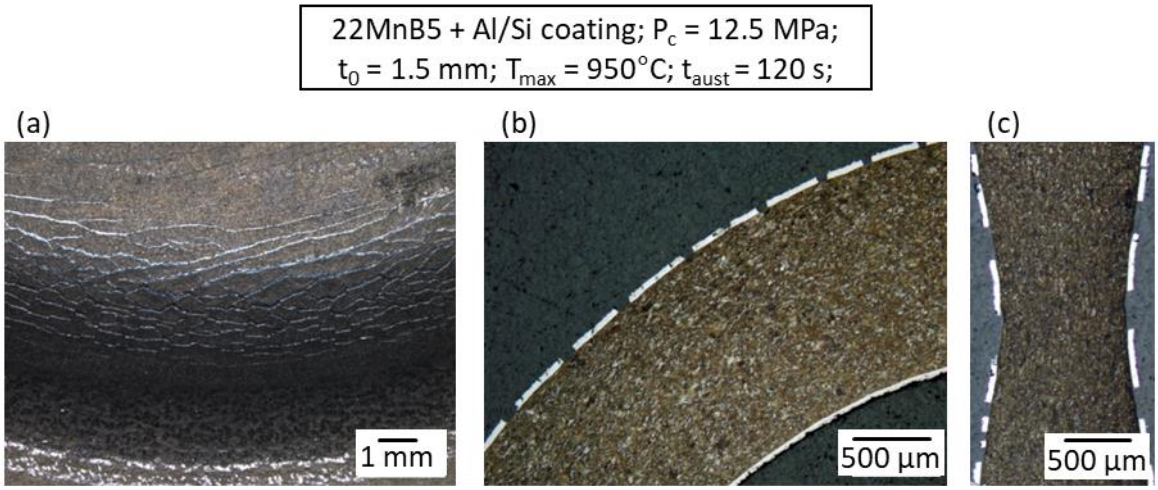

Figure 91: Rupture of the aluminized coating on cup C after direct hot samping: surface appearance (a), cross-sectional micrographs of the punch radius (b) and of the punch center of cup C (c).

Several defects (Figure 92) were observed during cross-sectional studies on aluminized steel after direct hot forming, in good accordance with the literature data discussed in Section 1.5.2. Pores can be observed on various areas of the coatings (Figure 92 a)), most probably due to the Kirkendall effect. The microcracks present in the coatings (Figure 92 b)) are most probably related to differences in the expansion coefficients of the different layers, and may act as nucleation sites for the appearance of macro-cracks in areas undergoing tensile deformation during forming. In addition, interfacial cracks were observed between coating and steel (Figure 92 a)) and sublayers of the aluminized coating (Figure 92 c)). It is important to note that no cracks propagate into steel substrate, which implies that the functional properties of the components may not be affected. However, the presence of bare steel areas could induce issues in terms of corrosion resistance.

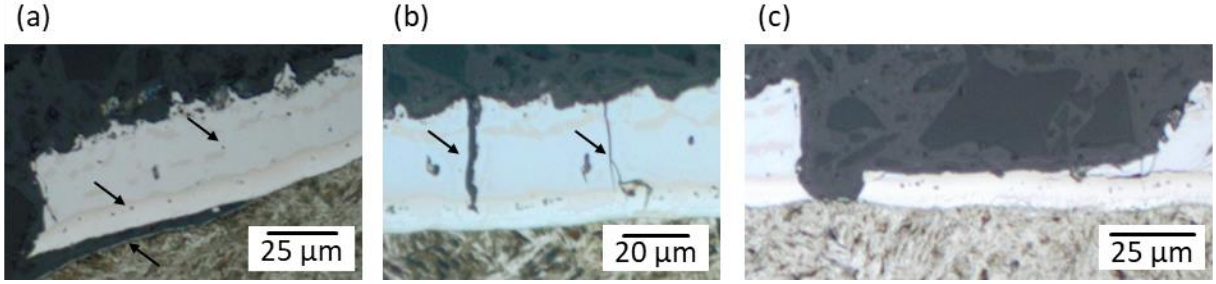

Figure 92: Presence of voids and coating delamination (a), micro-cracks (b) and partial delamination (c) of the aluminized coating after direct hot forming.

6.1.4 Hot forming behavior of galvanized coatings

Representative images of the surface appearance of cups A, B and C of a galvanized steel blank after direct hot stamping are presented in Figure 93. Cracks mainly located on the upper radius for cups A and B and on a wider area including the middle of the depth of cup C can be observed.

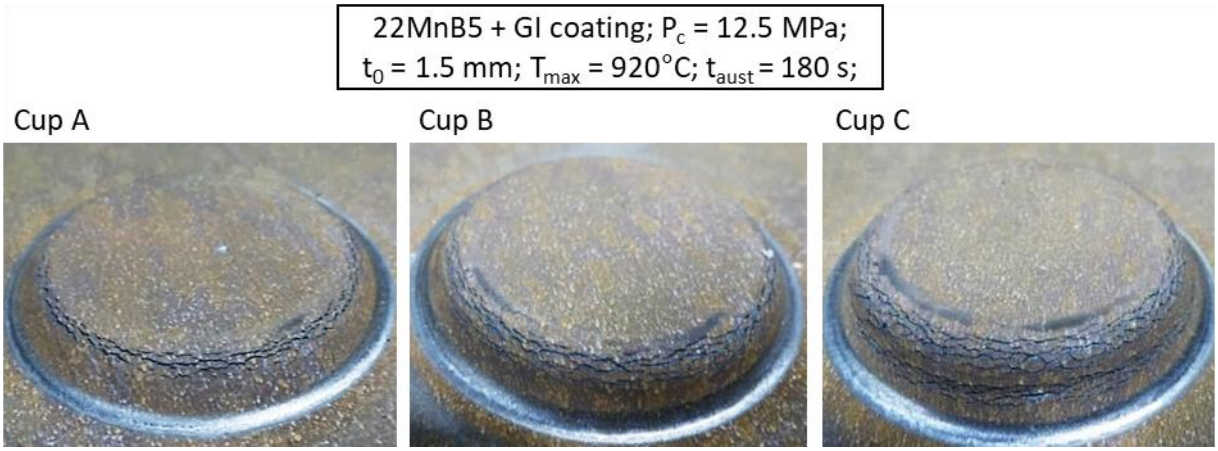

Figure 93: Surface appearance of cups A, B and C of a galvanized blank after direct hot stamping: cracking on the radii of the cups.

In order to prove the presence of cracks in the galvanized coating and determine their origin, cross-sectional microscope and SEM analyses were carried out on different cups of the large-scale plates (Figure 94).

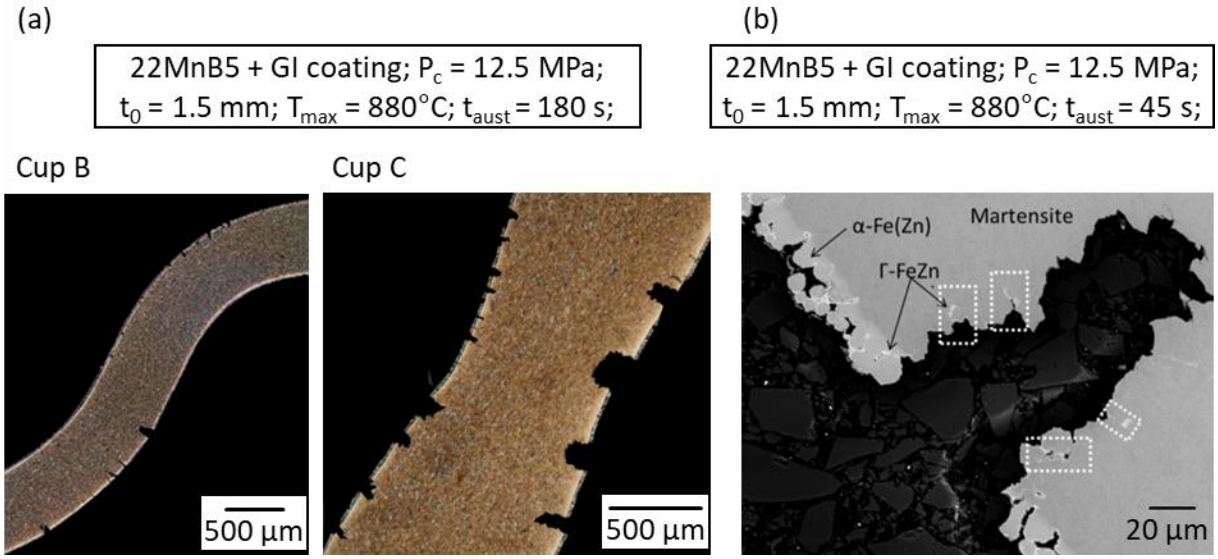

Figure 94: Cracking in galvanized steel plates after direct hot forming for cups B and C (a); SEM micrograph (BSE mode) of a crack: diffusion of zinc-rich Γ-FeZn phase in the grain boundaries of steel substrate (dashed areas) (b).

Contrarily to the aluminized coating, the cracks formed on areas undergoing tensile stresses appear to be present in the substrate of the galvanized product (Figure 94 a)). According to the SEM analyses presented in Figure 94 b) and carried out in the vicinity of cracks, Zn-rich phases can be observed in the grain boundaries of steel on areas subject to tensile stresses,

thereby confirming the appearance of LME mechanisms during direct hot stamping of galvanized steel, as discussed in Section 1.5.1. It should be noted that no cracks formed on areas undergoing compression stresses. It is important to note that no delamination of the coating could be observed in the case of the galvanized product with the exception of the walls of the cracks.

On the basis of the results obtained in this part, it appears that the above-mentioned geometries of the press equipments constitute an appropriate tool for studying the forming behavior of coating systems during direct hot stamping. A particular interest of this work, namely the evaluation of the formability of Zn-based coatings regarding to their susceptibility to LME, can be therewith studied.

The next section will be dedicated to the comparison of the behavior of commercial GI coatings and of alternative Zn-Mn coatings deposited and characterized in the previous chapters during direct hot stamping. This study will permit to assess the interest of the alloying of Zn with Mn and the suitability of Zn-Mn alloy layers for this application.

6.2 Direct hot stamping experiments with Zn-based coatings

The present part is focused on the study of the forming behavior and the material characterization of Zn-Mn and galvanized coatings after hot stamping with the press tools presented in the previous section. On the basis of the results reported in Section 5.3.2, it appears that Zn-Mn coatings are affected by evaporation when heated to a temperature of 900 °C in presence of argon, in particular when heating time increases.

In order to limit the influence of evaporation during the hot stamping studies, the coated plates were austenitized to a temperature of 860 °C in a furnace heated at a temperature of 920 °C in presence of argon and then transferred to the pressing unit. The temperature of 860 °C belongs to the temperature required for obtaining a full austenite structure in 22MnB5 press-hardened components for the hot stamping application (Section 1.3). The commercial galvanized product (PHS-Ultraform Z140) was heat treated and hot stamped after reaching the same temperature in order to evaluate the performance input of the alloying of Zn with Mn in terms of formability. More details about the parameters used and the experimental procedure are reported in Section 3.4.3. The studies of the hot stamping behavior of galvanized steel and of Zn-Mn-coated steels will be reported in Section 6.2.1 and Section 6.2.2, respectively.

Heating curves of both coated products are presented in Figure 95. A total heating time of 120 s was used for reaching the temperature of 860 °C in the case of Zn-Mn-coated large-scale plates, while a heating time of 220 s was required to attain this temperature in the case of the GI product. The heated blanks were removed from the furnace after reaching the latter durations, transferred to the press tools and quenched.

In these conditions, heating rates of approximately 10 °C.s^{-1} and 5 °C.s^{-1} were observed for Zn-Mn-coated and GI-coated 22MnB5 steel plates, respectively. The difference in the heating curves of both products can be explained by variations in the composition of their

respective steel substrates as well as by the influence of the coating materials on the behavior during heating. This study was conducted using five GI plates and two Zn-Mn-coated plates. It should be noted that alternative coating materials were electrodeposited on only one side of the large-scale plates, whereas GI plates were hot-dip coated on both sides.

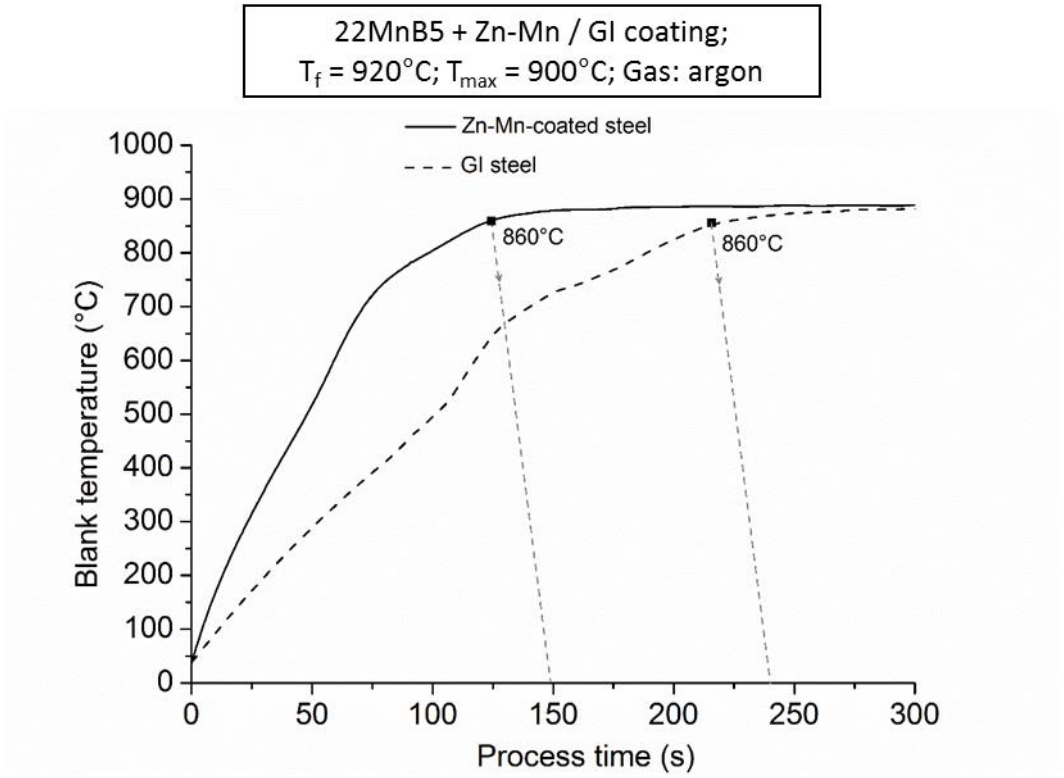

Figure 95: Representative heating curve of Zn-Mn-coated 22MnB5 steel (full line) and GI steel (dashed line) samples with dimensions of 200 x 200 mm during austenitizing treatment to 860 °C in a furnace heated at 920 °C in presence of argon.

6.2.1 Hot stamping of galvanized steel

The surface appearance of the commercial GI product after heat treatment to 860 °C in a furnace heated at 920 °C in presence of argon is presented in Figure 96.

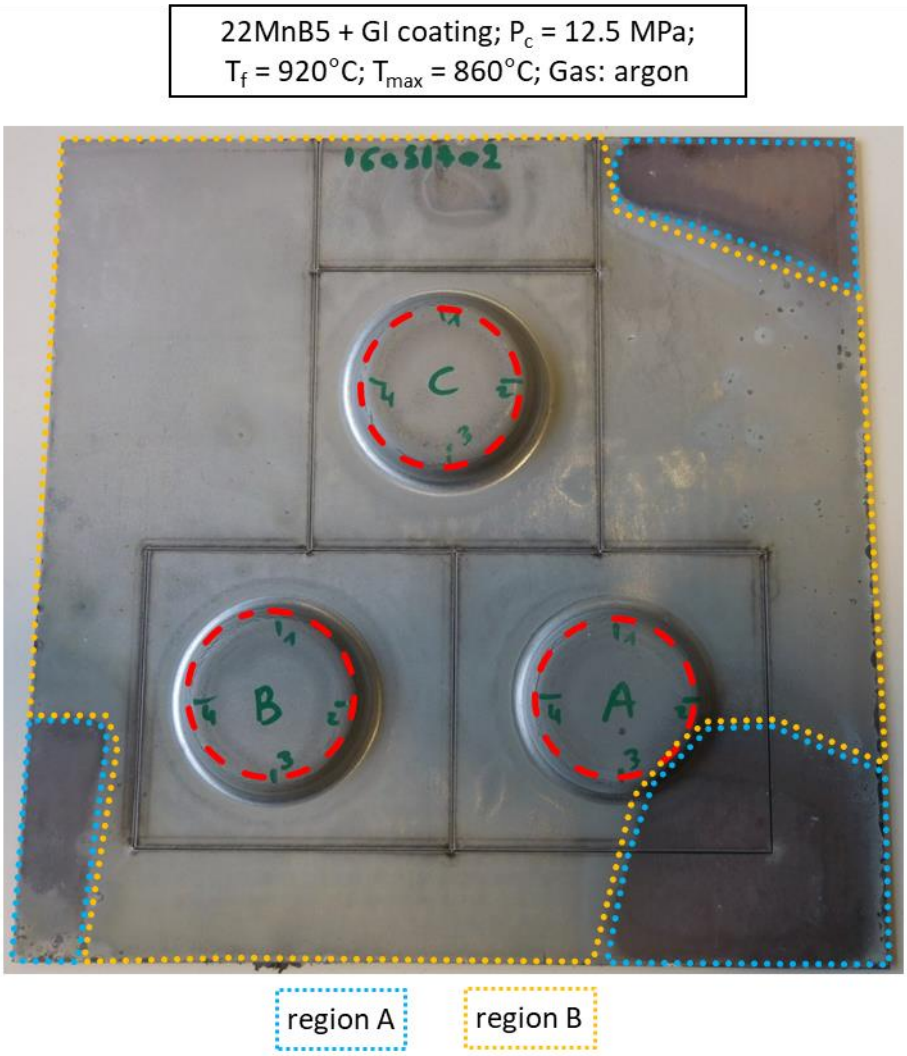

Figure 96: Surface appearance of a commercial GI steel plate post to heat treatment to 860 °C in a furnace heated at 920 °C in presence of argon and hot stamping in press tools; presence of two regions A and B; appearance of cracks in the coating (red dots).

On the one hand, dark gray colored regions (region A in Figure 96) can be observed on the corners of the plates. On the other hand, the main surface of the large-scale plates has a light gray color (region B in Figure 96). Cracks are visible on the radii of all cups located in region B.

Representative galvanostatic dissolution curves obtained from measurements carried out in both regions of the galvanized product are presented in Figure 97. It appears that the region A has a potential 100 mV lower than that of steel, while region B provides a much higher cathodic protection to steel, with the presence of several phases. The thickness of region B appears to be much higher than that of region A. Both regions will be characterized separately in the next parts.

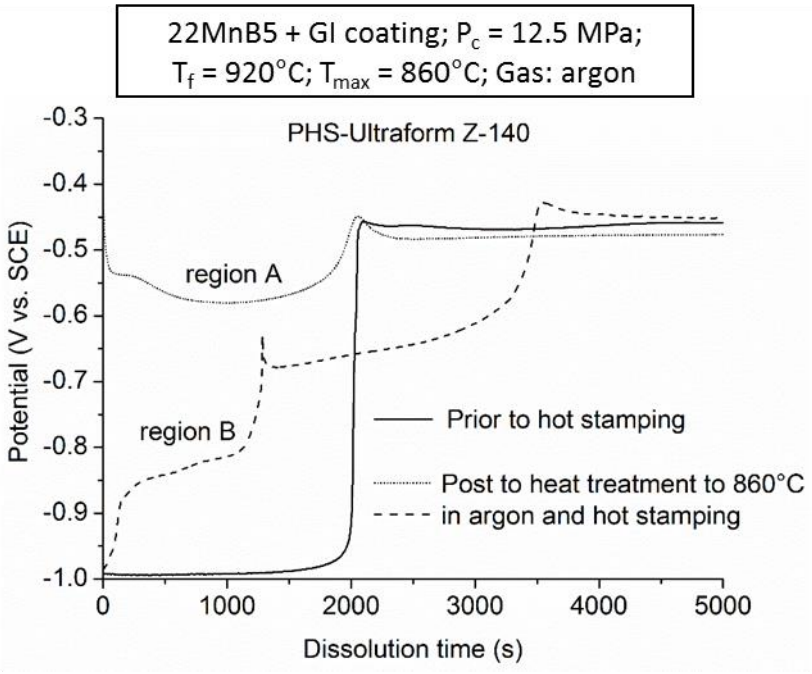

Figure 97: Evolution of the electrochemical potential of coating and substrate materials during galvanostatic dissolution of a commercial GI coating heat treated to 860 °C in a furnace heated at 920 °C in presence of argon and hot stamped, in V vs. SCE; presence of two regions A and B with different behaviors.

Materials characterization of galvanized coatings: region A

Representative cross-sectional micrographs of the layer observed on the region A of galvanized steel plates is presented in Figure 98. The coating appears to contain open porosities, cavities and cracks. A mean coating thickness of 14.8 ± 1.6 µm was obtained on the basis of a set of 12 values.

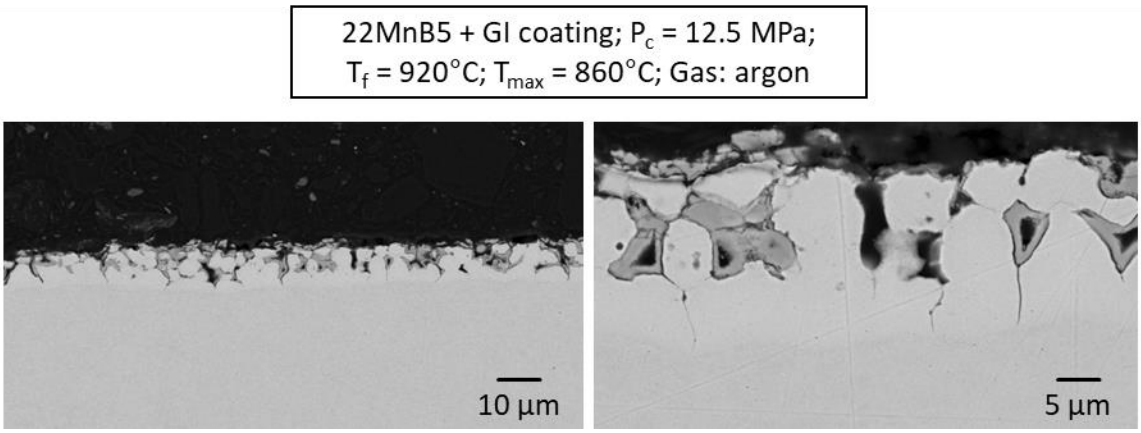

Figure 98: Cross-sectional SEM micrographs (BSE mode) of a commercial GI coating of region A (Figure 96) of large-scale steel plates heat treated to 860 °C in a furnace heated at 920 °C in presence of argon and hot stamped.

According to the results from Figure 97, the coating located in region A consists of a single phase which contains approximately 83 wt.% Fe (Table 21). From the literature data reported in Section 1.5.1 and regarding the composition of hot stamped galvanized steel, this composition is likely to correspond to the Fe-rich α-Fe phase with Zn in solid solution.

The low amount of remaining Zn in the coating explains the low difference in the electrochemical potentials of coating and substrate materials (Figure 97).

Table 21: Chemical composition of a commercial GI coating of region A (Figure 96) of large-scale steel plates heat treated to 860 °C in a furnace heated at 920 °C with argon and hot stamped, determined by semi-quantitative EDS analyses.

	Composition (wt.%)	
	Zn	Fe
region A	17.1 ± 2.3	82.9 ± 2.3

Materials characterization of galvanized coatings: region B

The galvanized coating located in region B (Figure 96) of the hot stamped large-scale plates has a microstructure containing two characteristic areas, as shown in Figure 99. A coating thickness of 17.3 ± 2.6 µm was obtained on the basis of 30 measurements.

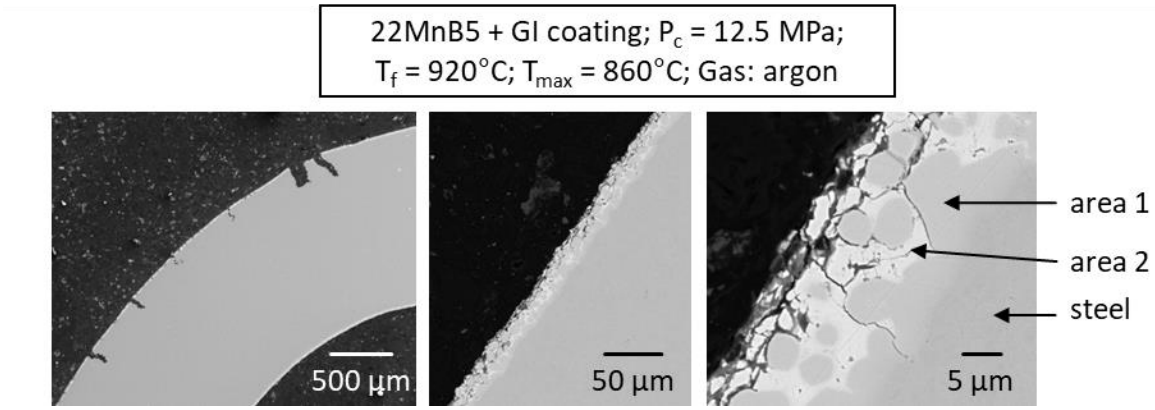

Figure 99: Cross-sectional SEM micrographs (BSE mode) of a commercial GI coating of region B (Figure 96) of large-scale plates (cup B) heat treated to 860 °C in a furnace heated at 920 °C in presence of argon and hot stamped.

According to EDS measurements carried out in both areas (Table 22), it appears that the island-type grains (area 1) mostly consist of iron and are surrounded by a Zn-rich phase corresponding to area 2. Similar phase distributions and compositions were already reported in Section 1.5.1 for this coating. The presence of cracks on areas in presence of tensile stresses, namely on the radii of all three cups, can be attributed to the appearance of LME due to the presence of the above-mentioned Zn-rich phase. This result is in good accordance with the literature data reported in Section 1.5.1.

Table 22: Chemical composition of the two areas (Figure 99) observed in a commercial GI coating after heat treatment to 860 °C in a furnace heated at 920 °C in presence of argon, determined by semi-quantitative EDS analyses.

Analysed area	Composition (wt.%)	
	Zn	Fe
area 1	33.9 ± 2.5	66.1 ± 2.5
area 2	88.0 ± 1.2	12.0 ± 1.2

Conclusion

The study of heat treatment of standard commercial galvanized products during heat treatment to 860 °C in a furnace in presence of argon permitted to reveal the presence of Zn-rich phases in the coatings, which were responsible for the formation of cracks due to LME. The electrochemical potentials of the phases formed in the galvanized coating post to hot stamping were found to be much lower than that of steel and can therefore provide sacrificial protection to steel.

Areas with a lower coating thickness and containing no Zn-rich phases were observed on the corners of the large-scale plates, in the same way as in the case of Zn-Mn coatings heat treated in the same conditions. The most probable explanation for this result is the fact that the plates were placed on firebricks during heat treatment in the furnace and that a faster heating by conduction is likely to have taken place on these areas. This could have reduced the time for atomic diffusion to occur and thereby increased the amount of Zn-rich which are susceptible to evaporation at high temperature.

6.2.2 Hot stamping of Zn-Mn-coated steel

In a similar way to the last part, this section is dedicated to the study of the behavior of Zn-Mn-coated large-scale plates during direct hot stamping after heat treatment in a furnace in presence of argon. It is important to note that the lower part of the Zn-Mn-coated large-scale specimens was found to have different properties, in particular a lower Mn content (Section 4.2.1) than the rest of the large-scale plates. In order to avoid the influence of the inhomogeneity of the coatings, only cups A and B of the large-scale plates will be investigated in the present part. Heat treatment to 860 °C and hot stamping of Zn-Mn-coated steel plates was found to lead to coatings with a non-homogeneous appearance, as presented in Figure 100.

In fact, several regions A, B and C with different colors were observed, which may indicate that the underlying materials have different compositions and properties. Region A is dark brown and is located on the corners of the plates. Region B has a gray color and was found to undergo cracking on areas located at the cups radii. On the other hand, no cracks could be observed on the deformed areas of region C, which is light brown. None of the surfaces of the latter regions were found to be powdery, which could indicate the presence of only a thin oxide layer, or an oxide layer with a good adhesion with the underlying materials.

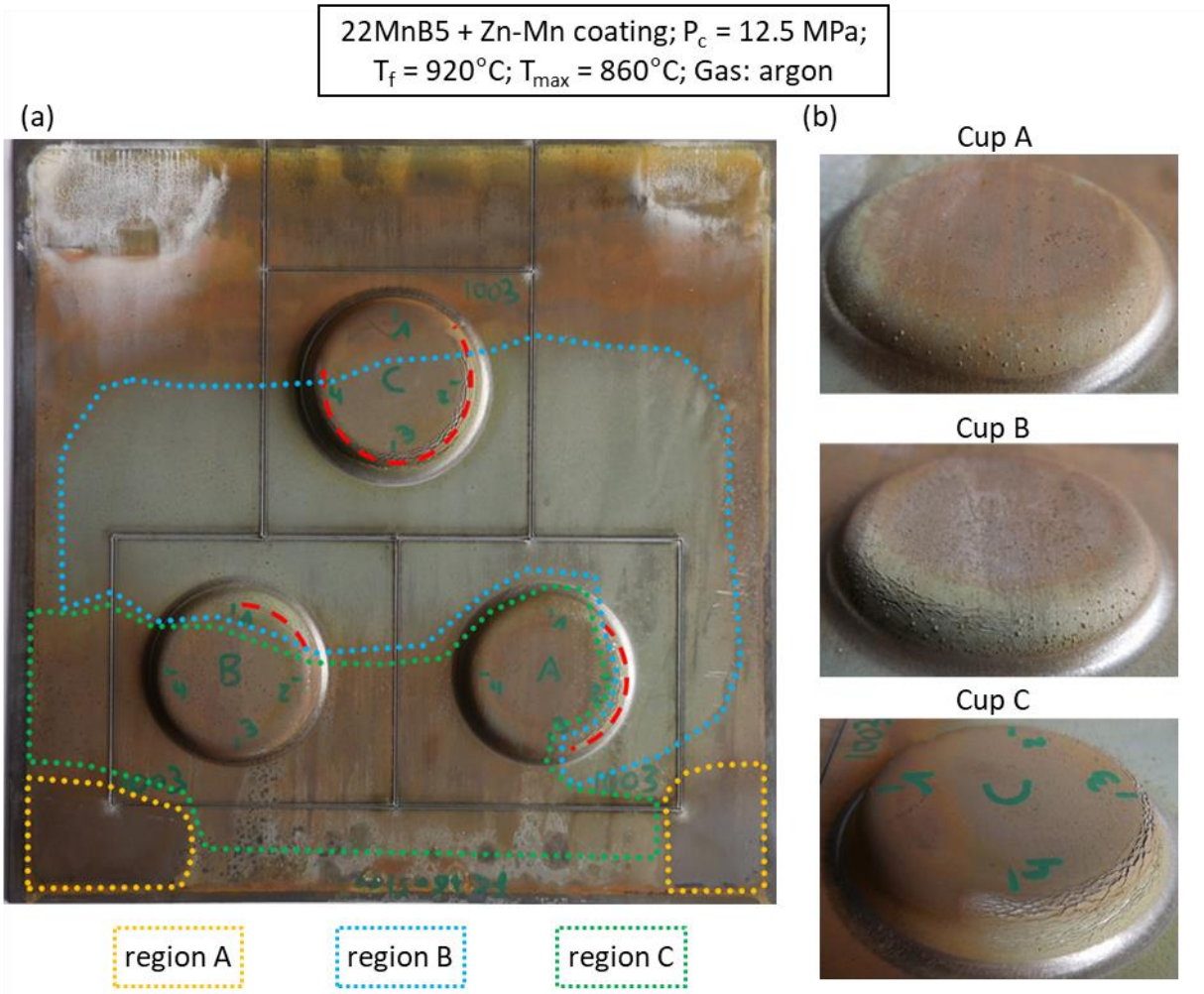

Figure 100: Surface appearance (a) of a Zn-Mn-coated steel plate after heat treatment to 860 °C in a furnace heated at 920 °C in presence of argon and hot stamping in press tools; presence of different regions A, B and C; appearance of cracks on the radii of the cups (red dots); surface appearance of cups A, B and C (b).

The material characterization of the three regions of the coatings will be reported separately in the next parts.

Materials characterization of Zn-Mn coatings: region A

Galvanostatic measurements (Figure 101) carried out on region A of the Zn-Mn-coated plates revealed the presence of materials with electrochemical potentials very similar to that of steel on the surface of the plates. This result indicates that no or barely no coating is present on the steel substrate. Similar results were obtained for the same regions in the case of galvanized steel (Section 6.2.1) and are most likely related to a much higher heating rate compared to the rest of the plates.

As the contact surface and the geometrical configuration during heat treatment considered in the present work is not representative of the industrial manufacturing processes with the use of roller furnaces, it should be noted that the results obtained in this area are unlikely to be observed at the industrial scale.

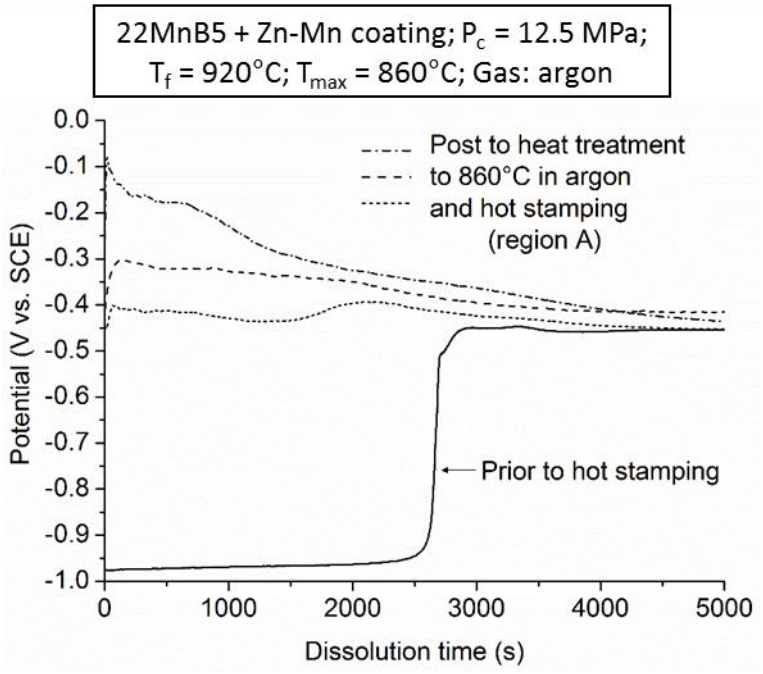

Figure 101: Evolution of the electrochemical potential of coating and substrate materials during galvanostatic dissolution of Zn-Mn coatings of region A (Figure 100) heat treated to 860 °C in a furnace heated at 920 °C in presence of argon and hot stamped in press tools, in V vs. SCE.

Materials characterization of Zn-Mn coatings: region B

According to Figure 102, Zn-Mn coatings located in region B are likely to consist of three phases with electrochemical potentials lower than that of steel.

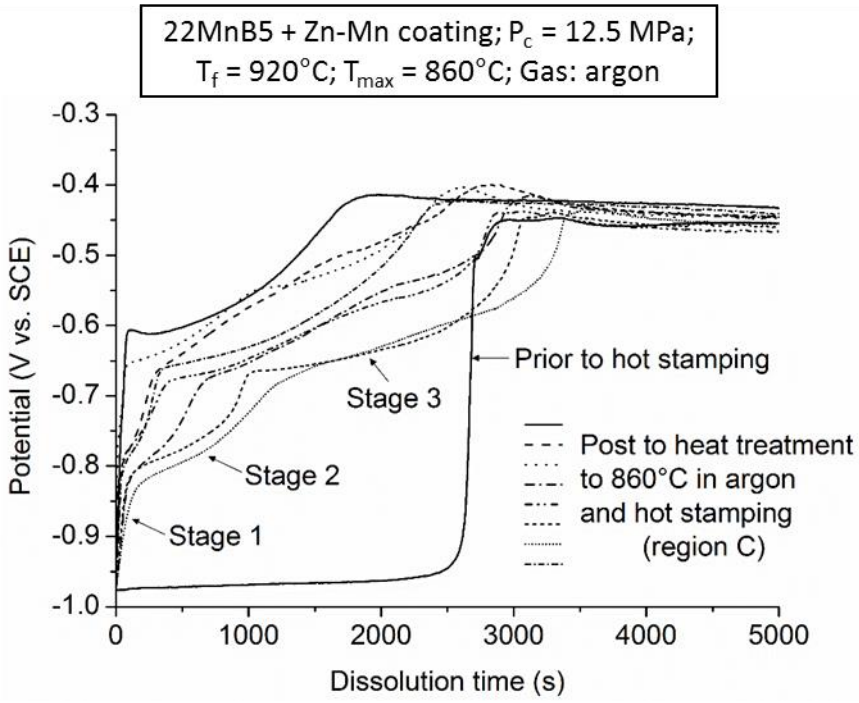

Figure 102: Evolution of the electrochemical potential of coating and substrate materials during galvanostatic dissolution of Zn-Mn coatings of region B heat treated to 860 °C in a furnace heated at 920 °C in presence of argon and hot stamped in press tools, in V vs. SCE.

The respective amount of the corresponding phases, as well as the time for the total dissolution of the coatings were found to vary, which indicates that the distribution and the composition of the phases in the coating are not homogeneous. A good adhesion between coating and substrate seems to be obtained.

The cross-sectional micrographs of the corresponding Zn-Mn coatings presented in Figure 103 prove the presence of several phases in the layers, in addition to the oxide scale formed on the coating surface and particles located between the oxide scale and the underlying materials. A mean coating thickness of 11.5 ± 2.4 µm was measured on the basis of a set of 51 values.

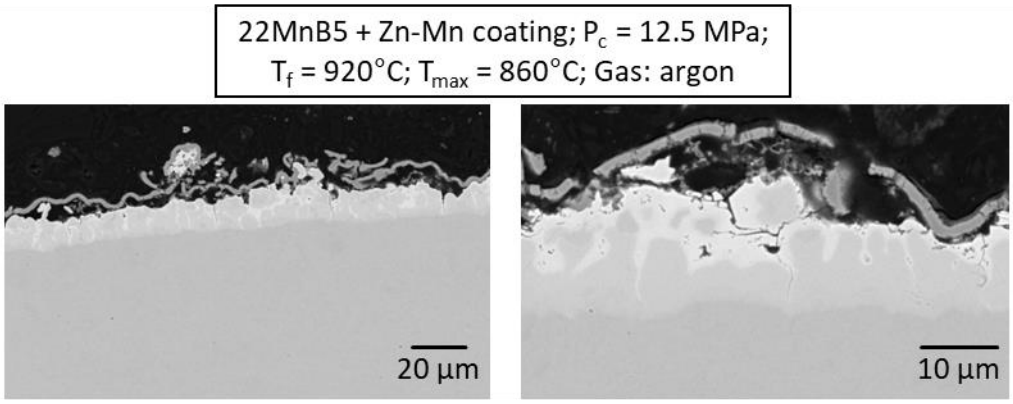

Figure 103: Cross-sectional SEM micrographs (BSE mode) of the Zn-Mn coating of region B (Figure 100) of large-scale plates post to heat treatment to 860 °C in a furnace heated at 920 °C in presence of argon and hot stamping.

According to the cross-sectional elemental mappings presented in Figure 104, the microstructure of the coatings consists of island-type grains with different sizes randomly distributed in the coating thickness and separated with domains with a light BSE contrast which appear to contain a higher amount of Zn. The island-type grains were found to have different BSE contrasts, as observed in the case of areas 2 and 3, which could be explained by the presence of different compositions.

From the EDS composition measurements listed in Table 23, it appears that areas 2 and 3 have different compositions with higher Mn and Fe contents for grains corresponding to area 2. The presence of the two latter phases with different compositions may explain the non-regular transition of the electrochemical potential in Stage 3 (Figure 102) of dissolution.

On the other hand, the Zn-rich phase contains about 82.5 wt.% Zn (Table 23) and can be most probably related to stage 2 observed during galvanostatic dissolution measurements (Figure 102).

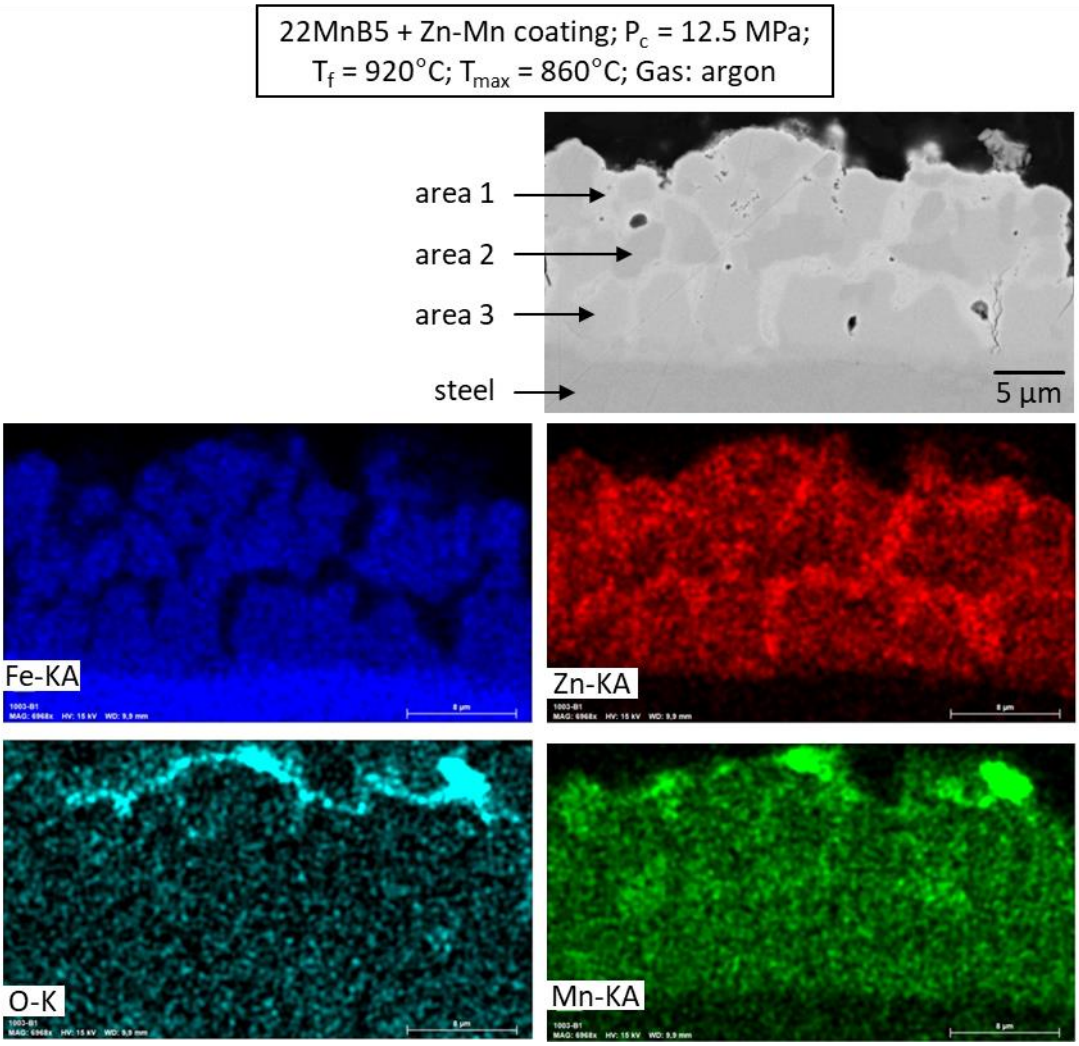

Figure 104: Cross-sectional SEM micrograph (BSE mode) with characteristic phase areas and EDS elemental mapping of Zn-Mn-coated 22MnB5 steel of region B (Figure 100) of large-scale plates post to heat treatment to 860 °C in a furnace heated at 920 °C in presence of argon and hot stamping.

Table 23: Chemical composition of the different phase areas (areas 1, 2 and 3 shown in Figure 104) observed in region B (Figure 100) of a Zn-Mn-coated large-scale steel plate heat treated to 860 °C in a furnace heated at 920 °C with argon, determined by semi-quantitative EDS analyses.

	Composition (wt.%)		
	Zn	Mn	Fe
area 1	82.5 ± 5.0	2.7 ± 1.3	14.9 ± 5.0
area 2	31.5 ± 2.3	9.9 ± 2.1	58.6 ± 2.6
area 3	40.6 ± 2.4	4.5 ± 1.5	54.9 ± 2.5

As mentioned earlier, cracks were observed on the surface of the Zn-Mn coatings in region B of the large-scale plates, as illustrated in Figure 105 a). On the basis of cross-sectional SEM micrographs (Figure 105 b) and c)) and EDS elemental mappings (Figure 106) on the corresponding areas, it appears that cracks are related to the presence of a zinc-rich phase at the grain boundaries of steel substrate, which is an evidence of the appearance of LME on areas undergoing tensile stresses. It is important to note that cracking due to LME takes place for all cups, namely for blank thinnings of at least 10 %.

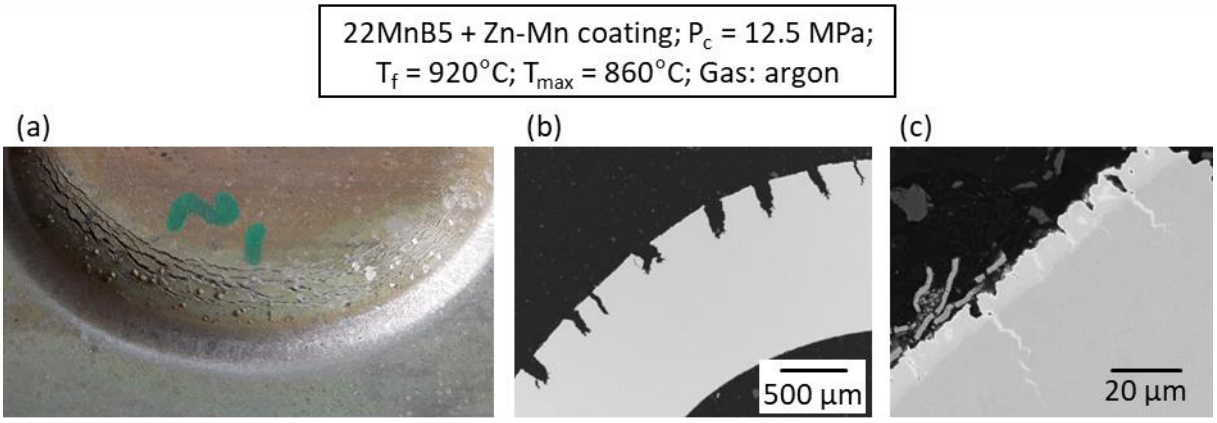

Figure 105: Surface appearance (a), cross-sectional SEM micrograph (BSE mode) of the cup radius (cup A) in presence of cracks (b) and SEM micrograph (BSE mode) of the corresponding cracks (c) due to LME in the case of region B (Figure 100) of Zn-Mn-coated large-scale plates post to heat treatment to 860 °C in a furnace heated at 920 °C in presence of argon and hot stamping; cup A of hot stamped plates.

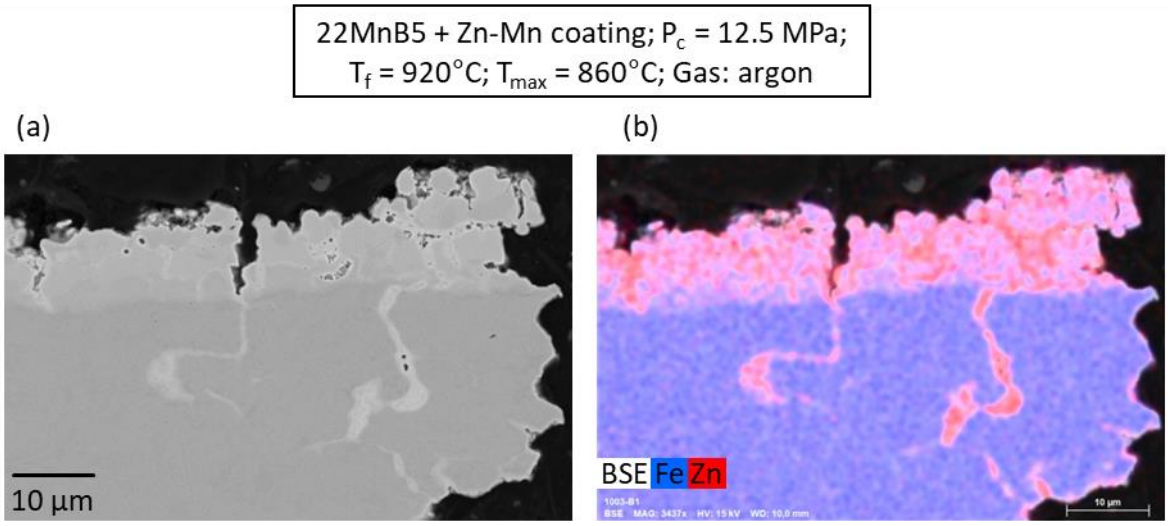

Figure 106: Cross-sectional SEM micrograph (a) (BSE mode) and EDS elemental mapping (b) of the presence of cracks due to LME in region B of Zn-Mn-coated 22MnB5 steel during hot stamping post to heat treatment to 860 °C in a furnace heated at 920 °C in presence of argon; cup B of hot stamped plates.

Materials characterization of Zn-Mn coatings: region C

According to Figure 107, a low difference in the electrochemical potential of the Zn-Mn coating and steel was obtained in region C (Figure 100) of the large-scale plates. In addition, the presence of only one dissolution stage during galvanostatic dissolution may be explained by the presence of a single phase in the coating.

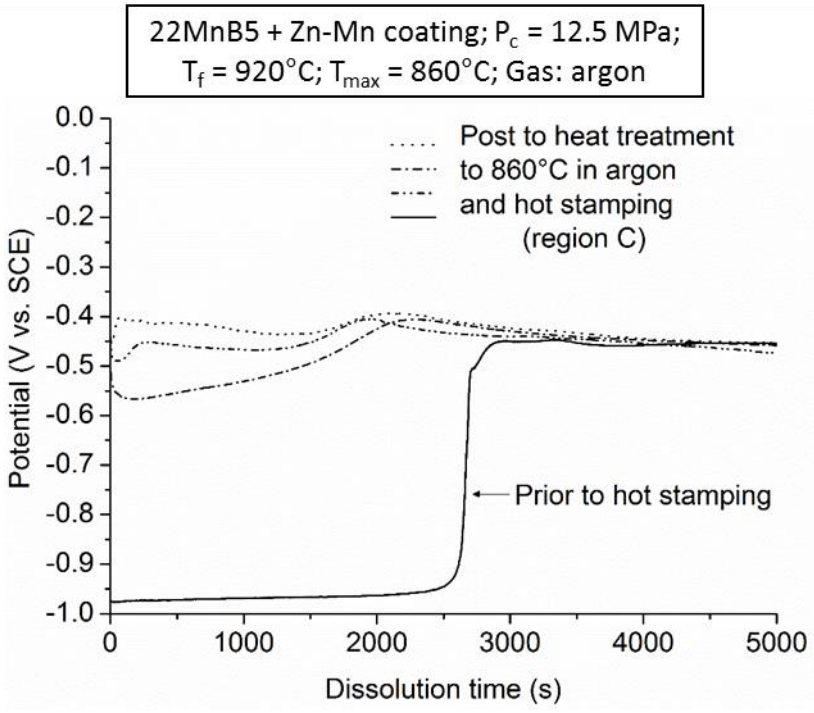

Figure 107: Evolution of the electrochemical potential of coating and substrate materials during galvanostatic dissolution of Zn-Mn coatings of region C (Figure 100) heat treated to 860 °C in a furnace heated at 920 °C in presence of argon and hot stamped, in V vs. SCE.

The absence of color contrast in the BSE image of cross-sectional micrographs of the coatings presented in Figure 108 confirms this result. A mean coating thickness of 8.4 ± 1.3 µm was measured on the basis of a set of 72 values. Cracks were partly observed in the coatings, but did not propagate into steel substrate.

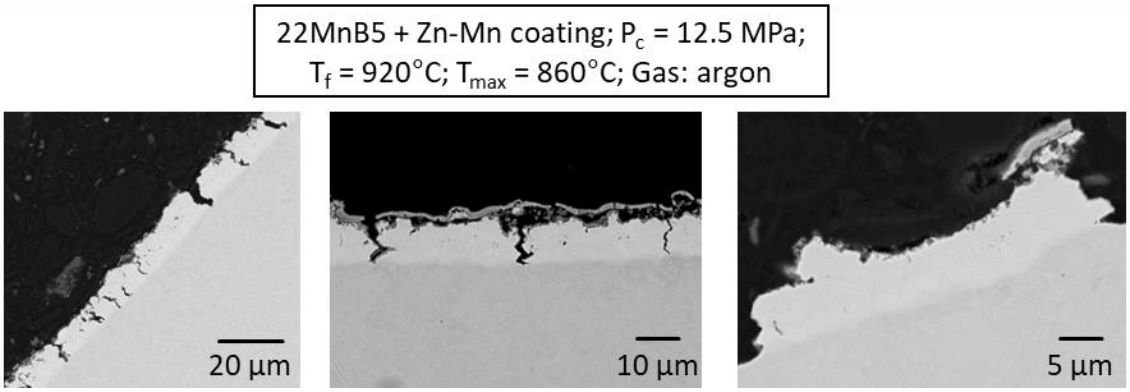

Figure 108: Cross-sectional SEM micrographs (BSE mode) of the region C of Zn-Mn-coated large-scale plates post to heat treatment to 860 °C in a furnace heated at 920 °C in presence of argon and hot stamping; cup B of hot stamped plates.

An oxide scale is visible on the top surface of the coating and does not have a good adhesion with the underlying coating, presumably due to the presence of sulfur particles between the oxide scale and the coating, as proved by the cross-sectional EDS mappings presented in Figure 109 and in a similar way to Zn-Mn coatings heated to 900 °C in argon (Section 5.3.3). The coating is very likely to consist of a mixture of Zn, Fe and Mn (Figure 109).

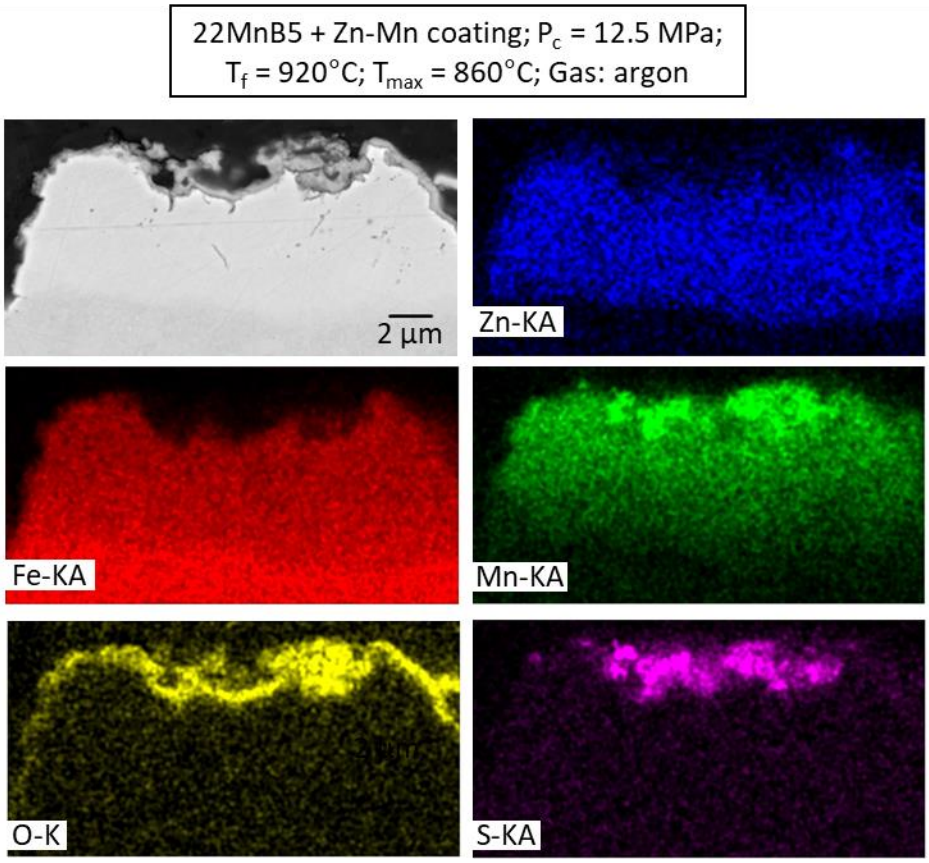

Figure 109: Cross-sectional SEM micrograph (BSE mode) and EDS elemental mapping of region C of Zn-Mn-coated 22MnB5 steel post to heat treatment to 860 °C in a furnace heated at 920 °C in presence of argon and hot stamping.

Elemental composition analyses listed in Table 24 indicate that the coatings contain approximately 22.5 wt.% Zn, 15.2 wt.% Mn and 62.4 wt.% Fe. The high Fe content is most likely the reason for the low sacrificial effect to steel provided by the coating. It should be noted that the high standard deviation for Mn and Fe content are very probably related to a composition gradient in the coating.

Table 24: Chemical composition of the Zn-Mn coatings of region C (Figure 100) of large-scale steel plates heat treated to 860 °C in a furnace heated at 920 °C in presence of argon and hot stamped, determined by semi-quantitative EDS analyses.

	Composition (wt.%)		
	Zn	Mn	Fe
coating	22.5 ± 2.5	15.2 ± 6.2	62.4 ± 7.6

Conclusion

From this study, it appears that the properties of the Zn-Mn coating varies significantly over the surface of large-scale plates after heating to 860 °C and hot stamping.

First of all, areas located on the corners of the plates (region A) were found to contain almost no coating. This result could be related to the direct contact with firebricks during heat treatment. A rapid heating of the coatings by conduction may have taken place,

thereby reducing the time for interdiffusion to occur and increasing the exposure of the Zn-based alloy to evaporation.

Region B of the large-scale plates have a light gray color and were found to contain Zn-rich phases, which induced cracking on areas undergoing tensile stresses, namely on cups radii. Charaterization studies revealed the propagation of cracks into steel due to LME. The microstructure and the Mn content of the corresponding coatings were found to vary. This is presumably due to non-regular growth of the Fe-rich phases as well as oxidation and evaporation phenomena. The coating located in region B was found to provide good sacrificial protection to steel, which may fit the products requirements of OEMs. As this region was located in the center of the large-scale plates it is very likely that the heating rate of the coating was lower than that of the rest of the plates. Besides, a lower temperature may have been reached, which could explain the presence of Zn-rich phases which did not evaporate.

Finally, the region with a brown color (region C) did not exhibit issues related to LME cracking, presumably due to the absence of Zn-rich phases in the coating. The corresponding coating was found to contain a high Mn content of approximately 15 wt.%. Due to the low Zn content of 22.5 wt.% in the coating, a low difference in the electrochemical potentials of the coating and steel was obtained.

On the basis of these results, it appears that higher corrosion protection is likely to be achieved by the use of Zn-Mn coatings compared to aluminized steel, due to the achievement of sacrificial corrosion protection for steel post to hot stamping, in a similar way to galvanized steel. However, due to presumable non-uniform oxidation and evaporation phenomena as well as temperature distribution during austenitizing treatment, heterogeneous phase distribution and compositions were observed and partly induced the formation of cracks related to LME, in a similar way to galvanized steels.

6.3 Suitability of Zn-Mn coatings for direct hot stamping [EN + FR]

In this chapter, the microstructure, the anticorrosive properties and the forming behavior of Zn-Mn-coated steel was investigated on the basis of direct hot forming operations on large-scale plates. Press tools were specifically designed for the present study to evaluate the behavior of the coated materials in a wide range of thinning of the blanks on a unique specimen.

In order to assess the input of the use of Mn as alloying element in the Zn coating and identify any improvements by the use of the alternative coating developed in this work, the same hot forming experiments were carried out on galvanized steel.

As said earlier, this study constitutes the first publicated work on the investigation of the suitability and the behavior of Zn-Mn coatings for hot forming application. It is important to note that the investigations carried out in the present study provide preliminary results and depict only a tendency in the conclusions regarding the behavior and the properties of the Zn-Mn coatings during hot forming, as a limited amount of large-scale plates were coated with Zn-Mn alloy layers and used for hot stamping experiments.

In addition, it is very likely that the conditions used during heat treatment of both coated products, namely the type of experimental sample holder in the furnace induced the presence of non-homogeneous heating rates over the surface of the coatings. A particularly fast heating is assumed to have taken place at the corners of the plates and to have led to accelerated evaporation of the coatings, heterogeneous diffusion between coating materials and steel or to heterogeneous exposure to high temperature oxidation.

In the case of commercial GI steel plates, cracks were found to form in the radii of all cups with tensile stresses and to propagate into the steel substrate. On the basis of SEM measurements, it appears that the coating partly consists of Zn-rich phases, which may have induced the occurrence of LME.

In the case of Zn-Mn-coated plates, LME could not be fully avoided, as cracks were partly found to form on the upper radius of the cups along with the presence of Zn-rich phases along the grain boundaries of the steel substrate at the cracks. In a similar way to galvanized plates, non-homogeneous microstructures and compositions were observed over the surface of large-scale plates after austenitizing and hot forming. This particularity is in good accordance with the results obtained in Section 5.3 during heat treatment experiments on small specimens and can be related to evaporation of the coating materials and preferential oxidation of Mn. In addition, this observation can be explained by the presence of heterogeneities in the composition, in the thickness and in the properties of the as-deposited layers over the surface of the large-scale plates.

A sacrificial corrosion protection could be achieved in the case of Zn-Mn coatings. However, due to the non-homogeneous microstructure and composition of the coating, the amount of Zn-rich phases with a high sacrificial effect to steel was found to vary significantly.

Compatibilité des alliages Zn-Mn pour l'emboutissage à chaud direct [FR]

Dans ce chapitre, la microstructure, les propriétés anticorrosives et le comportement en mise en forme des aciers revêtus de couches de Zn-Mn ont été étudiés par des essais d'emboutissage à chaud direct sur des plaques de larges dimensions. Des outils de presse permettant d'évaluer les propriétés de mise en forme d'aciers revêtus dans un large domaine d'amincissements ont été conçus spécialement pour cette étude. Afin d'évaluer la contribution de l'utilisation du Mn en tant qu'élément d'alliage pour les couches de Zn et d'identifier d'éventuels avantages de l'utilisation de revêtements alternatifs développés dans le cadre de ce travail, les mêmes essais de mise en forme à chaud ont été réalisés sur un acier galvanisé commercial. Comme annoncé précédemment, cette étude constitue le premier travail publié sur l'évaluation de la compatibilité et du comportement d'alliages Zn-Mn pour l'application de la mise en forme à chaud. Il est important de noter que les essais menés dans cette étude ne fournissent que des résultats préliminaires et décrivent une tendance dans les conclusions concernant le comportement et les propriétés des alliages Zn-Mn pendant la mise en forme à froid dû au fait qu'un nombre limité de plaques revêtues a pu être mis à disposition et utilisé pour les essais de mise en forme. De plus, il est fort probable que les conditions utilisées pendant le traitement thermique des deux types de produits, notamment le type de support pour les plaques dans le four, ont induit la présence de vitesses de chauffe hétérogènes sur la surface des revêtements. En outre, une chauffe trop rapide a vraisemblablement eu lieu aux coins des plaques et aurait conduit à une évaporation accélérée des revêtements, une diffusion hétérogène entre les matériaux des couches et de l'acier ainsi qu'à une exposition hétérogène à l'oxydation à haute température.

Dans le cas des plaques galvanisées commerciales, des fissures ont été observées dans la couche ainsi que dans le substrat dans les rayons comportant des contraintes de traction de tous les poinçons. Des analyses de microscopie électronique à balayage ont permis d'observer que des phases riches en Zn se situent aux joints de grains de ces fissures, qui se sont vraisemblablement formées dû au phénomène de fissuration par métaux liquides. La fissuration par métaux liquides n'a pas pu être évitée dans le cas des plaques revêtues de couches de Zn-Mn du fait que des résultats similaires ont été obtenus pour les couches alternatives. Des microstructures et compositions hétérogènes ont été obtenues pour les deux types de matériaux sur la surface des grandes plaques après austénitisation et mise en forme à chaud. Cette particularité est en accord avec les résultats obtenus dans le chapitre 5.3 pendant le traitement thermique sur des petits échantillons et peut être expliquée par la présence d'hétérogénéités dans la composition, dans l'épaisseur et dans les propriétés des couches électrodéposées sur les grandes plaques. Une protection cathodique est obtenue pour les deux types de revêtements. Cependant, la quantité de phases riches en Zn procurant un effet sacrificiel au substrat varie sensiblement en raison du caractère hétérogène des propriétés des couches après traitement thermique sur la surface des grandes plaques.

7 Summary and outlook

As a response to evolving emissions regulations implying a constant decrease of the weight of passenger vehicles, along with high requirements in terms of passenger safety, press-hardened components are widely used in the automotive construction, in particular around the passenger compartment. In order to avoid issues related to the exposure of bare steel components to corrosive media, aluminized and galvanized coatings are generally used. The interest of OEMs for a widening of the range of coating products for hot stamped automotive body parts has been raising during the last decade in order to optimize the manufacturing process and improve performance of the final products. However, the coating materials require a complex profile on functionalities, mostly due to the austenitizing treatment to temperatures of about 900 °C which is required for obtaining ultra-high strength. Among the various solutions proposed on the market, the best anticorrosive properties appear to be provided by Zn-based layers due to the achievement of cathodic corrosion protection to steel. However, due to a low formability at high temperature as a result of LME, the manufacturing route of galvanized steel with the indirect hot stamping method involves higher costs than the standard direct hot stamping method.

The present work examines the properties and the suitability of alternative Zn-Mn alloy coatings for the direct hot stamping application. The properties of the coatings were investigated with regard to their growth by electrodeposition, microstructure, morphology, chemical composition, crystallographic structure and anticorrosive behavior. Moreover, the high temperature behavior was investigated with regard to interdiffusion and to the distribution of the phases formed during heat treatment and to the occurrence of evaporation and oxidation. Finally, hot press forming studies were carried out on Zn-Mn-coated steels to assess the hot formability of the coating materials with a particular focus on the susceptibility of the system to LME.

Electrodeposition of Zn-Mn alloys

The Zn-Mn coatings were deposited from chloride electroplating baths. Various electrochemical and characterization studies were carried out in order to define optimal additives and plating bath compositions, electric parameters and deposition procedures. On the basis of CV and EQCM studies, it appears that electrodeposition of Zn-Mn coatings undergoes a significant hydrogen evolution reaction, limiting the amount of Mn in the alloys. The simultaneous use of NH_4SCN and 4-HB additives in the electroplating bath permitted to facilitate codeposition of Mn and provided outstanding crystallographic, surface and microstructural properties compared to additive-free solutions. In addition, a deposition potential of -1.62 V and a $[Mn^{2+}]/[Zn^{2+}]$ ions concentration ratio of 8 were found to lead to Zn-Mn alloys with high and reproducible Mn contents. In order to better understand the influence of the use of additives on the properties of Zn-Mn alloys, comprehensive material characterization studies were carried out on coatings deposited in presence and in absence of additives.

Chemical composition

A significant increase of the Mn content from 11 wt.% to 17 wt.% was observed by the simultaneous use of both NH_4SCN and 4-HB additives in the present work. A synergistic effect may have taken place by the combination of both additives, as their separate use was reported in the literature to increase Mn content. Further investigations are required for a better understanding of the influence of the additives on the kinetic parameters of the deposition process and on the growth mechanisms. According to the binary diagram of Zn-Mn alloys, a melting point of approximately 725 °C should be obtained in these conditions, which is much higher than that of pure Zn coatings (419.6 °C). This result may play an important role in the reduction of LME mechanisms and the achievement of good anticorrosive properties due to a delayed melting of the coating during heating. Traces of sulfur were observed and were most probably due to the use of NH_4SCN additive.

Microstructural properties

Zn-Mn alloy coatings deposited without additives were found to be very rough and to consist of a non-regular cauliflower-like dendritic morphology. On the contrary, an outstanding surface state without well-defined geometric characteristics and with a very low roughness of approximately S_a = 76.46 nm was obtained for Zn-Mn coatings deposited in presence of additives. Such a noteworthy smooth surface is likely to be related to the combination of NH_4SCN and 4-HB additives, as the latter were reported in the literature to improve the surface morphology of Zn-Mn deposits when used separately. In addition, the surface state may be related to the formation of very fine grains with a mean size of 268 nm observed from SEM-EBSD analyses on the coating surface. These particularities may have an influence on the heat treatment behavior and anticorrosive properties of the alloys. Coatings were found to provide a remarkable leveling effect to the roughness of the substrate, which implies that the thickness of the coatings varies significantly. Cross-sectional studies indicated the presence of a transition in the microstructure of the coating during deposition. At the first stages of growth, a layer with a fine-grained structure forms on steel substrate, accompanied by a high amount of porosities most likely due to hydrogen evolution reaction. After a certain duration of deposition, a layer consisting of columnar grains appears, suggesting a change in the growth mechanisms of the deposits, presumably related to the evolution of the energy of the grains during deposition or to a change in the electroplating conditions. Regular ruptures of the columnar structure in the shape of sublayers with a thickness of at most 100 nm were observed in the upper part of the coatings and could not be explained.

Crystallographic structure

The Zn-Mn coatings deposited in presence of additives were found to consist of a single ε_2–Zn-Mn HCP phase. This crystallographic phase is metastable and belongs to the ε phase field, thermodynamically stable between 220 °C and 815 °C. A remarkably strong fiber texture with an intensity of 15 was observed along the <110> direction, indicating that the crystals are well oriented with their basal plane normal to the surface. This particularity may

have an influence on the performance of the Zn-Mn deposits, in particular on mechanical, anticorrosive, thermal and forming properties.

Anticorrosive properties

Potentiodynamic polarization studies showed that Zn-Mn alloy coatings deposited in presence of additives provided the best corrosion protection compared to Zn-Mn layers deposited without additives and pure Zn coatings, with a lower corrosion current density and a higher polarization resistance. This result can be associated with the high Mn content, the smooth surface of the layers and the preferential orientation of the crystals, which could decrease the dissolution rate of the alloys. It is important to note that the presence of Mn in the coating is not sufficient for improving corrosion protection of Zn layers, as Zn-Mn coatings deposited without additives (11 wt.% Mn) have a higher corrosion current density than pure Zn coatings. It can be presumed that this result is related to the surface state of the latter deposits, in particular to the dendritic morphology, rough surface and open porosities observed. A difference of approximately 500 mV was observed between the potentials of coating and substrate materials, which means that a significant sacrificial protection can be obtained with the coatings developed.

High temperature behavior

A study of heating Zn-Mn coatings to 900 °C in air showed that most of the Mn content of the coatings is lost by oxidation in presence of air. Therefore, heat treatment studies were carried out on Zn-Mn coatings in a furnace in presence of a protective atmosphere (argon) in order to reduce the exposure of the coating materials to oxidation. The coated specimens were heated up at a constant temperature for various durations corresponding to intermediary target temperatures comprised between room temperature and standard austenizing conditions in order to investigate diffusion processes and phase formation occurring during heat treatment. Various complementary characterization techniques were used for determining the influence of heat treatment on the microstructural, crystallographic and anticorrosive properties of the coatings.

After heating to 300 °C, the Zn-Mn coatings were similar to as-deposited layers. At a temperature of 500 °C, a thin interdiffusion layer forms at the interface between coating and steel. A significant change in the microstructure of the coating was observed after reaching a temperature of 700 °C, with the formation of a compact interdiffusion layer with a thickness of about 5 µm. It is important to note that the interdiffusion layers were found to contain a Mn content lower than that of the upper part of the coatings, presumably due to high interdiffusion coefficients of Zn and Fe. The columnar structure observed for the as-deposited Zn-Mn alloys disappears after heating to 700 °C. Instead, large grains without well-defined geometries are formed in the upper part of the coating, which was found to be inhomogeneous due to the presence of a high density of pores and precipitates at the grain boundaries. On the basis of STEM elemental studies, these areas appear to contain high amounts of S and Mn, presumably due to the formation of MnS observed during XRD measurements. The sulfur-rich areas observed at 700 °C migrate towards the top surface of

the coating by a further increase of the temperature. Despite the use of a protective atmosphere with an amount of O_2 lower than 1 % during heat treatment, a Mn-rich oxide scale forms on the top surface of the coatings, in particular for temperatures of at least 700 °C. At a temperature of 900 °C, various microstructures and phase distributions were observed. The amount of Mn in the remaining layers was found to vary, presumably due to heterogeneous exposure to oxidation. It is important to note that the preferential oxidation of Mn permitted to partly avoid the loss of metallic Zn by oxidation, thereby increasing corrosion protection. From the galvanostatic dissolution measurements, it appears that the amount of Zn-rich phases varies. This observation might be related to the leveling effect provided by the Zn-Mn coatings during electrodeposition, which resulted in a significant variation of the thickness of the initial coatings. Besides, the absence of Zn-rich phases for Zn-Mn coatings heated at 900 °C with different dwell times may support the hypothesis of heterogeneous evaporation of the Zn-rich phases at high temperature in presence of argon.

On the basis of these results, it appears that the use of a furnace in presence of inert gas is necessary to retain most of the initial Mn content in the coatings and to provide a sufficiently high melting point to the alloy, which influences the susceptibility to LME and the anticorrosive properties. This particularity may induce higher production costs than a conventional oxidizing atmosphere. In addition, loss of Zn by evaporation may take place at high temperature, affecting the anticorrosive properties of the coated products. Furthermore, as the loss of Mn by oxidation induces the formation of an oxide scale consisting of loose particles, it is very likely that a surface treatment is required to achieve a good paintability of the components.

Hot formability

The behavior of Zn-Mn-coated large-scale steel plates during direct hot stamping was assessed by heating to a temperature of 860 °C in a furnace heated at 920 °C with protective gas. Press tools with geometries providing blank thinning values of up to 20 % were specifically designed for this study in order to evaluate the behavior of current and alternative coatings. Preliminary experiments on current coating products permitted to determine the requirements of alternative coating materials in terms of hot forming behavior and to evidence the appearance of LME for galvanized steels with the corresponding press tools. The results obtained on direct hot stamped Zn-Mn-coated steel plates showed areas with cracks induced by LME on areas with tensile stresses, in a similar way to galvanized steel, due to the presence of Zn-rich phases. These areas were found to contain a low Mn content, which could be related to the loss of Mn by oxidation. Other regions of the deformed Zn-Mn-coated steel plates were found to be crack-free and to consist of a single Fe-rich layer containing a high Mn content of about 15 wt.%. Evaporation of Zn-rich phases may have taken place, presumably due to the use of high temperatures and inert gas.

On the basis of these results, it appears that Zn-Mn coatings heat treated to 860 °C in presence of argon and hot stamped undergo heterogeneous oxidation of Mn and

evaporation of Zn-rich phases at high temperature, inducing different behaviors in terms of hot formability and corrosion protection. It is important to note that the heterogeneity is not related to a variation of the initial composition of the layers but can be explained by a heterogeneous phase distribution after heat treatment due to the variation of the thickness of the layers due to the presence of a leveling effect. In addition, heterogeneous oxidation and evaporation mechanisms took place over the surface of the plates. Furthermore, it can be assumed that a non-uniform temperature distribution was obtained on the large-scale plates during austenitizing.

Outlook

The present work permitted to study the behavior of Zn-Mn coatings containing 17 wt.% during direct hot stamping. A further increase of the Mn content in the coating may delay the appearance of liquid phases in the coatings, thereby improving the anticorrosive properties of the final product. In addition, a reduction of the formation of cracks due to LME may be achieved thanks to an increase of the melting temperature of the alloys. The growth of Zn-Mn coatings with higher Mn contents may be achieved by the use of other baths and additives, such as PEG or sodium gluconate, or by the use of different electric parameters such as pulse plating or galvanostatic deposition. Further investigations are required to identify and understand the possible benefits of the use of Mn as alloying element for Zn and assess the suitability of Zn-Mn coatings to respond to the requirements of the hot stamping application.

A study of large-scale electroplating in different laboratory plating baths and parameters could be interesting to understand the heterogeneity of the properties of Zn-Mn coatings obtained in the present work and to possibly avoid it. The remarkable leveling effect of the substrate roughness by the Zn-Mn deposits may have induced heterogeneities in the distribution and the composition of phases formed during heat treatment due to a significant variation of the coating thickness. A more constant thickness of the coatings may be preferable for a better understanding of the behavior of the coatings at high temperature and is of great importance for future research works. In addition, the deposition of Zn-Mn layers with different experimental conditions, in other electrochemical cells or at the industrial scale could permit to avoid heterogeneities in the properties of the layers prior to and post to high temperature treatment. Furthermore, higher amounts of large-scale Zn-Mn-coated plates would be of interest to precise the results obtained and further study the behavior of the layers.

Additional investigations could also be focused on a more detailed study of the heat treatment behavior of Zn-Mn alloy coatings at temperatures comprised between 860 °C and 900 °C in order to further precise the suitability and the limits of the coatings for conventional austenitizing treatment. The use of industrial conditions in furnaces with controlled atmosphere and heating may reduce the heterogeneous effects of oxidation and evaporation observed in the present work at the laboratory scale. In fact, the achievement of a uniform temperature distribution during austenitizing is necessary to ensure a good

comprehension of high temperature and hot forming behaviors of Zn-Mn alloy coatings. In addition, hot forming operations under industrial conditions with roller furnace and optimized heating stages could permit to obtain blanks with homogeneous compositions and properties. Thereby, the susceptibility of Zn-Mn alloy layers to LME could be better assessed and limited.

In a similar way to the use of 0.2 wt.% Al in galvanized steel, the study of Zn-Mn alloy coatings with a low Mn content may permit to form a thin Mn oxide film on the top surface of the coating, possibly reducing the exposure of Zn to evaporation and oxidation and providing a better suitability for subsequent painting and joining processes compared to the Al_2O_3-containing surface of galvanized coatings. Finally, a further investigation track could be dedicated to the study of Zn-Mn-X ternary alloys. The use of an appropriate additional alloying element with high oxygen affinity may permit to reduce the loss of Mn by oxidation and thereby increase the melting temperature of the coating, beneficial for the reduction of the susceptibility of the coated products for LME.

8 Résumé et perspectives

Dans l'objectif de répondre aux exigences de plus en plus strictes en matière de sécurité routière, de protection de l'environnement et de réduction du poids des véhicules, les pièces embouties à chaud ont trouvé une place importante dans la carrosserie automobile, en particulier dans la structure de l'habitacle. Pour éviter les problèmes liés à l'exposition d'aciers nus aux environnements corrosifs, de nombreux systèmes de revêtements ont été développés, notamment les produits galvanisés ou aluminiés qui sont actuellement utilisés. L'intérêt des constructeurs automobiles pour un agrandissement du panel de produits disponibles pour l'application de l'emboutissage à chaud a récemment grandi dans l'espoir d'optimiser les procédés de fabrication et d'améliorer les performances des produits finaux. Cependant, les matériaux des revêtements nécessitent un profil complexe de propriétés, en grande partie à cause du traitement thermique d'austénitisation à des températures avoisinant les 900 °C afin d'obtenir les propriétés mécaniques désirées. Parmi les nombreuses solutions proposées par les sidérurgistes, les meilleures performances semblent être obtenues pour les aciers galvanisés grâce à la présence de protection cathodique de l'acier. Cependant, la méthode de fabrication de ces produits est plus coûteuse que d'autres solutions à cause de leur faible aptitude à la mise en forme à chaud.

Ce travail est dédié à l'étude de la compatibilité d'alliages Zn-Mn pour la mise en forme à chaud. Le comportement du système électrolytique de la déposition de ces alliages ainsi que les propriétés microstructurales, crystallographiques et anticorrosives de ces couches ont été examinés en détail. De plus, le comportement des couches à haute température et notamment la distribution des phases, l'oxydation et l'évaporation des couches a été étudié afin de déterminer les performances des matériaux sélectionnés. En outre, des essais d'emboutissage à chaud ont été effectués sur les revêtements afin de déterminer l'aptitude à la mise en forme des matériaux alternatifs comparé aux produits commerciaux et évaluer leur intérêt pour cette application.

Électrodéposition d'alliages Zn-Mn

Les alliages Zn-Mn ont été élaborés par voie électrolytique dans des bains à base chlorure. De nombreuses analyses électrochimiques et de caractérisation ont été menées afin de définir une composition de bain, des paramètres électriques et une procédure expérimentale de déposition optimaux. Les études CV et EQCM ont révélé que l'électrodéposition d'alliages Zn-Mn est sujette à une réaction d'évolution de l'hydrogène importante qui limite la quantité de Mn incorporée dans le revêtement. L'utilisation simultanée des additifs NH_4SCN et 4-HB dans le bain électrolytique a permis de faciliter la codéposition de Mn et d'obtenir de remarquables propriétés crystallographiques, microstructurales et un meilleur état de surface comparé aux couches élaborées en absence d'additifs. De plus, cette étude a permis de déterminer qu'un potentiel de déposition de -1.62 V et un ratio de concentration d'ions $[Mn^{2+}]/[Zn^{2+}]$ de 8 permettent d'obtenir des alliages Zn-Mn avec une haute teneur en Mn et une bonne reproductibilité. De nombreuses études de caractérisation ont été effectuées sur

les couches obtenues d'électrolytes avec et sans additifs afin de comprendre l'influence des conditions électrolytiques sur les propriétés des alliages Zn-Mn.

Composition chimique

L'utilisation simultanée des deux additifs NH_4SCN et 4-HB a permis d'augmenter la teneur de 11 % à 17 % en Mn dans les revêtements obtenus par électrodéposition. D'après les données reportées dans la littérature, ces deux additifs utilisés séparément conduisent à une augmentation de la teneur en Mn, ce qui suggère qu'un effet synergétique peut avoir eu lieu par la combinaison de ces derniers. Des analyses supplémentaires sont nécessaires pour mieux comprendre l'influence des additifs sur les conditions cinétiques du procédé d'élaboration par électrodéposition et sur les mécanismes de croissance des revêtements. D'après le diagramme de phases binaire des alliages Zn-Mn, une température de fusion d'environ 700 °C est obtenue dans ces conditions. Cette valeur est nettement supérieure à la température de fusion du zinc pur (419.6 °C), ce qui peut jouer un rôle important dans la réduction des mécanismes de LME et dans l'obtention de bonnes propriétés anticorrosives liées au retardement de la liquéfaction du revêtement pendant le traitement d'austénitisation. Des traces de sulfures ont été observées et peuvent être attribuées à l'utilisation de l'additif NH_4SCN.

Propriétés microstructurales

Les couches d'alliages de Zn-Mn déposées sans additifs comportent une forte rugosité et une morphologie dendritique non régulière. Au contraire, un état de surface remarquable sans caractéristiques géométriques définies avec une rugosité très faible de S_a = 76.46 nm est obtenu pour les alliages de Zn-Mn déposés en présence d'additifs. Un tel état de surface n'a pas été reporté dans la littérature et est vraisemblablement lié à la combinaison des additifs NH_4SCN et 4-HB qui sont connus de la littérature pour améliorer la qualité de surface d'alliages Zn-Mn lorsqu'ils sont utilisés séparément. De plus, cet état de surface peut être expliqué par la formation de grains très fins avec un diamètre de 268 nm observés par des analyses SEM-EBSD sur la surface du revêtement. Ces caractéristiques peuvent avoir une influence positive sur le comportement des revêtements à haute température pendant l'étape d'austénitisation et sur la protection contre la corrosion. Il est intéressant de remarquer que les revêtements obtenus permettent de niveler la rugosité de surface du substrat, ce qui, par conséquent, implique que l'épaisseur des couches varie considérablement. Des études de caractérisation en coupe ont permis d'observer une transition dans la microstructure du revêtement pendant l'élaboration avec, aux premiers instants de l'électrodéposition, une couche avec une structure très fine au contact avec le substrat et une grande quantité de porosités vraisemblablement induites par la réaction d'évolution de l'hydrogène. Après une certaine durée de déposition, une couche consistant de grains avec une microstructure colonnaire apparaît, ce qui indique une modification des mécanismes de croissance des revêtements, qui peut être expliquée par une évolution de l'énergie des grains pendant la déposition ou par un changement des conditions lors de la

déposition. La présence de ruptures de cette structure colonnaire sous forme de sous-couches avec une épaisseur de moins de 100 nm n'a pu être expliquée.

Structure crystallographique

Les études de caractérisations crystallographiques des alliages Zn-Mn électrodéposés ont montré que les revêtements élaborés en présence d'additifs sont constitués d'une phase unique ε_2–Zn-Mn HCP. Cette phase crystallographique est métastable et appartient au domaine de phases ε qui est thermodynamiquement stable entre 220 °C et 815 °C. Une très forte texture de fibre d'une intensité de 15 a pu être observée le long de la direction <110>, ce qui indique que les cristaux sont parfaitement orientés avec leur plan basal perpendiculaire à la surface. Ce résultat peut avoir une influence sur les performances des revêtements Zn-Mn, notamment sur le comportement thermique, sur les propriétés anticorrosives et sur l'aptitude à la mise en forme.

Propriétés anticorrosives

Les études de polarisations potentiodynamiques ont permis d'observer que les alliages Zn-Mn déposés en présence d'additifs comportent la meilleure résistance contre la corrosion comparé aux couches obtenues d'électrolytes sans additifs et à des couches de Zn pur avec une densité de courant de corrosion plus faible et une résistance à la polarisation plus forte. Ce résultat peut être associé à la plus forte teneur en Mn contenue dans le revêtement, à la présence d'une surface très lisse et à l'orientation préférentielle des cristaux qui peuvent réduire la vitesse de dissolution des alliages. Il est important de noter que la présence de Mn dans le revêtement n'est pas suffisante pour augmenter la protection contre la corrosion de couches de Zn. En effet, les résultats obtenus ont démontré que la densité de courant de corrosion des alliages Zn-Mn élaborés sans additifs et contenant 11 wt.% Mn est plus haute que celle de revêtements de Zn pur. Cette caractéristique peut être expliquée par l'état de surface de ces couches, en particulier par la présence d'une morphologie dendritique, d'une surface rugueuse et de la présence de porosités ouvertes. Une différence de 500 mV entre les potentiels des nouveaux revêtements et du substrat a été observée et indique que la couche confère une protection cathodique importante au substrat.

Comportement à haute température

Des études préliminaires effectuées à haute température dans un four sous air à 900 °C ont montré que la quasi-totalité du Manganese contenu dans les revêtements est perdue par oxydation. Par conséquent, la majorité des essais de traitements thermiques ont été effectués dans un four en présence d'une atmosphère protectrice sous Argon afin de réduire l'exposition des revêtements contre l'oxydation à haute température. Les plaques revêtues ont été chauffées dans le four réglé à une température fixe et ont été transférées dans les outils de presse après avoir atteint des températures comprises entre 300 °C et celles généralement utilisées dans les conditions industrielles d'austénitisation. Le but de cette étude à plusieurs températures est d'étudier les phénomènes de diffusion entre le substrat et le revêtement et de comprendre le comportement du système.

De nombreuses méthodes de caractérisation ont été utilisées pour déterminer l'influence du traitement thermique sur les propriétés microstructurales, crystallographiques et anticorrosives des revêtements. Les couches obtenues après chauffage à 300 °C se sont révélées être similaires aux couches initiales. À une température de 500 °C, une fine couche d'interdiffusion apparaît à l'interface entre le revêtement et le substrat. Un changement important de la microstructure du revêtement a été observé après avoir atteint une température de 700 °C avec la formation d'une couche d'interdiffusion compacte avec une épaisseur d'environ 5 µm. Il est important de noter que la partie inférieure des couches contient une teneur plus faible en Mn par rapport au reste du revêtement, probablement à cause de forts coefficients d'interdiffusion du Zn et du Fe. La structure colonnaire obtenue pour les couches initiales n'a pas été observée après traitement thermique à 700 °C. À la place, une microstructure hétérogène comportant de gros grains sans géométrie particulière et une forte densité de pores et de précipités aux joints de grains est formée dans la partie supérieure de la couche. Des études de microscopie à transmission ont permis de révéler que ces zones contiennent de fortes teneurs en S et en Mn, ce qui pourrait être expliqué par la présence de MnS détectée par diffraction des rayons X. Les zones riches en S observées à 700 °C ont migré vers la surface des revêtements lors du traitement thermique à de plus hautes températures. Malgré l'utilisation d'une atmosphère protectrice avec un faible taux de O_2 de moins de 1 % pendant le traitement thermique, une couche d'oxydes riche en Mn se forme à la surface des revêtements, en particulier dans le cas de températures supérieures à 700 °C. À 900 °C, différentes microstructures et distributions de phases ont été observées. La teneur restante en Mn dans les couches s'est vu varier, vraisemblablement dûe à l'exposition hétérogène des matériaux à l'oxydation. Il est important de noter que l'oxydation préférentielle du Mn permet en partie d'éviter la perte de Zn métallique, ce qui a pour effet d'augmenter la protection contre la corrosion. Les mesures de dissolutions galvanostatiques ont permis de vérifier la présence d'une microstructure hétérogène avec la présence de phases avec une teneur en Zn variable. Cette observation peut être expliquée par l'effet nivelant présenté par le revêtement qui induit une variation importante de l'épaisseur de la couche initiale. De plus, l'absence de phases riches en Zn pour les alliages Zn-Mn chauffés à 900 °C avec différents temps de chauffe renforce l'hypothèse de l'évaporation de phases riches en Zn à haute température en présence d'argon.

Les résultats obtenus dans le cadre de cette étude ont permis de constater que l'utilisation d'un four en présence de gaz inerte est nécessaire pour éviter la perte d'une grande partie du Mn du revêtement initial par oxydation à haute température et pour conserver une température de fusion de l'alliage suffisamment haute afin de réduire la fragilité du système au phénomène de fissuration par métaux liquides. De plus, étant donné que la perte de Mn par oxydation conduit à la formation d'une couche d'oxydes formée de fines particules à la surface des produits, il est probable qu'un traitement de surface soit exigé après le procédé d'emboutissage à chaud afin de conférer une bonne compatibilité à la peinture et à l'assemblage au produit. Cette exigence est susceptible d'augmenter les coûts de production comparé à des atmosphères oxydantes conventionnelles. En outre, la perte de Zn par

évaporation peut intervenir à haute température et affecter les propriétés anticorrosives des produits.

Mise en forme à chaud

Le comportement de plaques revêtues d'alliages de Zn-Mn pendant l'emboutissage à chaud direct a été étudié après chauffage à 860 °C dans un four chauffé à 920 °C en présence de gaz inerte. Des outils de presse avec des géométries permettant d'atteindre des amincissements de 20 % des plaques ont été conçus pour cette étude afin d'évaluer le comportement des produits standards et des nouveaux revêtements. Des essais préliminaires effectués sur des produits commerciaux ont permis d'observer que les outils de presse utilisés sont adaptés pour l'étude du phénomène de fissuration par métaux liquides dans le cas d'aciers galvanisés. Les résultats obtenus sur les plaques revêtues d'une couche d'alliage Zn-Mn ont révélé des fissures similaires à celles observées dans le cas des aciers galvanisés sur certaines zones des plaques présentant des phases riches en Zinc et une teneur faible en Mn, probablement dûe à l'oxydation préférentielle du Manganese. D'autres régions des grandes plaques ne comportent pas de fissures et sont constituées uniquement de phases riches en Fe et contenant une forte teneur en Mn d'environ 15 %. Une partie des phases riches en Zn a pu disparaître par évaporation, notamment à cause de l'utilisation de hautes températures et de gaz inerte.

Ces études ont permis d'observer que les alliages Zn-Mn chauffés à 860 °C en présence d'argon et emboutis à chaud subissent une oxydation hétérogène et préférentielle de Mn et une évaporation de phases riches en Zn à haute température, ce qui se traduit par des comportements différents en termes de mise en forme à chaud et de protection contre la corrosion. Il est important de noter que ces hétérogénéités ne sont pas causées par une variation de la composition initiale du revêtement mais plutôt par la forte variation de l'épaisseur de couche des revêtements initiaux, qui a pu induire une distribution hétérogène des phases formées dans la couche pendant le traitement thermique. De plus, l'oxydation et l'évaporation des matériaux à haute température de manière hétérogène peuvent expliquer ces résultats. En outre, il est probable qu'une distribution non-uniforme des températures pendant le traitement thermique a pu causer la formation de microstructures variables dans les couches.

Perspectives

Ce travail a permis d'étudier les conditions d'élaboration, les propriétés ainsi que la compatibilité pour l'application de l'emboutissage à chaud d'alliages Zn-Mn. Des revêtements contenant 17 % de Manganèse ont été obtenus et étudiés. Une piste intéressante consiste à augmenter la teneur en Mn dans les revêtements afin de retarder l'apparition de phases liquides à haute température et par conséquent de réduire l'apparition de fissuration par métaux liquides et d'améliorer l'aptitude à la mise en forme à chaud de par la hausse de la température de fusion des couches. De plus, les propriétés anticorrosives des alliages seraient ainsi améliorées. Des alliages Zn-Mn avec de plus fortes teneurs en Mn peuvent être obtenus en utilisant d'autres types de bains ou additifs tels que le PEG ou le

gluconate de sodium ou en utilisant différents paramètres électriques comme la méthode de déposition par pulses ou par déposition galvanostatique. D'autres études sont nécessaires pour mieux comprendre les avantages possibles de l'utilisation du Manganèse comme élément d'alliage pour le Zinc et évaluer la compatibilité des alliages Zn-Mn pour répondre aux exigences de l'application d'emboutissage à chaud. Les conditions expérimentales utilisées pour élaborer les alliages Zn-Mn restent à approfondir. En effet, l'utilisation d'autres cellules électrolytiques ou de différents paramètres de déposition serait intéressante pour mieux comprendre le caractère hétérogène des propriétés obtenues dans le cadre de ce travail sur des plaques à grandes dimensions et de les éviter. De plus, il se peut que la présence d'un effet nivelant obtenu avec les conditions choisies et par conséquent la variation importante de l'épaisseur de la couche ait engendré des hétérogénéités dans la distribution et la composition des phases formées après traitement thermique. C'est pourquoi il serait intéressant d'optimiser les conditions d'élaboration de ces alliages afin d'obtenir une épaisseur constante. En outre, un plus grand nombre de plaques revêtues pourrait permettre de préciser les résultats obtenus dans le cadre de ce travail, de mieux comprendre le comportement des nouveaux matériaux à haute température et d'évaluer leur aptitude à la mise en forme.

Il serait également important de conduire des études plus détaillées sur le comportement à haute température des alliages Zn-Mn à des températures supérieures à 860 °C afin de préciser la compatibilité et les limites des matériaux considérés pour cette application et de définir les paramètres optimaux pour obtenir les performances exigées. L'utilisation de conditions industrielles avec des atmosphères et des chauffages contrôlés pourrait réduire les effets hétérogènes liés à l'oxydation et à l'évaporation observés dans le cadre de ce travail à petite échelle. En effet, l'application d'une distribution de températures uniforme est nécessaire pour assurer une bonne compréhension du comportement des alliages Zn-Mn à haute température et pendant la mise en forme. De plus, des essais dans des conditions industrielles avec un four à rouleaux et différentes zones optimales de chauffage pourraient permettre d'obtenir des compositions et propriétés homogènes nécessaires à la bonne compréhension des phénomènes de fissuration par métaux liquides.

De la même manière que pour la formation d'une couche d'oxydes à la surface d'aciers galvanisés, l'étude d'alliages Zn-Mn avec une teneur en Mn faible pourrait permettre de former une fine couche d'oxydes à la surface du produit après traitement thermique. Cette couche permettrait de réduire l'exposition du Zn et du Mn à l'évaporation et à l'oxydation et pourrait présenter une bonne compatibilité avec les procédés de fabrication ultérieurs tels que la peinture et l'assemblage et, de ce fait, éviter l'étape de nettoyage des pièces après l'emboutissage à chaud. Enfin, une autre piste d'étude possible concerne l'utilisation d'alliages ternaires de type Zn-Mn-X avec X un élément d'alliage avec une affinité plus forte que celle de Zn et Mn et qui pourrait former une couche d'oxydes à la surface du revêtement et réduire l'exposition des matériaux à l'oxydation et l'évaporation. Ce concept permettrait de conserver une forte teneur en Mn dans les couches et donc une haute température de fusion et réduire les risques d'apparition de fissuration par métaux liquides.

Appendix

Appendix 1: Further protective coating systems

Al-Zn coatings

The hot-dip Al-Zn coating containing 55 wt.% Al, 43.4 wt.% Zn and 1.6 wt.% Si is generally available under the trade name Galvalume for appliance, construction or transportation applications [183]. Silicon is among other reasons added to the hot-dip bath to prevent a strong exothermic reaction between the steel substrate and the Al-Zn bath [62]. The study of the latter coating system for the hot stamping application was reported by Fan et al. [3]. The coating was stated to be first pre-conditioned by heat treatment at 550-730 °C for at least 9 min in order to stabilize the layer for subsequent heating for hot forming by increasing Fe content. A good paint adhesion was obtained and the phosphated and painted panels reportedly provided better corrosion resistance than hot stamped GA parts in cyclic corrosion test. Lee and De Cooman [184] investigated the microstructural evolution of the Al-Zn coating after heat treatment of the coating at temperatures between 600 and 900 °C in order to study its suitability for hot press forming. The coating consisted of a zinc-rich and a aluminium-rich layer prior to heat treatment. No change in the microstructure was observed up to 600 °C, whereas various interdiffusion layers appeared at temperatures of at least 700 °C, essentially due to Fe diffusion. At 900 °C, a zinc oxide layer and multiple voids related to zinc-rich phases appeared in the coating. A preferential formation of Fe-Al intermetallic compounds compared to Zn-Fe phases was reported to occur. Cracks formed in the coating, reportedly due to a crystallographic transformation on the steel surface, causing a volume expansion and a sufficient stress for inducing localized LME. No cracks propagated into the steel matrix. Lee et al. [185] reported that the heat treated Al-Zn coating was not susceptible to LME, although the coating contained a large volume fraction of liquid Zn at grain boundaries in the diffusion layer at the hot forming temperature. The corrosion potential of the heat treated coating was found to be similar to the corrosion potential of an as-deposited Zn coating due to the presence of isolated islands of pure metallic Zn [185]. This product is currently not commercially available for the hot stamping application and may find interest of OEMs in the near future as an alternative coating system.

Aluminide coatings

Fan et al. reported that cracks formed in the aluminized coating during deformation at 800 °C consisted of two areas with different characteristic fracture morphologies, namely the upper part of the coating was found to crack in a brittle manner and the lower part had a ductile fracture appearance [80]. The cracks reportedly initiate in the upper layer during plastic deformation and propagate into the lower layer. The authors proposed that cracks could be prevented if the entire coating consisted of the lower layer, which is able to deform plastically with the steel substrate. A Fe content of at least 83 wt.% was reported to be required to obtain a more formable coating consisting of the Fe_3Al phase [80]. The authors

studied the process window of the aluminized coating for obtaining a formable coating [80, 186]. The use of a thinner coating and higher heating temperatures than those used for the conventional hot stamping process of aluminized parts permits to obtain ductile coatings and to prevent cracks or delamination of the layer during high temperature deformation. However, a decrease in the steel strength should be considered by the use of higher heating temperatures. Moreover, a decrease of anticorrosive properties may occur due to the high Fe content in the coating after hot stamping.

Hybrid coatings

Fan et al. [3] reported the investigation of hybrid coatings called x-tec, deposited by coil-coating and composed of organic and inorganic materials and suitable for both direct and indirect hot stamping processes [14]. Several generations were developed with the aim of consecutively improving performance of the products and processability during the subsequent manufacturing processes. The first generation of the x-tec coating was used to prevent oxidation of bare steel during heat treatment and to increase the die lifetime by acting as a lubricant [187]. The E-Coat adhesion was found to be limited and Resistance Spot Welding process could not be used due to a too high electric resistance, affecting the work welding current. As a result, the component had to undergo a surface cleaning treatment to remove the coating prior to joining and painting processes [14, 87]. The second generation of the x-tec product was developed for improving surface properties of the coating post to hot stamping process. A good compatibility of the coating with the subsequent painting and welding processes was reported, even without surface treatment. However, no cathodic corrosion protection was provided after hot stamping [87]. The third generation was reported by Fan et al. [3] to be suitable for RSW and painting and to provide good protection against oxidation and cathodic corrosion protection. This last generation coating is deposited by a liquid painting spray process, during which the paints are synthesized in a sol-gel reaction from organosilane precursors or organic monomers. After painting, a paint drying step is carried out in a hot air atmosphere, which results in the formation of inorganic-organic matrix containing Mg, Al particles, graphite and waxy components. The graphite was stated to improve the tribological properties during hot forming, while wax improves the tribological properties during cold pre-forming in the indirect hot stamping method. Moreover, Mg aims for an increase of cathodic corrosion protection of steel [3]. Lenze et al. reported the use of the x-tec coating product in the serial production of the Volkswagen Passat in 2007 with the product MBW-K 1500 + x-tec commercialised by ThyssenKrupp [187]. No further industrial use was reported.

Zn-Al-Mg coatings

Zn-Al-Mg coatings generally contain from 0.2 to 11.0 wt.% Aluminium and 0.1 to 3.0 wt.% Magnesium and are commercially available for cold forming [188]. Genderen et al. [70] investigated the properties of Zn-Al-Mg alloy coatings for the hot stamping application in terms of microcrack formation, friction coefficient, weldability and corrosion performance after direct hot stamping. Although no composition was directly provided by the authors, the

studies were carried out with the MagiZinc product (Tata Steel) which is not commercially available for hot stamping. A composition of 1.6 % Al and 1.6 % Mg was reported in the literature for this coating system [189]. Although LME was found to be prevented in the case of the Zn-Al-Mg alloy, microcracks similar to those of the GA coating were observed. The weldability of the developed coating was as good as or better than GA coating for dwell times shorter than 4 min. However, a significant increase of the contact resistance occurs for higher dwell times, probably due to the formation of an oxide layer mainly composed of Mn and Al oxides, which was stated to be linked to the higher oxygen affinity of Al and Mg compared with Zn. This preferential oxidation was reported to possibly prevent Zn from evaporation and oxidation during heat treatment. A removal of the oxide scale may be required to ensure a good compatibility with subsequent processes [70]. Corrosion protection was studied with 10 weeks of VDA 621-415 cyclic corrosion test. Penetration depth at scribes were much lower for the ZnAlMg coating compared to a GA coating with a similar heat treatment and the scribe delamination was slightly improved. The heat treatment was found to have a significant influence on the anticorrosive performance. No beneficial contribution of the use of Mg and Al was stated to be obtained after hot forming [190]. The use of an additional ceramic-based superficial layer with a thickness of 2-5 µm was found to reduce excessive oxidation of the Zn-Al-Mg coating during heat treatment and permitted to obtain an improvement of the weldability and of the anticorrosive properties in a salt spray test [191]. No industrial use of this coating system for the hot stamping application was reported in the literature data.

Dual layer Al-Si + Zn coatings

Lupp et al. investigated multi-layer coatings at ThyssenKrupp Steel Europe AG consisting of an Al-Si alloy containing 10 wt.% Si with an additional protective Zn-based thin film containing at least 99 wt.% Zn, the rest being Al and unavoidable impurities, with a thickness comprised between 2 and 10 µm [192]. The use of the aluminized layer between base material and the Zn-based layer aims for avoiding the LME mechanisms, while the use of the Zn-containing layer aims for an enhancement of corrosion protection by providing cathodic protection to steel. In fact, the OCP value of the dual layer coating was found to be lower than that of a galvanized coating after heat treatment. A corrosion behavior similar to that of pure Zn coatings was observed in salt spray test. The authors reported that the coating is suitable for both indirect and direct hot stamping processes and that risks of LME could be avoided. Fan et al. reported that liquid Zn-Al phases may be present at high temperature, leading to adhesion to press dies and to LME risks [3]. However, a decrease of Zn evaporation and of the adhesion of coating materials to press tools was achieved by the use of an additional protective layer consisting of metal phosphates [192, 193]. No industrial application was reported in the literature, most probably due to increased maintenance costs on the hot stamping lines induced by the adhesion of coating particles on the tools [194].

Dual layer Al-Si + ZnO coatings

Similarly to the previous bi-layer coating system, several works were dedicated to the study of thin ZnO layers deposited on aluminized steels for the hot stamping application. Maki et al. studied the effect of an additional ZnO layer on morphology, formability, phosphatability, weldability and on corrosion properties of the products [83]. The ZnO layer was deposited from a water solution of fine ZnO particles and dried. A coating weight of 1 g/m² corresponding to a layer of around 0.5 µm was used. The authors reported that the use of the oxide layer resulted in a reduction of the friction coefficient of about 30 % during hot stamping compared to the aluminized coating and permitted to avoid adherence of particles to the die, as confirmed by the study of Azushima et al. [195]. Moreover, paint adhesion and corrosion resistance of the conventional aluminized product could be improved by the use of the additional layer, due to the possibility of depositing phosphate crystals on the coating surface before cataphoresis painting [83, 196]. An increase of the ZnO layer weight resulted in an increase of the weight of the phosphate treatment film along with a reduction of cosmetic corrosion on painted panels after 360 cycles of JASO M-609 cyclic corrosion test. The spot weldability of the bi-layer coating was stated to be similar to that of a conventional aluminized product [83]. A surface density of up to 7 g/m² was stated to provide best weldability and paint adhesion [196]. This coating system is currently under development and may find a commercial application in the near future.

Post-process coating

An alternative manufacturing route for press-hardened body parts is to carry out hot forming on bare steel with a subsequent surface treatment to remove oxide scale and to deposit protective coatings on press-hardened components by electrodeposition or by hot-dipping. This post-process coating method permits to avoid heat treatment of the coatings during hot stamping and to increase performance of the coated components. Fan et al. [3] reported that hydrogen uptake can occur during electrodeposition, for instance in the case of Zn coatings from aqueous electrolytes, and may induce risks of hydrogen embrittlement of the martensitic steel and lead to delayed fracture of the components.

Merklinger et al. investigated the hot-dipping process of zinc alloy coatings on 22MnB5 parts after press-hardening and surface cleaning [197]. The authors studied the mechanical, microstructural and anticorrosion properties of coated parts after annealing in a galvanizing bath with a constant duration and various temperatures. A molten bath of a Zn-Al-Mg alloy was used with the aim of reducing the melting temperature of the bath down to 350 °C and possibly reduce the tempering effect induced on the hardened steel substrate. A bath temperature of 450 °C resulted in a reduction of the steel tensile strength from 1650 to 950 MPa while temperatures of 350 °C and 375 °C permitted to achieve 1300 MPa. It should be noted that temperatures comprised between 450 °C and 620 °C are mainly used for conventional hot dip galvanized baths. The electrochemical potential of the alternative zinc alloy was found to be similar to that of a pure Zn coating. However, the authors

reported an influence of the melting bath composition and temperature on the coating thickness, microstructure and the phases [198, 199].

Although this process permits to increase corrosion protection of body components including on cut-edges that are not protected on conventional coil-coated products, additional costs are induced compared to standard hot stamped parts from coil-coating, due to the discontinuous deposition of coatings on individual body parts, which necessitate specific equipments. In addition, it may be presumed that this process has an influence on the dimensional accuracy of the components due to a possible release of stresses during annealing.

Appendix 2: Preliminary heat treatment studies of Zn-Mn coatings in air

In order to evaluate the behavior of Zn-Mn coatings during high temperature treatment, preliminary studies were carried out in a furnace under air. Coated specimens were cut out of large-scale plates and heat treated for 120 s in a furnace heated at 915 °C and subsequently cooled down in air. Representative pictures of the surface appearance of the coatings are presented in Figure 110. A brownish layer was formed on the surface of the coating, with the presence of blisters, presumably due to a low adhesion with the underlying materials during heat treatment.

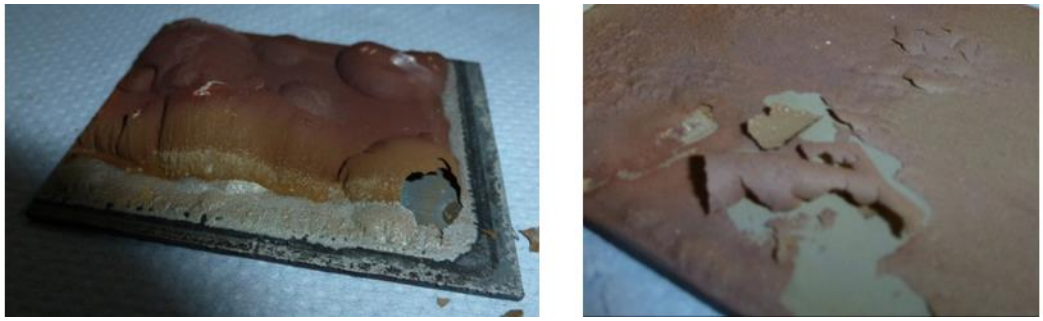

Figure 110: Surface appearance of Zn-Mn coatings heat treated at 915 °C for a duration of 120 s and cooled down under air (preliminary study); presence of a brownish superficial layer.

In order to determine the origin of the formation of the above-mentioned layer and determine its composition, Raman spectroscopy analyses were carried out on the brownish powder formed on Zn-Mn-coated specimens heat treated in a furnace at 915 °C for 120 s and cooled in press tools. The results are presented in Figure 111. Several Raman modes can be observed on the spectrum. Peaks formed at 292, 322, 377 and 667 cm^{-1} were found to be similar to those reported in the literature data for hausmannite Mn_3O_4 [200-203]. The peak visible at 204 cm^{-1} was stated by Bouchard et al. to be associated to ZnO [204]. The same authors reported the presence of two peaks at 330 cm^{-1} and 380 cm^{-1}, which could be included with the peaks associated to Mn_3O_4 and observed at 322 cm^{-1} and 377 cm^{-1}, respectively, as confirmed by the work of Gandhi et al. [205]. The intense peak located at 435 cm^{-1} can be attributed to one of the fundamental optical modes of ZnO [204, 206]. It should be noted that a low and broad peak appears at 520-560 cm^{-1}. Values of 544, 537 and 527 cm^{-1} corresponding to MnO [200] and a peak at 582 cm^{-1} related to ZnO [204] could be associated to the signals observed.

The major conclusion of this study is that Zn-Mn coatings, in particular Mn, oxidize during high temperature processes. Several oxides such as MnO, ZnO and Mn_3O_4 were found to form on the surface of the coatings.

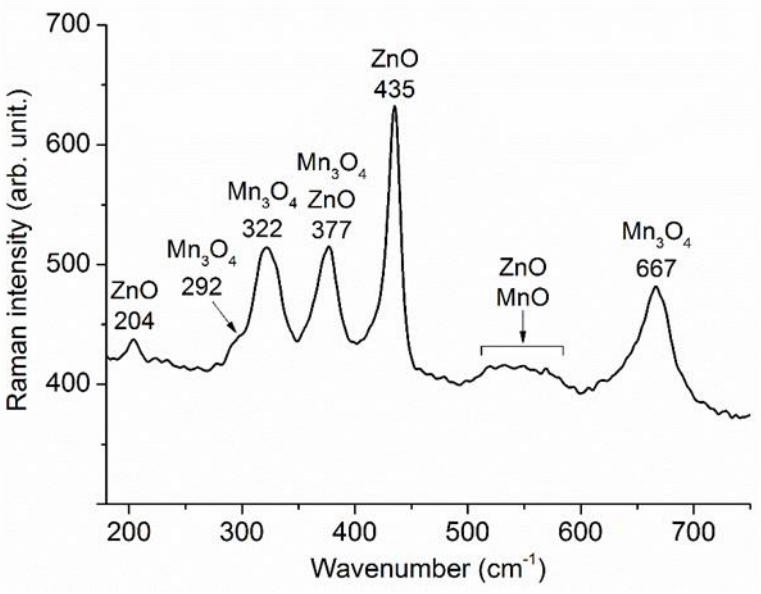

Figure 111: Raman spectrum of loose particles formed on Zn-Mn coatings during heat treatment recorded using a λ = 785 nm laser line.

Appendix 3: Zn-Mn-Fe phase diagrams

Table 25: Composition of Layer 2 (Figure 71 b) and Table 15) formed in a Zn-Mn coating heat treated to 500 °C in a furnace heated at 920 °C in presence of argon, calculated in weight and atomic percent.

Unit	Zn content	Mn content	Fe content
wt.%	78.2	5.7	16.1
at.%	75.3	6.5	18.2

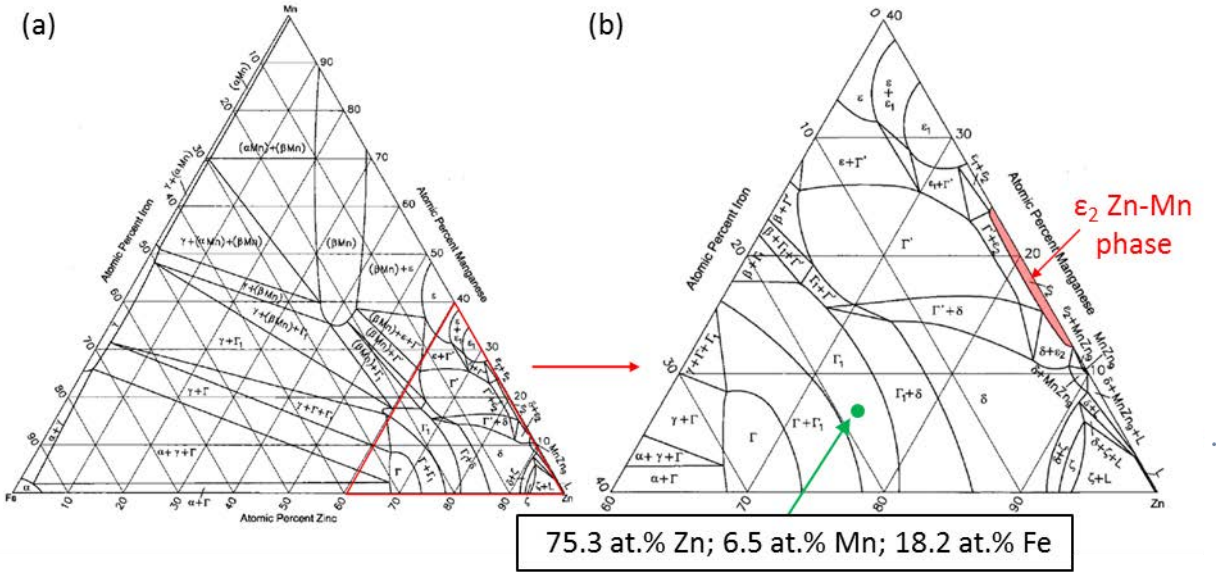

Figure 112: Experimental Zn-Mn-Fe ternary phase diagram at a temperature of 450 °C (a); (b): zoom of the Zn-rich region of diagram (a) with the position of the ε_2-Zn-Mn phase field and of the composition of Layer 2 (Figure 71 b)) and Table 15) formed in a Zn-Mn coating heat treated to 500 °C in a furnace heated at 920 °C in presence of argon (green dot) [108].

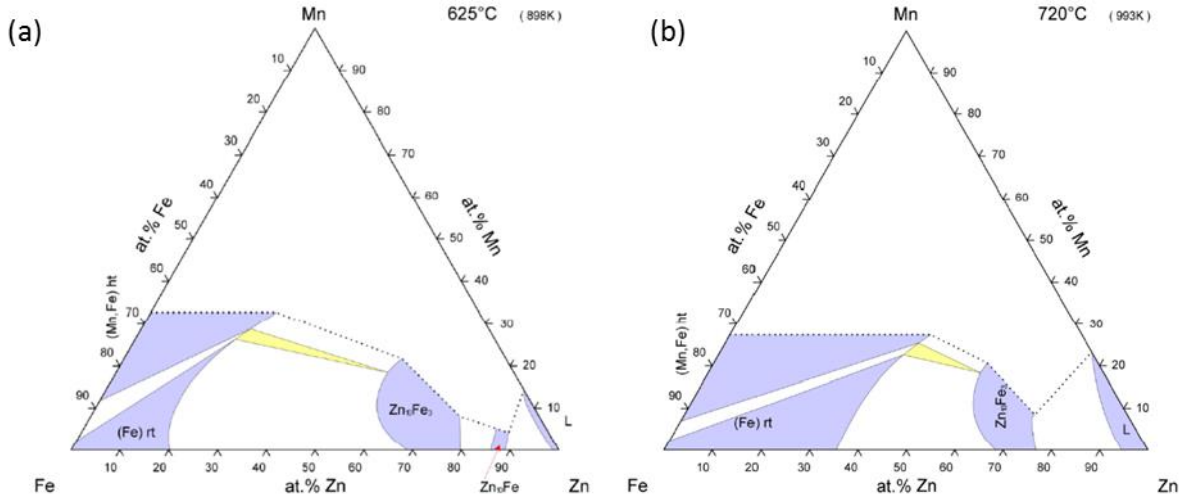

Figure 113: Experimental Zn-Mn-Fe ternary phase diagrams at temperatures of 625 °C and 720 °C [109].

Appendix 4: Ellingham diagram

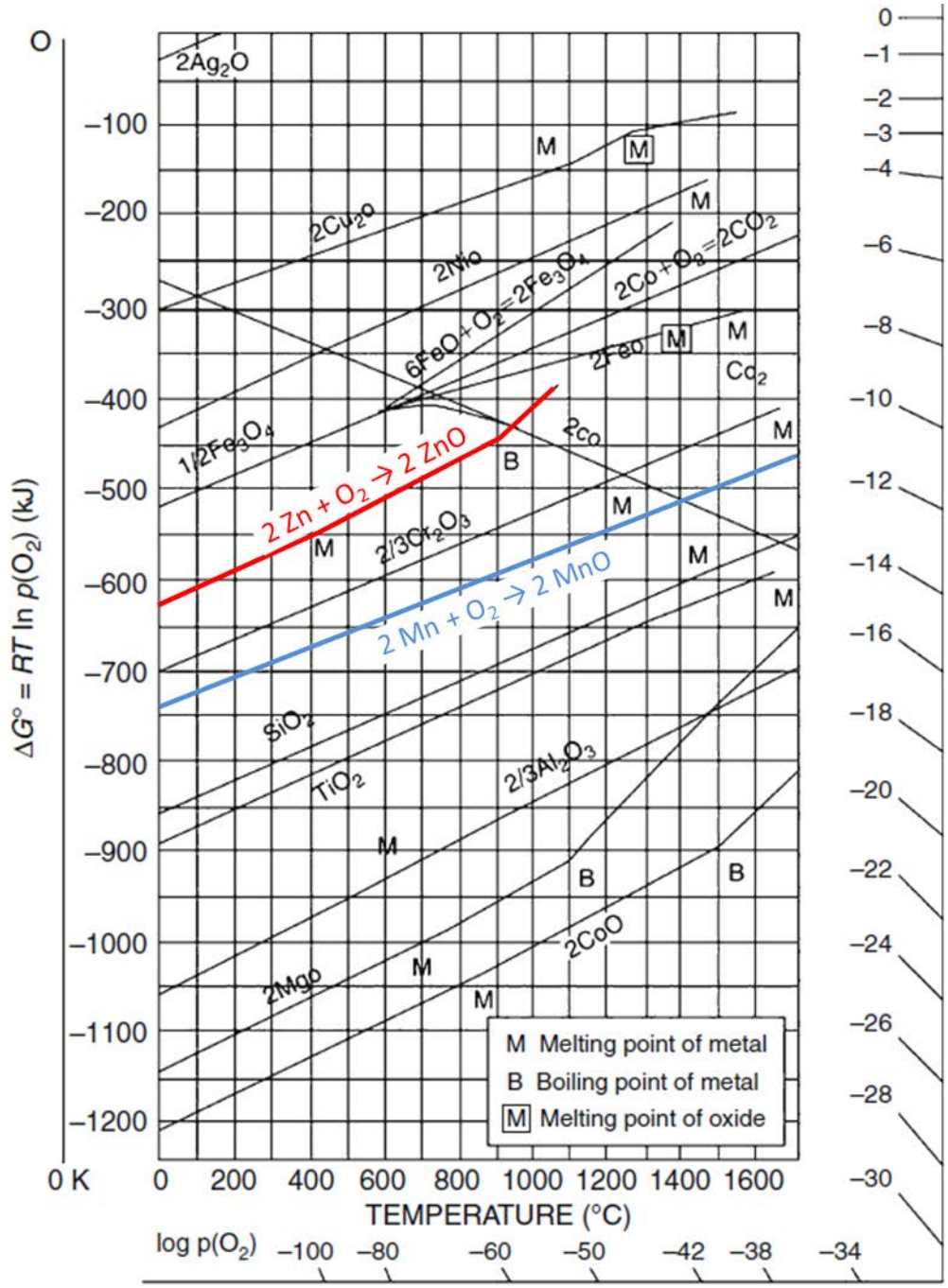

Figure 114: Evolution of standard free energy of the reaction of formation of common oxides in dependency of temperature (Ellingham diagram); Gibbs energy of ZnO (red line) and MnO oxides formation (blue line); from [207].

Appendix 5: Comparative AAS and SEM-EDS studies

Table 26: Comparative study of the composition of Zn-Mn coatings deposited from electrolytes in presence of additives by means of AAS and SEM-EDS analyses; SEM-EDS mean values obtained on the basis of sets of 9 measurements on the surface of the coatings.

	Mn content (wt.%)	Zn content (wt.%)
Specimen 1		
AAS analyses	22.4	77.6
SEM-EDS analyses	22.4 ± 1.4	77.6 ± 1.4
Specimen 2		
AAS analyses	21.9 ± 1.1	78.1 ± 1.1
SEM-EDS analyses	22.2	77.8

Bibliography

1. WorldAutoSteel, *Advanced High-Strength Steels Application Guidelines Version 5.0*, S. Keeler and M. Kimchi, Editors. 05/2014.
2. Feuser, P., *Ein Ansatz zur Herstellung von pressgehärteten Karosseriekomponenten mit maßgeschneiderten mechanischen Eigenschaften: Temperierte Umformwerkzeuge. Prozessfenster, Prozesssimulation und funktionale Untersuchung*. 2012, Friedrich-Alexander-Universität Erlangen-Nürnberg: Erlangen. p. 195.
3. Fan, D.W. and B.C. De Cooman, *State-of-the-Knowledge on Coating Systems for Hot Stamped Parts.* Steel Research International, 2012. **83**(5): p. 412-433.
4. Schupfer, M. and K. Steinhoff, *Market Development and Technological Perspectives in Press Hardened of UHSS*, in *3rd International Conference on Hot Sheet Metal Forming of High-Performance Steel*, M. Oldenburg, K. Steinhoff, and B. Prakash, Editors. 2011. p. 271-281.
5. Todzy, T., *Prozessfenster beim Presshärten bei schneller Erwärmung von Stahlplatinen mit Aluminium-Silizium-Beschichtung*. Forschungsberichte des Lehrstuhls für Umformtechnik. 2016: Shaker. 200.
6. Steinhoff, K., et al. *Marktentwicklung und Technologietrends in der Warmumformung von höchstfesten Vergütungsstählen*. in *7. Erlanger Workshop Warmblechumformung*. 2012. Erlangen, Germany.
7. Skrikerud, M. and J. Friberg. *Press Hardening, Process Design and Tool Systems*. in *4th International Conference on Hot Sheet Metal Forming of High-Performance Steel*. 2013. Luleå, Sweden.
8. *ThyssenKrupp Steel Europe - Warmumformung im Automobilbau*. Die Bibliothek der Technik (BT), ed. S.V. onpact. 2012: Verlag Moderne Industrie. 84.
9. Lee, C.W., et al., *Liquid-Metal-Induced Embrittlement of Zn-Coated Hot Stamping Steel.* Metallurgical and Materials Transactions A, 2012. **43**(13): p. 5122-5127.
10. Naganathan, A. and L. Penter, *Hot Stamping*, in *Sheet Metal Forming: Processes and Applications*, T. Altan and A.E. Tekkaya, Editors. 2012, ASM International. p. 133-156.
11. Fan, D.W., H.S. Kim, and B.C. De Cooman, *A Review of the Physical Metallurgy related to the Hot Press Forming of Advanced High Strength Steel.* Steel Research Int., 2009. **80**(No. 3): p. 241-248.
12. *Manufacturing a hardened steel article*, N.J. AB, Editor. 1977: Lulea, Sweden.
13. Behrens, B.A., *Hot Stamping*, in *CIRP Encyclopedia of Production Engineering*, C.I.R.P, L. Laperrière, and G. Reinhart, Editors. 2013, Springer Berlin Heidelberg: Berlin, Heidelberg. p. 1-7.
14. Karbasian, H. and A.E. Tekkaya, *A review on hot stamping.* Journal of Materials Processing Technology, 2010. **210**(15): p. 2103-2118.
15. Lagneborg, R., *New steels and steel applications for vehicles.* Materials and Design, 1991. **12**(1): p. 3-14.
16. Jesner, G. and S. Gelder. *New High Performance Hot Work Tool Steel for Hot Stamping Applications*. in *4th International Conference on Hot Sheet Metal Forming of High-Performance Steel*. 2013. Luleå, Sweden.
17. Michalak, F., M. Hoefer, and M. Ebner. *Body-in-white of the New Mercedes-Benz S-Class*. in *EuroCarBody*. 2013. Bad Nauheim, Germany.
18. Wurth, P. and B. Aranha, *Arcelormittal: Worldwide Auto Steel Business*, Arcelormittal, Editor. 2011: Paris. p. 40.

19. Spittel, M. and T. Spittel, *Steel symbol/number: 22MnB5/1.5528*, in *Metal Forming Data of Ferrous Alloys - deformation behaviour*, H. Warlimont, Editor. 2009, Springer Berlin Heidelberg: Berlin, Heidelberg. p. 930-935.
20. *22MnB5 - Boron-alloyed quenched and tempered steel*, S. Flachstahl, Editor. 01/2014.
21. Fan, D.W., et al., *Influence of Isothermal Deformation Conditions on The Mechanical Properties of 22MnB5 HPF Steel.* steel research international, 2010. **81**(4): p. 292-298.
22. ArcelorMittal, *Steels for hot stamping - Data sheet*. 04/2014.
23. Naderi, M., A. Saeed-Akbari, and W. Bleck, *The effects of non-isothermal deformation on martensitic transformation in 22MnB5 steel.* Materials Science and Engineering: A, 2008. **487**(1–2): p. 445-455.
24. Liu, W.J., *An Introduction to Advanced Hot-Formed Steel for Automobile.* Acta Metallurgica Sinica (English Letters), 2014. **27**(3): p. 373-382.
25. Somani, M.C., et al., *Dimensional Changes and Microstructural Evolution in a B-bearing Steel in the Simulated Forming and Quenching Process.* ISIJ International, 2001. **41**(4): p. 361-367.
26. Kuepferle, J., et al., *Thermo-physical properties of heat-treatable steels in the temperature range relevant for hot-stamping applications.* Journal of Materials Science, 2015. **50**(6): p. 2594-2604.
27. Merklein, M. and J. Lechler, *Investigation of the thermo-mechanical properties of hot stamping steels.* Journal of Materials Processing Technology, 2006. **177**: p. 452-455.
28. Merklein, M., J. Lechler, and M. Geiger, *Characterisation of the Flow Properties of the Quenchenable Ultra High Strength Steel 22MnB5.* CIRP Annals - Manufacturing Technology, 2006. **55**(1): p. 229-232.
29. Merklein, M., J. Lechler, and T. Stoehr. *Characterization of Tribological and Thermal Properties of Metallic Coatings for Hot Stamping Boron-Manganese Steels*. in *7th International Conference "THE" Coatings in Manufacturing Engineering*. 2008. Chalkidiki, Greece.
30. Brosius, A., et al. *Modellierung und Simulation der Warmblechumformung: Aktueller Stand und zukünftiger Forschungsbedarf*. in *Proceedings of the 2nd Erlanger Workshop Warmblechumformung*. 2007. Erlangen, Germany: Meisenbach Bamberg.
31. Merklein, M., J. Lechler, and T. Stoehr, *Investigations on the thermal behavior of ultra high strength boron manganese steels within hot stamping.* International Journal of Material Forming, 2009. **2**(S1): p. 259-262.
32. Geiger, M., M. Merklein, and J. Lechler, *Determination of tribological conditions within hot stamping.* Production Engineering, 2008. **2**(3): p. 269-276.
33. Siebert, P., M. Alsmann, and H.J. Watermeier. *Influence of Different Heating Technologies on the Coating Properties of Hot-Dip Aluminized 22MnB5*. in *3rd International Conference on Hot Sheet Metal Forming of High-Performance Steel*. 2011. Kassel, Germany.
34. Senuma, R. and Y. Takemoto. *Effect of Rapid Heating on Evolution of Microstructures and Coating Layers in Hot Stamping Processes*. in *3rd International Conference on Hot Sheet Metal Forming of High-Performance Steel*. 2011. Kassel, Germany.
35. Karbasian, H., et al., *Einfluss der Prozessführung auf die Eigenschaften pressgehärteter Bauteile*, in *Tagungsband zum 5. Erlanger Workshop Warmblechumformung*, M. Merklein, Editor. 2010, Meisenbach-Verlag Bamberg 2010: Erlangen, Germany. p. 103-118.
36. Karbasian, H., A. Brosius, and A.E. Tekkaya. *Experimentelle und numerische Untersuchung der prozessabhängigen Eigenschaften pressgehärteter Bauteile*. in

Tagungsband zum 4. Erlanger Workshop Warmblechumformung. 2009. Erlangen, Germany: Meisenbach Bamberg.

37. Dosdat, L., Petitjean, J, Vietoris, T, Clauzeau, O, *Corrosion Resistance of Different Metallic Coatings on Press-Hardened Steels for Automotive.* Steel Research Int., 2011. **82**: p. 726-733.
38. Faderl, J. and K.M. Radlmayr, *Ultraform und Ultraform_PHS - Innovation made by Voestalpine*, in *1. Erlanger Workshop Warmblechumformung 2006*, M. Geiger and M. Merklein, Editors. 2006, Meisenbach Bamberg 2006: Erlangen, Germany. p. 130-149.
39. Ademaj, A., U. Weidig, and K. Steinhoff. *Phenomenological Thermo-Physical Approach on Process Monitoring in Hot Stamping of Coated Boron Steel*. in *4th International Conference on Hot Sheet Metal Forming of High-Performance Steel*. 2013. Luleå, Sweden.
40. Kojima, N., et al. *Metallurgical Behaviour of Uncoated and Galvannealed Boron Steels in Hot Stamping Process*. in *3rd International Conference on Hot Sheet Metal Forming of High-Performance Steel*. 2011. Kassel, Germany.
41. Schrenk, M., et al. *Oxidation of Uncoated 22MnB5 Steel Grades for Hot Stamping Applications*. in *4th International Conference on Hot Sheet Metal Forming of High-Performance Steel*. 2013. Luleå, Sweden.
42. Mori, K. and D. Ito, *Prevention of oxidation in hot stamping of quenchable steel sheet by oxidation preventive oil.* CIRP Annals - Manufacturing Technology, 2009. **58**(1): p. 267-270.
43. Close, D., et al., *Challenges in Corrosion Protection for Press-Hardened Steels*, in *Tagungsband zum 9. Erlanger Workshop Warmblechumformung*. 2014: Erlangen, Germany. p. 31-52.
44. Lefèvre, B., *Corrosion des aciers revetus de zinc dans les zones confinées des carrosseries automobiles*. 2004, Chimie ParisTech.
45. A/SP, *A Guide To Corrosion Protection - An analysis of corrosion-related issues for passenger car and light truck underbody structural components*. 1999.
46. Amirudin, A. and D. Thierry, *Corrosion mechanisms of phosphated zinc layers on steel as substrates for automotive coatings.* Progress in Organic Coatings, 1996. **28**(1): p. 59-75.
47. Autengruber, R., G. Luckeneder, and A.W. Hassel, *Corrosion of press-hardened galvanized steel.* Corrosion Science, 2012. **63**: p. 12-19.
48. Allély, C., J. Petitjean, and T. Vietoris. *Corrosion Resistance of Zinc Based and Aluminized Coatings on Press-Hardened Steels for Automotive*. in *3rd International Conference on Hot Sheet Metal Forming of High Performance Steel*. 2011. Kassel, Germany: Verlag Wissenschaftliche Scripten.
49. Köyer, M., et al. *Zinc Alloy Coating for the Hot Forming Process*. in *4th International Conference on Hot Sheet Metal Forming of High-Performance Steel*. 2013. Luleå, Sweden.
50. LeBozec, N., N. Blandin, and D. Thierry, *Accelerated corrosion tests in the automotive industry: A comparison of the performance towards cosmetic corrosion.* Materials and Corrosion, 2008. **59**(11): p. 889-894.
51. Singh, J.P., J.N. Hall, and J.J. Coryell. *Challenges with Zinc-Coated Press Hardened Steels*. in *4th International Conference on Hot Sheet Metal Forming of High-Performance Steel*. 2013. Luleå, Sweden.
52. Miyoshi, Y., *Evaluation Technology of Corrosion Behavior for Automotive Steel Sheet.* ISIJ International, 1991. **3**(2): p. 122-133.

53. Fleischanderl, M., et al., *Method for producing a hardened steel part*. 2007.
54. Luckeneder, G., et al. *Einflussfaktoren auf die Korrosionsschutzleistung von pressgehärteten Stahlwerkstoffen*. in *3-Länder Korrosionstagung*. 2014. Linz, Austria.
55. Schwinghammer, H., et al., *Zinc Coated Press Hardening Steel for the Direct Process*, in *4th International Conference on Hot Sheet Metal Forming of High-Performance Steel*, M. Oldenburg, B. Prakash, and K. Steinhoff, Editors. 2013, Verlag Wissenschaftliche Scripten: Luleå, Sweden.
56. Allély, C., et al., *Anticorrosion mechanisms of aluminized steel for hot stamping.* Surface and Coatings Technology, 2014. **238**: p. 188-196.
57. Maki, J., et al. *Effect of Heating Condition and Hot Forming on Corrosion Resistance of Hot Stamped Aluminized Steels*. in *3rd International Conference on Hot Sheet Metal Forming of High-Performance Steel*. 2011. Kassel, Germany.
58. Maki, J. and M. Suehiro, *Effects of heating atmosphere and steel chemistry on delamination of the surface layer of aluminized steel.* Surface and Coatings Technology, 2012. **206**(19-20): p. 3869-3874.
59. Autengruber, R., et al., *Surface and Coating Analysis of Press-Hardened Hot-Dip Galvanized Steel Sheet.* Steel Research In., 2012. **83**: p. 1005-1011.
60. Fleischanderl, M., et al., *Method for producing a hardened steel part*. 2007.
61. Shibli, S.M.A., B.N. Meena, and R. Remya, *A review on recent approaches in the field of hot dip zinc galvanizing process.* Surface and Coatings Technology, 2015. **262**: p. 210-215.
62. Marder, A.R., *The metallurgy of zinc-coated steel.* Progress in Materials Science, 2000. **45**(3): p. 191-271.
63. Huh, Y., et al. *Characterization of the Galvanizing Behaviors Depending on Annealing Conditions in 22MnB5 Steel and the High Temperature Phase Evolution of Zn Coatings with Hot Press Forming*. in *9th International Conference on Zinc and Zinc Alloy Coated Steel Sheet*. 2013. Beijing, China.
64. Kurz, T., et al. *Trends and Developments in the Usability and Production of Press-Hardened Components with Cathodic Corrosion Protection*. in *3rd International Conference on Hot Sheet Metal Forming of High-Performance Steel*. 2011. Kassel, Germany.
65. Zhu, G., et al. *Effect of Heating Process on Microstructure of Press Hardened Steel Zinc Coating*. in *9th International Conference on Zinc and Zinc Alloy Coated Steel Sheet*. 2013. Beijing, China.
66. Kim, S., et al. *Cracking Issues of Zn Coated Press Hardening Steel in Direct Hot Press Forming*. in *4th International Conference on Hot Sheet Metal Forming of High-Performance Steel*. 2013. Luleå, Sweden.
67. Su, Y.M., *A determination of the rate of evaporation of zinc at atmospheric pressure*, in *Scholars' Mine*. 1957, Missouri University of Science and Technology.
68. Drillet, P., et al., *Study of cracks propagation inside the steel on press hardened steel zinc based coatings*, in *8th International conference on zinc and zinc alloy coated steel sheet*. 2011: Genova, Italy.
69. Janik, V., et al., *Role of Heating Conditions on Microcrack Formation in Zinc Coated 22MnB5*, in *Materials Science & Technology Conference and Exhibition 2014* 2014, Materials Science and Technology (MS&T) Pittsburgh, USA.
70. Genderen, M.J.V., et al. *Zinc-Coated Boron Steel, ZnX: Direct Hot Forming for Automotive Applications*. in *3rd International Conference on Hot Sheet Metal Forming of High-Performance Steel*. 2011. Kassel, Germany.

71. Hensen, G., et al. *Developing Zinc Coated Boron Steel: Balancing Microcrack Performance and Corrosion Protection*. in *4th International Conference on Hot Sheet Metal Forming of High-Performance Steel*. 2013. Luleå, Sweden.
72. Li, J., et al. *Study of Crack Generation and Propagation Mechanism Inside Zinc-coated Press-Hardened Steel*. in *9th International Conference on Zinc and Zinc Alloy Coated Steel Sheet*. 2013. Beijing, China.
73. Takahashi, M., et al. *Liquid Metal Embrittlement Behavior and Bendability of Hot V-Bent Galvannealed Boron Steel*. in *4th International Conference on Hot Sheet Metal Forming of High-Performance Steel*. 2013. Luleå, Sweden.
74. Yoshikawa, Y.S.M.I.L., et al., *Hot press formed product and method for production thereof*. 2009, Google Patents.
75. Knezar, K., et al. *Formhärten von feuerverzinktem 22MnB5*. in *Proceedings of the 2nd Erlanger Workshop Warmblechumformung*. 2007. Erlangen, Germany: Meisenbach Bamberg.
76. Windmann, M., A. Röttger, and W. Theisen, *Formation of intermetallic phases in Al-coated hot-stamped 22MnB5 sheets in terms of coating thickness and Si content.* Surface and Coatings Technology, 2014. **246**: p. 17-25.
77. Fan, D.W., et al., *Coating Degradation in Hot Press Forming.* ISIJ International, 2010. **50**(4): p. 561-568.
78. Ghiotti, A., S. Bruschi, and F. Borsetto, *Tribological characteristics of high strength steel sheets under hot stamping conditions.* Journal of Materials Processing Technology, 2011. **211**(11): p. 1694-1700.
79. Windmann, M., A. Röttger, and W. Theisen, *Phase formation at the interface between a boron alloyed steel substrate and an Al-rich coating.* Surface and Coatings Technology, 2013. **226**: p. 130-139.
80. Fan, D.W. and B.C.D. Cooman, *Formation of an Aluminide Coating on Hot Stamped Steel.* ISIJ International, 2010. **50**(11): p. 1713-1718.
81. Zhong-Xiang, G., Kai, Wang, Yi-Sheng, Zhang, Bin, Zhu, *Cracking and interfacial debonding of the Al–Si coating in hot stamping of pre-coated boron steel.* Applied Surface Science, 2014. **316**: p. 595-603.
82. Suehiro, M., et al., *Properties of Aluminum-Coated Steels for Hot-Forming*, in *Nippon Steel Technical Report*. 2003. p. 16-21.
83. Maki, J., et al., *Effect of ZnO Coating on the Performance of Alu-Minized Steels after Hot Stamping*, in *4th International Conference on Hot Sheet Metal Forming of High-Performance Steel*, M. Oldenburg, B. Prakash, and K. Steinhoff, Editors. 2013, Verlag Wissenschaftliche Scripten: Luleå, Sweden. p. 451-458.
84. Zhang, J., S. Jiang, and Q.-F. Zhang. *Effect of Temperature on Microstructure and Formability of Press Hardened Steel Al-Si Coating*. in *9th International Conference on Zinc and Zinc Alloy Coated Steel Sheet*. 2013. Beijing, China.
85. Laurent, J.-P., et al., *Tôle d'acier laminée à chaud et à froid revêtue et présentant une très haute résistance après traitement thermique*. 2000.
86. Voestalpine. *phs-directform: product information*. 2016 [cited 2016; Available from: http://www.voestalpine.com/thinkzinc/en/phs-directform-R.
87. Köyer, M., et al., *Oberflächenveredelungen für die Warmumformung - Serienprodukte und Neuentwicklungen*, in *Tagungsband zum 5. Erlanger Workshop Warmblechumformung*, M. Merklein, Editor. 2010, Meisenbach-Verlag Bamberg 2010: Erlangen, Germany. p. 15-28.

88. Kondratiuk, J., et al., *Zinc coatings for hot sheet metal forming: Comparison of phase evolution and microstructure during heat treatment.* Surface and Coatings Technology, 2011. **205**(17-18): p. 4141-4153.
89. Kuhn, P., et al., *Method for producing a steel component provided with a metal coating protecting agains corrosion and steel component*. 2011, ThyssenKrupp Steel Europe AG.
90. Kuhn, P., et al., *Verfahren zum Herstellen eines mit einem metallischen, vor Korrosion schützenden Überzug versehenen Stahlbauteils und Stahlbauteil*. 2012, ThyssenKrupp Steel Europe AG.
91. Kondratiuk, J. and P. Kuhn, *Tribological investigation on friction and wear behaviour of coatings for hot sheet metal forming.* Wear, 2011. **270**(11-12): p. 839-849.
92. Reini, L.A., M. Choi, and A. Wendorf. *Development of Zn-Coated PHS Components for Automotive Applications*. in *4th International Conference on Hot Sheet Metal Forming of High-Performance Steel*. 2013. Luleå, Sweden: Verlag Wissenschaftliche Scripten.
93. Kasprzak, K.S., F.W. Sunderman Jr, and K. Salnikow, *Nickel carcinogenesis.* Mutation Research/Fundamental and Molecular Mechanisms of Mutagenesis, 2003. **533**(1–2): p. 67-97.
94. Feuser, P., *Personal Communication*. 2016: Daimler AG, Sindelfingen, Germany.
95. Close, D., et al., *DE102014004652 (A1) - Bauteil, insbesondere Strukturbauteil für einen Kraftwagen, sowie Verfahren zum Herstellen eines solchen Bauteils*. 2015, Daimler AG.
96. Close, D., et al., *WO2015149918 (A1) - COMPONENT, PARTICULARLY A STRUCTURAL COMPONENT FOR A MOTOR VEHICLE, AND A METHOD FOR PRODUCING SUCH A COMPONENT*. 2015, Daimler AG.
97. Boshkov, N., et al., *Influence of the alloying component on the protective ability of some zinc galvanic coatings.* Electrochimica Acta, 2005. **51**(1): p. 77-84.
98. De Lima-Neto, P., et al., *Corrosion study of electrodeposited Zn and Zn-Co coatings in chloride medium.* Journal of the Brazilian Chemical Society, 2007. **18**: p. 1164-1175.
99. Close, D., et al., *DE102014004650 (A1) - Bauteil, insbesondere Strukturbauteil für einen Kraftwagen sowie Verfahren zum Herstellen eines Bauteils*. 2015, Daimler AG.
100. Close, D., et al., *DE102014004656 (A1) - Bauteil, insbeseondere Strukturbauteil für einen Kraftwagen sowie Verfahren zum Herstellen eines Bauteils*. 2015, Daimler AG.
101. Close, D., et al., *WO2015149901 (A1) - COMPONENT, PARTICULARLY A STRUCTURAL COMPONENT, FOR A MOTOR VEHICLE, AS WELL AS A METHOD FOR PRODUCING A COMPONENT*. 2015, Daimler AG.
102. Close, D., et al., *DE102014004657 (A1) - Bauteil, insbesondere Strukturbauteil, für einen Kraftwagen, sowie Verfahren zum Herstellen eines Bauteils*. 2015, Daimler AG.
103. Close, D., et al., *DE102014004651 (A1) - Bauteil, insbesondere Strukturbauteil für einen Kraftwagen sowie Verfahren zum Herstellen eines Bauteils*. 2015, Daimler AG.
104. Close, D., et al., *DE102014004649 (A1) - Bauteil, insbesondere Strukturbauteil für einen Kraftwagen sowie Verfahren zum Herstellen eines Bauteils*. 2015, Daimler AG.
105. Close, D., et al., *WO2015149900 (A1) - COMPONENT, PARTICULARLY A STRUCTURAL COMPONENT FOR A MOTOR VEHICLE, AND A METHOD FOR PRODUCING A COMPONENT*. 2015, Daimler AG.
106. Okamoto, H. and L.E. Tanner, *The Mn-Zn (Manganese-Zinc) System.* Bulletin of Alloy Phase Diagrams, 1990. **11**(No.4): p. 377-384.
107. Tsuchiya, Y., et al., *Structure of Electrodeposited Zn-Mn Alloy Coatings.* ISIJ International, 2000. **40**(No. 10): p. 1024-1028.

108. Raghavan, V., *Fe-Mn-Zn (Iron-Manganese-Zinc).* Journal of Phase Equilibria, 2003. **24**(6): p. 556-557.
109. Bhan, S., A. Lal, and S. Singh, *The Fe-Mn-Zn system (iron-manganese-zinc).* Journal of Phase Equilibria, 1991. **12**(6): p. 667-672.
110. Reumont, G., G. Dupont, and P. Perrot, *The Fe-Mn-Zn system at 450°C*, in *ASM Alloy Phase Diagrams Center*, P. Villars, Editor. 2012, ASM International: Materials Park, OH, USA.
111. Baumgart, H. and R. Sanders, *STEEL SHEET AND FORMED PART*, GM, Editor. 2014.
112. Zoestbergen, E., J. Van De Langkruis, and R. Bleeker, *Steel substrate provided with corrosion resistant coating with high melting temperature*, T.S.N.T. B.V., Editor. 2015.
113. Brandstätter, W., et al., *Method for producing a hardened profile part*. 2010, Voestalpine Stahl GmbH.
114. Ortiz, Z.I., et al., *Characterization of the corrosion products of electrodeposited Zn, Zn–Co and Zn–Mn alloys coatings.* Corrosion Science, 2009. **51**(11): p. 2703-2715.
115. Boshkov, N., S. Vitkova, and K. Petrov, *Corrosion Products of Zinc-Manganese Coatings: Part I - Investigations Using Microprobe Analysis and X-Ray Diffraction.* Metal Finishing, 2001. **99**(9): p. 56-60.
116. Boshkov, N., K. Petrov, and S. Vitkova, *Corrosion Products of Zinc-Manganese Coatings - Part III: Double-Protective Action of Manganese.* Metal Finishing, 2002. **100**(6): p. 98-102.
117. Boshkov, N., et al., *Galvanic alloys Zn–Mn—composition of the corrosion products and their protective ability in sulfate containing medium.* Surface and Coatings Technology, 2005. **194**(2-3): p. 276-282.
118. Bučko, M., et al., *Initial corrosion protection of Zn–Mn alloys electrodeposited from alkaline solution.* Corrosion Science, 2011. **53**(9): p. 2861-2871.
119. Boshkov, N., *Galvanic Zn–Mn alloys—electrodeposition, phase composition, corrosion behaviour and protective ability.* Surface and Coatings Technology, 2003. **172**(2-3): p. 217-226.
120. Savall, C., et al., *Morphological and structural characterisation of electrodeposited Zn–Mn alloys from acidic chloride bath.* Materials Science and Engineering: A, 2006. **430**(1-2): p. 165-171.
121. Bakhtiari, A., *Effects of a small addition of Mn on modifying the coating thickness, structure and corrosion resistance of hot-dip galvanized coatings.* Metallurgical and Materials Engineering, 2011. **18**: p. 1-7.
122. Zhang, B., et al., *Effects of a small addition of Mn on the corrosion behaviour of Zn in a mixed solution.* Electrochimica Acta, 2009. **54**(26): p. 6598-6608.
123. Tomić, M.V., et al., *Corrosion Stability of Electrochemically Deposited Zn-Mn Alloy Coatings.* Contemporary Materials, 2010. **1**(1): p. 87-93.
124. Müller, C., M. Sarret, and T. Andreu, *Electrodeposition of Zn-Mn Alloys at Low Current Densities.* Journal of The Electrochemical Society, 2002. **149**(11): p. C600.
125. Eyraud, M., et al., *Morphology and Composition of Electrodeposited Zinc-Manganese Alloys.* Plating and Surface Finishing, 1994. **82**: p. 63-70.
126. Crousier, J., F. Soto, and M. Eyraud, *Des alliages de zinc et de manganèse aptes au revêtement protecteur de plaques d'acier.* Matériaux & Techniques, 1999. **87**(n°3-4): p. 47-51.
127. Bučko, M., et al., *The influence of anion type in electrolyte on the properties of electrodeposited ZnMn alloy coatings.* Surface and Coatings Technology, 2013. **228**: p. 221-228.

128. Sylla, D., et al., *Electrodeposition of Zn–Mn alloys on steel using an alkaline pyrophosphate-based electrolytic bath.* Surface and Coatings Technology, 2005. **200**(7): p. 2137-2145.
129. Losey, M.W. and J.J. Kelly, *1.10 - Electrodeposition*, in *Comprehensive Microsystems*. 2008, Elsevier: Oxford. p. 271-292.
130. Thiery, L., G. Schiavon, and N. Pommier, *Acid dip for zinc-manganese alloy electrodeposition*. 2006, Coventya (Clichy, FR): United States.
131. Sylla, D., et al., *Electrodeposition of Zn–Mn alloys in acidic and alkaline baths. Influence of additives on the morphological and structural properties.* Journal of Applied Electrochemistry, 2005. **35**(11): p. 1133-1139.
132. Sylla, D., et al., *Electrodeposition of Zn–Mn alloys on steel from acidic Zn–Mn chloride solutions.* Thin Solid Films, 2003. **424**(2): p. 171-178.
133. Ganesan, S., G. Prabhu, and B.N. Popov, *Electrodeposition and characterization of Zn – Mn coatings for corrosion protection.* Surface and Coatings Technology, 2014. **238**: p. 143-151.
134. Díaz-Arista, P., et al., *Electrodeposition and characterization of Zn–Mn alloy coatings obtained from a chloride-based acidic bath containing ammonium thiocyanate as an additive.* Surface and Coatings Technology, 2009. **203**(9): p. 1167-1175.
135. Díaz-Arista, P. and G. Trejo, *RETRACTED: Electrodeposition and characterization of manganese coatings obtained from an acidic chloride bath containing ammonium thiocyanate as an additive.* Surface and Coatings Technology, 2006. **201**: p. 3359-3367.
136. Dietz, H., et al., *Influence of substituted benzaldehydes and their derivatives as inhibitors for hydrogen evolution in lead/acid batteries.* Journal of Power Sources, 1995. **53**(2): p. 359-365.
137. Bucko, M., U. Lacnjevac, and J. Bajat, *The influence of substituted aromatic aldehydes on the electrodeposition of Zn-Mn alloy.* Journal of the Serbian Chemical Society, 2013. **78**(10): p. 1569-1581.
138. Bučko, M., et al., *Electrodeposition of Zn–Mn alloys at high current densities from chloride electrolyte.* Journal of Solid State Electrochemistry, 2013. **17**(5): p. 1409-1419.
139. Paunovic, M. and M. Schlesinger, *Fundamentals of electrochemcial deposition - Second edition*. 2006: John Wiley & Sons, Inc. 388.
140. Geiger, M., M. Merklein, and C. Hoff, *Basic Investigations on the Hot Stamping Steel 22MnB5.* Advanced Materials Research, 2005. **6-8**: p. 795-804.
141. Sotto, F., *Électrocristallisation de revêtements zinc-manganèse: comportement à la corrosion*. 1998, Université de Provence - Aix-Marseille 1.
142. Marken, F., A. Neudeck, and A.M. Bond, *Cyclic Voltammetry*, in *Electroanalytical Methods: Guide to Experiments and Applications*, F. Scholz, et al., Editors. 2010, Springer Berlin Heidelberg: Berlin, Heidelberg. p. 57-106.
143. Bilal, S., *Cyclic Voltammetry*, in *Encyclopedia of Applied Electrochemistry*, G. Kreysa, K.-I. Ota, and R.F. Savinell, Editors. 2014, Springer New York: New York, NY. p. 285-289.
144. Broch, L., et al., *Real time in situ ellipsometric and gravimetriy monitoring for electrochmistry experiments.* Review of scientific instruments, 2007. **78**: p. 064101.
145. Suryanarayana, C. and M.G. Norton, *X-Rays and Diffraction*, in *X-Ray Diffraction: A Practical Approach*. 1998, Springer US: Boston, MA. p. 3-19.

146. Wang, G.-C. and T.-M. Lu, *X-Ray Diffraction*, in *RHEED Transmission Mode and Pole Figures: Thin Film and Nanostructure Texture Analysis*. 2014, Springer New York: New York, NY. p. 55-71.
147. Birkholz, M., *Thin Films Analysis by X-Ray Scattering - Principles of X-ray Diffraction*. 2006.
148. Jenkins, R., *X-ray Techniques: Overview.* Encyclopedia of Analytical Chemistry, 2006: p. 13269-13288.
149. Trampert, M., *Properties of Sputter Deposited Zinc and Zinc Alloy Coatings*. 2006, Universität des Saarlandes. p. 183.
150. Fundenberger, J.-J. and B. Beausir, *JTEX - Software for Texture Analysis*. 2015, Université de Lorraine - Metz: http://jtex-software.eu/.
151. Goldstein, J., et al., *Scanning Electron Microscopy and X-ray Microanalysis*. 2003. XIX, 689.
152. Reimer, L., *Scanning Electron Microscopy - Physics of Image Formation and Microanalysis*. Springer Series in Optical Sciences. Vol. 45. 1998: Springer-Verlag Berlin Heidelberg.
153. Piccolo, B. and R.T. O'Connor, *Atomic Absorption Spectroscopy.* Journal of the American Oil Chemists' Society. **45**(11): p. 789-792.
154. Bayol, E., K. Kayakirilmaz, and M. Erbil, *The inhibitive effect of hexamethylenetetramine on the acid corrosion of steel.* Materials Chemistry and Physics, 2007. **104**: p. 74-82.
155. Zinin, P. *Lecture 14 - Transmission Electron Microscope*. 2011 03/05/2016]; Available from: http://www.soest.hawaii.edu/HIGP/Faculty/sksharma/GG711/GG711Lec15TEM.pdf.
156. Maitland, T. and S. Sitzman, *Backscattering Detector and EBSD in Nanomaterials Characterization*, in *Scanning Microscopy for Nanotechnology - Techniques and Applications*, W. Zhou and Z.L. Wang, Editors. 2007, Springer New Yorek. p. 41-75.
157. Shimizu, K., et al., *Radiofrequency GDOES: a powerful technique for depth profiling analysis of thin films.* Surface and Interface Analysis, 2003. **35**(7): p. 564-574.
158. Standard, I., *ISO 14707:2015 - Surface chemical analysis - Glow Discharge Optical Emission Spectrometry (GD-OES) - Introduction to use*. 2015.
159. Galindo, R.E., et al., *Towards nanometric resolution in multilayer depth profiling: a comparative study of RBS, SIMS, XPS and GDOES.* Analytical and Bioanalytical Chemistry, 2010. **396**(8): p. 2725-2740.
160. Szymanski, H.A., *Raman Spectroscopy - Theory and Practice*. 1967.
161. AG, D., *DBL 4093 - Karosserieteile aus pressgehärteten Stahlblechen*, in *9.4 Galvanostatische Auflösung des ZnFe-Überzugs*. 2015.
162. *Princeton Applied Research - Application Note CORR-1 - Basics of Corrosion Measurements*. 27.04.2016; Available from: www.princetonappliedresearch.com/download.asbx?AttributeFileId=228c5c3f-69dc-495e-afde-06aefc513779.
163. McCafferty, E., *Introduction to Corrosion Science*. 2010: Springer-Verlag New York.
164. Close, D., et al., *Electrodeposition, microstructural characterization and anticorrosive properties of Zn-Mn alloy coatings from acidic chloride electrolyte containing 4-hydroxybenzaldehyde and ammonium thiocyanate.* Surface and Coatings Technology, 2016. **298**: p. 73-82.

165. Nayana, K.O. and T.V. Venkatesha, *Bright zinc electrodeposition and study of influence of synergistic interaction of additives on coating properties.* Journal of Industrial and Engineering Chemistry, 2015. **26**: p. 107-115.
166. Trejo, G., R. Ortega, and Y. Meas, *Nucleation and Growth of Zinc from Chloride Concentrated Solutions.* Journal of The Electrochemical Society, 1998. **145**(12): p. 4090-4097.
167. Díaz-Arista, P., et al., *EQCM study of the electrodeposition of manganese in the presence of ammonium thiocyanate in chloride-based acidic solutions.* Electrochimica Acta, 2006. **51**(21): p. 4393-4404.
168. Zimmer, A., et al., *Growth Mechanisms during the Early Stages of electrodeposition of Bismuth telluride films.* Electrochimica Acta, 2015. **174**: p. 376-383.
169. Reinhold, B., S.G. Klose, and J. Kopp, *Schutzsysteme für Verschraubungselemente in Kontakt mit Leichtmetall.* Materialwissenschaft und Werkstofftechnik, 1998. **29**(1): p. 1-8.
170. Fels, C.C. and W. Plieth, *Zink-Mangan-Legierungselektrolyte im Test.* JOT Journal für Oberflächentechnik, 2001. **41**(11): p. 64-67.
171. Chung, P.P., et al., *Electrodeposition of zinc–manganese alloy coatings from ionic liquid electrolytes.* Transactions of the IMF, 2008. **86**(4): p. 211-219.
172. Olea-Mejía, O., O. Olea-Cadoso, and R. Lopez-Castañares, *FIB-SEM Combination Technique for Characterization of Polymer Composites*. Polymer science: research advances, practical applications and educational aspects, ed. A. Méndez-Vilas and A. Solano-Martín. Vol. 2. 2012: Formatex Research Center.
173. Li, J., *Advanced Techniques in TEM Specimen Preparation, The Transmission Electron Microscope*, K. Maaz, Editor. 2012, InTech. p. 69-84.
174. Schlesinger, M. and M. Paunovic, *Modern Electroplating*. 2011: Wiley.
175. Nee, C.C. and R. Weil, *The banded structure of Ni-P electrodeposits.* Surface Technology, 1985. **25**(1): p. 7-15.
176. Blonde, R., et al., *Evolution of texture and microstructure in pulsed electro-deposited Cu treated by Surface Mechanical Attrition Treatment (SMAT).* Journal of Alloys and Compounds, 2010. **504, Supplement 1**: p. S410-S413.
177. Pangarov, N.A., *Preferred orientations in electro-deposited metals.* Journal of Electroanalytical Chemistry, 1964: p. 16.
178. Ramanauskas, R., *Structural factor in Zn alloy electrodeposit corrosion.* Applied Surface Science, 1999. **153**: p. 53-64.
179. Baumgart, H. and R. Sanders, *Stahlblech und Formteil daraus*, G.G.T.O. LLC, Editor. 2014.
180. Mita, K., T. Ikeda, and M. Maeda, *Phase diagram study of Fe-Zn intermetallics.* Journal of Phase Equilibria, 2001. **22**(2): p. 122-125.
181. Close, D., P. Feuser, and R. Lallement, *Design of Press Tools to Investigate the Hot Stamping Behaviour of Alternative Coatings for Press-Hardened Steel Parts.* Key Engineering Materials, 2015. **639**: p. 227-234.
182. Close, D., P. Feuser, and R. Lallement, *DE102014006136 (A1) - Werkzeug zum Presshärten eines Blechbauteils*. 2015, Daimler AG.
183. Zhang, X., et al., *The initial release of zinc and aluminum from non-treated Galvalume and the formation of corrosion products in chloride containing media.* Applied Surface Science, 2012. **258**(10): p. 4351-4359.

184. Lee, C.W. and B.C. De Cooman, *Microstructural Evolution of the 55 Wt Pct Al-Zn Coating During Press Hardening.* Metallurgical and Materials Transactions A, 2014. **45**(10): p. 4499-4509.
185. Lee, C.W., et al., *Microstructure evolution of a 55 wt.% Al–Zn coating on press hardening steel during rapid heating.* Surface and Coatings Technology, 2015. **281**: p. 35-43.
186. Fan, D.W. and B.C. De Cooman. *A Ductile Aluminide Coating for Hot Stamping*. in *3rd International Conference on Hot Sheet Metal Forming of High-Performance Steel*. 2011. Kassel, Germany.
187. Lenze, F.-J., J. Bian, and S. Sikora. *Einsatz pressgehärteter Stähle im Karosseriebau: Stand und Trends der Entwicklung*. in *Proceedings of the 2nd Erlanger Workshop Warmblechumformung*. 2007. Erlangen, Germany: Meisenbach Bamberg.
188. Schürz, S., et al., *Chemistry of corrosion products on Zn–Al–Mg alloy coated steel.* Corrosion Science, 2010. **52**(10): p. 3271-3279.
189. Landschoot, N., et al., *Zinc-Magnesium Coated Hot Dip Galvanised Steel.* ATZ worldwide, 2013. **115**(4): p. 4-8.
190. Hensen, G., *ZnAlMg for Hot Stamping*, D. Close, Editor. 2013.
191. Rout, R.K., J. Go, and A.V. Gaikwad, *Strip, sheet of blank suitable for hot forming and process for the production thereof*. 2001, Tata Steel LTD.
192. Lupp, B., et al., *Method for the production of a steel component by thermoforming, and steel component produced by thermoforming*. 2009, ThyssenKrupp Steel AG.
193. Lupp, B., et al., *Method for producing a coated steel component by means of hot forming and steel component produced by means of hot forming*. 2009, ThyssenKrupp Steel Europe AG.
194. Köyer, M., *DoubleProtect*. 05.12.2013.
195. Azushima, A., et al., *Frictional behavior of ZnO coated aluminized steels under hot drawing tests with coated tools.* Journal of Materials Processing Technology, 2016. **228**: p. 106-111.
196. Maki, J., M. Kurosaki, and S. Sugiyama, *Plated steel sheet and method of hot-stamping plated steel sheet*. 2013.
197. Merklinger, V., et al., *Entwicklung einer niedrigschmelzenden Legierung und deren Applikation zum Korrosionsschutz hochfester Stähle.* Materialwissenschaft und Werkstofftechnik, 2008. **39**(12): p. 888-891.
198. Merklinger, V. and B. Reinhold, *Coating of Automobile Structural Components from Ultra-High Strength Steels*, in *5th International Conference on Sustainable Automotive*. 2013: Ingolstadt, Germany.
199. Kurzynski, J., C. Strobl, and V. Merklinger, *Entwicklung und Erprobung von kathodischen Korrosionsschutzsystemen für höchstfeste Stähle: Development and test of corrosion protection systems for HSS grades*. Forschung für die Praxis. Vol. 640. 2013: Verlag und Vertriebsges. mbH.
200. Buciuman, F., et al., *Vibrational spectroscopy of bulk and supported manganese oxides.* Physical Chemistry Chemical Physics, 1999. **1**(1): p. 185-190.
201. Malavasi, L., et al., *Raman spectroscopy of AMn2O4 (A = Mn, Mg and Zn) spinels.* Physical Chemistry Chemical Physics, 2002. **4**(15): p. 3876-3880.
202. Mironova-Ulmane, N., A. Kuzmin, and M. Grube, *Raman and infrared spectromicroscopy of manganese oxides.* Journal of Alloys and Compounds, 2009. **480**(1): p. 97-99.

203. Silva, G.C., et al., *Raman and IR spectroscopic investigation of As adsorbed on Mn3O4 magnetic composites.* Spectrochimica Acta Part A: Molecular and Biomolecular Spectroscopy, 2013. **100**: p. 161-165.
204. Bouchard, M. and D.C. Smith, *Catalogue of 45 reference Raman spectra of minerals concerning research in art history or archaeology, especially on corroded metals and coloured glass.* Spectrochimica Acta Part A: Molecular and Biomolecular Spectroscopy, 2003. **59**(10): p. 2247-2266.
205. Gandhi, A.C., et al., *In Situ Confocal Raman Mapping Study of a Single Ti-Assisted ZnO Nanowire.* Nanoscale Research Letters, 2009. **5**(3): p. 581-586.
206. Damen, T.C., S.P.S. Porto, and B. Tell, *Raman Effect in Zinc Oxide.* Physical Review, 1966. **142**(2): p. 570-574.
207. Li, F., et al., *Thermodynamic consideration on selective surface oxidation of high strength steels prior to hot-dip galvanizing.* Journal of Coatings Technology and Research, 2011. **8**(5): p. 639-647.